CRANFIELD INSTITUTE OF TECHNOLOGY

SCHOOL OF MECHANICAL ENGINEERING

PhD THESIS

Academic Year 1987-88

P A Hobson

Thermosyphon solar water heaters; validated numerical simulation and design correlations

Supervisor: Dr. B Norton

March 1988

This thesis is submitted for the degree of Doctor of Philosophy

ABSTRACT

A detailed analysis of the heat transfers and fluid flows within a direct thermosyphonic solar-energy water-heater has been undertaken. The collector energy equations when cast in a two-dimensional form enabled heat transfer and thermal capacitance effects to be simulated accurately at the small flow rates encountered commonly in such systems. An investigation of thermocline relaxation processes within the store indicated negligible mixing at the store inlet over a wide range of Richardsons numbers ($43{,}608 < Ri < 729{,}016$). Thermal relaxation under conditions of no flow was shown to be due predominantly to axial conduction along the store wall. The use of an appropriate non-isothermal friction factor correlation when calculating frictional losses in the collector's riser pipes, produced predicted steady-state flow rates which were corroborated experimentally to within 2%. An indoor test facility, monitored and controlled by a microcomputer, enabled "real" operating conditions to be simulated. The predicted responses of the system to identical conditions showed good agreement with the corresponding experimental observations, the predicted heat delivery being within 2.8% of the measured value.

A technique for correlating the daily performances of thermosyphon solar-energy water-heaters has been developed. The five dimensionless groups which form the basis of the correlations and the functional relationships between these groups were derived from an analytical solution of a linear first-order differential transient heat balance carried out on a generic system. Thermal performance data used in the correlations was generated by the numerical simulation using representative U.K. hourly weather data and operating conditions. The minimum amount of data required to establish a characteristic curve for an individual system was found to be thirty days. Using such a curve, the total annual solar fraction agreed with that predicted by the high level model to within 3%. Two universal curves were determined in which the gradients of characteristic curves were correlated against the derived dimensionless groups. The accuracy of the resulting two-stage algorithm in determining annual solar fractions was established as ranging from 5.5% for predominantly multiple-pass systems to a mean of 10.5% for single-pass systems.

ACKNOWLEDGEMENTS

Without the generous funding of the School of Mechanical Engineering, Cranfield and latterly, the Science and Engineering Research Council, this work would not have been possible.

I am indebted to all the academic, research and technical staff at Cranfield who have, at various stages, proffered advice and assistance. In particular, I would like to thank:

Brian Norton for his guidance and enthusiasm in all aspects of this study,

Steve Lo for his time and patience in handling much of the data used in the initial correlation work,

Dave Whittington for the general practical advice, initial construction of and subsequent modifications to, the experimental rig,

Brian Moffitt and John Dawe for their assistance in solving many of the remote-monitoring and control hardware problems, and

Barry Highfield for the benefit of his computing expertise.

Finally I should like to thank my wife, Patricia, not only for her support and tolerance throughout this venture, but also for her practical contribution to the preparation of this thesis.

SUMMARY OF CONTENTS

TABLE OF CONTENTS

LIST OF FIGURES IN THE MAIN BODY OF THE TEXT

LIST OF FIGURES APPEARING IN THE APPENDICES

LIST OF TABLES IN THE MAIN BODY OF THE TEXT

LIST OF TABLES APPEARING IN THE APPENDICES

NOMENCLATURE

Where units are not specified, quantities are dimensionless

A	Area	(m^2)
a	Factor defined by equation 4.4	
a_1-a_{23}	Factors defined in chapter 3	
b	Factor defined by equation 4.4	
C	Specific heat capacity	($Jkg^{-1}K^{-1}$)
D	Internal diameter of considered pipe	(m)
Dn	Dean number for the flow through a pipe bend	
e	error value	(%)
E	Electrical potential across a thermocouple junction	(V)
F	Fin efficiency factor	
F_{AV}	Collector efficiency factor based on the mean fluid temperature within the collector	
F'	Collector efficiency factor based on the local fluid temperature at the fin base	
F_R	Collector heat removal factor	
F^*	Force acting on a control volume of water	(N)
f	Friction factor for the flow through a cylindrical pipe	
f'	Solar fraction	
G	Solar fraction predicted by equation 8.22	
Gr	Grashof number for flow	
Gz	Graetz number	
g	Acceleration due to gravity	(ms^{-2})
H	Total global radiation	(Jm^{-2})
h	Convective heat transfer coefficient	($Wm^{-2}K^{-1}$)
h_1	Vertical height of store downcomer port above collector inlet	(m)
h_2	Vertical distance between collector inlet and outlet	(m)
h_3	Vertical height of store upriser port above collector inlet	(m)
I	Insolation	(Wm^{-2})
K	System parameter defined by equation 11.3	

K^*	System parameter defined by equation 11.2	$(kgs^{-1}K^{-1})$
K_{BEND}	Frictional loss coefficient for flow through a pipe bend	
K_i	Incident angle modifier	
K_s	Clearness index	
K_{TEE}	Frictional loss coefficient for flow through a pipe "tee" section	
K'	Collector constant defined by equation 6.9	
k	Thermal conductivity	$(Wm^{-1}K^{-1})$
L	Component length	(m)
L^*	Dimensionless form of penetration depth defined by equation 5.4	
M	Mass of water	(kg)
m	Mass flow rate	(kgs^{-1})
m	Gradient of characteristic curve for a system defined by equation 10.1	
m'	Factor in definition of fin efficiency	
m^*	Correlating function defined in equation 11.4	
N	Number of riser pipes in collector	
Nd	Number of days in a month	(days)
Np	Mean daily circulation number	$(days^{-1})$
Nr	Hourly number of air changes within the roof space	(hr^{-1})
Nu	Nusselt number	
P	Internal perimeter of a component	(m)
Pr	Prandtl number	
p	Fluid pressure on the surface of a control volume	(Nm^{-2})
Q	Total heat transfered	(J)
Q'	Dimensionless form of total heat transfered defined by equation 8.18	
q	Instantaneous rate of heat transfer	(W)
R	Radius of curvature of a uniformly-curved pipe bend	(m)
Re	Reynolds number	
Ri	Richardson number defined by equation 5.5	
r	Internal radius of considered pipe	(m)
S	Radiative heat transfer shape factor	

T	Temperature (units in K unless indicated otherwise)	(K)
T^*	Dimensionless store outlet temperature defined by equation 5.9	
T'	Dimensionless mean store temperature defined by equation 5.9	
t	time	(s)
t^*	Store reaction time defined by equation 5.6	(s)
t'	Dimensionless time defined by equation 8.12	
U	General effective heat transfer coefficient	($Wm^{-2}K^{-1}$)
V	Volume of fluid within a control volume	(m^3)
v	Fluid velocity	(ms^{-1})
W	Specific load ratio	
W_c	Width of collector fin	(m)
w	Total electrical power supplied to heater mats	(W)
X	Brooks number defined by equation 8.30	
X'	f-chart parameter defined by equation 8.1	
x	Distance perpendicular to the riser pipe	(m)
Y	Heywood number defined by equation 8.15	
Y'	f-chart parameter defined by equation 8.2	
y	Distance along a component	(m)
Z	Bailey number defined by equation 8.16	
z	Vertical height from datum	(m)
z^*	Dimensional form of penetration depth defined by equation 5.8	(m)
α	Absorptance of collector absorber plate surface	
α'	Thermal diffusivity	
β	Temperature difference between mean collector and store values	(K)
Γ	Collector time constant defined by equation 6.11	(s)
γ	Cubic expansivity	(K^{-1})
$\Delta()$	Small increment in the quantity in parenthesis	
δ	Thickness of solid components	(m)
ε	Thermal emissivity	
ζ	Angle subtended by a pipe bend	(degrees)
η	Collector efficiency	
θ	Angle of general component from the horizontal	(degrees)
μ	Dynamic viscosity	(Nsm^{-2})

ν	Kinematic viscosity	(m^2s^{-1})
ρ	Density	(kgm^{-3})
σ	Stefan Boltzmann constant	$(Wm^{-2}K^{-4})$
σ'	Root mean square deviation from a mean value (units are variable)	
τ	Transmittance of glass collector cover	
ϕ	Angle of incident light (from normal) on the glass collector cover	(degrees)
ψ	Difference between ambient and mean store temperature	(K)
Ω	Theoretical store charge period (= $M_s/\dot{m}_c$)	(s)

Subscripts:

a	Refers to ambient conditions
BODY	Refers to forces acting on entire mass of fluid within a control volume
CJC	Pertaining to conditions at or in the vicinity of the cold junction card
C	Pertaining to properties of the ceiling structure
c	Pertaining to the collector
ce	Pertaining to the edge of the collector
cell	Referring to the cell number of a node
cor	Refers to a value calculated using a correlation technique
D	Based on the internal diameter of the pipe
d	Pertaining to the downcomer pipe
dp	Refers to the dew point state
e	Representing an effective overall value
f	Pertaining to the collector absorber plate
g	Pertaining to the glass collector cover
i	Refers to properties of an insulant
in	The value of a fluid quantity at the inlet to a component
J	Refers to a value calculated using operating conditions and meteorological data pertinant to the month of June

j	refers to a node in the j th column of a finite difference matrix
k	refers to a node in the k th row of a finite difference matrix
L	Refers to thermal load on solar water heater
l	Refers to conditions within the roof space
M	Refers to "minor" frictional flow losses
m	Refers to mains water supply
max	Refers to a maximum value
min	Refers to a minimum value
n	Pertaining to the n th riser pipe from the collector inlet
90	Representing optical properties at normal angles of incidence
o	The value of a fluid quantity at the outlet to a component
p	Pertaining to characteristic common to both the upriser and downcomer pipes
r	Pertaining to the collector riser pipes
ref	Refers to a reference value
R	Refers to properties of external surface of roof
s	Pertaining to the storage tank
sb	Pertaining to local heat transfer at the base of the storage tank
sim	Refers to a value calculated using the numerical simulation model
sol	Pertaining to solar heated water
st	Pertaining to local heat transfer at the top of the storage tank
SURF	Refers to forces acting over the surface of a fluid contained within a control volume
sw	Pertaining to storage tank walls
T	Refers to properties at the local fluid temperature
tot	Refers to total values heating requirements
u	Pertaining to the upriser
w	Local property or state of water in component
wind	Refers to heat transfer processes associated with forced air flow across a collector

z Pertaining to the penetration depth of a jet of fluid into a reservoir

Superscripts:

~ Denotes a vector quantity

e Refers to end conditions

i Refers to initial conditions

id Refers to a specific day

im Refers to a specific month

t Refers to the current state of a node in the finite difference scheme

td Refers to daily values

tm Refers to monthly values

ty Refers to yearly values

CHAPTER ONE

INTRODUCTION: PREVIOUS INVESTIGATIONS

1.1 The general approach

To predict analytically the performance of a natural-circulation solar-energy water heater, three alternative broad approaches can be adopted, these being:

i) Simplified models (1,2)

ii) Correlation of performance characteristics from either the simulation or monitoring of generic systems (3-6)

iii) Rigorous simulation models (7-18)

The first two approaches are intended for the estimation of the long-term performance of a system and for the determination of the system size that achieves the optimum solar fraction. Because of the simplifications inherent in the first approach, such models are limited by the range of operating conditions and system configurations over which the simplifying assumptions are valid. Models refered to in this category often require experimentally-determined information which is only obtainable once the system has been constructed. The second approach cannot be applied reliably to those systems for which dimensions and climatic conditions a correlation has not been determined.

The third approach, that is the use of a rigorous simulation model has three principle roles. These are,

i) the engineering optimisation of systems from short-term performance simulations,

ii) to establish the long-term correlation of system behaviour over a wide range of system types and operating conditions, and

iii) to determine the limits of the validity of simplified models.

This paper describes the development and validation of a comprehensive model of the third kind.

1.2 Previous Modelling of Thermosyphon Solar Water Heaters

A thorough review of previous experimental and analytical work in the field of the present investigation is given by Norton and Probert (19). Experimental observations by Close (7) indicated that in practical multiple-pass thermosyphon solar-energy water heaters, the mean collector temperature was only slightly higher than the mean storage tank temperature. Based on this, a simple analytical model was developed for predicting the day-time performances of such a water heater. Conditions of no water draw off and sinusoidal variations with time in both insolation and ambient temperature were assumed. Using a simple heat balance for the entire system, a differential equation was developed, the solution permitting the mean tank temperature to be predicted. The analysis proved to be simple and accurate when applied to specific systems under known conditions. However it was unable to provide information on a systems' performance as a function of its parameters or environmental conditions. Gupta and Garg (8) improved on the Close (7) analysis by introducing a collector plate efficiency factor. A Fourier series expansion was used to model variations in the ambient temperature. In validating this model experimentally, a close correlation was obtained during the day-time. The observed night-time system loss was almost half way between the loss rates predicted for the two extreme cases of,

i) perfect coupling, high reverse flow and

ii) perfect decoupling, no reverse flow between the collector and storage tank.

An empirical analysis of the criteria for natural reverse thermosyphon circulation to occur has been provided by Norton and Probert (20).

Ong (9,10) was the first to employ a finite difference method to predict the system temperature distribution and thermosyphonic flow rates. The use of a numerical solution to the governing equations meant that actual hourly values of ambient temperature and insolation could be used as inputs rather than the Fourier series approximations necessary in previous analytical solution methods. In addition, this solution technique enabled fluid properties and therefore heat transfer and fluid flow frictional loss coefficients to be evaluated based on current operating temperatures. There was some agreement between predicted temperatures and those measured in one particular system near the middle of the insolation period, but large discrepancies were noted at other times. These may be attributable to the inadequate representation of the thermal capacities of the flat plate collector and connecting pipes. Baughn and Dougherty (11) extended Ongs analysis (10) to include the transition from laminar to turbulent flow.

Morrison et al (12) examined experimentally the transient dynamic behaviour of a thermosyphonic loop which included an electrically heated tube to simulate the solar energy collector. Laser-Doppler anemometry was used to measure the flow rate, thus introducing no additional fluid flow resistance. This study demonstrated the inadequacy of using fully developed flow friction factor correlations in determining the mass flow rate. A correction factor based on work by Langhaar (21) was proposed, to account for developing flow in the collector risers and connecting pipes.

Huang (13) developed an analysis of the behaviour of direct thermosyphon systems by solving a dimensionless form of the momentum and continuity equations. Ten dimensionless parameters for characterising the system were evolved and the sensitivity of the system performance to changes in these parameters was investigated. Huang (13) noted that the performance of a low resistance direct thermosyphon system was largely insensitive to the storage tank elevation.

Vaxman and Sokolov (14), using a numerical simulation similar to that

of Huang (13), highlighted the phenomenon that despite the small heat transfer area represented by the external surface of the upriser, insufficient thermal insulation on this component can trigger reverse circulation and cause significant night losses from the store. The diurnal performance of a thermosyphon system was shown to be insensitive to the degree to which the downcomer was insulated.

A theoretical and experimental study of the effects of draw-off on the stratification in a horizontal solar-energy heated hot water storage tank was carried out by Young (15). The observed destratification of the temperature profile within the tank, due to the inertial and buoyancy forces which ensue as hot water from the collector enters the store, was modelled in his analysis by the introduction of mixing coefficients into the boundary conditions. The mixing coefficients had to be adjusted by trial and error to give accurate results. The mixing which occurs when warm water is introduced above a cooler layer was simulated by a turbulent mixing term analagous to the axial conduction term in the storage tank energy equation. This mathematical model was found to give tank temperature profile predictions in close agreement with experimental observations.

An alternative approach to destratification due to unstable temperature inversions within the store was proposed by Morrison et al (1). This involved a distributed return model where gradual mixing of the collector return fluid was assumed as this fluid reached its equilibrium position in the storage tank thermocline. Perfect stratification was found to overestimate the system performance. The "Detailed Loop Model" (16) extended Huangs approach (13) in order to develop the most comprehensive parametric study to date. Unlike previous analyses, the coupled energy and momentum equation were solved assuming unsteady flow. All parameters were in a non-dimensional form. The simulated mode of heat transfer to the storage water was indirect (ie. via a heat exchanger). The performance of the system was found to be insensitive to both the degree of stratification within the store and the relative vertical orientation of the store and collector (during the insolation period). This latter observation for indirect systems is consistent with Huang's findings (13) for direct systems.

Defects in this analysis severely limit its usefulness in predicting performance over a wide range of system configurations and operating conditions. These problems include:

i) an empirically-determined, one-dimensional, linear vertical temperature profile was assumed for the hot water storage tank and an unnecessarily simplified approach used to model withdrawal of water from the tank,

ii) fluid density was assumed to vary linearly with temperature in determining the buoyancy forces and

iii) constant heat transfer coefficients were employed.

Although this simulation model remains unvalidated, experimental observations made later by Webster et al (22) verified, at least quantitatively, some of the characteristics of indirect solar energy water heaters identified using the Detailed Loop Model.

The correlation techniques used in predicting long-term system thermal performances and more detailed discussions of the methods employed in simulating the individual components in the models described above, are presented in the ensuing chapters.

CHAPTER TWO

DEVELOPMENT OF THE THERMOSYPHON SIMULATION MODEL

2.1 The Collector Model

2.1.1 Collector models used in previous thermosyphon simulations

In order to predict the fluid outlet temperature in their models, both Ong (9,10) and Young (15) used a collector heat removal factor. This factor developed by Hottel, Whillier and Bliss, as presented by Duffie and Beckman (23), gives the overall heat transfer characteristics of a fin and tube arrangement, under steady state conditions and is the ratio of the actual amount of heat transferred to the collector fluid, to the heat which would be transferred if the entire collector plate was at the fluid inlet temperature. This is defined mathematically as:

$$F_R = (\dot{m}_c C_w / A_c U_L)/[1 - \exp[-(A_c U_L F'/\dot{m}_c C_w)]]$$

equation 2.1

where F', the collector efficiency factor, is given by

$$F' = \frac{1/U_L}{W_f[U_L(D_r + F(W_f - D_r))] + (1/\pi D_r h_{f,w})}$$

equation 2.2

where F, the fin efficiency factor, is

$$F = \frac{\tanh[m'(W_f - D_r)/2]}{m'(W_f - D_r)/2}$$

equation 2.3

the factor m' being defined as

$$m'^2 = U_L/(k_f \delta_f)$$

equation 2.4

Although equation 2.1 assumes effectively a non-linear temperature profile along the collector tube, errors were introduced because:

i) as it was applied to the complete length of the collector tube, equation 2.1 gives no information on the actual temperature variation

along the collector and so the contribution of the water in the collector to the buoyant force in a thermosyphonic circuit has to be calculated from the arithmetic mean of the inlet and outlet temperatures, and

ii) the thermal capacity of all components within the collector were effectively neglected.

Some of the techniques used in the steady state analysis of flat-plate solar-energy collectors have been incorporated into existing non-steady state models. The collector efficiency factor F' defined in equation 2.2 was employed by Huang (13) in a form adapted for parallel plate absorbers. This form was also used in the "Detailed Loop Model" (16). The physical interpretation of equation 2.2 is that F' represents the ratio of the the actual amount of heat absorbed by the fluid at a particular point along the collector, to the amount of heat that would be absorbed were the whole fin at the local fluid temperature. The collector tubes could therefore be divided up along their lengths into a series of nodes and F' assumed to hold constant for the length of each node. A transient thermal analysis was then carried out on the fluid within this node, the heat transfer from the absorber plate to the fluid being calculated using the local F' value. This gave the additional advantage that since the fluid temperature of each node is known, the contribution due to buoyancy forces within the collector can be calculated accurately when determining the mass flow rate in the system, without having to assume a linear temperature profile between the inlet and outlet. Although the thermal capacity of the fluid in the collector was accounted for, the capacity due to the remainder of the collector components was in effect, neglected. Experimental work carried out by Shitzer et al (24) under the climatic conditions of Israel indicated that the centreline plate temperatures (ie. the plate temperatures midway between, and parallel to, the risers) of a collector in a natural-circulation loop reached a maximum value over the day approximately two hours before the maximum fluid temperature at the corresponding axial distance along the risers. The time lag between these particular maximum plate and fluid temperatures was attributed in part to the transient behaviour of the collector plate and was shown to have a significant effect on the collector outlet temperature.

A comparison was made by Kirchhoff and Billups (25) of the Hottel-Whillier-Bliss model with a steady-state finite-difference model of a flat plate collector which allowed for two-dimensional conduction in the collector absorber plate. Results showed good agreement between the water temperature distributions predicted by the two analyses (23,25) at high mass flow rates. However, the Hottel-Whillier-Bliss model was shown to predict too high an efficiency at thermosyphonic mass flow rates (ie. down to $5x10^{-3}$ $kgs^{-1}m^{-2}$). This discrepancy was attributed to a substantial component of heat flux in the collector plate, parallel to the risers which becomes significant at low flow rates and which is not accounted for in the Hottel-Whillier-Bliss analysis. A similar steady-state, two-dimensional analysis was carried out by Rao et al (26) and the resulting energy equations solved analytically. The isotherms predicted by this model confirmed the findings of Kirchhoff and Billups (25), namely that conduction within the absorber plate increases significantly in a direction parallel to that of the flow through the riser pipes at low flow rates. Although it was stated that this model was in good agreement with experimental observations, the significance of this phenomenon for collector performance was not explicitly investigated.

2.1.2 The collector model used in the simulation

A two dimensional finite difference model was developed based on that of Kirchhoff and Billups' (25), but with transient terms added. The main advantages of this over previously used Hottel-Whillier-Bliss (23) relationships are:

i) the fluid, collector plate and glass cover assume individual thermal masses and temperature profiles, and

ii) fewer assumptions are made about the heat transfer processes within the collector plate and between the collector plate and fluid.

The following assumptions are made in the derivation of the energy equations for the collector model.

i) The collector plate is of a fin and parallel tube configuration.

ii) For the purposes of radiative heat exchange the glass cover and collector plate are treated as two large, parallel, grey bodies.

iii) The glass cover is represented by a single node and is therefore considered to be at a single uniform temperature at each moment in time.

iv) The glass cover is opaque to long wave radiation.

v) Because the fin material is thin, the temperature gradient through the fin is assumed constant; ie. two dimensional heat flow only.

vi) Conduction within the collector fluid in the direction of flow is negligible.

The collector geometry considered was similar to that of a commercially manufactured collector (29) a section of which is shown in figure 2.1. Water flows in tubes of diameter D_r and length L_r attached to fins of thickness δ_f. Geometrical symmetry allows for the consideration of a representative plate segment of width W_f which has a water tube located at $W_f/2$. An energy balance on an incremental volume dx.dy. δ_f of fin, after dividing through by dx.dy gives an equation for the two-dimensional plate temperature distribution.

$$(\rho C\delta)_f \frac{\partial T_f}{\partial t} = (k\delta)_f \left[\frac{\partial^2 T_f}{\partial x^2} + \frac{\partial^2 T_f}{\partial y^2}\right] + h_{f,g}(T_g - T_f)$$

(i) (ii) (iii)

$$+ (U_{f,a} + U_{ce,a}A_{ce}/A_c)(T_a - T_f)$$

(iv)

$$+ S_{f,g}(T_g^4 - T_f^4) + (\tau\alpha)_e I$$

(v) (vi)

equation 2.5

where $S_{f,g} = (\varepsilon_f^{-1} + \varepsilon_g^{-1} - 1)^{-1}$

The components of the equation represent:

FIGURE 2.1

Heat transfers within a flat-plate solar-energy collector

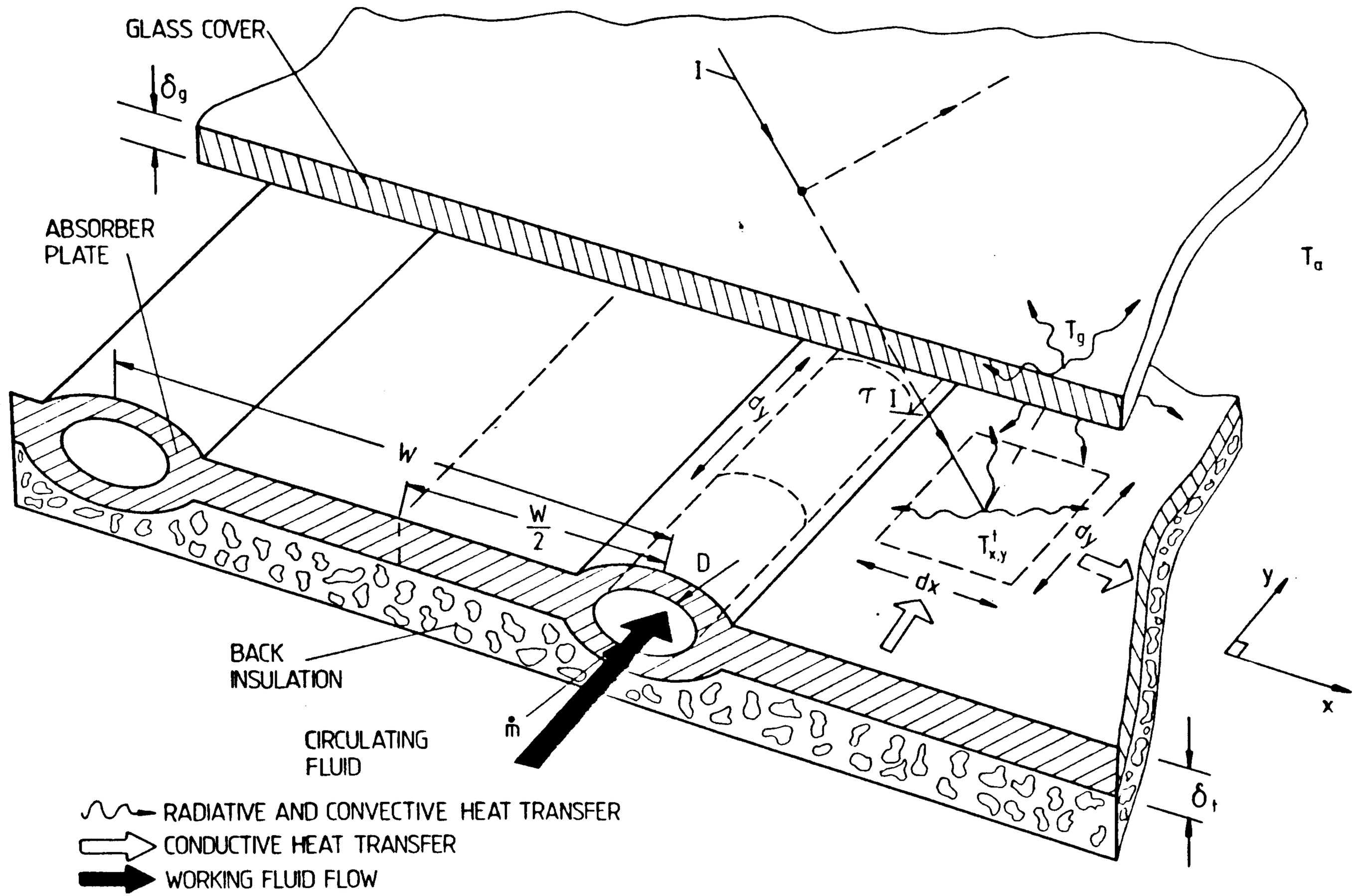
GLASS COVER
δ_g
ABSORBER PLATE
I
T_a
T_g
α_y
τ I
W
$\frac{W}{2}$
D
$T'_{x,y}$
α_y
dx
y
x
BACK INSULATION
$\dot{m}$
CIRCULATING FLUID
δ_t
RADIATIVE AND CONVECTIVE HEAT TRANSFER
CONDUCTIVE HEAT TRANSFER
WORKING FLUID FLOW

i) the rate of change of internal energy,

ii) two-dimensional heat conduction,

iii) convective heat transfer between the fin and glass cover,

iv) heat transfer through the back and edges of the collector,

v) radiative heat exchange between the glass cover and fin,

vi) solar radiation incident on the fin. The transmittance-absorptance product calculation is based on the angle of light incident on the cover using the method presented by Duffie and Beckman (23).

Boundary conditions on the fin temperature profile T(x,y,t) are from symmetry of adjacent nodes

$$\left.\frac{\partial T_f}{\partial x}\right|_{x=W_f/2} = 0$$

equation 2.6

and since there is no heat flux through the ends of the plate (collector edge losses have been spread over the absorbing area of the collector),

$$\left.\frac{\partial T_f}{\partial y}\right|_{y=0} = \left.\frac{\partial T_f}{\partial y}\right|_{y=L_r} = 0$$

equation 2. 7

The boundary condition connecting the fluid temperatures to the plate temperatures is obtained from a heat balance on an incremental area of the plate at x = 0. In the limit as dx tends to zero,

$$\left.\frac{\partial T_f}{\partial x}\right|_{x=0} = \frac{h_{f,w}\pi D_r}{2(k\delta)_f}(T_{f,x=0} - T_w)$$

equation 2.8

The pipe wall is assumed to take on the same temperature (defined by equation 2.4) as that of the fin at $x = W_f/2$. A heat balance on an incremental section of fluid within the riser pipes (shown in figure 2.1) then gives,

$$(\rho C)_w(\pi D_r^2/4)\frac{\partial T_w}{\partial t} + \frac{C_w \dot{m}_c}{N}\frac{\partial T_w}{\partial y} = h_{w,f}\pi D_r(T_{f,x=0} - T_w)$$

(i) (ii) (iii)

equation 2.9

where the components represent:

i) the rate of increase in internal energy,

ii) the heat convected into the incremental fluid volume from the "down-stream" direction,

iii) convective heat transfer between the fin and fluid.

To avoid the use of complex shape factors, assumption (iii)-that the glass cover is at a single uniform temperature at any instant in time-is used and the cover temperature is obtained in the following energy balance. The mean temperature of the collector plate is employed to determine the heat transfer between plate and cover.

$$(\rho C)_g\frac{\partial T_g}{\partial t} = h_{g,f}(\bar{T}_f - T_g) + \sigma S_{f,g}(\bar{T}_f^4 - T_g^4)$$

(i) (ii) (iii)

$$+ h_{wind}(T_a - T_g) + \sigma\varepsilon_g(T_s^4 - T_g^4)$$

(iv) (v)

equation 2.10

The components of this equation are:

i) the rate of increase in internal energy of the glass cover,

ii) the heat transferred by convection between the absorber plate and cover,

FIGURE 2.2

Assumed flow distribution within the risers and headers of a solar-energy collector

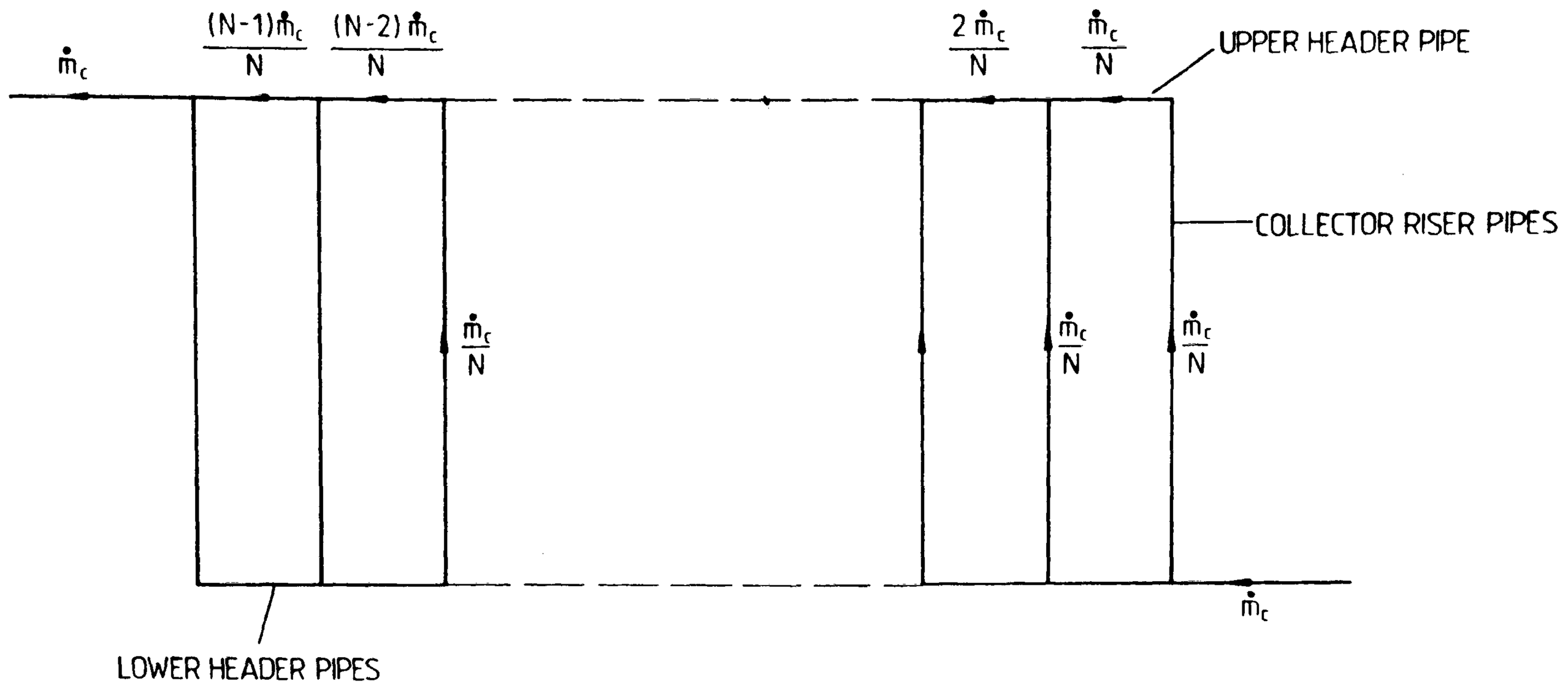
$\dot{m}_c$
$\frac{(N-1)\dot{m}_c}{N}$
$\frac{(N-2)\dot{m}_c}{N}$
$\frac{2\dot{m}_c}{N}$
$\frac{\dot{m}_c}{N}$
UPPER HEADER PIPE
COLLECTOR RISER PIPES
$\frac{\dot{m}_c}{N}$
$\frac{\dot{m}_c}{N}$
$\frac{\dot{m}_c}{N}$
$\dot{m}_c$
LOWER HEADER PIPES

FIGURE 2.3

Designation of flows and temperatures within the header pipe of a solar-energy collector

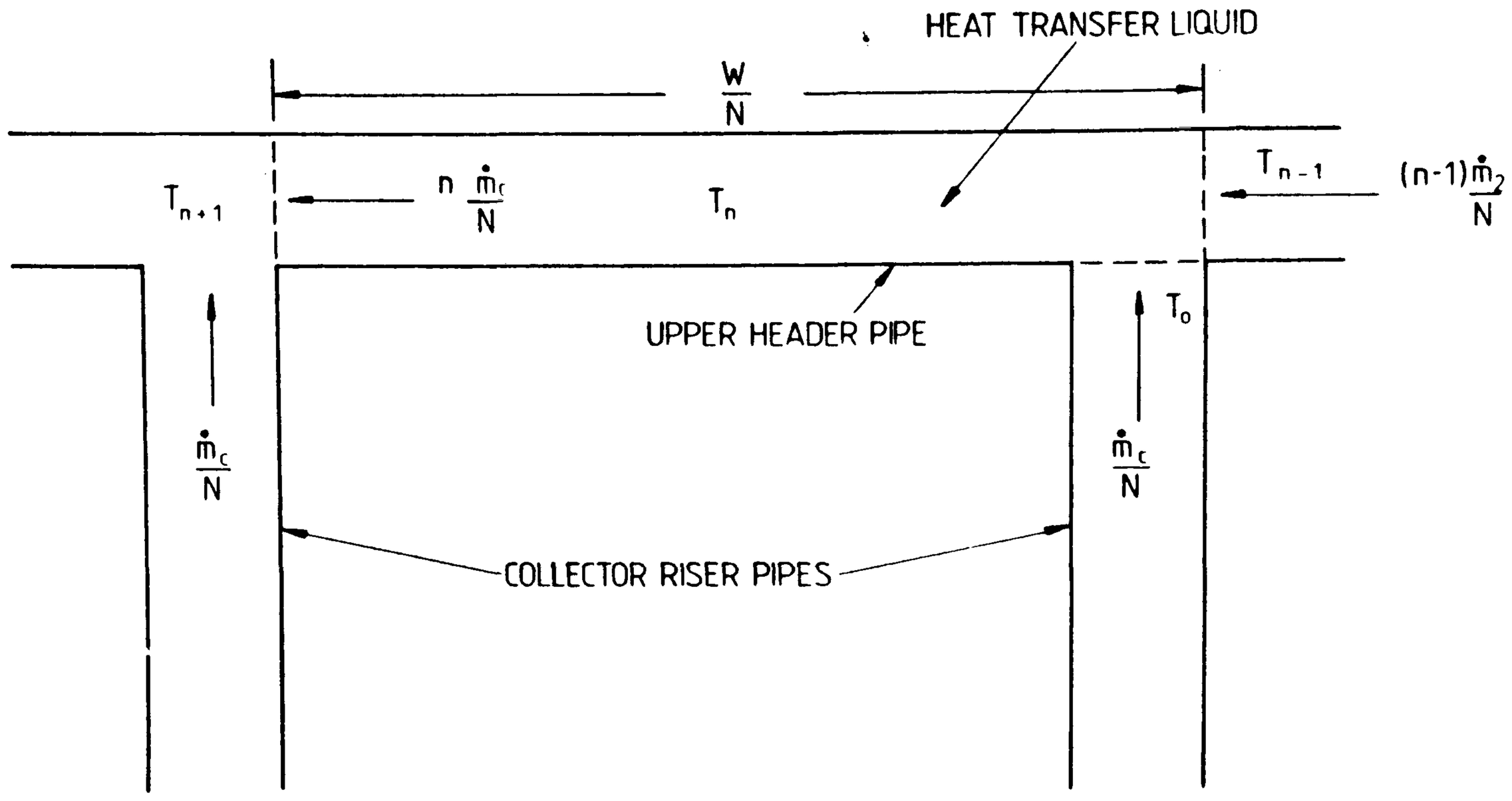
HEAT TRANSFER LIQUID
W/N
T_{n+1}
$n\frac{\dot{m}_c}{N}$
T_n
T_{n-1}
$(n-1)\frac{\dot{m}_2}{N}$
UPPER HEADER PIPE
T_o
$\frac{\dot{m}_c}{N}$
$\frac{\dot{m}_c}{N}$
COLLECTOR RISER PIPES

iii) radiative heat transfer between plate and cover,

iv) convective heat transfer between the outer surface of the glass cover and surroundings (due predominantly to wind effects),

v) radiative heat transfer between glass cover and sky, where the sky temperature is given by

$$T_{sky} = T_a[0.8 + (T_{dp} - 273)/250]^{0.25}$$

equation 2.11

In order to simulate accurately the transient response time of the collector, it is necessary to take into account the thermal mass of water in the collectors header pipes. The transient response of fluid in this component has been shown (27) to account for the experimentally-observed "retardation time". The retardation time is the time lag between a change in the temperature of the fluid leaving the end of the riser pipes and the time when this change appears at the outlet of the header pipe. The mass flow rates in the sections of the header pipes associated with each of the riser pipes will each have different values (figure 2.2). It is therefore necessary to consider each of these sections individually although (since only one riser pipe is being considered) the incoming fluid temperature and mass flow rate from the assosiated riser pipe is the same in each section. In order to keep the required computational time to a minimum, the section of header pipe associated with each riser pipe is considered as a single node as shown in figure 2.3. A heat balance on the nth section of the header pipe gives,

$$(W_f \rho_w / \dot{m}_r)(\pi D_h^2/4)\frac{\partial T_w}{\partial t} = n(T_{n-1} - T_n) + (T_o - T_{n-1})$$

equation 2.12

2.2 Storage Tank Model Used in the Simulation

An energy balance neglecting the thermal capacity of the insulation on an incremental section (figure 2.4) of fluid in the tank which is not

in contact with the end sections of the tank gives

$$A_s(\rho C)_w\frac{\partial T_w}{\partial t} + C_w\dot{m}_s\frac{\partial T_w}{\partial y} = k_w A_s\frac{\partial^2 T_w}{\partial y^2} + U_{s,a}P_s(T_a - T_w)$$

(i) (ii) (iii) (iv)

equation 2.13

where $\dot{m}_s = \dot{m}_c - \dot{m}_L$

Term (iii) in equation 2.13 represents one dimensional axial thermal conductivity within the storage tank fluid, and term (iv) the heat loss through the vertical tank walls only.

The boundary conditions for the storage tank are determined by considering incremental sections of fluid of thickness dy (figure 2.4) in contact with the top and base of the tank. For the top of the tank, as dy approaches zero,

$$(U_{st}/k_s)(T_a - T_w) + \frac{\partial T_w}{\partial y} = 0$$

equations 2.14

Similarly for the base of the tank shown in figure 2.4,

$$(U_{sb}/k_s)(T_a - T_w) - \frac{\partial T_w}{\partial y} = 0$$

equations 2.15

Because of the discontinuous nature of the temperature profile at the fluid inlets and outlets in the store, an exact differential equation has not been derived. The boundary conditions at the planes in which water is added or removed from the store and which therefore divide volumes in which there is no through-flow of water and volumes in which a through flow exists, are derived directly in finite difference form. A simple mixing model based on that suggested by Morrison and Tran (1) was introduced into the storage tank simulation. If a layer of warm fluid exists below a cooler layer, complete mixing is assumed to occur and the two adjacent nodes take on a single temperature. This process

FIGURE 2.4

Fluid flows and temperatures within an unpressurised storage tank

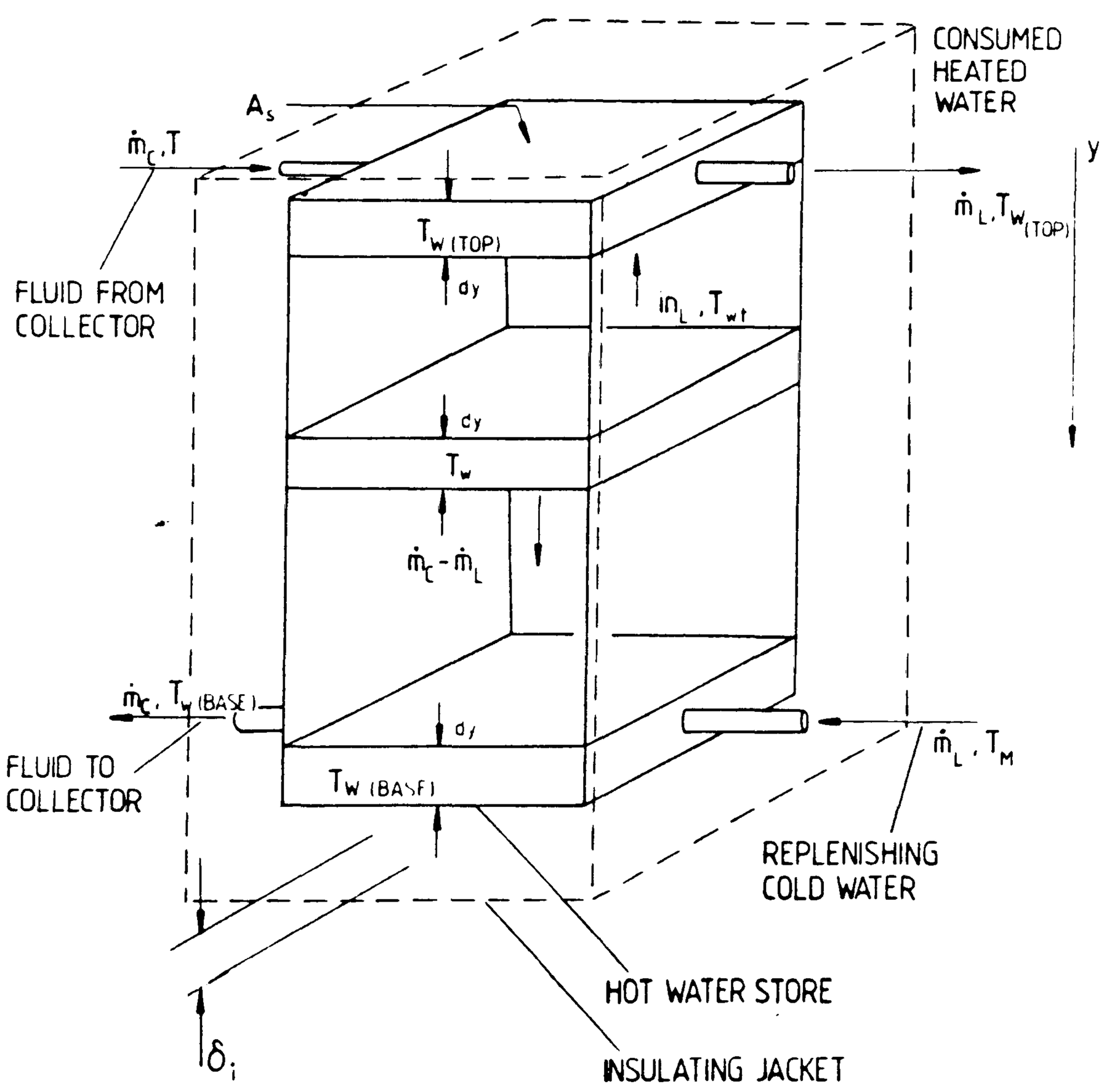
CONSUMED
HEATED
WATER
A_s
$\dot{m}_c, T$
y
$\dot{m}_L, T_{W(TOP)}$
$T_{W(TOP)}$
dy
in_L, T_{wt}
FLUID FROM
COLLECTOR
dy
T_w
$\dot{m}_c - \dot{m}_L$
$\dot{m}_c, T_{W(BASE)}$
d_1
FLUID TO
COLLECTOR
$T_{W(BASE)}$
$\dot{m}_L, T_M$
REPLENISHING
COLD WATER
HOT WATER STORE
δ_i
INSULATING JACKET

FIGURE 2.5

Fluid flows and temperatures within a general section of an upriser or downcomer pipe

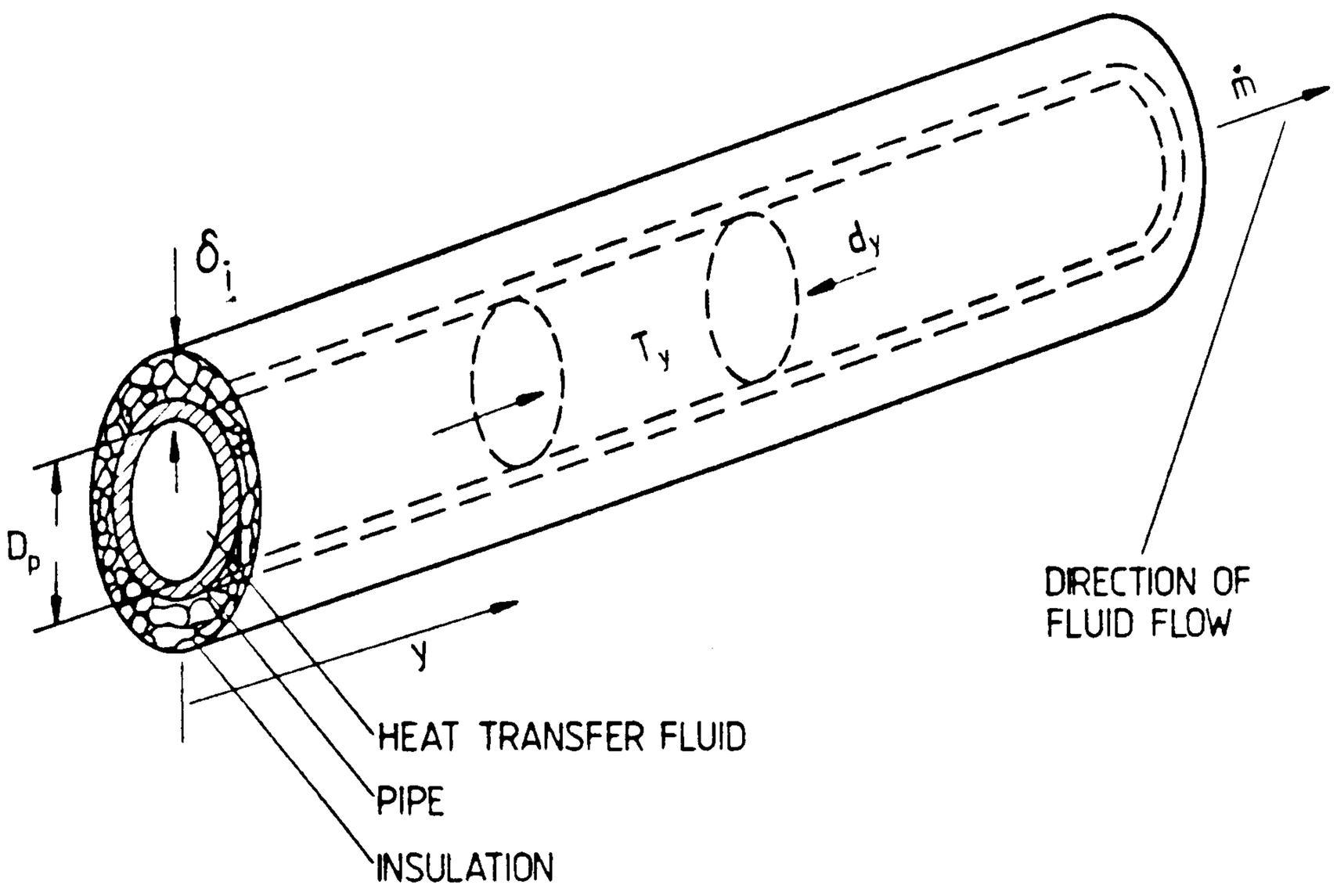
δ_i
D_p
d_y
T_y
y
$\dot{m}$
DIRECTION OF
FLUID FLOW
HEAT TRANSFER FLUID
PIPE
INSULATION

is repeated throughout the tank until the thermocline is restored.

2.3 The Simulation of the Connecting (Upriser and Downcomer) Pipework

Neglecting the thermal mass of the insulation surrounding the upriser and downcomer pipes, a heat balance on an element of fluid (figure 2.5) within the pipes gives

$$(\rho C)_w \pi D_p^2 \frac{\partial T_w}{\partial t} + C_w \dot{m}_c \frac{\partial T_w}{\partial y} = U_{p,a} \pi D_p (T_a - T_w)$$

equation 2.16

2.4 The Momentum Equation

The general form of the integral momentum equation is

$$\tilde{F}^*_{SURF} + \tilde{F}^*_{BODY} = \frac{\partial}{\partial t}\int \tilde{v}\rho dV + \int \tilde{v}\rho\tilde{v}.d\tilde{A}$$

equation 2.17

For the four components comprising the thermosyphon loop, equation 2.17 becomes, for one-dimensional, incompressible flow,

$$P_{SURF} + P_{BODY} = (L_r/A_r + L_u/L_p + L_s/A_s + L_d/A_p)\frac{\partial \dot{m}_c}{\partial t}$$

equation 2.18

Pressure losses due to surface forces (ie. friction) are given by

$$P_{SURF} = \frac{-\dot{m}_c|\dot{m}_c|}{2}\left[\frac{(fL)_r}{\rho_w(DA^2)_r N^2} + \frac{(fL)_u}{\rho_w(DA^2)_p} + \frac{(fL)_d}{\rho_w(DA^2)_p}\right] - \Sigma p_M$$

equation 2.19

Where Σp_M is the sum of the pressure losses due to turns, elbows and tees.

Pressure terms due to body forces acting on the fluid arise from the

total vertical hydrostatic head integrated around the thermosyphon loop,

$$P_{BODY} = g \oint \rho_w \sin(\theta) dy$$

equation 2.20

where θ is the angle of the incremental length dy from the horizontal. Substituting equations 2.19 and 2.20 into 2.18 gives

$$(L_r/A_r + L_u/A_p + L_s/A_s + L_d/A_p)\frac{\partial \dot{m}_c}{\partial t} = g \oint \rho_w \sin(\theta) dy - \sum p_M$$

$$-\frac{\dot{m}_c|\dot{m}_c|}{2}\left[\frac{(fL)_r}{\rho_w (DA^2)_r N^2} + \frac{(fL)_u}{\rho_w (DA^2)_p} + \frac{(fL)_d}{\rho_w (DA^2)_p}\right]$$

equation 2.21

Using the technique of finite differences equations 2.5, 2.9, 2.10, 2.12, 2.13, 2.16 and 2.21 representing the main energy and momentum transfer processes, were solved simultaneously with their associated boundary conditions.

2.5 The Assembled Model

A summary of the main features which form the basis on which the governing equations developed in the preceeding sections of this chapter are founded and the operating conditions used as basic inputs to the numerical simulation, has been compiled below.

1. A finite difference, transient heat transfer analysis is applied to the circulating liquid in all the components (ie. collector, upriser, storage tank and downcomer) of the thermosyphon loop.

2. Collector plate and cover thermal capacitance terms are included in the simulation.

3. The density, specific heat, viscosity, conductivity and Prantl number of the circulating liquid are represented as second-order

polynomial functions of temperature.

4. All heat transfer coefficients are temperature dependent and based on the ambient and mean component temperatures. These coefficients are updated at each time step in the numerical solution.

5. A simple simulation of buoyancy-induced mixing between stratified layers - which occurs when warmer fluid exists below a cooler layer - is included in the storage tank model.

6. Water is drawn off from the storage tank according to a time-dependent draw-off profile. The draw-off data is taken from the monitoring of three dwellings in the village of Wharley End in each of which similar thermosyphon solar energy water heaters have been installed (28).

7. "Real" insolation and ambient temperatures are used as inputs to the simulation.

8. The transmission coefficient of the glass collector cover is a function of the sun hour angle.

9. In determining the mass flow rate, a form of the momentum equation which includes transient terms is used.

10. Friction factors are calculated using correlations appropriate to both non-isothermal thermally destabilised low Reynold numbers flow and isothermal developing laminar flow in the straight sections of the ducting.

11. Empirically determined laminar loss coefficients for bends in the ducting is included in the simulation rather than the previously used turbulent "minor" loss coefficients.

CHAPTER THREE

METHOD OF SOLUTION AND FINITE DIFFERENCE FORMULATION

3.1 The Choice, Accuracy and Stability of the Chosen Solution Method

The partial differential terms in the energy and momentum equations are approximated by finite difference relationships employing the following solution scheme.

i) First order forward difference for temporal transient terms (truncation error $O[\Delta t]$)

ii) First order windward difference for spatial convective terms (truncation error $O[\Delta y]$)

iii) Second order central difference for spatial conductive terms (truncation error $O[\Delta y]$ and $O[\Delta x]$)

Young (15) has shown that unless small time steps Δt and small node dimensions Δy are used, considerable errors can be introduced by the windward differencing scheme due to artificial diffusion. Replacing the convective terms in the main equation by a second order, central differencing rather than a first order accurate windward differencing scheme would at first sight appear advantageous. However such a scheme does not prevent artificial diffusion and indeed introduces oscillations in the solution if the ratio v/α' (velocity/thermal diffusivity) is greater than 100. For a typical thermosyphon solar energy water heater, $v/\alpha' \simeq 150$ and consequently, oscillations could be expected. Artificial diffusion can be eliminated by employing an explicit scheme which is accurate to second order in time and space. However, this would only produce a stable solution when the cell Reynolds number ($Re_{CELL} = v\,\Delta x/\alpha'$) is less than or equal to 2. For the dimensions and operating conditions of the particular collector and tank system to which the derived simulation model is currently applied, this particular restraint would not prove impractical, but may be limiting when alternative system geometries and operating conditions are considered.

An implicit method of solution was employed in which J equations are set up for J nodes. The simultaneous equations were solved using a

Gauss-Seidel iterative method in order to find $(T_{j,k})^{t+1}$ for each node. Using such a method, the solution is unconditionally stable (see appendix A) and the only limit on the size of the time step employed is the required accuracy of the solution.

3.2 The Energy and Momentum Equations in Finite-Difference Form

3.2.1 The collector

Substituting finite-difference approximations into the differential equations and associated boundary conditions derived in the previous section gives the following.

For the collector plate, equation 2.5 becomes

$$(T_{j,k})^{t+1} = [(T_{j,k})^{t} + a_1(T_{j+1,k} + T_{j-1,k})^{t+1} + a_2(T_{j,k+1} + T_{j,k-1})^{t+1} + a_3 T_g + a_4 T_a + a_5]/[1 + 2a_1 + 2a_2 + a_3 + a_4] \qquad \text{equation 3.1}$$

where

$$a_1 = \frac{k_f \Delta t}{(\rho C)_f \Delta x^2}$$

$$a_2 = \frac{k_f \Delta t}{(\rho C)_f \Delta y^2}$$

$$a_3 = [\Delta t/(\rho C \delta)_f][h_{f,g} + \frac{\sigma (T_g^2 + T_{j,k}^2)^t (T_g + T_{k,j})^t}{1/\varepsilon_f + 1/\varepsilon_g - 1}]$$

$$a_4 = \frac{U_{f,a} \Delta t}{(\rho C \delta)_f}$$

$$a_5 = \frac{(\tau\alpha)_e I \Delta t}{(\rho C \delta)_f}$$

The finite difference expressions resulting from the boundary condition

given by equations 2.6 and the two boundary conditions implicit in equation 2.7 are, respectively

$$(T_{jmax+1,k})^{t+1} = (T_{jmax-1,k})^{t+1}$$

equation 3.2

$$(T_{j,kmin-1})^{t+1} = (T_{j,kmin+1})^{t+1}$$

equation 3.3

$$(T_{j,kmax+1})^{t+1} = (Tj,kmax-1)^{t+1}$$

equation 3.4

and for the base of the fin in contact with the riser pipe, the boundary condition given by equation 2.8 becomes,

$$(T_{jmin-1,k})^{t+1} = \frac{(T_{jmin,k} + a_6 T_{w,k})^{t+1}}{(1 + a_6)}$$

equation 3.5

where

$$a_6 = \frac{h_{f,w}\pi D_r \Delta x}{4(k\delta)_f}$$

The fluid temperature within the collector riser pipes from equation 2.9 is

$$(T_k)^{t+1} = \frac{(T_k)^t + a_7(T_{f,k})^{t+1} + a_8(T_{k-k'})^{t+1}}{1 + a_7 + a8}$$

equation 3.6

where

$$a_7 = \frac{4h_{w,f}\Delta t}{(\rho C)_w D_r}$$

$$a_8 = \frac{4\dot{m}_c \Delta t}{ND_r{}^2\pi\rho_w \Delta y}$$

$k' = 1$ for $\dot{m}_c > 0$ (ie. forward circulation)

$k' = -1$ for $\dot{m}_c < 0$ (reverse circulation)

and from equation 2.10 for the glass collector cover,

$$(T_g)^{t+1} = \frac{(T_g)^t + a_9(T_f)^{t+1} + a_{10}(T_f)^{t+1} + a_{11}T_a + a_{12}T_{sky}}{1 + a_9 + a_{10} + a_{11} + a_{12}}$$

equation 3.7

where

$$a_9 = \frac{\Delta t h_{g,f}}{(\rho \delta C)_f}$$

$$a_{10} = \frac{\Delta t \sigma (\bar{T}_f^2 + T_g^2)^t (\bar{T}_f + T_g)^t}{(\rho \delta C)_g}$$

$$a_{11} = \frac{h_{wind} \Delta t}{(\rho \delta C)_g}$$

$$a_{12} = \frac{\sigma \varepsilon_g \Delta t (T_{sky}^2 + T_g^2)^t (T_{sky} + T_g)^t}{(\rho \delta C)_g}$$

For the collector header pipes, rearanging equation 2.12 gives

$$(T_n)^{t+1} = \frac{(T_n)^t + na_{13}(T_{n+1})^{t+1} + (n-1)a_{13}(T_{n-1})^{t+1} + a_{13}(T_o)^{t+1}}{1 + na_{13} + (n-1)a_{13} + a_{13}}$$

equation 3.8

where

$$a_{13} = \frac{4|\dot{m}_c|\Delta t}{W_f \rho_w \pi D_h^2}$$

During forward circulation equation 3.8 represents the fluid

temperature in the upper header pipes. The temperature in the lower header pipes is assumed to take on that of the outlet temperature from the downcomer. Conversely, during reverse circulation when fluid is being discharged from the risers into the lower header pipes, equation 3.8 is used to represent the temperatures in the lower header pipes. The upper header pipes are then assumed to be at the temperature of the fluid flowing from the upriser.

3.2.2 The connecting pipework

The temperature of a node within the fluid contained in the upriser or downcomer is given (from equation 2.16) as

$$(T_k)^{t+1} = \frac{(T_k)^t + a_{15}(T_{k-k'})^{t+1} + a_{16}T_a}{1 + a_{15} + a_{16}}$$

equation 3.9

with

$$a_{14} = \frac{4\Delta t}{\rho_w D_p^2}$$

$$a_{15} = \frac{a_{14}|\dot{m}_p|}{\pi \Delta y}$$

$$a_{16} = \frac{a_{14}U_p, a^{D_p}}{C_w}$$

with $k' = 1$ for $\dot{m}_p > 0$

and $k' = -1$ for $\dot{m}_p < 0$

3.2.3 The storage tank

Equation 2.13 for the bulk of the water in the storage tank becomes

$$(T_k)^{t+1} = \frac{(T_k)^t + a_{18}(T_{k-k'})^{t+1} + a_{19}(T_{k-1} + T_{k+1})^{t+1} + a_{20}T_a}{1 + a_{18} + 2a_{19} + a_{20}}$$

equation 3.10

where

$k' = 1$ when $\dot{m}_s > 0$

$k' = -1$ when $\dot{m}_s < 0$

and

$$a_{17} = \frac{\Delta t}{(\rho C)_w A_s}$$

$$a_{18} = \frac{a_{17} |\dot{m}|_s C_w}{\Delta y}$$

$$a_{19} = \frac{a_{17} k_w A_s}{\Delta y^2}$$

$$a_{20} = a_{17} U_{w,a} P_s$$

The boundary conditions to equation 3.10 are, from equations 2.14 for the node at the top of the store (ie. k = kmin)

$$(T_{kmin-1})^{t+1} = (T_{st})^{t+1}$$

where

$$(T_{st})^{t+1} = \frac{(T_{kmin})^{t+1} + (U_{st,a} \Delta y / k_w) T_a}{1 + (U_{st,a} \Delta y / k_w)}$$

equation 3.11

and for the node in contact with the store base, (ie. k = kmax)

$$(T_{kmax+1})^{t+1} = (T_{sb})^{t+1}$$

with

$$(T_{sb})^{t+1} = \frac{(T_{kmax})^{t+1} + (U_{sb,a}\Delta y/k_w)T_a}{1 + (U_{sb,a}\Delta y/k_w)}$$

equation 3.12

For the k th node immediately above the plane representing the boundary condition at the inlet to the store from the upriser (also corresponding to the water draw-off point),

$$(T_{k+1})^{t+1} = (T_{in})^{t+1}$$

where,

$$(T_{in})^{t+1} = \frac{[(T_{k+1})^{t+1}/\Delta y + (T_k)^{t+1}/\Delta y + C_w(\dot{m}_c(T_{kmin-1})^{t+1} + \dot{m}_L(T_{k+1})^{t+1})/(k_w A_s)]}{[2/\Delta y + C_w(\dot{m}_c + \dot{m}_L)/(k_w A_s)]}$$

equation 3.13

Similarly the equation for the boundary condition of the k th node immediately above the plane of the store outlet and replenishing water inlet is given by,

$$(T_{k+1})^{t+1} = (T_o)^{t+1}$$

where,

$$(T_o)^{t+1} = \frac{[(T_{k+1})^{t+1}/\Delta y + (T_k)^{t+1}/\Delta y + C_w(\dot{m}_c(T_{kmax+1})^{t+1} + \dot{m}_L(T_m)^{t+1})/(k_w A_s)]}{[2/\Delta y + C_w(\dot{m}_c + \dot{m}_L)/k_w A_s)]}$$

equation 3.14

The subscripts kmin-1 and kmax+1 in equations 3.13 and 3.14 refer respectively, to the nodes immediately preceeding and following the first and last node in the finite difference matrix representing the storage tank. In effect $(T_{kmin-1})^{t+1}$ and $(T_{kmax+1})^{t+1}$ represent the node temperatures of water within the upriser and downcomer pipes at the inlet and outlet to the store, respectively.

For the nodes representing sections of water in the store in which there is no through flow ie. above the plane defined by equation 3.13 and below that of equation 3.14, the term a_{18} in equation 3.10 is set

to zero.

3.2.4 The total mass flow-rate through the collector

The final equation required (from equation 2.21) in order to determine the mass flow rate is given in finite difference form as

$$(\dot{m}_c)^{t+1} = \frac{a_{22} + a_{21}(\dot{m}_c)^t}{a_{21} + a_{23}\,(\dot{m}_c)^{t+1}}$$

equation 3.15

where

$$a_{21} = [(L_r/A_r) + (L_u/A_p) + (L_s/A_s) + (L_d/A_d)]/\Delta t$$

$$a_{22} = \sum[\rho_k g \sin(\theta_k)\Delta y]$$

$$a_{23} = \frac{[(fL)_r + (fL)_u + (fL)_d]/2}{(\rho_w DA^2)_r N \quad (\rho_w DA^2)_p \quad (\rho_w DA^2)_p} + \sum p_M$$

The finite difference formulations (represented by equations 3.1 to 3.15) of the main energy and momentum transfer processes and the associated boundary conditions were solved using a program written in FORTRAN 77 and run on a Digital TU80 VAX 11/750 main-frame computer at the School of Mechanical Engineering, Cranfield Institute of Technology. A flow diagram of the main program is given in appendix I.

CHAPTER FOUR

EXPERIMENTAL APPARATUS AND INSTRUMENTATION

4.1 The Thermosyphon Hot Water System

An indoor facility for the control and detailed monitoring of a thermosyphon solar-energy water-heater has been constructed. The basic system (shown in figure 4.1) consisted of a non-irradiated collector connected by insulated upriser and downcomer pipes to a well insulated storage tank. Energy normally absorbed by an irradiated solar collector was supplied by heater mats bonded to the back surface of the absorber plates. Both control of the power supplied to the heaters and monitoring of the system performance were carried out by a microcomputer interfacing with suitable peripheral devices.

The collector employed in the system was a comercially-produced model manufactured and supplied by Gull Air Ltd. and had an effective aperture area of 1.936 m^2 More complete construction details and basic physical data for the collector (28) are supplied in appendix C. Two 2m x 1m x 0.0007m Flexel Thermomat flexible mat heaters (supplied by Jimi-Heat Ltd., Watford. Herts.) each with a specified power density of 930 Wm^{-2} at 240V and with a maximum operating temperature of 100^{o}C, were stuck, as shown in figure 4.1, to the reverse surface of the collector absorber plate. The heater mats were electrically conducting flexible sheet material consisting of a glass cloth substrate coated with a uniform layer of conducting polymer to which electrode strips had been attached; the whole is encapsulated in a transparent insulating envelope. The heaters were bonded to the absorber by covering the plate with 0.05m double sided heat resistant adhesive tape supplied by Advance Tapes (U.K.) Ltd., Leicester. Figure 4.2 shows the heaters in place on the absorber plate before being re-installed in the glass-fibre collector box.

Initially, heater mats were installed that would permit a higher power density and maximum operating temperature of 1200Wm^{-2} and 150^{o}C respectively. The heaters were fabricated from a flexible polymer on a glass cloth substrate but a loosly-fitting Nomex envelope was used to electrically insulate the element. The heater mats in this form were found to produce an unacceptably high thermal contact resistance between the elements and plate. This phenomenon was made manifest by the high response time and low steady-state efficiency observed for the

FIGURE 4.1

The experimental rig

FIGURE 4.2

The flexible electrical heater mats bonded to the reverse suface of the collector absorber plate

collector. The poor thermal performances of these heaters were due to:

i) the lack of flexibility of the Nomex envelope giving uneven adhesion to the plate surface, and

ii) the lack of any form of bonding between the elements and the inside of the Nomex envelope surface.

To improve the thermal contact, the Nomex envelopes were replaced by repeated coatings of anti-tracking varnish (supplied by R.S. Components, U.K.) applied directly on to the heating elements. This provided a layer of insulant with a breakdown voltage of 73 MVm^{-1} capable of withstanding temperatures of upto 130°C. When cured, the coated elements were then bonded to the reverse surface of the absorber using the adhesive properties of a further layer of varnish applied to the plate itself. The varnish, however, was found to have insufficient mechanical integrity and was repeatedly punctured by imperfections (such as seams and brazed joints) in the copper absorber plate, thereby causing leakages of current to earth. These heaters were therefore abandoned in preference to the lower powered, lower temperature, but more robust and efficient Flexel Thermomat heaters described at the beginning of this section.

The downcomer and upriser were formed from sections of 0.0254 m internal diameter copper pipe insulated with 0.007 m thick Armour Flex foamed plastic sleeving. All bends, tee sections and reductions in the pipework were soft-soldered to reduce the frictional resistance to fluid flow.

The storage tank detailed in appendix C was a 0.49 m diameter cylindrical copper vessel with a capacity of approximately 0.111 m^3. The base of the storage tank was internally-domed to provide rigidity. The base and walls were insulated by mounting the store on a 0.07 m thick disc of expanded polystyrene and encapsulating the whole in a 0.63 m diameter aluminium cylinder, the annular cavity formed between the two cylinders being filled with granular vermiculite. Holes were bored in the wall of the outer cylinder for the inlet and outlet pipes to the store, all such pipes being fitted with nylon collars to prevent

thermal short-circuiting between the pipes and the aluminium cylinder and leakage of the vermiculite grains. The store top was insulated with a further 0.07 m thick expanded polystyrene disc. Water draw-offs were made via a pipe positioned opposite the upriser inlet at a distance of 0.101 m from the top of the store. Water drawn off is replenished from an adjacently-mounted constant head tank via a pipe positioned opposite the outlet to the downcomer at a distance of 0.099 m from the base of the store. The positioning of the upriser and cold water replenishing pipes was at the minimum distance from the base to prevent disruption of flow (and therefore of the thermocline) by the internally-domed structure of the store base. The constant-head tank maintained the water level at a depth of 0.026 m from the top of the unpressurised store. The very low pressure head differential between the water in the store and that in the constant head tank was intended to be such that the velocity of the replenishing water entering the store was not high enough to have a significantly disruptive effect on thermal stratification.

Air was blown across the glass collector cover to ensure that the heat-loss to the ambient was predominantly due to forced rather than buoyancy-driven convection as will be the case when the collector is in a normal outside environment. This was achieved using a 500 W vertically-mounted fan positioned at one end of the collector. The air from the fan was directioned to give an air-flow across the width, and in the plane of, the collector. A further two smaller 25 W fans were installed to give a constant velocity up the length of the collector. Measurements of the air velocity using a hot-wire anemometer indicated that after an initial rapid fall-off in the velocity at the leading edge, the velocity remained constant at 1.1 ms^{-1} for the remaining width of the collector. The measured air velocity profile across the width of the collector at a height of 0.22 m above the collector (the height at which the velocity was found to be a maximum) is shown in figure 4.3.

FIGURE 4.3

Measured air velocity profile across the width of the collector

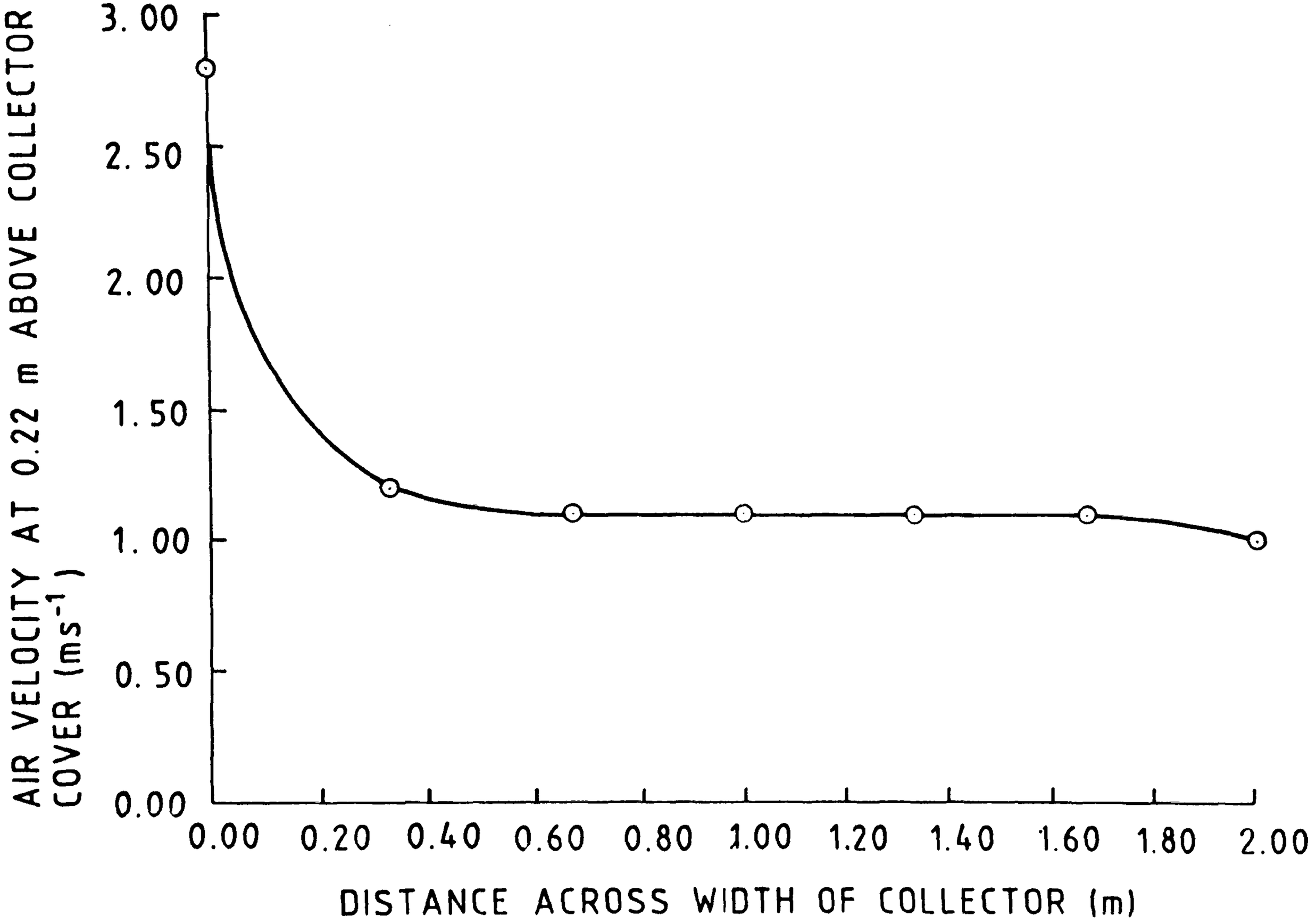
AIR VELOCITY AT 0.22 m ABOVE COLLECTOR COVER (ms^{-1})
3.00
2.50
2.00
1.50
1.00
0.50
0.00
0.00
0.20
0.40
0.60
0.80
1.00
1.20
1.40
1.60
1.80
2.00
DISTANCE ACROSS WIDTH OF COLLECTOR (m)

4.2 The Data Acquisition and Control System

The data logging was accomplished by a modular system (shown schematicaly in figure 4.4). This consisted of a microcomputer, visual display unit, disc drive, a specialist instrumentation peripheral and an IEEE-488 interface.

A BBC Model B microcomputer was used in conjunction with a multi-application peripheral system (M.A.P.S) manufactured by Harlyn Automation Ltd., Congleton. The two MAPS type R6B main-frames accomodate up to six plug-in modules each, of which four were utilised, the remaining eight being allocated to other users. The four modules comprised two type 3700-10a ten channel four-pole scanner modules, a type 3700-11 four-range bipolar analogue-to-digital converter (A.D.C), and a three channel type 3700-09 digital-to-analogue converter (D.A.C).

The scanner modules were programmed by transmitting, from the microcomputer, a sequence of ASCII command strings via the IEEE interface to the M.A.P.S. mainframe. When a sensor was being read, a series of three basic command strings were transmitted causing the following sequence of events to take place:

1. The appropriate analogue input pair was selected and switched onto the A.D.C. for measurement.

2. The A.D.C. range was set and a measurement taken after an internal delay (set nominally at 120 mS) had timed out. This delay permitted the input amplifiers to settle when range changing has occurred.

3. After a delay greater than the internal delay set in the A.D.C., the reading was requested and outputed by the A.D.C. in the form of a twelve bit, three character ASCII string.

A choice of four settings were available for the A.D.C.. These gave ranges of 10, 1, 0.1, and 0.01 volts.

The D.A.C. control module was programmed using two different ASCII command strings. These were loaded into the register of the appropriate

FIGURE 4.4

Schematic block diagram of hardware used in the monitoring and control of the indoor test rig

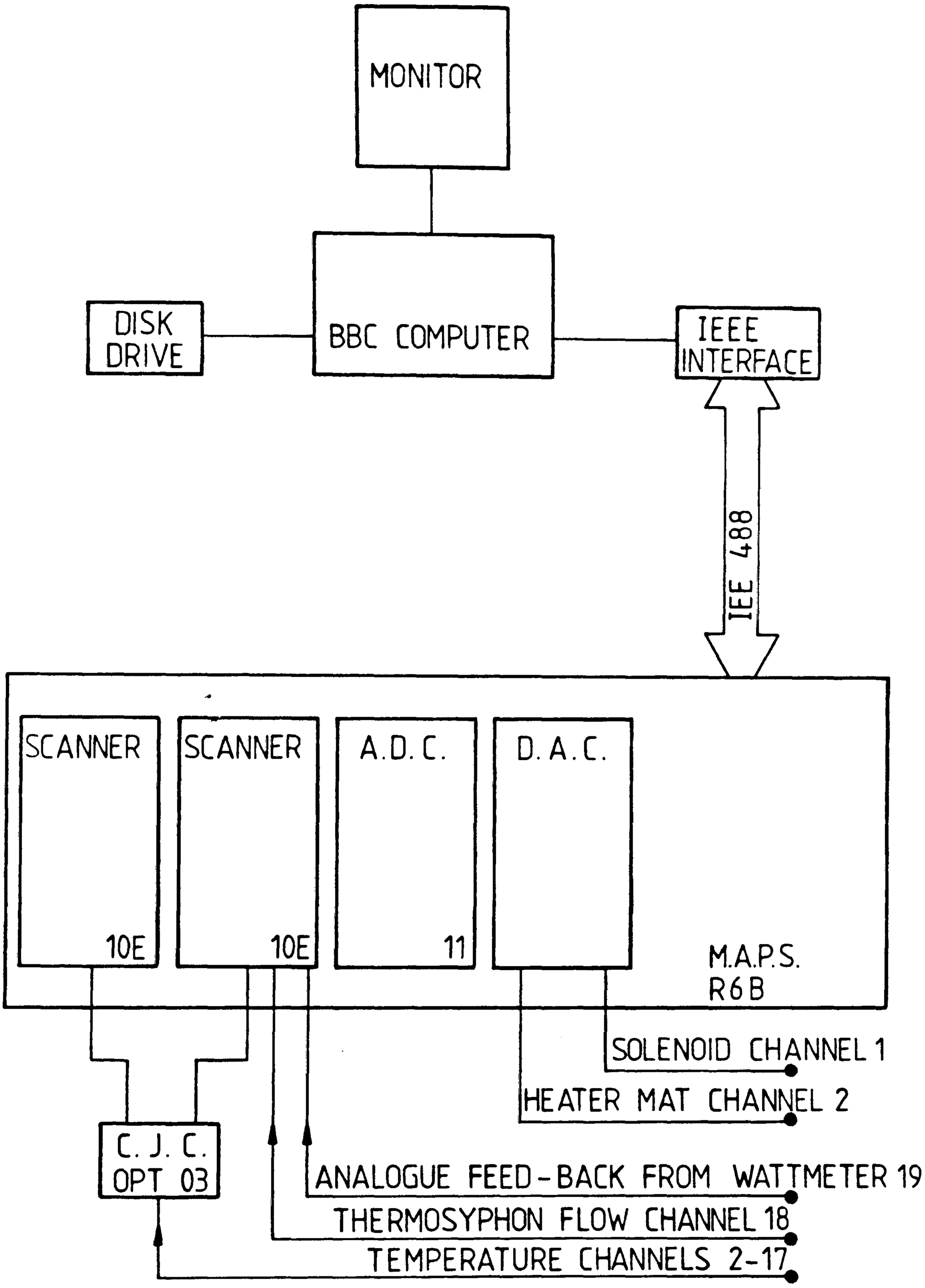
MONITOR
DISK DRIVE
BBC COMPUTER
IEEE INTERFACE
IEE 488
SCANNER
10E
SCANNER
10E
A.D.C.
11
D.A.C.
M.A.P.S.
R6B
SOLENOID CHANNEL 1
HEATER MAT CHANNEL 2
C.J.C.
OPT 03
ANALOGUE FEED-BACK FROM WATTMETER 19
THERMOSYPHON FLOW CHANNEL 18
TEMPERATURE CHANNELS 2-17

control channel (ie. one of the three available in the module) via the IEEE interface. These two strings carried the following information.

i) The relevant data (ie. information on the required analogue output) was expressed in the form of a twelve bit binary number. This was divided up into three four-bit "nibbles" and the ASCII equivalents inserted into a nibble setting string.

ii) The DAC output would only change to a new value when the nibble setting string was followed by the output setting string. This string contains the module code letter and DAC channel number being addressed.

The DAC supplied a control signal beteen 0 and 5 volts. This analogue output was "latched" and remained at the value at which it was set until reset by a further command sent out by the computer. A listing of the control and monitoring program written in BBC/IEEE basic is given in appendix D.

4.3 Instrumentation

4.3.1 Temperature measurement

All temperature measurements were made using 0.0002 m solid core type "T" PTFE covered copper constantan twisted pair thermocouple flex. The sensor junctions were spot welded. The resultant of the two opposing electrical potentials set up by the sensor junction and the junction formed by the copper terminal block and the constantan lead, were then measured. The temperature in the near vicinity of the terminal block was determined using a cold junction card (CJC) supplied by Harlyn Automation. The CJC was powered by a 12 volt externally-supplied stabilised voltage. The CJC consisted of a PCB supporting a semiconductor based temperature sensor and a pair of twelve way terminal strips, two terminals of which were connected up for measurement of the semiconductor output potential. The semiconductor was calibrated to give a reference output potential the value of which, when measured in volts was one tenth (1/10) of the temperature in degrees centigrade. The equivalent potential (E_{CJC}) set up by the copper constantan junction at the terminal block was then calculated

from the empirically determined correlation (31) given in equation 4.1

$$E_{CJC}=-2.308x10^{-6}+T_{CJC}[3.8616x10^{-5}+T_{CJC}(4.4503x10^{-8}-T_{CJC}2.041x10^{-11})]$$

equation 4.1

The value of E_{CJC} is then subtracted from E_{tot}, the total potential measured, to give E_T,the actual potential across the thermocouple sensor junction. E_T was then converted to a temperature (in degrees centigrade) using the correlation represented by equation 4.2.

$$T=-0.104797+E_T[25.945x10^{-3}+E_T(-6.895x10^{-5}+E_T2.3512x10^{7})]$$

equation 4.2

Equations 4.1 and 4.2 are included in the monitoring software and cold junction compensation is carried out prior to a temperature value being recorded on magnetic disk.

The CJC was mounted in an aluminium alloy diecast box together with a further two independently-mounted ten-way terminal strips. By keeping the dimensions to a minimum, isothermal conditions could be assumed within the box and for the purposes of cold junction compensation, all the terminal strips would be at the same temperature as that recorded by the semiconductor sensor.

The temperature measurement points are given in table 4.1. All fluid temperatures were taken by immersing the thermocouples directly in the fluid. In the cases of the storage tank temperatures, the thermocouples were mounted on a length of 0.0075 m diameter "Tefflon" dowel. Fluid temperatures taken in pipe sections were set in "Binda" plugs using an epoxy resin glue. The thermocouples protruded into the fluid in the pipes. The ambient temperature was taken as room temperature measured at a height equivalent to the mean height of the collector. This thermocouple was mounted in a ventilated container to eliminate radiation effects. The thermocouple measuring the room surface temperature was embedded 0.002 m into an area of the ceiling "seen" by the upwardly-inclined collector. Repeated consecutive measurements were recorded for a thermocouple in a steady-state isothermal environment of

Table 4.1: Allocation of channels

MODULE, CHANNEL	READING
C,0	cold junction reference temperature
C,1	zero off-set
C,2	T1,store base temperature
C,3	T2
C,4	T3 intermediate
C,5	T4 store
C,6	T5 temperatures
C,7	T6
C,8	T7
C,9	T8,store top temperature
D,0	collector inlet temperature
D,1	collector outlet temperature
D,2	upriser temperature (first bend)
D,3	upriser temperature (store inlet)
D,4	mains temperature
D,5	ambient temperature
D,6	wall surface temperature
D,7	wattmeter analogue output voltage
D,8	flow meter
D,9	draw-off water temperature

known temperature (in this case taken as the constant head tank). By this means the combined uncertainty of thermocouple readings taken via the A.D.C. and cold junction card was estimated as $\pm$ 0.3 C.

4.3.2 Mass flow measurement

The velocity flow rate was measured using a non-invasive Eckardt type 514 Inductive flow meter (32) with a 0.025 m diameter bore. The flow meter consisted of a transmitter and a converter which existed as separate devices and were connected to one another by electrically-screened cables to form a functional unit. As fluid flowed through the transmitter, a voltage was induced and was tapped off by electrodes which were insulated against the meter tube. The induced voltage was proportional to the mean velocity and largely independant of flow profile. Precautions did however have to be taken to avoid excessively unstable flow. Steadying sections of at least three and two times the internal diameter of the pipe upstream and downstream respectively were fitted between the nearest pipe bend or fitting and the transmitter. In addition, the transmitter was installed between the collector inlet and the storage tank outlet, the section of pipe in which there was a minimum difference between the fluid and ambient temperatures. This ensured minimum distortion of the flow profile by thermal destabilisation. The transmitter was mounted in a vertical section of the downcomer to avoid air locks and the accumulation of sediment within the meter. The installed meter is shown in figure 4.5.

The converter supplied a load-independent DC current of 4 to 20 mA. The current was converted to a voltage output for measurement by the ADC by connecting two 1000 ohm resistors in parallel across the converter output. The combined resistance of 500 ohms gave an analogue voltage output of 2 to 10 V.

Although factory calibrated, the flow meter was being operated at the lower end of the manufacturers specified range. A check was therefore made on the indicated flow rate (see appendix E). By this means, the fluid velocity through the meter was determined and found to differ from the value measured by the flow meter. By multiplying all velocity flow rate readings from the converter by appropriate factors, agreement

FIGURE 4.5

The installed inductive flow meter

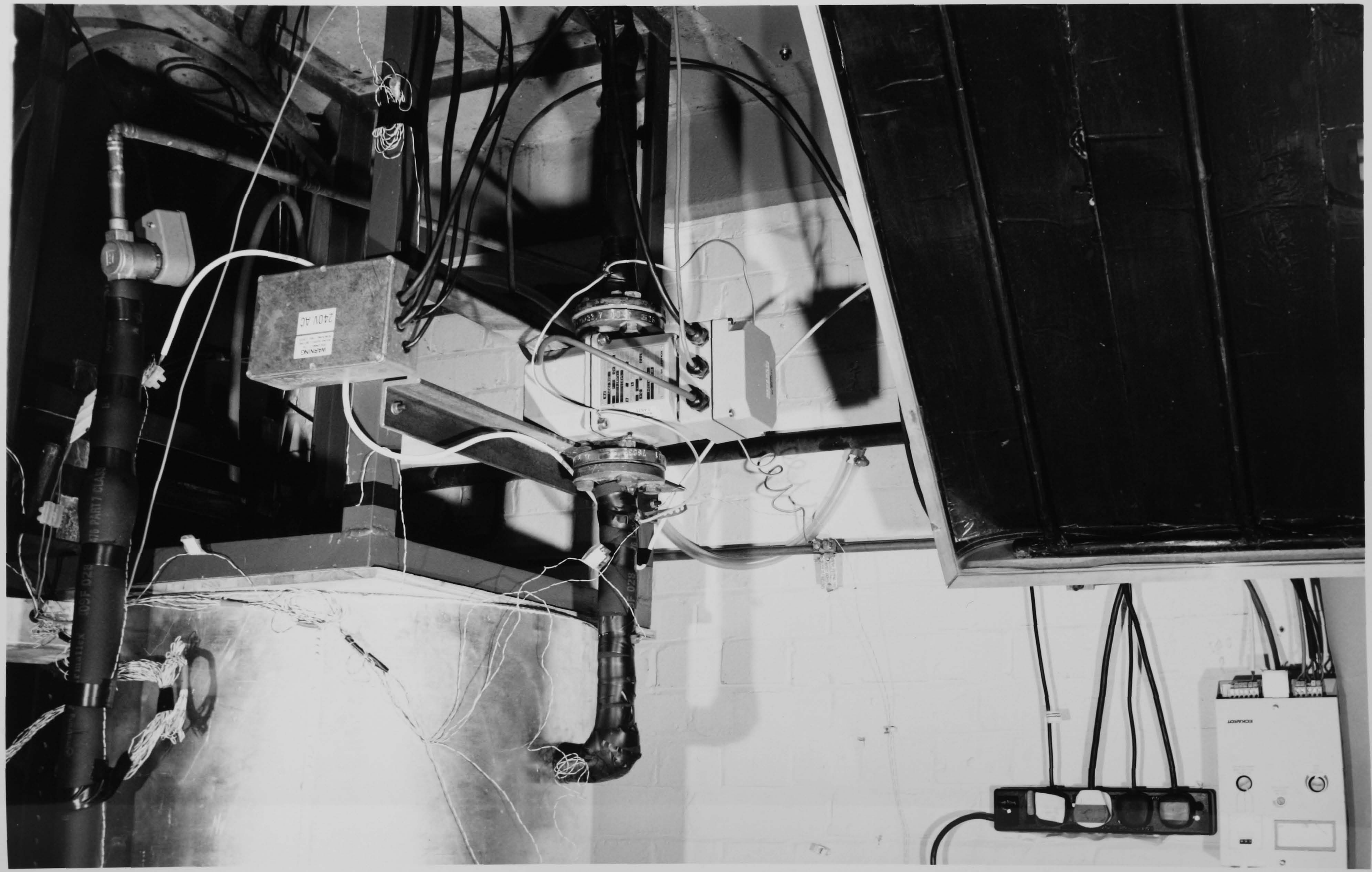
240V AC

FIGURE 4.6

Schematic of circuitry used in the control of the power supply to the elecrical heater mats and solenoid valve

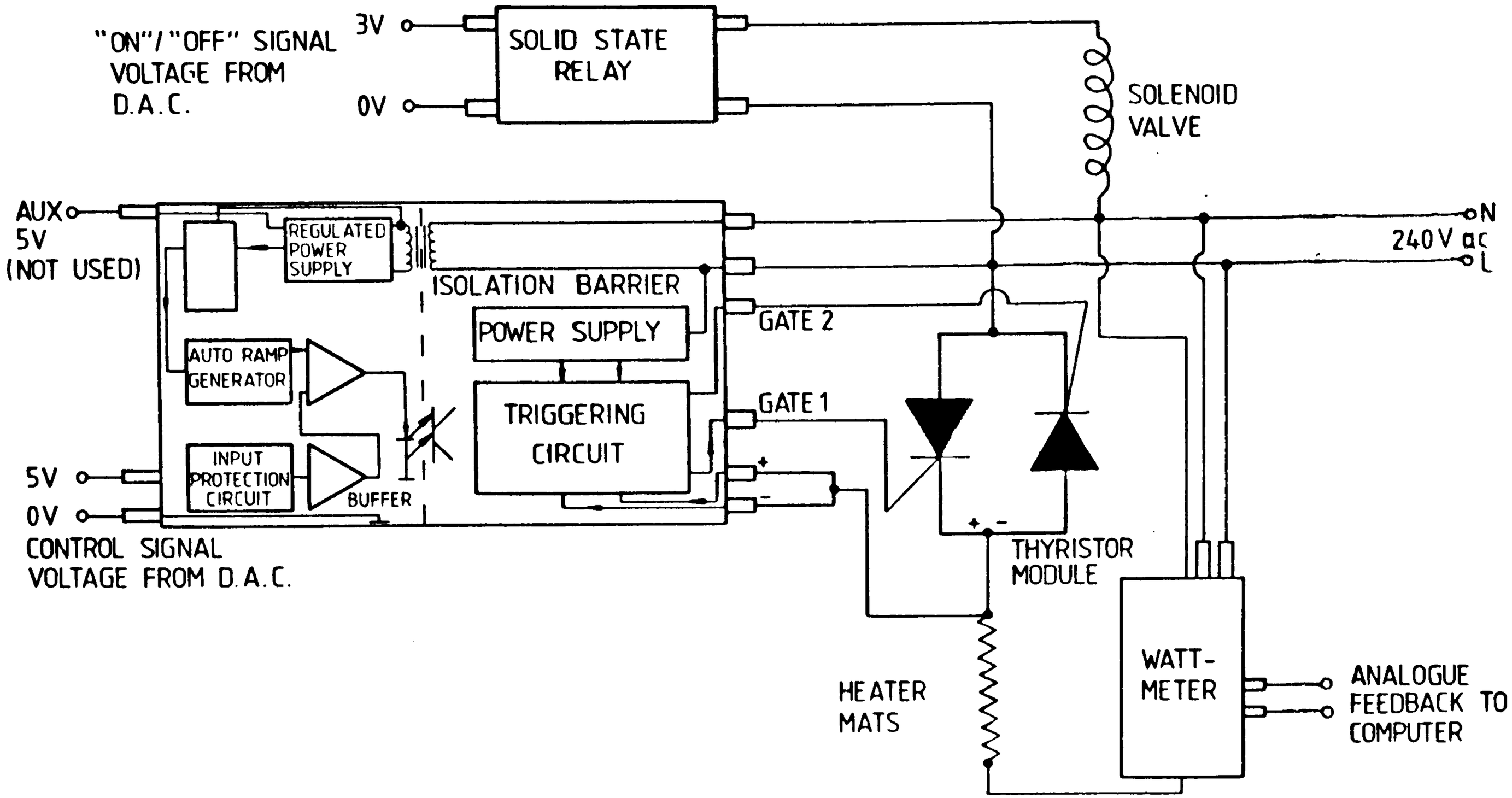
"ON"/"OFF" SIGNAL VOLTAGE FROM D.A.C.
3V
0V
SOLID STATE RELAY
SOLENOID VALVE
AUX 5V (NOT USED)
REGULATED POWER SUPPLY
ISOLATION BARRIER
POWER SUPPLY
AUTO RAMP GENERATOR
INPUT PROTECTION CIRCUIT
BUFFER
TRIGGERING CIRCUIT
GATE 2
GATE 1
N
240 V ac
L
5V
0V
CONTROL SIGNAL VOLTAGE FROM D.A.C.
THYRISTOR MODULE
HEATER MATS
WATT-METER
ANALOGUE FEEDBACK TO COMPUTER

to within an estimated $\pm$ 0.2×10^{-3} kgs^{-1} of the directly measured values were achieved in the range 0 to 6×10^{-2} kgs^{-1}.

Very low flow rates are encountered in thermosyphon systems giving correspondingly low signal outputs from the flow meter transmitter. The change in path length between the electrodes caused by the deposition of sediment can therefore cause significant drift of the zero point setting and a reduction in the accuracy of the flow reading. An attempt was made to remedy this situation by reducing the area of the electrodes in contact with the fluid thereby reducing the possible variation in path length. A 0.0005 m wide strip of tape was placed over the electrodes at right angles to the direction of flow. A layer of "nail lacquer" was painted on the electrodes and allowed to set after which the tape was removed leaving a reduced area of electrode exposed to the fluid. This procedure was found not to significantly improve the performance of the meter and the lacquer was subsequently removed. The problem of sediment on the electrodes means that the zero point had to be frequently re-set and tests repeated when deposition becomes apparent.

After measuring the voltage output across the resistances, the velocity flow rate was converted by the microcomputer into a mass flow rate and recorded on magnetic disk. The instantaneous temperature of the fluid flowing through the transmitter was measured at a point three diameters upstream (to avoid affecting the flow profile). With the temperature dependant correlation given in the procedure PROCflow (see appendix D), the density of the fluid stream was determined and used in calculating the mass flow rate.

4.4 Control aspects

The control circuitry employed in converting the low voltage (and current) DC output signals from the DAC into 240 V AC outputs is shown schematically in figure 4.6.

4.4.1 Power supply to heaters

The signal voltage from the DAC controlling the power supply to the

heater was converted into a 240 V supply via a RS components phase angle trigger module. The input signal was varied between 0 and 5 V. The power output varies non-linearly with the input and it was therefore necesary to calibrate the response of the phase angle trigger module to an input signal for the particular load across the output. The results of the calibration were analysed using a least squares curve fitting computer software package. A polynomial which adequately described the relationship between the input and output signal could not be found. The data was therefore used directly in the main monitoring and control program and intermediate values determined by linear interpolation. This method alone was found to be insufficiently accurate in determining the power input to the heaters. This was due to two main factors.

i) The impedences and therefore the power outputs of the heaters vary with temperature. This results in a droping off, with time, of the actual power disipated by the heater compared with the required power value. Compensation for this effect based on a simple temperature-impedence relationship was not feasable as the exact temperature of the encapsulated heater element was unknown.

ii) Fluctuations in the mains supply voltage of the order of ±15% were observed. These fluctuations could persist for periods of time (up to 15 minutes) which were comparable to the response time of the collector and thereby cause significant changes to occur in the state of the collector.

A feed-back system was therefore employed. A wattmeter giving an analogue voltage output enabled the actual power being disipated by the heaters to be read, at two minute intervals, by the microcomputer. This value was compared with the required output and by extrapolation methods a correction was made to the power supply. Repeated itterations were performed untill the required and actual values agreed to within ±5% of the measured value. The relationship between the analogue output from the wattmeter and the power measurement was found, from the calibration of the instrument, to be linear. The calibration procedure and results are given in appendix F.

The required power supplied to the mat heaters was calculated from,

$$w = (\tau\alpha)_e A_c I$$

equation 4.3

where $(\tau\alpha)_e$ was the effective transmittance-absorptance product, the value of which was dependent on the simulated angle of the solar radiation incident on the collector cover. A single collector with fixed optical properties was used in the experimental validation of the simulation model. A simplifying correlation was therefore employed relating the experimentally-simulated angle of the incident radiation to the incident angle modifyer coefficient (K_i) defined (23) as

$$K_i = \frac{(\tau\alpha)_e}{(\tau\alpha)_{90^\circ}} = 1 + a[1/\cos(\phi_i) - 1] + b[1/\cos(\phi_i) - 1]^2$$

equation 4.4

The values of a and b were determined semi-empirically for a particular collector. A computer program incorporating the method out lined by Duffie and Beckman (23) and based on the subroutine TORALF (given in appendix I) has been used to generate values of K_i for angles between 0 and 90°. By inputing into the program the optical properties of the collector used in the experimental work, the values of a and b were obtained from a second order least-squares polynomial fit on the values of $[1/\cos(\phi_i) - 1]$ and the generated values of K_i, giving

$(\tau\alpha)_{90^\circ} = 0.88$

$a = 0.05$

and $b = 0.03$

The resulting function is shown graphically in figure 4.7.

4.4.2 Water draw-off

The solenoid valve was operated via a solid state relay supplied by RS Components. A 3 V signal from the DAC activates the relay which in turn operated the 240 V solenoid valve. The relay remained conducting until the DAC analogue output was reset to 0 V.

FIGURE 4.7

Curve representing the calculated angle-dependent incident angle modifier based on the optical properties of the collector

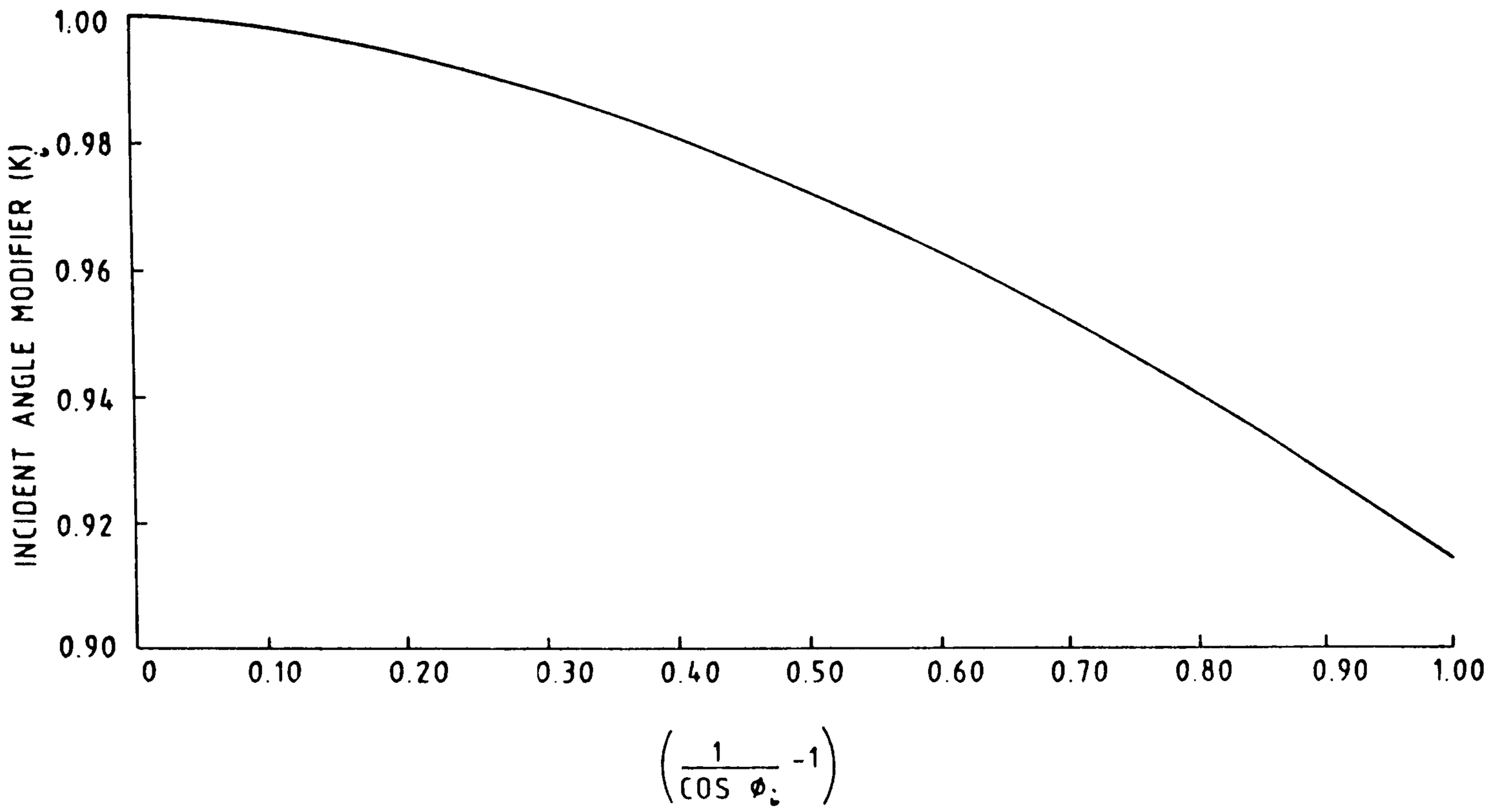

INCIDENT ANGLE MODIFIER CALCULATED FROM OPTICAL PROPERTIES OF COLLECTOR

The mass of water withdrawn from the storage tank was determined by the length of time for which the solenoid valve was permitted to remain open. The relationship between time and water draw-off was determined empirically (see appendix G). A linear relationship was established between time and mass draw-off. Using this linear relationship, the water draw off could be controlled to within + 0.02 kg within a range of draw-offs between 0 and 12 kg.

CHAPTER FIVE

EXPERIMENTAL VALIDATION OF THE STORAGE TANK MODEL USED IN THE SIMULATION

5.1 Modification of the Basic experimental Thermosyphon System to Investigate the Thermal Performances of Individual Components.

A preliminary comparison between the experimental and predicted performance of the thermosyphon water heater indicated the necessity for a more detailed appraisal of the veracity of the predicted temperatures in each of the various components. Because of the interdependance of the temperature and flow rate of the circulating fluid in a buoyancy-driven system, it was decided that a series of component tests under conditions of either constant forced flow or no flow at all would significantly simplify the initial model validation.

Constant forced circulation through the components of the system (represented schematically in figure 5.1) was achieved by connecting the inlet of the collector to the constant pressure head tank mounted adjacent to the storage tank. Water was passed through the collector and upriser into the top of the storage tank and drained away via the flow meter at the base of the tank. The flow through the system was governed by a manually-operated valve fitted at the drain-off end of the circuit.

In the transient testing of the collector, a step input could be supplied electrically to the collector heater mats. However, because of thermal transience in the collector, the temperature of the fluid entering the store in response to the step input of electrical power to the collector heaters can take from 10 to 30 minutes to reach a maximum value. In order, therefore, to achieve a true thermal step input to the store, as was required in the tests described in section 5.3, a three-way valve was installed in the upriser. This enabled heated water to be drained away untill the collector attained thermally steady-state conditions whereupon the flow was redirected into the store. The drain-away pipe from the three-way valve was connected to the drain-away pipe from the base of the store. This had the effect of maintaining a constant pressure drop between the inlet to the three-way valve from the collector and the common drain-away irrespective of whether or not the flow was being directed into the store. The three way valve was positioned a distance of 32 pipe diameters along the

FIGURE 5.1

Schematic diagram of flows through the solar water-heater under conditions of forced flow

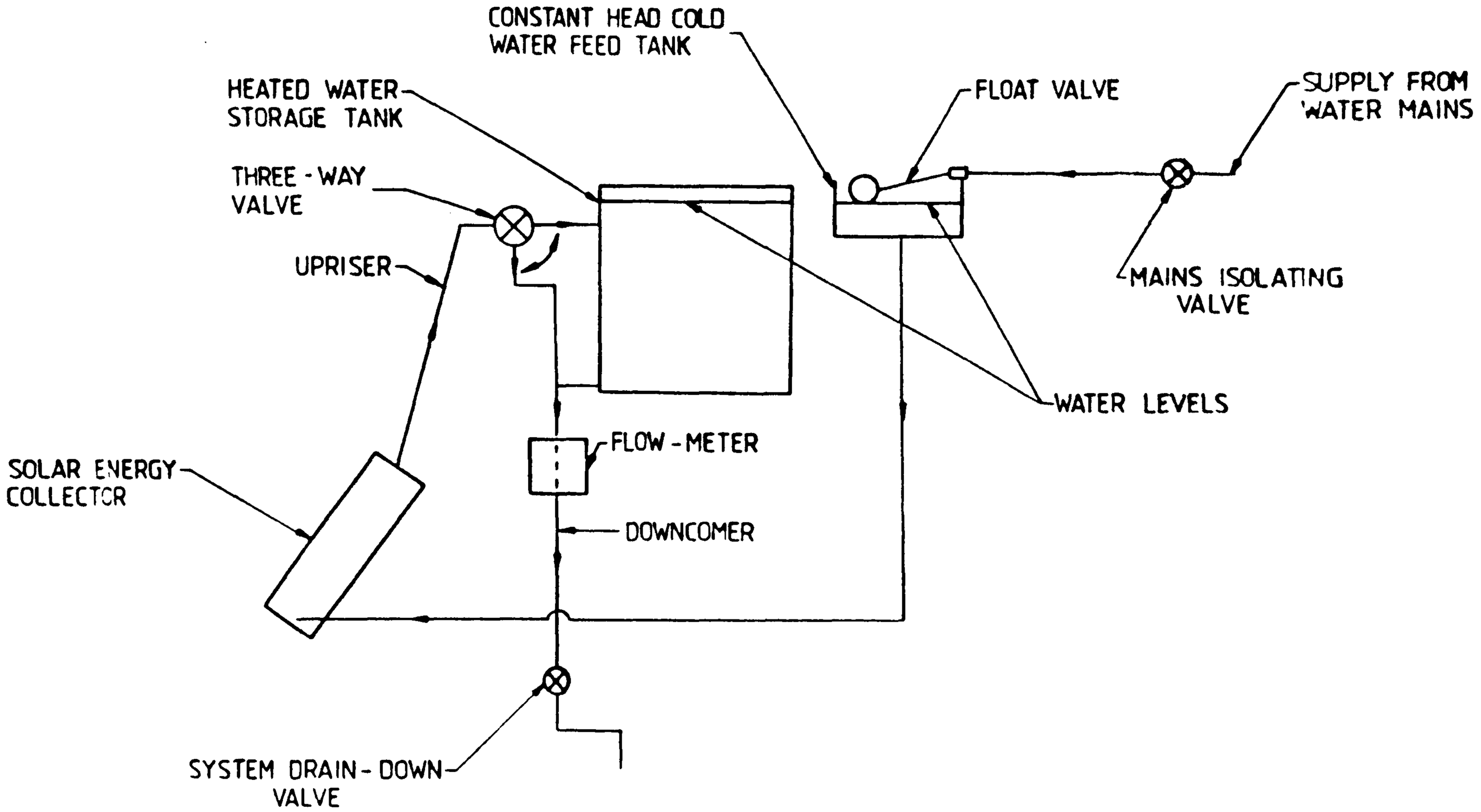
CONSTANT HEAD COLD WATER FEED TANK
HEATED WATER STORAGE TANK
FLOAT VALVE
SUPPLY FROM WATER MAINS
THREE - WAY VALVE
UPRISER
MAINS ISOLATING VALVE
WATER LEVELS
FLOW - METER
SOLAR ENERGY COLLECTOR
DOWNCOMER
SYSTEM DRAIN - DOWN VALVE

upriser from the point of entry into the store. This ensured that any turbulence caused by the passage of water through the valve was reduced by the viscous damping along this section of pipe and fully developed, laminar flow restored before the fluid entered the store.

5.2 Heat Loss from the Fully Mixed Store

The cooling characteristics of a low aspect ratio (ie. height/diameter) store in which there is significant heat loss from the top and base of the store, are dependant on both the overall heat loss coefficient of the store and the degree of thermal stratification. In establishing the suitability of the heat transfer coefficients used in simulating heat loss through the store walls independently of the accuracy with which stratification effects can be predicted, a cooling curve was obtained for the store whilst ensuring fully mixed (initial) conditions.

The initially-cool water was drained off from the base of the store and replaced by hot water from the collector until the mean store temperature reached 21^{o}C above ambient. Subsequent thermal isolation from other components was achieved, as far as this was possible, by shutting off any flow going into or comming out of the store. The water was then stirred manually to eliminate thermal stratification, and the store allowed to cool over a period of 16 hours. During this period, the mean store and ambient temperatures were measured and recorded at 5 minute intervals. Identical initial store temperature and ensuing ambient temperatures were used as inputs to the simulation and the heat loss from the store under no-flow conditions was predicted. Because of the absence of flow and thermal stratification in the store, the minimum of three nodes was used in the finite difference solution scheme (ie. top and base nodes in contact with the end surfaces and a central node representing the main bulk of the water in the store). The time step was 30 s.

For the purposes of comparison, a simple analysis has been used from which the overall rate of heat loss from the store $(UA)_s$ could be established. An energy balance for a fully mixed store in which fluid was neither entering nor leaving can be represented by,

$$M_s C_w \frac{d\bar{T}_s}{dt} = (UA)_s(T_a - \bar{T}_s)$$

equation 5.1

Integrating equation 5.1 gave the time-dependant mean store temperature as,

$$In(\bar{T}_s - T_a) = In(\bar{T}_s^i - T_a) - \frac{(UA)_s \Delta t}{M_s C_w}$$

equation 5.2

Equation 5.2 implies a linear relationship between $In(T_s - T_a)$ and time, t with a gradient of $(UA)_s/(M_s C_w)$. These measured and predicted log-linear values were plotted and the respective $(UA)_s$values were calculated. An experimentally-determined value of $(UA)_s$= $1.54(\pm 0.03) W^oC^{-1}$was obtained from the predominantly linear region of the plot between t = 0 and t = 10 hours in figure 5.2. In deriving heat loss coefficients for the store top, walls and base the insulant around the store was originally assumed to take the form of a simple disk of insulant of the same internal diameter as the store on the top and base, with a cylinder of insulant around the walls of the store which was of the same length as the store height. This simple representation neglected the heat loss through the insulant at the edges between the flat and cylindrical surfaces of the store and gave an overall $(UA)_s$ value of 1.24 W^oC^{-1}. This was rectified by assuming that the cylinder of insulant around the store had an internal length equal to the length of the store and an external length extended beyond both ends of the store, a distance equal to the repective thickness' of insulant on the top and base. This gave an internally-bevelled cylinder. The insulant on the top and base were assumed to "plug" the bevelled ends and were therefore parallel-faced frustrums with the smaller, inner circular, surface having the same diameter as that of the store and the external surface, equal to the outer diameter of the insulating cylinder. An expression was then derived (see appendix H) for the one dimensional heat conduction through these component sections of the store insulation. The resulting modified heat transfer relationships gave an overall $(UA)_s$ value of 1.53 W^oC^{-1}, this value being in agreement to within the experimental uncertainty associated with the measured value.

FIGURE 5.2

Experimental and predicted cooling curve for the store

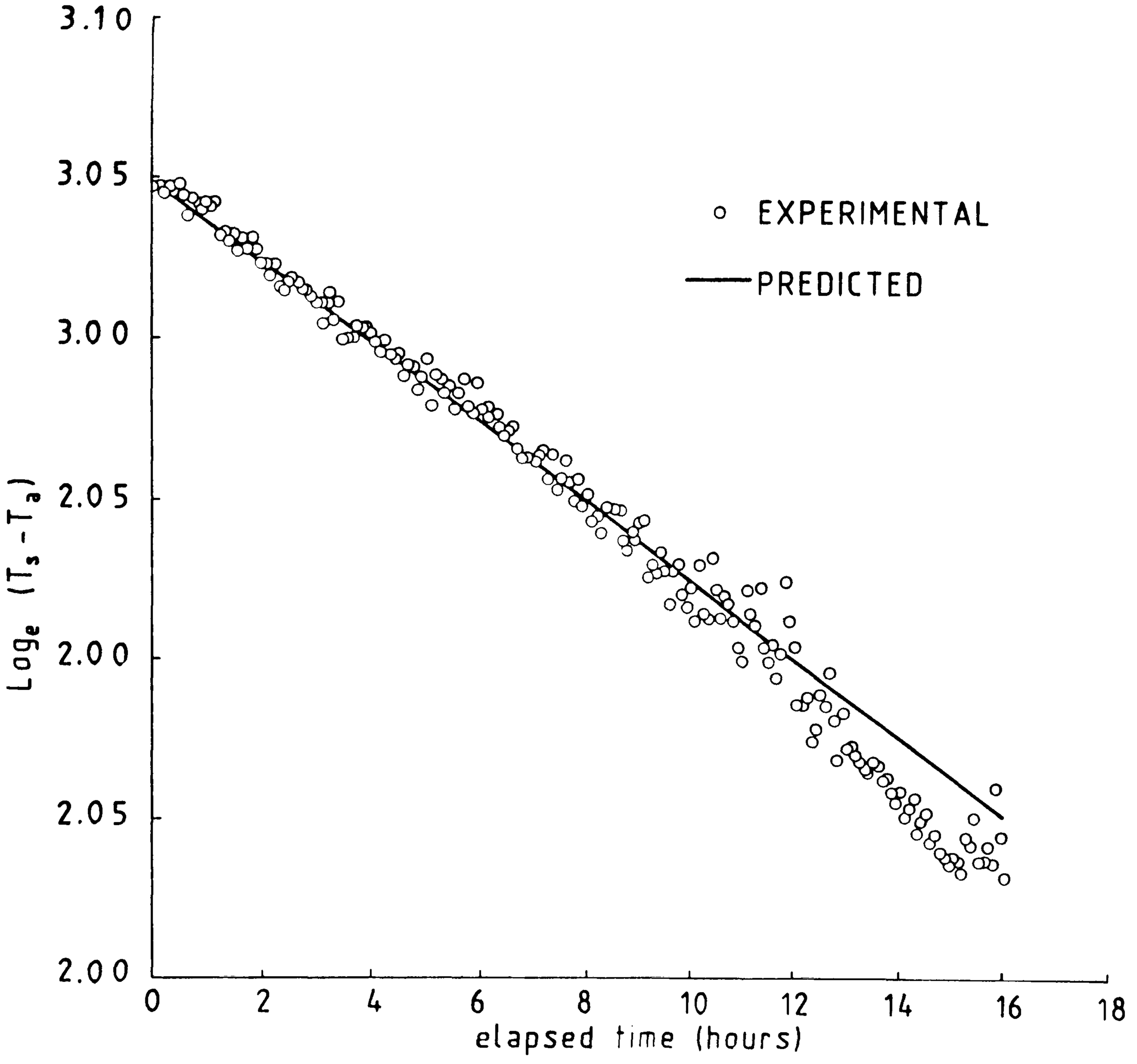
3.10
3.05
3.00
2.05
2.00
2.05
2.00
$Log_e\ (T_s - T_a)$
0
2
4
6
8
10
12
14
16
18
elapsed time (hours)
EXPERIMENTAL
PREDICTED

Any attempt to take into account the additional thermal resistance, between the external surfaces of the store insulant and the ambient, using buoyancy driven convection correlations, resulted in a considerable underestimate of the heat loss processes.

Figure 5.2 indicates an increase in the heat loss from the store after t = 10 hours. This may be due to condensation from the unpressurised store permeating the expanded polystyrene top cover and the surrounding vermiculite granules. Also the fully-mixed store will eventually start to stratify as heat is lost from water in immediate contact with the store walls, this cooler liquid sinking to the base of the store and displacing warmer liquid upwards. The accumulation of the warmer water at the top of the store where heat losses are relatively high, will accelerate the heat-loss processes to a level higher than that for a fully mixed store. The resulting observed non-linearities (after t = 10 hours) were not apparent in the simulated rate of heat loss because of the inaccuracies in predicting thermocline relaxation effects within the store at this stage in the development of the simulation model.

5.3 Energy Distribution within the Store

5.3.1 Development of the thermocline in response to a thermal step input

As part of an initial study, the development, with time, of experimental and measured store temperature profiles in response to a thermal step input at a constant mass flowrate, were compared. The forced flow conditions were achieved using the system described in section 5.1. At the onset of the experiment, the drain-off valve was adjusted to give a measured mass flow rate of aproximately $0.005 kgs^{-1}m^{-2}$. This value was chosen as being representative of a system operating in the thermosyphon mode. The power supplied to the collector heater mats was sufficient to give a heat delivery rate to the store of approximately 1KW. Temperatures were monitored and recorded at 2 minute intervals over a period of 4 hours.

The experimentally-measured flow-rate, store inlet and ambient temperatures were used as inputs to the simulation. The bulk of the

fluid in the store was represented in the simulation by a 100-node grid with an additional two nodes for the sections above and below the inlet and outlet respectively, in which there could be no through-flow. A time step of 5 seconds was used in the simulation.

In this preliminary study, it was assumed that heat transfer between nodes was due solely to buoyancy-induced mixing (where the appropriate conditions occured), mass transport due to the through-flow of water, and axial conduction through the store water. The development of the temperature profiles within the storage tank at 20, 60, 100, and 180 minutes from the start of the test are shown in figure 5.3. There are two main differences between the predicted and observed profiles.

i) The boundary dividing the bulk of the hot water at the top of the store and the cooler layer below is predicted as being more distinct than is actually observed indicating a higher predicted degree of stratification.

ii) Predicted temperatures in the warmer, upper section of the store are higher than the corresponding measured values. The converse is true in the lower cooler section of the store.

These two observations indicate that in addition to conduction through the water, occurring between the hot and cold sections of the store, destratification is increased further by other mechanisms. Two such possible mechanisms are:

i) cooling of water in immediate contact with the wall of the store container causes local recirculation and mixing between stratified layers. In addition, conduction down the wall of the store causes heating of cooler layers of water which further increases local convection currents and consequently decreases the degree of stratification within the store.

ii) Radial momentum is converted to axial momentum by both viscous forces acting on the "jet" of warm water entering the side of the cooler store from the upriser and deflection of this "jet" on reaching

FIGURE 5.3

Experimental and predicted storage tank temperature-height profiles under conditions of forced flow

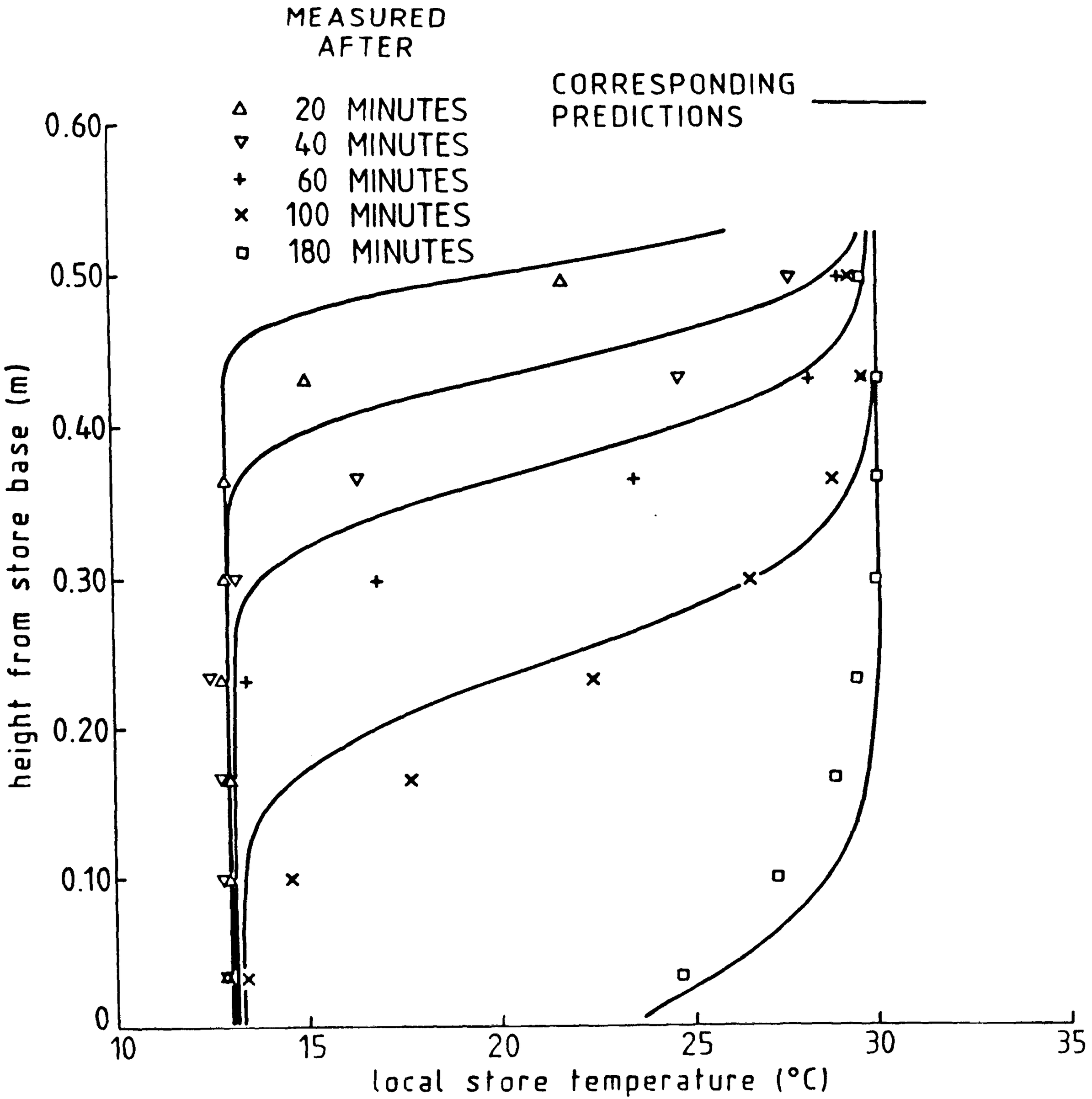
MEASURED
AFTER
20 MINUTES
40 MINUTES
60 MINUTES
100 MINUTES
180 MINUTES
CORRESPONDING
PREDICTIONS
0.60
0.50
0.40
0.30
0.20
0.10
0
height from store base (m)
10
15
20
25
30
35
local store temperature (°C)

the opposite side of the store. The warm jet of water travelling down the store is opposed by a buoyancy force and after initially reaching a certain depth, rises through and subsequently mixes with, the cooler water above it.

Thermal relaxation in the store by whatever mechanism results in an increase in the inlet temperature thereby decreasing the collector efficiency. It was decided therefore to investigate the significance of these two mixing phenomena.

5.3.2 Conduction in the store walls

Heat is always transferred down the store walls in a direction such as to cause a relaxation of the store temperature profile. The degree to which this phenomenon significantly alters the thermocline within the store will depend on, amongst other factors, the thermal conductivity and thickness of the tank wall. In order to separate store relaxation due to axial conduction from that of any mixing effects at the inlet or outlets, an equilization test was carried out under no-flow conditions. This entailed the setting up of a high temperature gradient within the store and comparing the predicted and experimental rate at which heat was redistributed throughout the thermocline. As in section 5.3.1, a thermal step-input was imposed on the store using a low flow-rate for a period of time equal to $t = \Omega/2$. This theoretical charge period, Ω, is defined as $\Omega = M_s/\dot{m}_c$. This resulted in a steep thermocline positioned approximately in the middle region of the store. The root-mean-square (R.M.S) deviations of the temperatures from the mean store temperatures, σ', was used as the index to measure the instantaneous degree of stratification, where

$$\sigma' = \frac{[\sum(T_k - \bar{T}_s)^2]}{kmax}$$

The simulation model was run to investigate three values of the effective conductivity, these being:

i) no axial conduction in the store.

ii) axial conduction through the water alone, and

iii) axial conduction through both the water contained within and the walls of the store using an approximate effective conductivity (33) defined by,

$$k_e = \frac{k_w A_s + k_{sw} A_{sw}}{A_s + A_{sw}}$$

equation 5.3

for $0 \quad \frac{k_{sw} A_{sw}}{k_w A_s} \leq 3$

A grid of 102 nodes was used to simulate the water in the store with a time step of 5s. The initial distribution of temperatures within the finite difference grid was initially set to give an equivalent thermocline to that of the measured temperatures at time t = 0 from the eight axially-positioned thermocouples.

The predicted and measured values of σ' over a period of 16 hours have been plotted in figure 5.4.

For the simulated case of no axial conduction, relaxation of the store thermocline is slight, with a change in the R.M.S. deviation of only 2.7 ^{o}C over the 16 hour test period. This apparent relaxation was due entirely to the higher rate of heat loss from the warmer water at the top of the store rather than any internal redistribution of energy. With axial conduction in the fluid alone, the predicted change in the R.M.S. deviation was 4.7^{o}C representing a 52% error when compared with the corresponding measured value. In the third case in which the simulated effective axial conduction was given by equation 5.3, the R.M.S. deviation of the store temperatures had changed by 10.0^{o}C. This is in close agreement with the experimentally-measured change in the R.M.S. value of 9.9 ($\pm$ 0 .3)^{o}C. The value of $(k_{sw}A_{sw})/(k_w A_s)$ for the copper-walled store was 3.8 and therefore outside the stated range of equation 5.3. However, because of its effectiveness in predicting store thermocline relaxation it was decided to retain equation 5.3 in the analysis.

FIGURE 5.4

Experimental and predicted variation with time of the root mean square of the storage tank temperature variation from the mean value

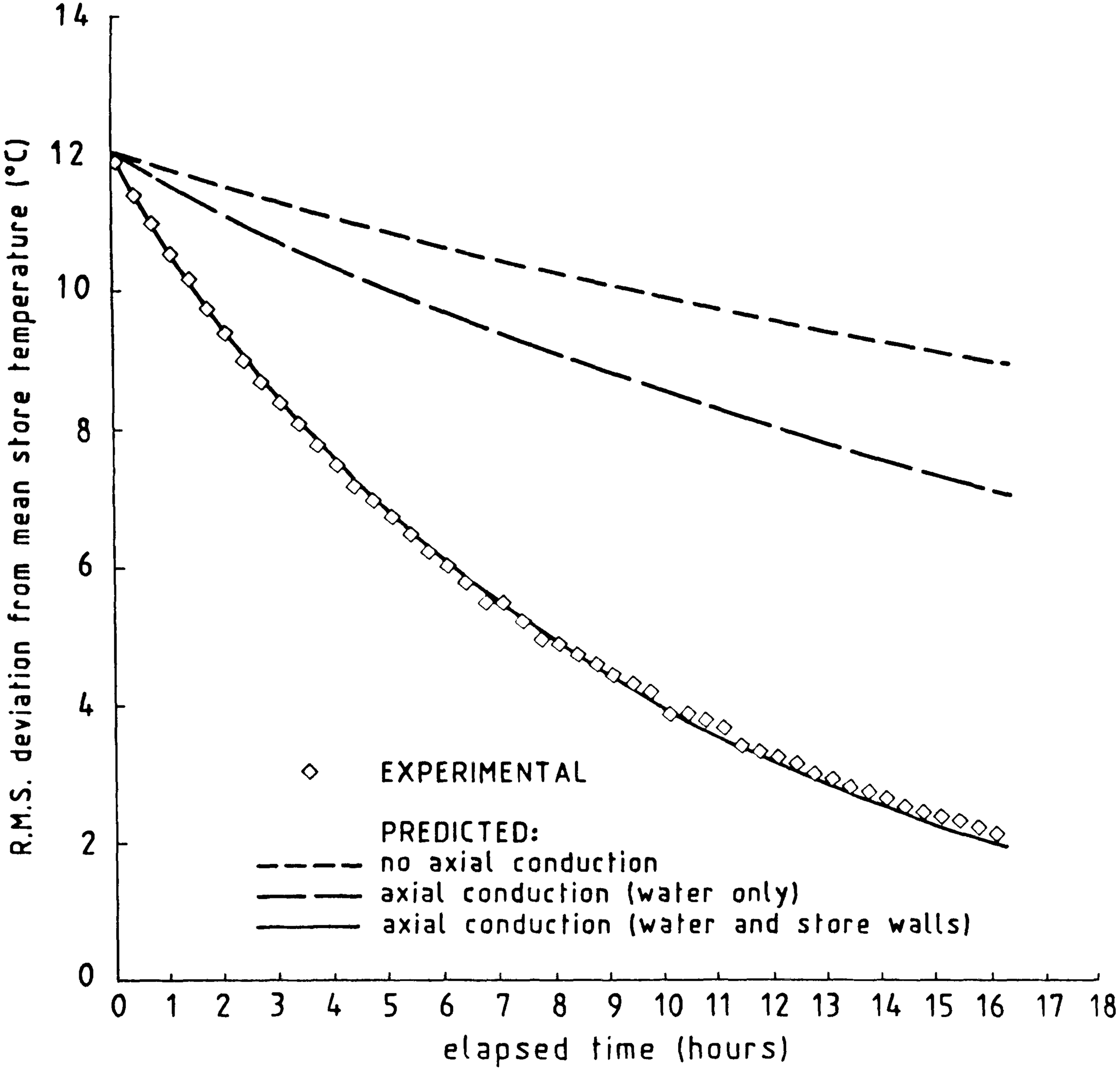
R.M.S. deviation from mean store temperature (°C)
14
12
10
8
6
4
2
0
0 1 2 3 4 5 6 7 8 9 10 11 12 13 14 15 16 17 18
elapsed time (hours)
EXPERIMENTAL
PREDICTED:
no axial conduction
axial conduction (water only)
axial conduction (water and store walls)

In addition to establishing an appropriate effective thermal conductivity, this test served to demonstrate the degree to which store thermocline relaxation would occur in a domestic-sized store over what would be equivalent to an overnight period in which there is no buoyancy-driven flow. It was evident that the resulting rise in the collector inlet temperature apparent at the subsequent onset of the insolation period would be significantly underestimated (in copper-walled stores) and the predicted diurnal efficiency of the system overestimated, if the contribution to the axial thermal conductivity of the store wall were neglected.

5.3.3 Jet penetration depth and mixing

Empirically-derived correlations have previously been developed for both ports which enter a store vertically (34) and, as is the case with the present configuration, horizontal ports (35-37). It has been demonstrated using dimensional analysis techniques (37) that the dimensionless depth of penetration, L^* of a jet of water entering a store may be correlated with the dimensionless Richardson number, Ri, (sometimes refered to as the Archimedes number) according to

$$L^* = z^*/r_s = CONST(Ri)^{-0.5}$$

equation 5.4

where Ri is based on the properties of the fluid entering the store and the internal radius of the nozzle ie.

$$Ri = \frac{g\rho\Delta T r}{v_{in}^2}$$

equation 5.5

Equation 5.4 only applies to turbulent flow and has been shown to break down at lower, transitional region, Reynold number flows. No such equivalent data or correlation exists for the predominantly laminar flow regime which prevails in thermosyphon systems.

An attempt has been made in this present study to obtain measurements

for jet penetration depths for laminar flows. The technique used was similar to that used by Cohen (37) as opposed to the flow visualisation methods employed by the other investigators. The technique involved the measurement of the time taken for the outlet temperature to change in response to a thermal step input. By assuming an initial mixed zone of depth z^* shown schematically in figure 5.5(a), the temperature front produced will reach the store outlet after a time t^*, the reaction time, defined by

$$t^* = \frac{(L_s - z^*)\rho_{in}A_s}{\dot{m}_s}$$

equation 5.6

where $\dot{m}_s$ is the mass flow rate of fluid through the store and the density of fluid at the store inlet. Cohen (37) measured this reaction time t^* directly from the experimental results by detecting the temperature front as a rise in temperature at the the store outlet, of 0.1 C since the previous reading. Because of the low Reynold number, laminar flow rates being investigated, and the relatively high rate of axial conduction in the store, this direct method of detecting t^* was found not to be feasible as conduction effectively extended the temperature front travelling down the store. The method finally adopted was to compare the predicted and measured response at the outlet of the store. By this means, the forward extension of the thermal front by conduction which was shown in section 5.3.2 to be accurately modelled by the simulation, will be the same as the corresponding conduction effects indicated by the experimentally-measured output temperature. Any initial mixing effects at the onset of the applied thermal step function would therefore appear as a displacement Δt^*, shown schematically in figure 5.5(b), in the reaction time, between the otherwise identical predicted and measured temperature-time response curves. Since both temperature fronts are travelling down the store at the 'plug' velocity, v_s, of the flow, where

$$v_s = \frac{\dot{m}_s}{\rho_{in}A_s}$$

equation 5.7

FIGURE 5.5

(a) Schematic representation of the penetration depth of the mixed zone due to hot water entering at the top of the storage tank from a horizontal port.

(b) Schematic graph indicating the displacement of the reaction time (due to mixing), between the experimental and predicted temperature-time profiles

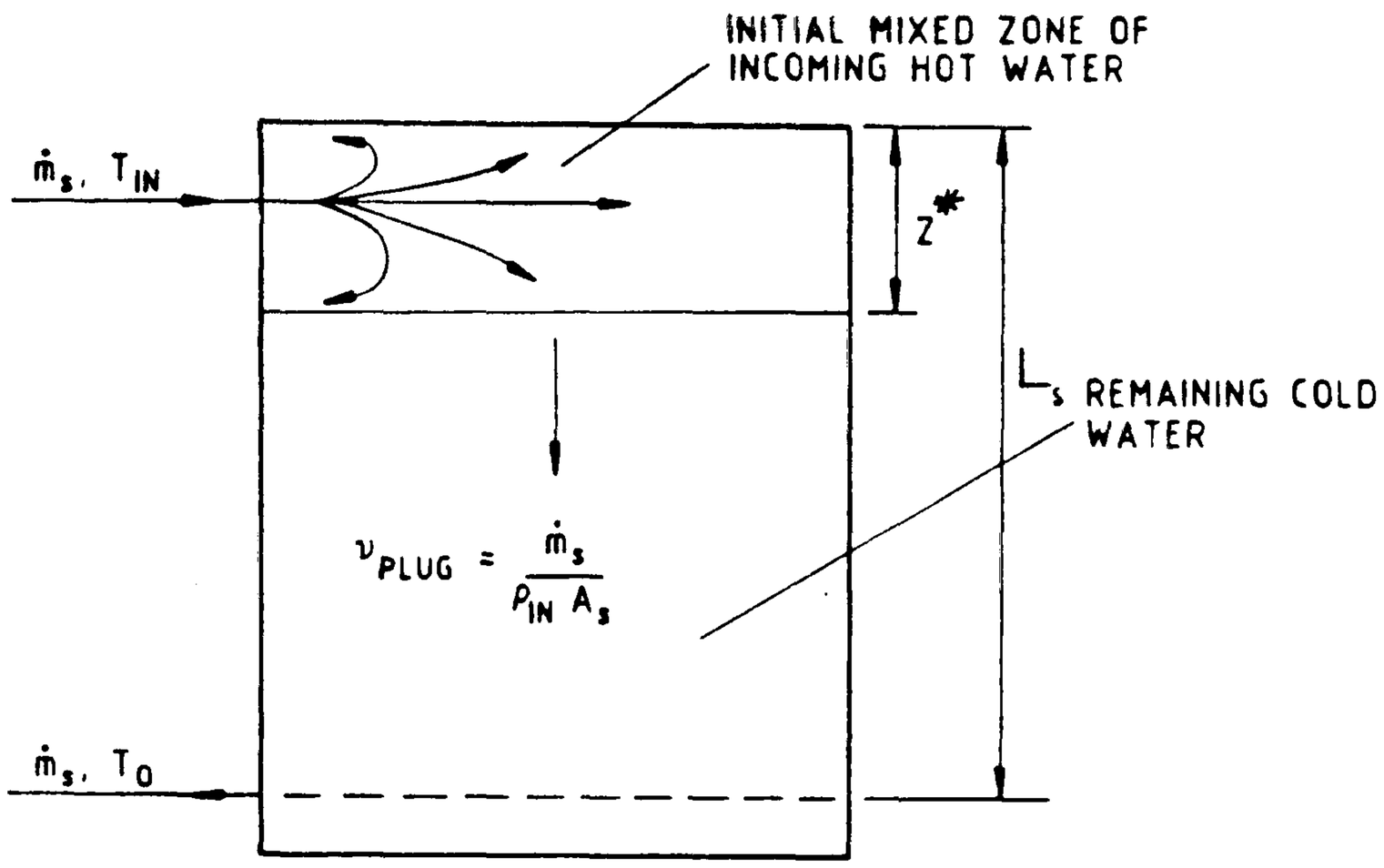
INITIAL MIXED ZONE OF INCOMING HOT WATER
$\dot{m}_s$, T_{IN}
Z^*
L_s REMAINING COLD WATER
$v_{PLUG} = \frac{\dot{m}_s}{\rho_{IN} A_s}$
$\dot{m}_s$, T_O

(a)

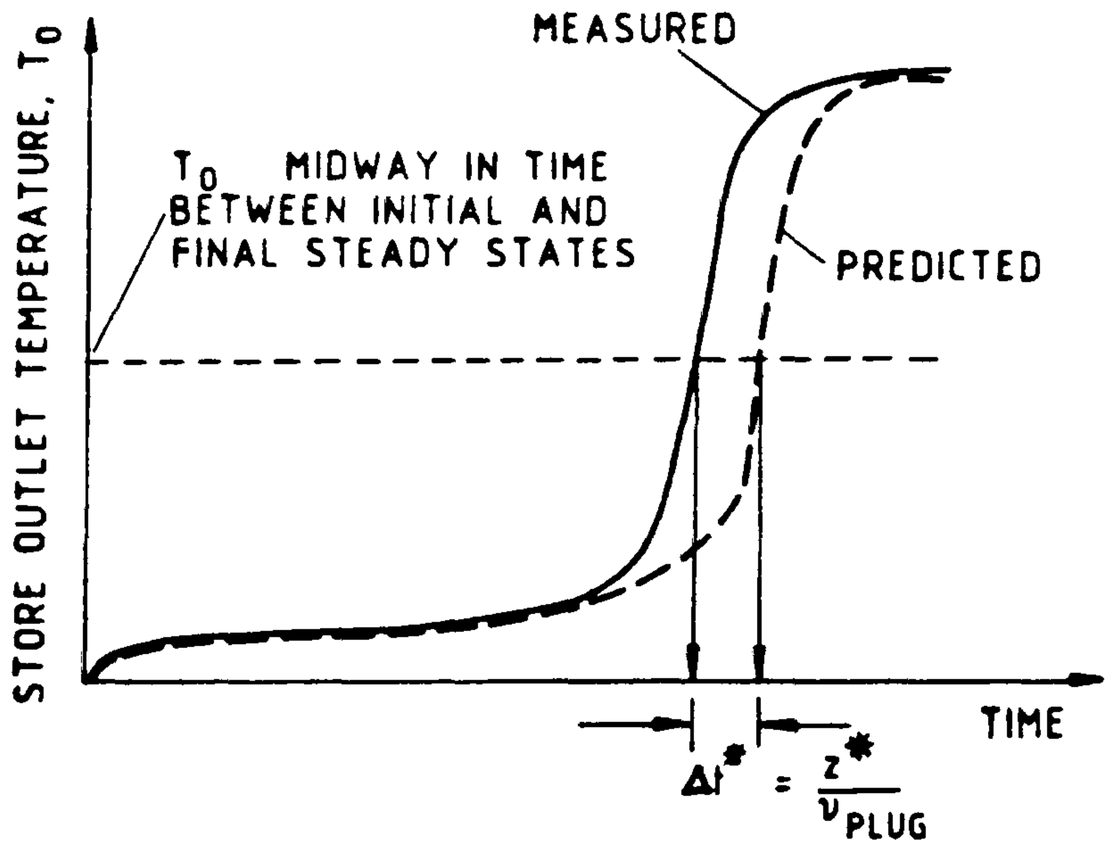
STORE OUTLET TEMPERATURE, T_O
MEASURED
T_O MIDWAY IN TIME BETWEEN INITIAL AND FINAL STEADY STATES
PREDICTED
TIME
$\Delta t^* = \frac{Z^*}{v_{PLUG}}$

(b)

then the penetration depth, z^* will be related to the time displacement, Δt^* by

$$z^* = v_s \Delta t^*$$

equation 5.8

Using the configuration described in section 5.1, six thermal step functions over a range of flow rates and power inputs were imposed, giving corresponding Re_D and Ri numbers, measured at the store inlet, in the range 357 to 975 (ie. laminar) and 729016 to 43608 respectively. The resulting two extremes and an intermediate comparison of the experimental and predicted outlet temperatures are shown in figure 5.6. These temperatures T^* are presented, for comparison purposes in a non-dimensional form according to

$$T^* = \frac{(T_{s,o} - \bar{T}_s{}^i)}{(T_{s,in} - \bar{T}_s{}^i)}$$

equation 5.9

Although some displacement was evident at the higher Ri numbers, the difference between the predicted and measured outlet temperatures was not significantly greater than the experimental uncertainty of $\pm$ 0.3 associated with the thermocouple measurements. Therefore for the system configuration and range of tests (corresponding to the normal operating conditions of a domestic thermosyphon solar- energy water-heater), thermocline relaxation within the store was shown to be accurately simulated by modelling the predominantly conduction rather than mixing effects at the inlet port.

It has been shown (37) that for the same correlating parameter, the penetration depth and therefore mixing effects of a jet entering a store is higher as the laminar flow regime is approached. This is because in laminar flow, the rate of mixing between the inlet flow and store water is lower than in the fully turbulent case and the momentum of a laminar jet will therefore be dissipated much less rapidly. However, physical laws dictate that the penetration depth cannot increase indefinitely with decreasing Re_D number in the laminar region, as no mixing would occur if there is no flow (ie. $Re_D = 0$) and

FIGURE 5.6

Variation with time of the dimensionless outlet temperature during charging of the storage tank

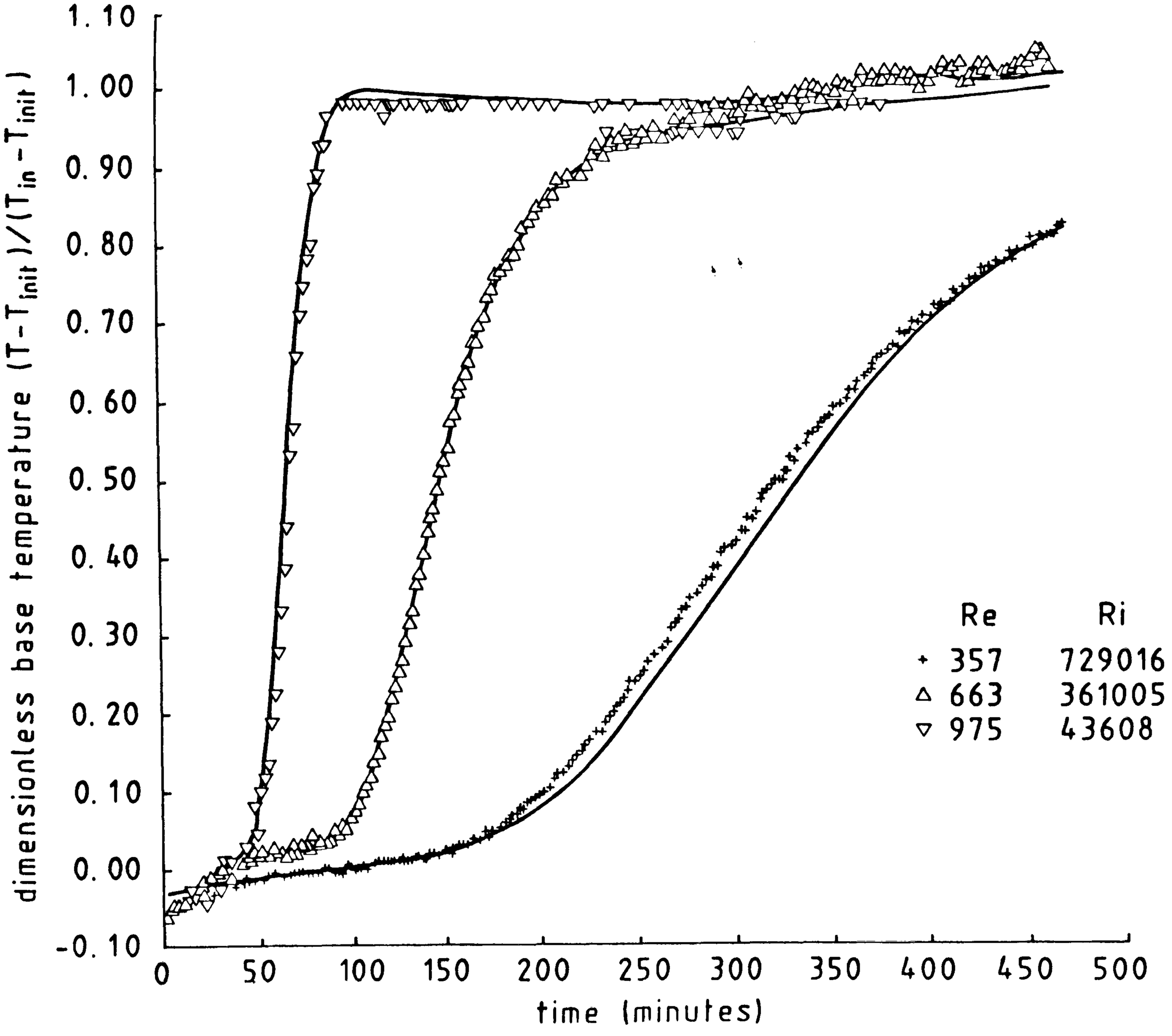
dimensionless base temperature $(T-T_{init})/(T_{in}-T_{init})$
1.10
1.00
0.90
0.80
0.70
0.60
0.50
0.40
0.30
0.20
0.10
0.00
-0.10
0
50
100
150
200
250
300
350
400
450
500
time (minutes)
Re
Ri
357
729016
663
361005
975
43608

so there must eventually be a downward trend in the penetration depth with decreasing Reynold's number. It is therefore assumed that the series of tests described in this section fall within the laminar region in which there is a low penetration depth.

CHAPTER SIX

VALIDATION OF SIMULATED THERMAL PERFORMANCE OF COLLECTOR AND ASSOCIATED PIPEWORK

6.1 Steady-State Thermal Characteristics of the Collector

A method of test similar to that outlined by the British Standards Institution (38) was used in determining the steady-state thermal performance of the collector under conditions of a constant mass flow-rate. The analysis employed in processing the results is based on a Hottel-Whillier-Bliss-type model (23) of a collector in which the heat output is given by

$$\dot{q}_{sol} = F_{AV}A_c[(\tau\alpha)_e I - U_L(\bar{T}_c - T_a)] \qquad \text{equation 6.1}$$

from which the efficiency is

$$\eta = F_{AV}(\tau\alpha)_e - F_{AV}U_L(\bar{T}_c - T_a)/I \qquad \text{equation 6.2}$$

The efficiency is therefore directly proportional to $(\bar{T}_c - T_a)/I$ with a gradient of $F_{AV}U_L$ and an intercept on the ordinate axis representing $F_{AV}(\tau\alpha)_e$.

The tests were carried out using the configuration described in section 5.1. As a value more representative of buoyancy-driven conditions, a flow rate of 0.005 $kgs^{-1}m^{-2}$ was used during the test rather than the stated standard (38) of 0.016 $kgs^{-1}m^{-2}$ for pumped systems. An insolation level of 600 Wm^{-2} with a simulated angle of incidence for the radiation of 0 degrees was imposed. These conditions were maintained for a period of 2 hours to ensure that thermally steady-state conditions were achieved in the collector. A range of efficiencys were obtained by varying the collector inlet temperature between 21°C and 62°C. This was achieved by heating the water in the constant-head tank using a 3 KW electrical immersion-heater, the power to the heater being controlled via a variac. The efficiency, η, was determined from measurements of flow rate and collector inlet and outlet temperatures from which,

$$\eta = \dot{m}_c C_w (T_{c,o} - T_{c,in})/(IA_c)$$

equation 6.3

Identical conditions of flow rate, prevalent ambient temperatures, air velocity across the glass cover and insolation were supplied as inputs to the two-dimensional collector model for a simulated period of time equivalent to the test period. A 7x20 node grid was employed in simulating the collector plate temperature field in the x and y directions respectively, with a time step of 5 s. The appropriate collector heat loss coefficients (39-41) used in the simulation are summarised in appendix H. A plot of against $(\bar{T}_c - T_a)/I$ for the predicted and measured results is shown in figure 6.1. The best straight line through the experimental results gives, for the steady-state thermal characteristics of the collector,

$$\eta = 0.64(\pm 0.03) - 3.3(\pm 0.8)(T_c - T_a)/I$$

equation 6.4

The corresponding non-linear relationship obtained in the case of the predicted performance is given by

$$\eta = 0.64 - 2.47(\bar{T}_c - T_a)/I - 3.35[(\bar{T}_c - T_a)/I]^2$$

equation 6.5

The predicted characteristics agree to within the associated experimental margin of error. The non-linear characteristics indicated by equation 6.5 was evidence of the effects of temperature on the heat-transfer coefficients given in appendix H. The scatter of the corresponding experimental results did not permit confirmation of this predicted trend with a sufficient degree of confidence.

The effect on steady state efficiency, of longitudinal conduction (ie. parallel to the direction to flow) within the absorber plate was investigated numerically at the low thermosyphon-type flow rate at which the collector had been validated.

Insufficient available data pertaining to the simulated operating conditions on which Kirchhoff and Billups (25) and Rao et al (26) based

FIGURE 6.1

Experimental and predicted collector steady-state thermal efficiency performance characteristics

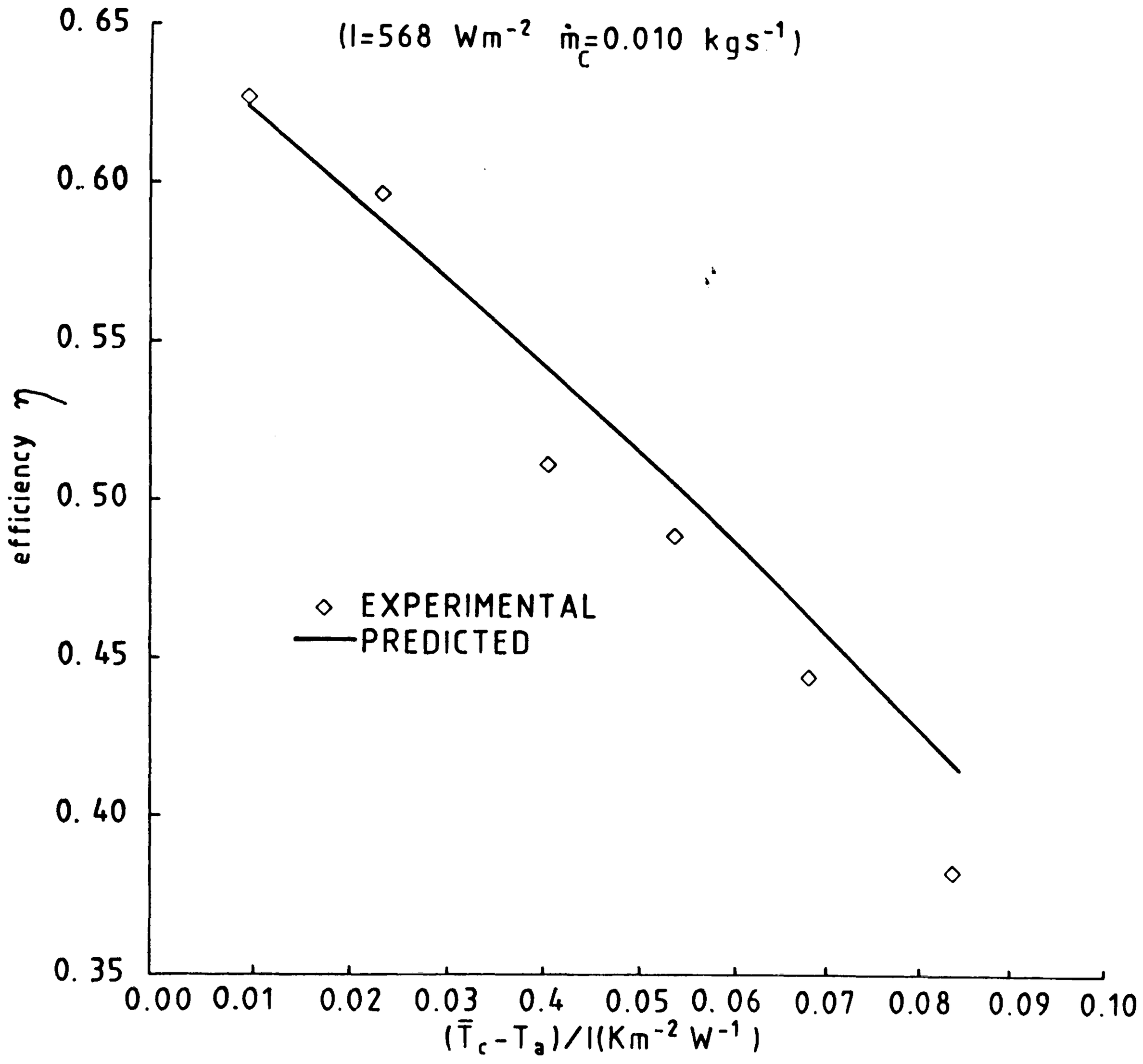
(I=568 Wm⁻² ṁc=0.010 kgs⁻¹)
0. 65
0. 60
0. 55
0. 50
0. 45
0. 40
0. 35
efficiency η
◇ EXPERIMENTAL
PREDICTED
0.00 0.01 0.02 0.03 0.4 0.05 0. 06 0.07 0.08 0.09 0.10
(T̄c - Ta)/I(Km⁻² W⁻¹)

their observations , made any direct comparisons of the two-dimensional temperature distributions in the absorber plate with those predicted by the present collector model, impractical. However, a comparison of the isotherms predicted by the present collector model under steady-state conditions at high (0.028 $kgs^{-1}m^{-2}$) and low (0.005 $kgs^{-1}m^{-2}$) collector fluid flow rates (shown in figures 6.2(a) and 6.2(b) respectively) confirm previous findings (25,26) that a significant component of thermal conduction occurs in the direction parallel and opposite to the direction of flow.

An example of predicted steady-state absorber plate temperatures are shown in figure 6.3 for the two cases of

i) no longitudinal plate conduction (as the Hottel-Whillier-Bliss model assumes), and

ii) longitudinal conduction in the plate.

For the case of no longitudinal plate conduction, an almost linear profile was observed between the ends corresponding to the collector fluid inlet and outlet. This was in contrast to the distinctly non-linear profile observed when a longitudinal component of heat conduction in the collector plate was simulated. However, despite differences between the two cases, in maximum and minimum plate temperatures, of 3.5°C and 0.6°C respectively, the mean plate temperatures integrated over the entire fin surfaces were found, for all practical purposes, to be equal. The efficiency predicted by the simulation with longitudinal conduction was compared with a corresponding value obtained by neglecting longitudinal conduction. Longitudinal conduction was found not to play a significant role in the accurate prediction of steady-state or near steady-state collector performance at thermosyphonic flow rates. This was due to the near-identical mean absorber plate temperatures, and therefore heat losses, predicted in both cases.

6.2 Transient Results

The transient response of a solar collector is generally characterised

FIGURE 6.2

Predicted isothermal mappings of a section of the collector absorber fin

(a) with $\dot{m}_c = 0.016\ kgs^{-1}m^{-2}$

(b) with $\dot{m}_c = 0.005\ kgs^{-1}m^{-2}$

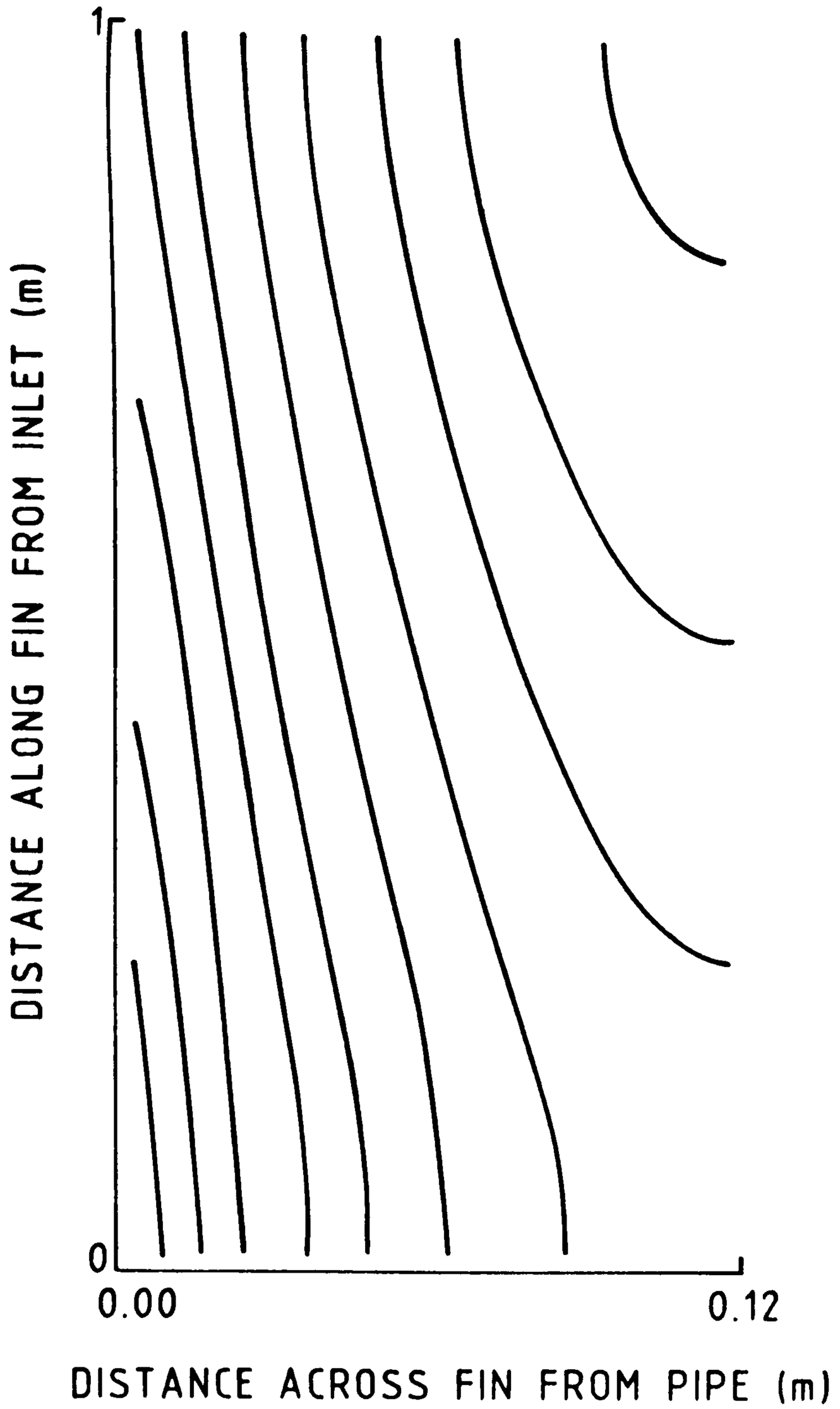
1
0
0.00
0.12
DISTANCE ALONG FIN FROM INLET (m)
DISTANCE ACROSS FIN FROM PIPE (m)

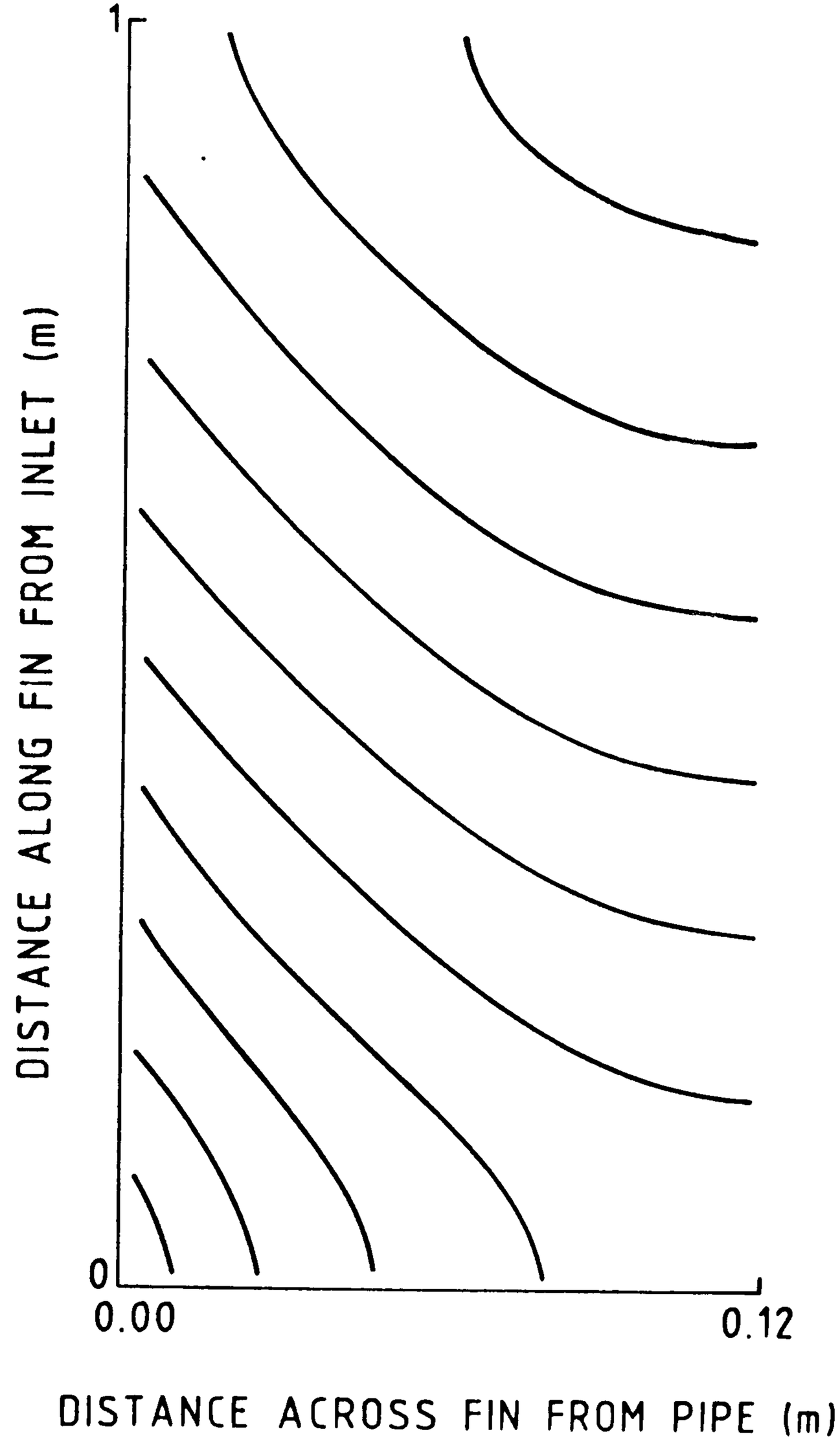
1
0
0.00
0.12
DISTANCE ALONG FIN FROM INLET (m)
DISTANCE ACROSS FIN FROM PIPE (m)

FIGURE 6.3

Carpet plot of predicted temperature distribution over a section of collector absorber plate fin

(a) without longitudinal conduction, and

(b) with longitudinal conduction

1) WITHOUT LONGITUDINAL CONDUCTION

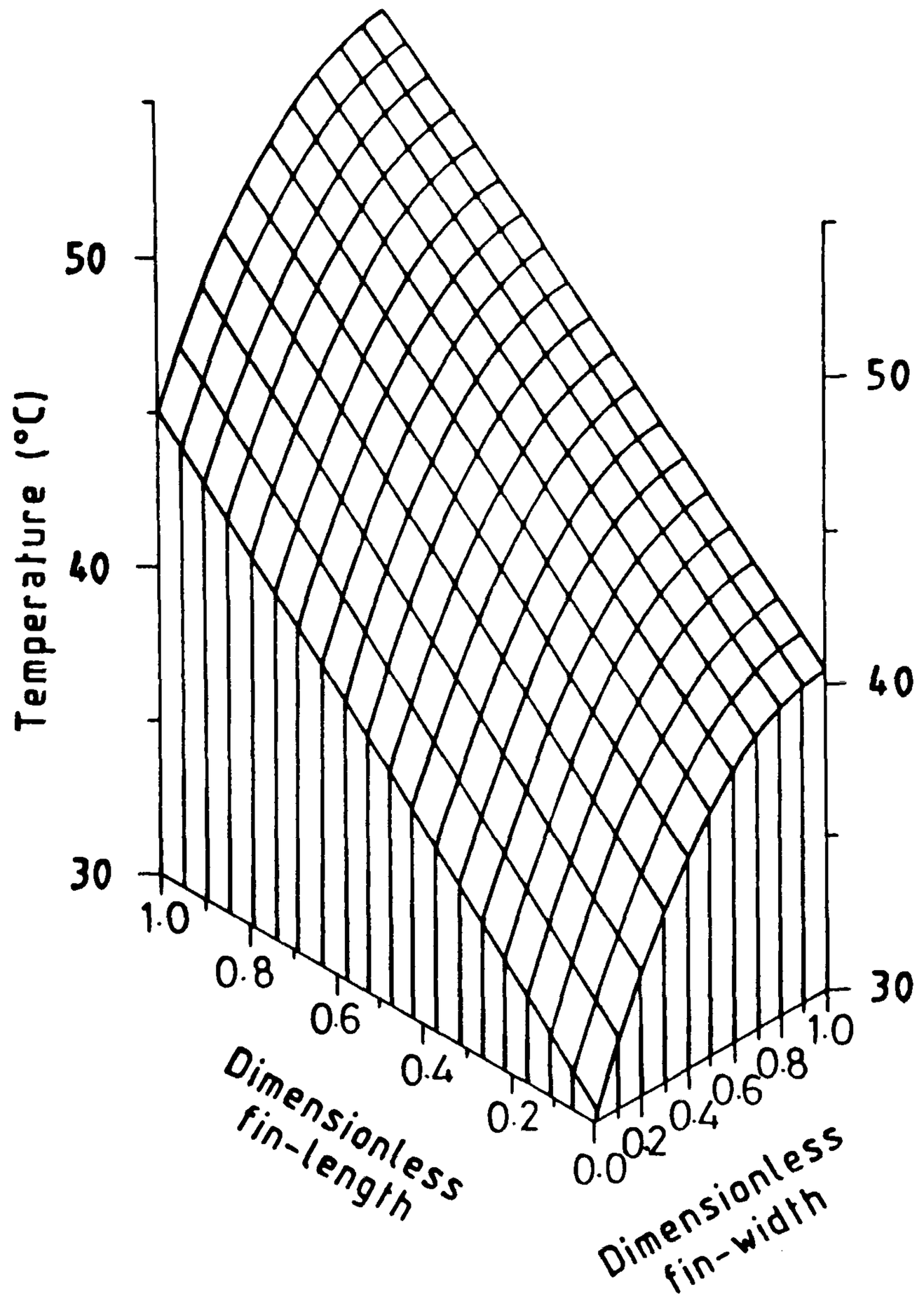

2) WiTH LONGITUDINAL CONDUCTION

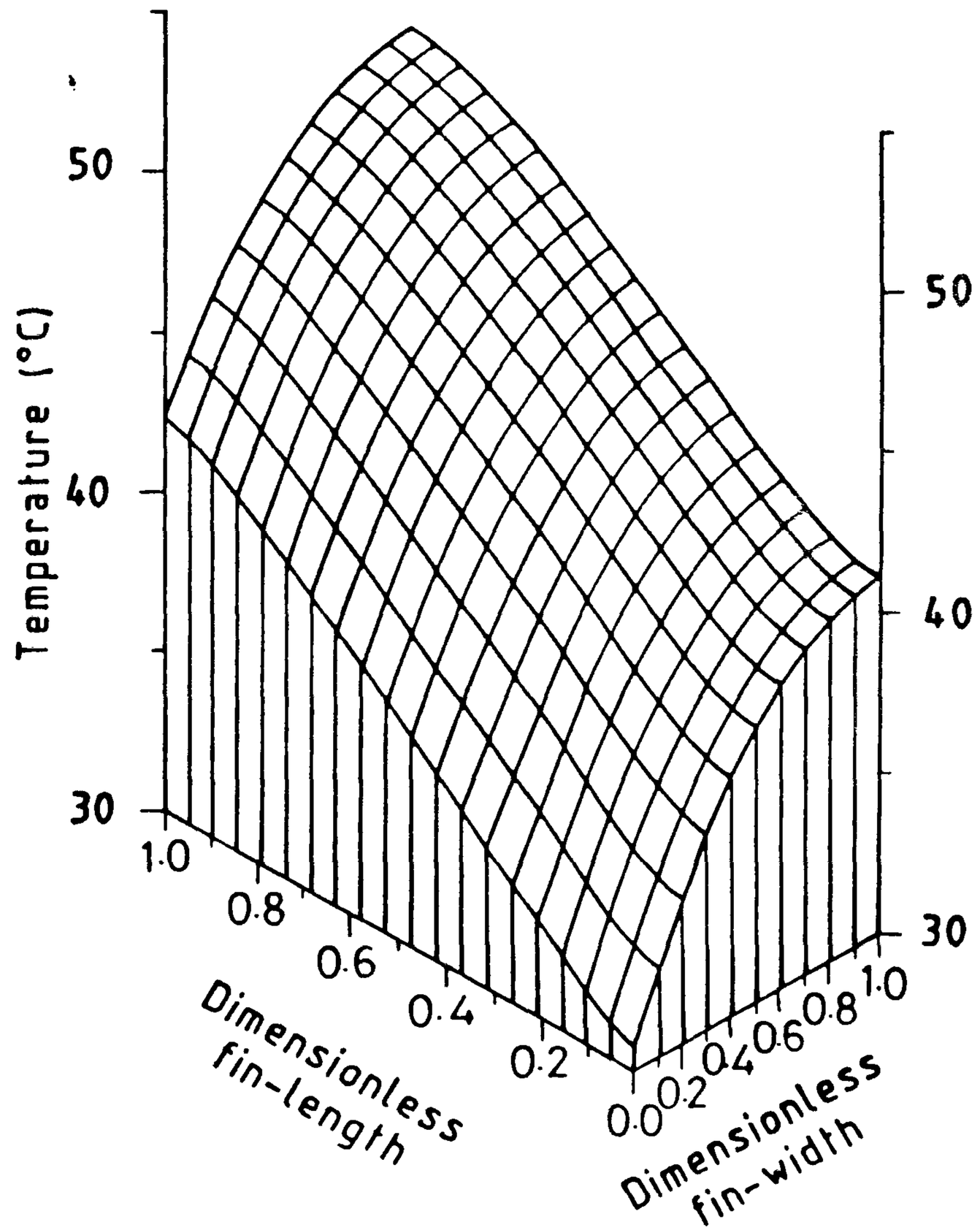

by a time constant, Γ . A simplified approach (42) in determining Γ is to consider a simple heat balance on the collector represented by equations 6.6 and 6.7.

$$\frac{C_c}{A_c}\frac{d\bar{T}_c}{dt} = F_{AV}[(\tau\alpha)_e - U_L(\bar{T}_c - T_a)]$$

equation 6.6

$$\frac{C_c}{A_c}\frac{d\bar{T}_c}{dt} = \frac{\dot{m}_c C_w}{A_c}(T_{c,o} - T_{c,in})$$

equation 6.7

where C_c represents an effective lumped capacitance for the collector which includes the fluid within and the fabric of the collector.

The exit and mean temperature of the fluid in the collector are related by

$$\frac{d\bar{T}_c}{dt} = K'\frac{dT_{c,o}}{dt}$$

equation 6.8

where

$$K' = [\dot{m}_c C_w/(F_{AV}U_L A_c)][(F_{AV}/F_R)-1]$$

equation 6.9

By assuming the whole collector is initially at the inlet temperature equations 6.6, 6.7 and 6.8 can be solved simultaneously to give the time-dependent mean fluid temperature.

$$\frac{F_{AV}[(\tau\alpha)_e I - U_L(\bar{T}_c - T_a)] - (\dot{m}_c C_w/A_c)(T_{c,o} - T_{c,in})}{F_{AV}[(\tau\alpha)_e I - U_L(\bar{T}_c - T_a)}$$

$$= \underset{(i)}{\exp}-[\dot{m}_c C_w/(K'C_c)]$$

$$\underset{(ii)}{}$$

equation 6.10

From equation 6.10 Γ is then defined as

$$\Gamma = K'C_c/\dot{m}_c C_w$$

equation 6.11

The response time therefore coresponds to the time at which

$$\frac{F_{AV}[(\tau\alpha)_e I - U_L(\bar{T}_c - T_a)] - (\dot{m}_c C_w/A_c)(T_{c,o} - T_{c,in})}{F_{AV}[(\tau\alpha)_e I - U_L(\bar{T}_c - T_a)]} = e^{-1}$$

Using the empirically-determined values from equation 6.4, of

$$F_{AV}(\tau\alpha)_e = 0.64 \ (\pm 0.03)$$

and

$$F_{AV}U_L = 3.3 \ \ (\pm 0.8)$$

A plot of the response factor (term (i) in equation 6.10) against the time t, from the onset of the insolation step function was obtained (figure 6.4). From figure 6.4, the experimentally-measured and predicted response times are 583 and 529 seconds respectively, representing a discrepancy of 9% for the predicted value. Although every effort was made to obtain a good thermal contact, a finite contact resistance will still exist between the absorber plate and the heater mats. This resistance will reduce the rate of heat transfer between the heaters and absorber plate. In effect this gives an apparent increase in the response time of the collector and will partially account for the discrepancy between the predicted and observed values.

6.3 Heat Transfer Processes in the Upriser and Downcomer Pipes

The development of the mean upriser temperature with time during the transient testing of the collector described in section 6.2 was used to establish the most suitable choice of heat transfer processes at the pipe wall. The measured flow rate, collector outlet and ambient temperatures were used as inputs to the upriser component in the

FIGURE 6.4

Experimental and predicted variation with time, in the collector response function

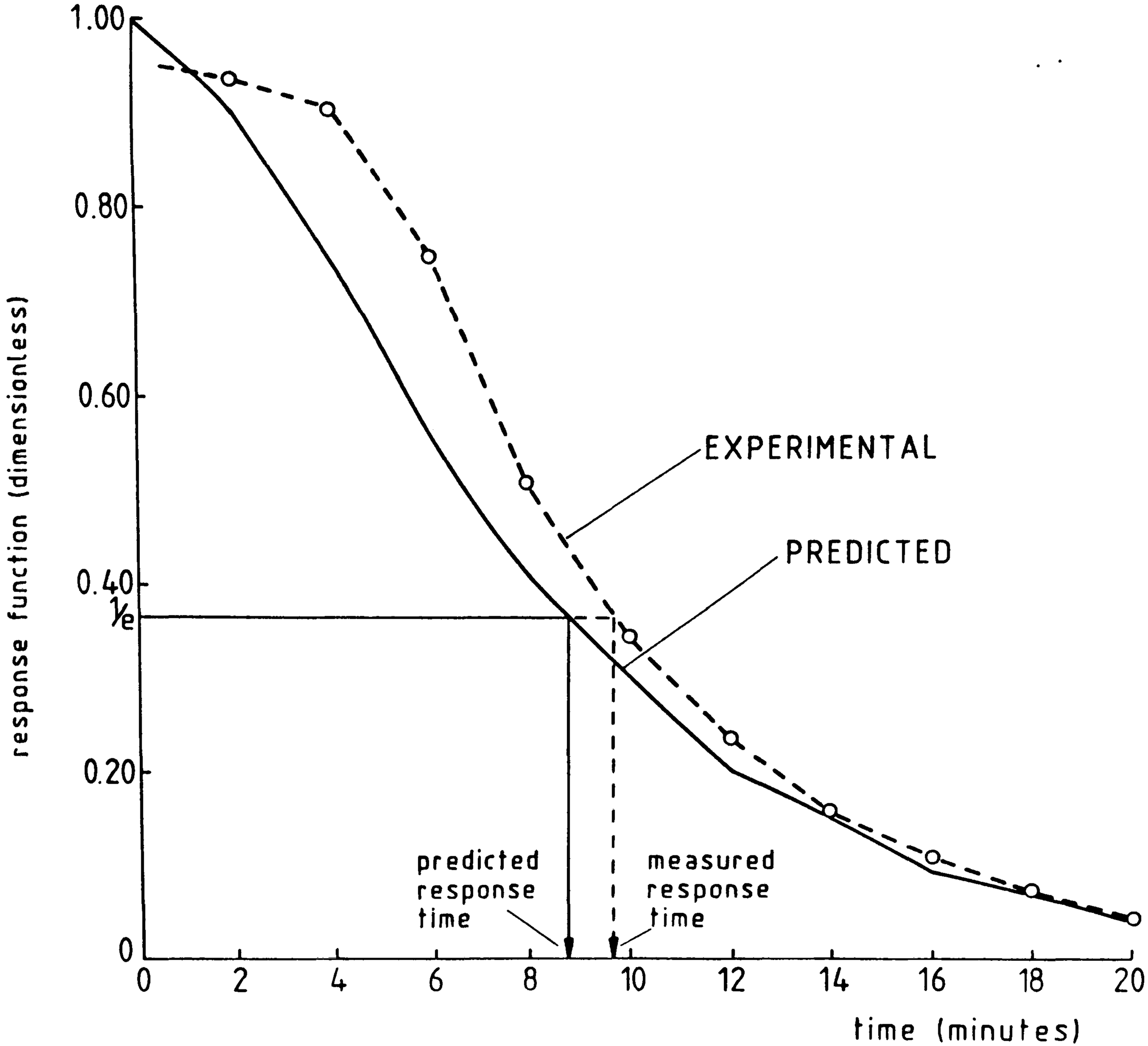
1.00
0.80
0.60
0.40
1/e
0.20
0
response function (dimensionless)
EXPERIMENTAL
PREDICTED
predicted response time
measured response time
0
2
4
6
8
10
12
14
16
18
20
time (minutes)

FIGURE 6.5

Experimental and predicted response of the mean upriser temperature to a thermal step input

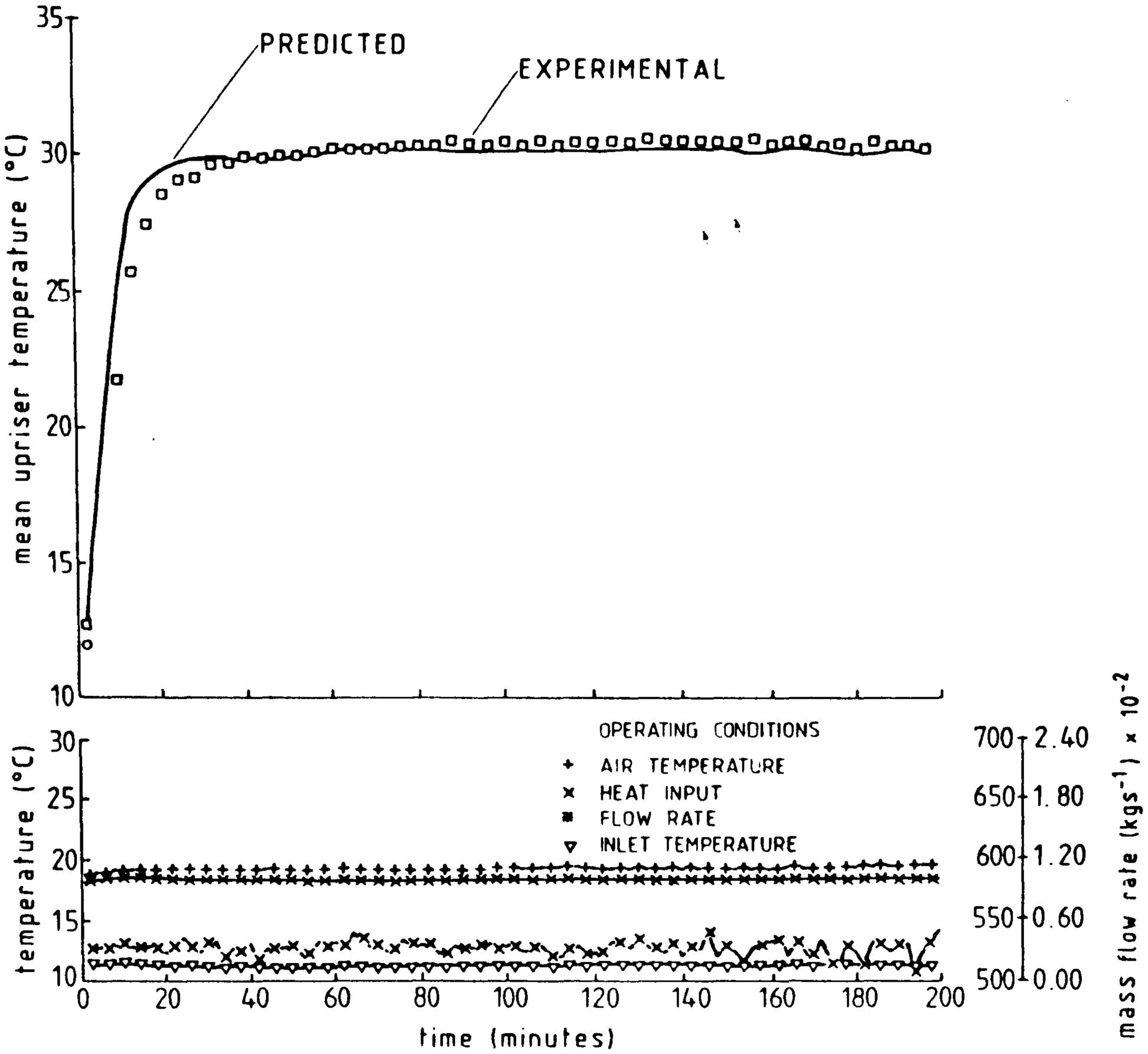
PREDICTED
EXPERIMENTAL
mean upriser temperature (°C)
35
30
25
20
15
10
OPERATING CONDITIONS
AIR TEMPERATURE
HEAT INPUT
FLOW RATE
INLET TEMPERATURE
temperature (°C)
30
25
20
15
10
0
20
40
60
80
100
120
140
160
180
200
time (minutes)
700
650
600
550
500
2.40
1.80
1.20
0.60
0.00
mass flow rate (kgs^{-1}) x 10^{-2}

simmulation model. A total of five nodes was found to adequately represent the finite difference approximation of the predicted fluid temperature field within the upriser pipe. By assuming a finite rate of heat transfer between the fluid and pipe wall (due to forced convection) and also between the external surface of the insulant and the ambient (buoyancy-driven convection), the simulated thermally steady-state mean upriser temperature indicated a rate of heat loss which was 20% less than that indicated by the corresponding experimentally-measured value. However, with the simulated heat loss from the pipework due entirely to radial conduction through the cylindrically configured insulation according to the relationship presented in appendix H, the predicted and measured mean upriser temperatures agreed to within the associated experimental uncertainty of $\pm$ 0.3 ^{o}C over both the transient and steady-state regions of the temperature histories plotted in figure 6.5. Heat transfer rates associated with the downcomer pipe (which was of the same internal diameter and identically insulated) were assumed to be equivalent to those experienced in the upriser.

CHAPTER SEVEN

VALIDATION OF SYSTEM THERMAL PERFORMANCE WITH BUOYANCY-DRIVEN FLOW

7.1 Available Data Pertinent to Flow Resistances in Solar-Energy Stimulated Liquid Thermosyphons

7.1.1 The problem

The literature abounds with studies concerning the thermal performances of natural-circulation solar-energy water-heaters (19), yet few mention the flow losses encountered let alone indicate their magnitudes for given geometries and operating conditions. However such information is essential for accurate predictions of the prevailing flow rate and hence the time variations of system performance.

The assumption of fully-developed isothermal laminar flow leads usually to underpredictions of the flow rate at Reynolds numbers less than 300 and over-estimates at higher "laminar" flow rates (9,10,24,12). The former discrepancy has been attributed (12) to the calculation of the thermosyphon head based on the mean bulk temperature of the liquid without correction for the flow structure and temperature profile. This effect is dominant at very low Reynolds number ($Re_D < 300$) so that any underestimate of the frictional resistance of the circulating fluid is masked by an overestimate of the thermosyphon head.

However, in the range $300 \geqslant Re_D \geqslant 1200$ (within which many solar energy water-heater systems operate) the effects of neglecting the increased frictional resistance due to flow development and thermal destabilisation become significant. The use of the correct pipe-loss coefficients therefore becomes imperative if an overestimate of the mass flow rate is to be avoided.

At present, turbulent flow pipe fitting loss coefficients are frequently used (13,15,16). The veracity of flow-rate estimates could be further improved by employing coefficients for flow losses arising at pipe fittings that are relevant to laminar flow.

A series of preliminary measurements on the pressure differential across the Gull Air collector were carried out prior to installing the collector in the solar water heater system, the results of which are

presented in appendix K. A comparison of these measured pressures with corresponding predicted values based on the measured flow rate, confirmed the need for a more comprehensive review of the available literature on friction factor correlation data.

7.1.2 Entrance effects under isothermal conditions

Many theoretical analyses dealing with laminar flow after entry into a pipe have been formulated (21,43-47). The range of values of the entrance Reynolds number ($(L/D)/Re_D$), over which the solutions are valid depends on the intial simplifying assumptions. Pertinent experimental studies (44,48,49) are rare and thus only limited data are available.

The present approach is to derive the friction factor correlations of experimental data (44,49). These are supplemented where necessary by numerically-predicted theoretical data (21) in order to produce a single continuous function.

Kline and Shapiro (44) measured, experimentally, apparent local friction factors at the entrance to a cylindrical duct. Air was used as the test fluid. At the air velocities ($<61\ ms^{-1}$) employed, compression effects were considered to be negligible. Thus the resulting generalisations should be applicable also to liquids. Non-isothermal tests were also carried out in which the cooling of the fluid was induced by temperature differences of up to 156 ^{o}C between the free air stream and the duct wall. In the non-isothermal case, provided that the value of the fluid properties used in the calculation of the Reynolds number were based on the mean of the free stream and wall temperatures, both the isothermal and non-isothermal experimentally determined friction factors could be uniquely correlated by

$$f(L/D) = 13.74[(L/D)/Re_D]^{0.5} \qquad \text{equation 7.1}$$

for $10^{-5} \leq (L/D)/Re_D \leq 5 \times 10^{-3}$

All the experimental data fell within $\pm 6\%$ of this correlation (44).

In the course of the experiments, three distinct laminar regions were identified, namely:-

i) For $0 < (L/D)/Re_D \leq 5 \times 10^{-3}$, the flow behaves as that over a flat plate because the boundary layer is thin compared with the internal diameter of the pipe.

ii) Within a transition region, $5 \times 10^{-3} < (L/D)/Re_D \leq 10^{-1}$, the flow alters to the fully developed laminar viscous flow as $(L/D)/Re_D$ increases.

iii) For $10^{-1} < (L/D)/Re_D \leq \infty$, steady Poiseuille-type flow prevails.

A macroscopic momentum balance was derived (44) for a boundary layer which was assumed to be thin when compared with the duct's internal diameter. When solved, the friction factor correlation obtained from this simplified analysis was:-

$$f(L/D) = 14.3[(L/D)/Re_D]^{0.5}$$

equation 7.2

Equation 7.2 agrees to within $\pm 4\%$ with the experimentally determined correlation given by equation 7.1. Outside the given limits for $(L/D)/Re_D$ in equation 7.1 the velocity profile of the flow undergoes a transformation to Poiseuille-type flow. Thus the use of equation 7.1 in those regions is not recommended. Similarly, equation 7.2 is inappropriate other than for $(L/D)/Re_D \leq 5 \times 10^{-3}$ as above this value for $(L/D)/Re_D$ the assumption of a thin boundary layer then becomes invalid.

A solution of the Navier-Stokes equation for steady flow in the entrance region of a pipe was derived by Langhaar (21) by means of a linearising approximation. Based on this study, a correction factor to account for the effects of developing flow in thermosyphon solar-energy water heaters was proposed by Morrison and Ranatunga (12), namely

$$f(L/D) = 64\frac{(L/D)}{Re_D}\left[1 + \frac{0.038}{[(L/D)/Re_D]^{0.96}}\right]$$

equation 7.3

Equation 7.3, however was found to predict friction factors significantly higher than those measured by Kline and Shapiro (44) in the upper applicable range of $(L/D)/Re_D$ (ie.$(L/D)/Re_D = 10^{-3}$). The principle reason for this discrepancy is that the pressure drop (Δp) in the dimensionless pressure term ($\Delta p/\rho v^2/2$), from which equation 7.3 was derived (12), was defined (21) as the pressure difference between still water in the supply reservoir and a point at a distance y from the entrance to the pipe. This term includes a pressure drop ($\rho v^2/2$) due to neither viscous nor boundary layer momentum effects but to the acceleration of the static fluid in the reservoir to the mean flow velocity just before its entry to the pipe. Thus the total pressure difference will be given by

$$p = \rho v^2/2 + (p_{in} - p_y)$$

equation 7.4

$(p_{in} - p_y)$ is the static pressure drop between the entry and the distance y along the pipe due to viscous forces and boundary layer development. Rearranging equation 7.4 gives

$$\frac{p_{in} - p_y}{\rho v^2/2} = \frac{\Delta p}{\rho v^2/2} - 1$$

equation 7.5

A value of unity has to be subtracted from the values of the $(\rho v^2/2)$ terms presented by Langhaar (21) if the apparent friction factor for the pipe alone is to be determined. Making this adjustment to equation 7.3 gives

$$f(L/D) = 64\frac{(L/D)}{Re_D}\left[1 + \frac{0.038}{[(L/D)/Re_D]^{0.96}}\right] - 1$$

equation 7.6

As can be seen in figure 7.1, equation 7.6 is corroborated by Langhaars

FIGURE 7.1

Friction factor correlations for isothermal developing laminar flow in pipes

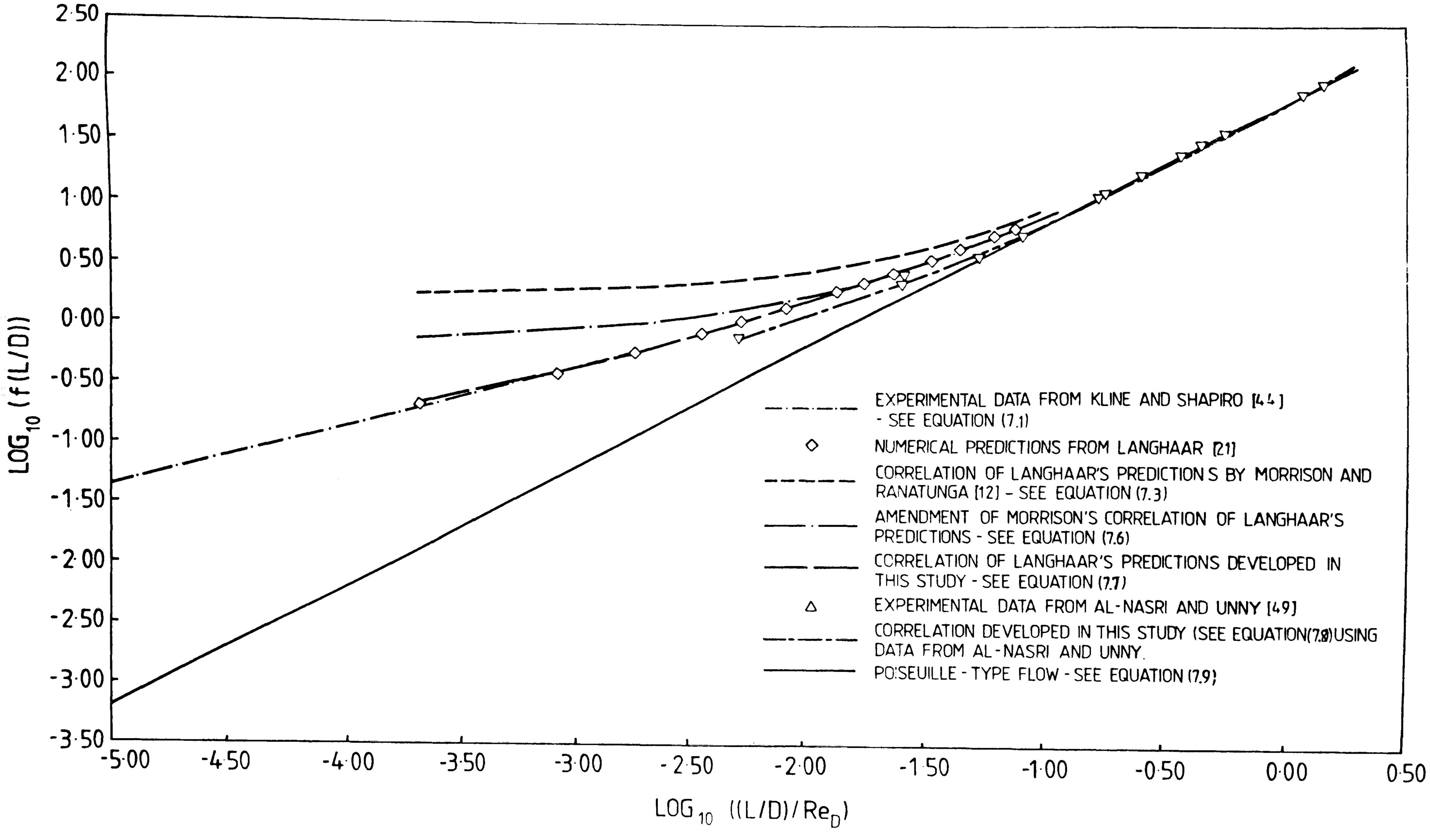
2·50
2·00
1·50
1·00
0·50
0·00
-0·50
-1·00
-1·50
-2·00
-2·50
-3·00
-3·50
LOG10 (f(L/D))
-5·00
-4·50
-4·00
-3·50
-3·00
-2·50
-2·00
-1·50
-1·00
-0·50
0·00
0·50
LOG10 ((L/D)/ReD)
EXPERIMENTAL DATA FROM KLINE AND SHAPIRO [44] - SEE EQUATION (7.1)
NUMERICAL PREDICTIONS FROM LANGHAAR [21]
CORRELATION OF LANGHAAR'S PREDICTIONS BY MORRISON AND RANATUNGA [12] - SEE EQUATION (7.3)
AMENDMENT OF MORRISON'S CORRELATION OF LANGHAAR'S PREDICTIONS - SEE EQUATION (7.6)
CORRELATION OF LANGHAAR'S PREDICTIONS DEVELOPED IN THIS STUDY - SEE EQUATION (7.7)
EXPERIMENTAL DATA FROM AL-NASRI AND UNNY [49]
CORRELATION DEVELOPED IN THIS STUDY (SEE EQUATION(7.8)USING DATA FROM AL-NASRI AND UNNY.
POISEUILLE - TYPE FLOW - SEE EQUATION (7.9)

predicted data (21) only within the range $0.01 < (L/D)/Re_D \leq 0.08$, yet over-estimates the friction factor for $(L/D)/Re_D \leq 0.01$. No correlation of the form of equation 7.6 which would represent adequately Langhaars data over the pertinent range of $(L/D)/Re_D$ could be derived. A logarithmic plot of the data revealed that a more suitable correlation was given by

$$f(L/D)/Re_D = 50.698[(L/D)/Re_D]^a$$

equation 7.7

where $a = 0.90 + 0.07 \log[(L/D)/Re_D]$

for $10^{-3} < (L/D)/Re_D \leq 0.1$

The mean deviation of Langhaars predicted data from equation 7.7 Over the range of $(L/D)/Re_D$ was $\pm 2\%$. The mean deviation of equation 7.6 from Langhaar's numerical results was $\pm$ 19% over the same range of $(L/D)/Re_D$. Equation 7.7 is plotted in figure 7.1. As can be seen, it exhibits continuity with equation 7.1 at $(L/D)/Re_D = 10^{-3}$.

Experimental observations were presented by Al-Nasri and Unny (49) for apparent friction factors in the entrance region of a pipe under isothermal conditions and high values of $(L/D)/Re_D$. Values were obtained for seven different entry lengths in the range $16.5 < (L/D) \leq 919$. However, no overall correlation was derived relating friction factors to entry length and Reynolds number. Using the graphical data provided, a correlation between $f(L/D)$ and $(L/D)/Re_D$ has been obtained in this study. This is also shown in figure 7.1. Two points were taken from the best-fit straight line in the linear laminar region of the $\log(f)$against $\log(Re_D)$ plots for each of the seven entry length results. Using these data, a plot of $\log[f(L/D)]$ against $\log[(L/D)/Re_D]$ was obtained giving a curve which could be descibed by

$$f(L/D) = 64.416[(L/D)/Re_D]^b$$

equation 7.8

where $b = 1.10 + 0.11 \log[(L/D)/Re_D]$

This function was found to be reasonably continuous with equation 7.7 (that is the correlation obtained from Langhaar's results) at approximately $(L/D)/Re_D = 0.1$ - see figure 7.1. Equation 7.8 corresponds to

$$f(L/D) = 64[(L/D)/Re_D] \qquad \text{equation 7.9}$$

for $(L/D)/Re_D > 0.4$, that is Poiseuille flow prevails.

Equation 7.8 represents the remaining part of a continuous set of functions which permit the estimation of apparent friction factors in pipes under conditions of isothermal, laminar, developing flow for all entrance Reynolds numbers.

7.1.3 Thermal destabilisation and developing flow

When fluids flowing through a horizontal cylindrical tube are heated by conduction through the tube walls, the buoyancy forces cause an internal circulation in the plane normal to the direction of flow. The circulation is upwards in the fluid adjacent to the pipe wall and downward through the central region of the pipe. This flow is illustrated schematically in figure 7.2(a). This secondary flow induces a flow resistance and thereby increases the overall friction factor compared with that for isothermal flow.

Both for a heated fluid flowing vertically upwards and a cooled fluid flowing vertically downwards, buoyancy forces increase the velocity of the fluid near the tube wall, thereby distorting the isothermal laminar velocity profile as illustrated schematically in figure 7.2(b). Thus an increase in the total friction encountered is experienced. The situation in inclined pipes is intermediate between those shown in figure 7.2(a) and 7.2(b).

Accurate measurements were carried out by Kemeny and Somers (50) of the pressure drop across a vertical heated pipe in which both free and forced convection ensued simultaneously. Either water or oil was used as the circulating fluid: the range of Reynolds number investigated in

FIGURE 7.2

Flows in horizontal and vertical pipes

(a) vertical cross-sectional view of secondary flows
in a heated horizontal tube

(b) schematic indication of the fluid velocity distributions
in laminar vertical upward flow

(a) VERTICAL CROSS-SECTIONAL VIEW OF SECONDARY FLOWS IN A HEATED HORIZONTAL TUBE.

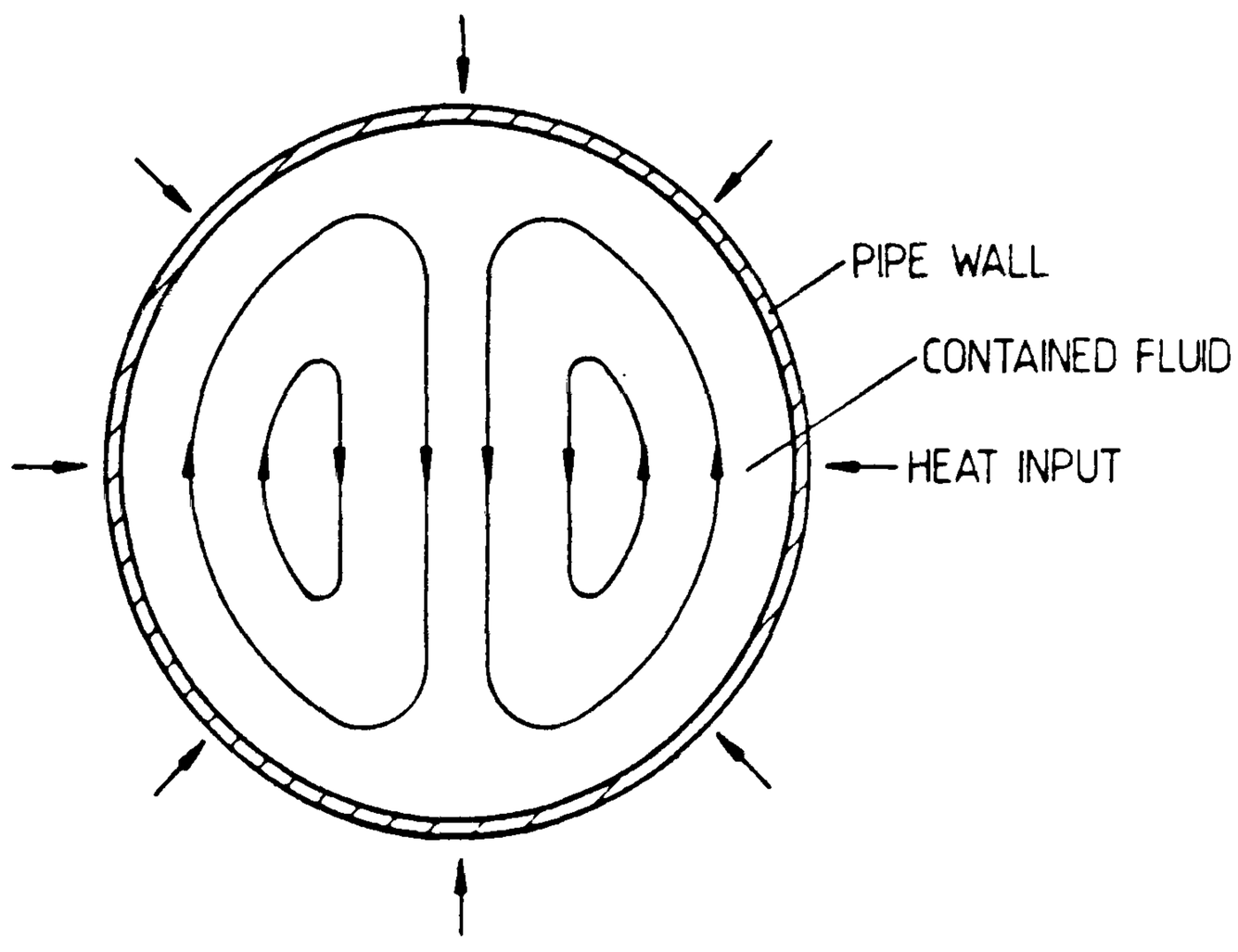

(b) SCHEMATIC INDICATION OF THE FLUID VELOCITY DISTRIBUTIONS IN LAMINAR VERTICAL UPFLOW

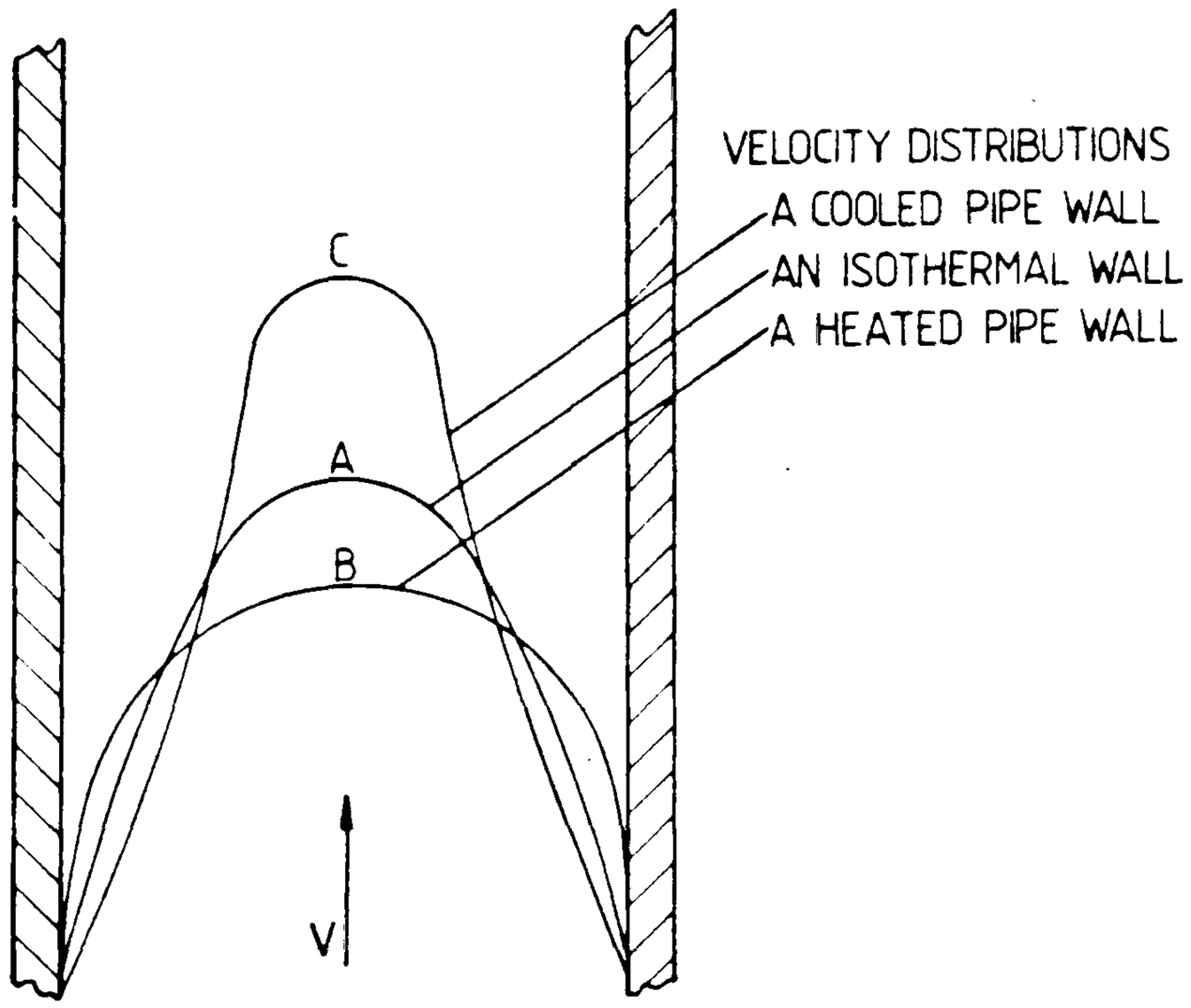

the case of water was $61 < Re_D \leq 6800$. The electrical heat input was $53 < q \leq 5200$ W, which gave Graetz numbers in the range $5 < Gz \leq 320$. No overall correlation was given for the data obtained.

Creveling et al (51) measured friction factors in a simple circular, toroidal, natural circulation loop and obtained the correlation :-

$$f = 604(Re_D)^{-1.17}$$

equation 7.10

for $200 < Re_D \leq 1500$

Addlesee (52) investigated experimentally the relationship between friction factor, Reynolds number and Rayleigh number. A natural circulation loop was used, consisting of two vertical pipes connected at either ends by short lengths of larger diameter tubing. Water in the lower connecting length was heated electrically, thereby causing circulation of the fluid. The effect of cooling of the vertical pipes on the friction factor was investigated. The friction factor was dependent on the Reynolds number alone, the correlation given being

$$f = 600(Re_D)^{-1.19}$$

equation 7.11

for $50 < Re_D \leq 2500$

Despite the differences in geometries of the two systems considered, the friction factors predicted by equation 7.10, obtained by Creveling et al (51) agree to within 15% of those predicted using equation 7.11. However, equation 7.11 describes experimental results for an experimental configuration closer to the component geometries encountered in thermosyphon solar water heating systems.

A more comprehensive correlation, relevant to buoyancy effects in vertical pipes has been proposed by Bishop et al (53). The ratio Gr/Re_D is identified as the most appropriate correlating parameter for fully-developed, thermally-destabilised flow and using a numerical simulation was found to be related to the friction factor by

FIGURE 7.3

Friction factor data correlations for isothermal and non-isothermal flows with

(a) L/D = 5

(b) L/D = 20

(c) L/D = 100

(d) L/D = 400

a)

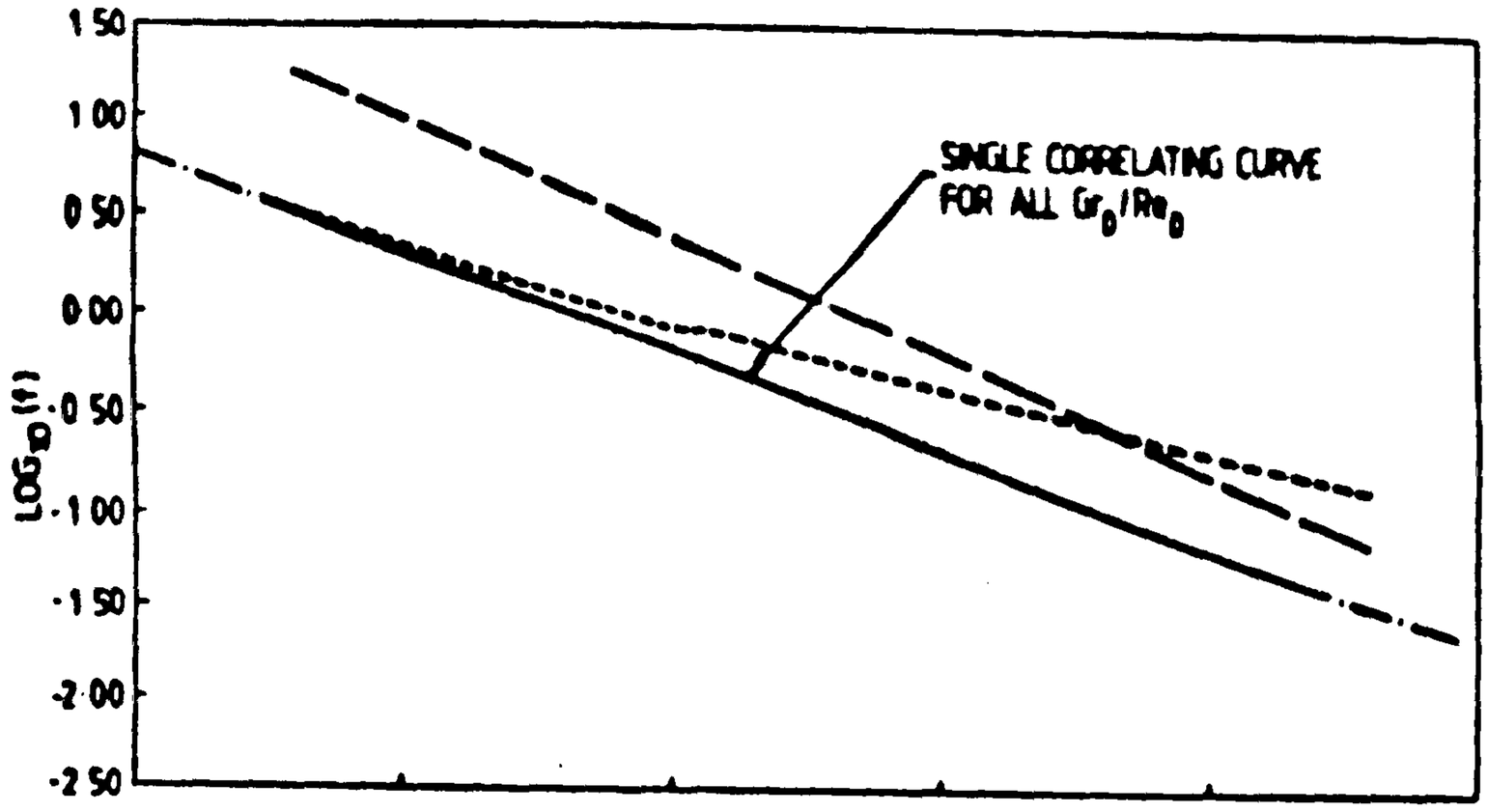
SINGLE CORRELATING CURVE FOR ALL Gr_0/Re_0
$LOG_{10}(f)$

b)

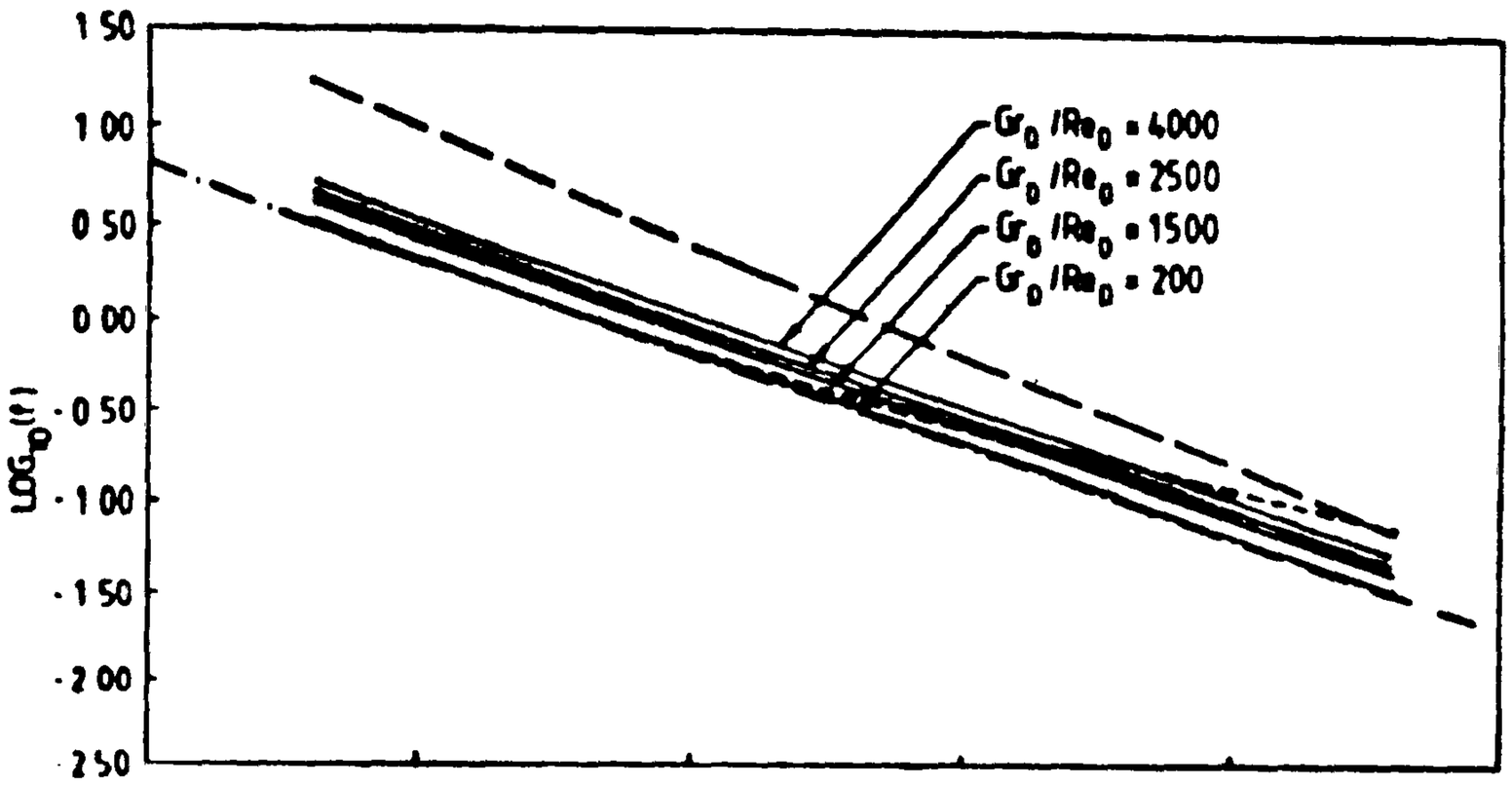
Gr_0/Re_0 = 4000
Gr_0/Re_0 = 2500
Gr_0/Re_0 = 1500
Gr_0/Re_0 = 200
$LOG_{10}(f)$

c)

Gr_0/Re_0 = 4000
Gr_0/Re_0 = 2500
Gr_0/Re_0 = 1500
Gr_0/Re_0 = 200
$LOG_{10}(f)$

d)

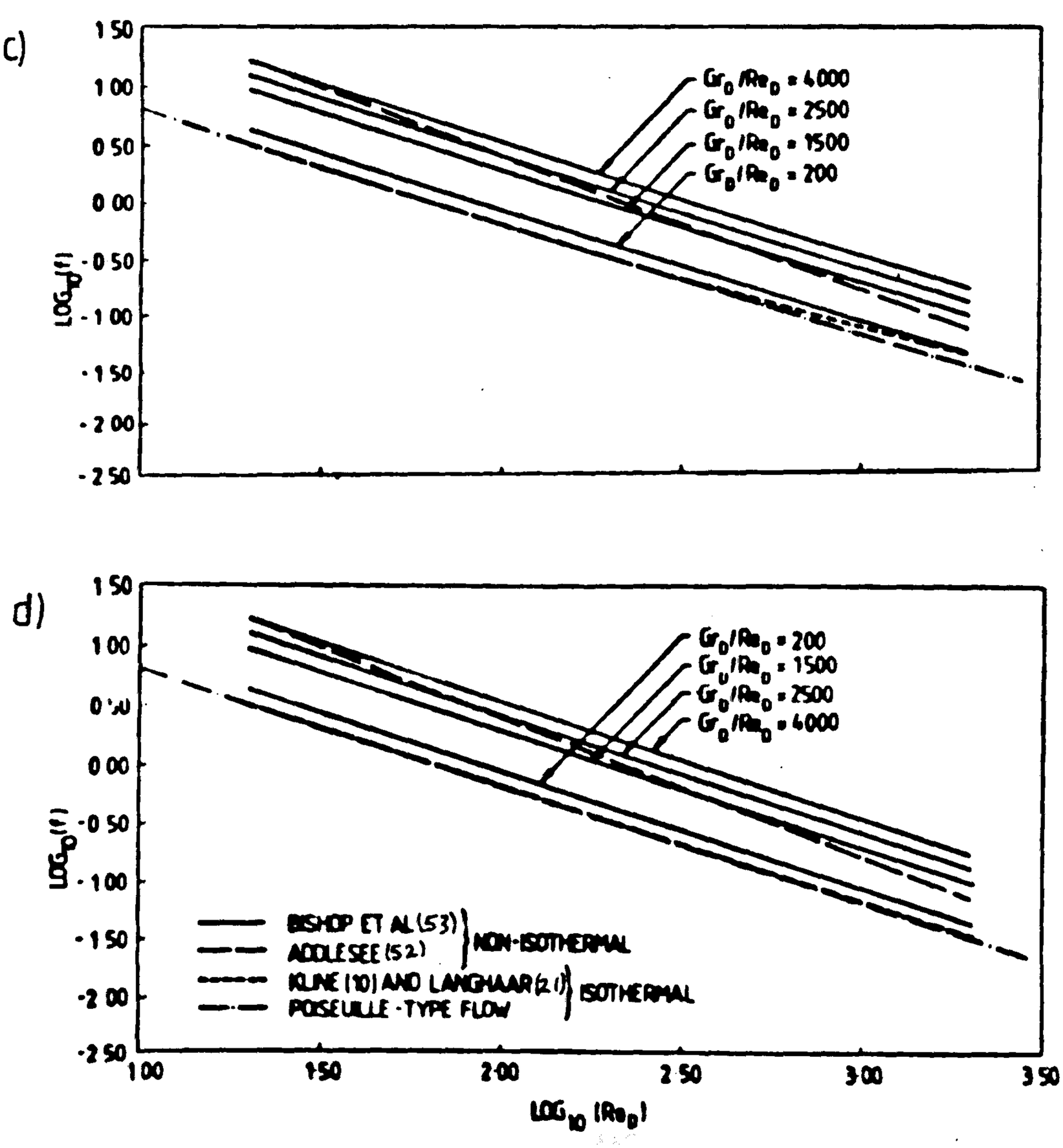
Gr_0/Re_0 = 200
Gr_0/Re_0 = 1500
Gr_0/Re_0 = 2500
Gr_0/Re_0 = 4000
BISHOP ET AL (53)
ADDLESEE (52)
NON-ISOTHERMAL
KLINE (10) AND LANGHAAR (21)
POISEUILLE - TYPE FLOW
ISOTHERMAL
$LOG_{10}(f)$
$LOG_{10}(Re_0)$

$$f(Re_D/64) = [1+2.97(Gr/Re_D)/1000)]^{0.655}$$

equation 7.12

Using experimentally-determined velocity-profile distribution data for different L/D locations, and a constant Gr/Re_D value of 465, the following correlation was obtained:-

$$f(Re_D/64) = 1 + 1.6\left[\frac{1}{1 + 0.36[50/(L/D)]^3}\right]$$

equation 7.13

Combining equations 7.12 and 7.13, Bishop et al (53) derived the expression

$$f(Re_D/64) = 1 + \frac{[1+2.97(Gr/Re_D)/1000]^{0.655} - 1}{1 + 0.36[50/(L/D)]^3}$$

equation 7.14

for $Gr/Re_D \leq 10^6$

When equation 13 was plotted for the two cases of L/D = 20 and L/D =∞, the region bounded by these two lines was shown (53) to contain 93% of the Kemeny and Somers data.

An important consequence of the L/D factor in equation 7.14 is that it results in the converse effect to that which occurs under isothermal conditions. Low values of L/D in non-isothermal developing flows act to reduce the apparent friction factor that would occur at equivalent Re_D and Gr/Re_D numbers under conditions of fully-developed non-isothermal flow.

At very low values of L/D (namely < 10), the friction factor is almost totally independent of the Gr/Re_D ratio. This is illustrated in figures 7.3(a) to 7.3(d) where equation 7.14 is plotted for different L/D values. In each case, four different Gr/Re_D ratios are shown, (Gr/Re_D = 200,1500,2500,4000). For the purposes of comparison the Addlesee correlation given in equation 7.11 and isothermal correlations are

also presented.

A shortcoming of using equation 7.14 is that as isothermal conditions are approached (ie. $Gr/Re_D \rightarrow 0$), the flow increasingly approxim ates to the fully-developed Poiseuille-type, regardless of the value of L/D. This is attributed to the L/D correction factor used (see equation 7.13) which is determined at a fixed value of Gr/Re_D and is assumed thereafter to be independent of temperature. Where near isothermal conditions exist, and L/D effects are likely to be significant, more accurate results would be expected using the isothermal correlations, that is equations 7.1, 7.7 and 7.8.

7.1.4 "Minor" losses

Few correlations for loss coefficients applicable to laminar fluid flow exist. Thus most flow loss coefficients for bends and tees, used in thermosyphon simulations, are based on the comparatively flat velocity profile associated with turbulent flow.

Integrating across a laminar velocity profile, the following relationship is obtained:

$$\int \frac{v^2 dV}{2g} = \int_0^R \frac{v^3 \pi r dr}{g} = \frac{2\bar{v}^2 V}{2g}$$

equation 7.15

The exact kinetic energy is therefore twice the value calculated using the mean velocity. It was thus sugested by Morrison and Ranatunga (14) that a 100% correction factor on the relevant turbulent loss coefficient should be employed.

An equation has been deduced (54) based on previous experimental studies (55,56) , that permits laminar flow losses in bends to be predicted for a wide range of flow rates and bend types. The resulting correlations are dependant on both Reynolds and Dean numbers and are given by:-

For Dn $\lesssim$ 13.5

$$K_{BEND} = 1.17\,\zeta(R/D)/Re_D$$

equation 7.16

For 13.5 $\lesssim$ Dn $\leq$ 463.5

$$K_{BEND} = 0.17\,\zeta\,(1+2R/D)(Re_D)^{-0.72} + (Dn - 13.5)/450$$

equation 7.17

For Dn > 463.5

$$K_{BEND} = 0.17\,\zeta(1+2R/D)(Re_D)^{-0.72} + 1$$

equation 7.18

where Dn is the Dean number defined as

$$Dn = Re_D(2R/D)^{-0.5}$$

equation 7.19

It was tentatively suggested (57) that branch-loss coefficients are independent of Reynolds number and a single correlation can be used based on mass flow rate alone. There does not however appear to be any experimental data to corroborate this assertion for laminar flows. A velocity dependent branch loss coefficient has been given by (58,59) as,

for dividing flow (see figure 7.4(a))

$$K_{TEE} = 0.792 - 0.304(\dot{m}_1/\dot{m}_3) + 0.723(\dot{m}_1/\dot{m}_3)^2$$

equation 7.20

and for confluent flow (see figure 7.4(b))

$$K_{TEE} = 0.062 + 1.207(\dot{m}_1/\dot{m}_3) - 0.761(\dot{m}_1/\dot{m}_3)^2$$

equation 7.21

K_{TEE} represents the branch loss coefficient in terms of the kinetic

FIGURE 7.4

Designation of fluid mass flows at tee junctions of pipes for

(a) dividing flow, and

(b) confluence:

m_1, m_2 and m_3 represent flows in the minor branch and in the confluent branch respectively.

(a)

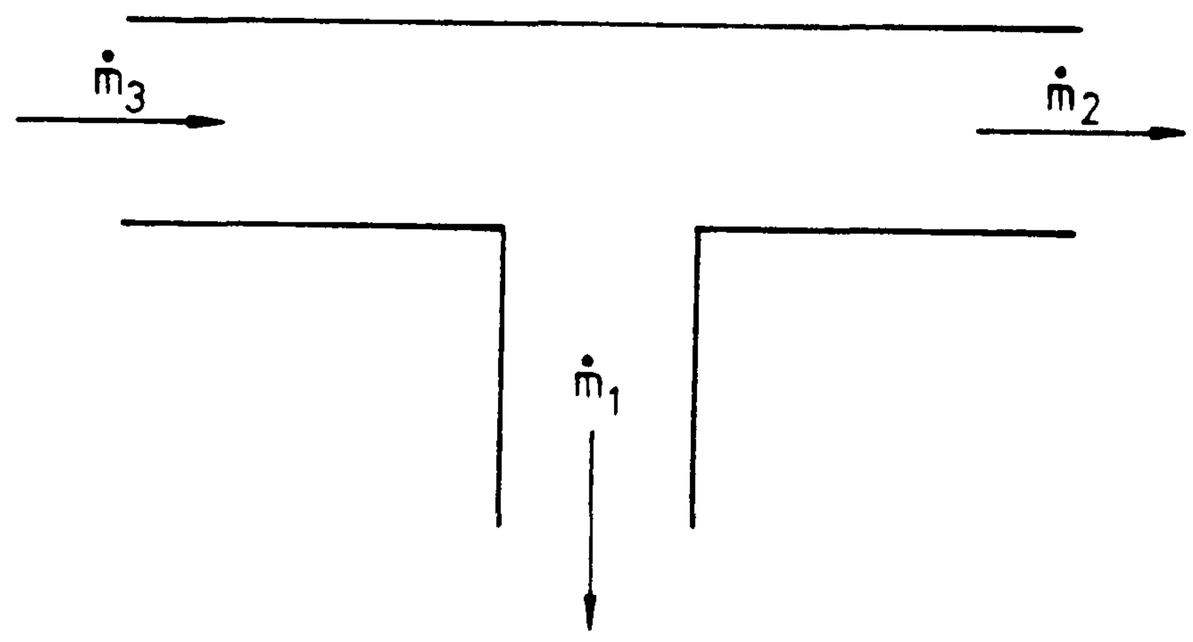

(b)

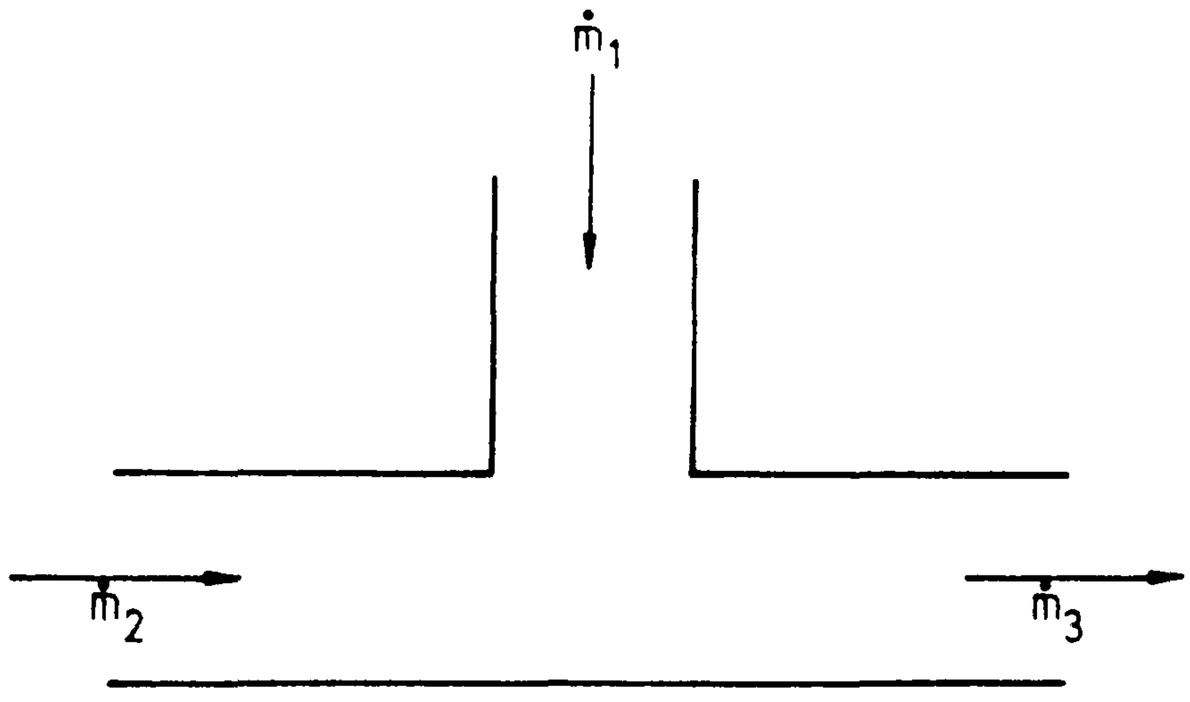

energy head of the flow approaching the branch (ie. in terms of $\dot{m}_3$ for dividing flow and $\dot{m}_2$ for confluent flow).

The applicability to thermosyphon system simulation models of the non-isothermal frictional flow loss relationships collated in this section were entirely uncorroborated. Where an attempt had been made to derive an expression for isothermal developing flow in the riser pipes of a collector (12), this expression was shown to be inconsistent with other available data and a new correlation was determined. The next step was therefore to determine by experimental validation, the most suitable of the available friction factor correlations.

7.2 Response of System to Step Function Under Conditions of Buoyancy Driven Circulation.

The collector inlet was disconnected from the mains water supply and directly coupled via the insulated downcomer pipe and flow meter, to the storage tank, thereby restoring the system to that described in section 4.1 and shown schematically in figure 7.5. Power was supplied in the form of a step function to the absorber plate heaters and the development of the resulting buoyancy-driven flow-rate, recorded. The computer simulation was run using simultaneously recorded operating conditions. By comparing the predicted and experimental values when an approximately constant flow rate had been attained, the appropriate frictional loss correlations for flow through the various pipe work components was established.

Flow within the insulated upriser and downcomer pipes was assumed to be isothermal and inreased frictional losses due to thermal destabilisation of the flow to be negligible. With the low buoyancy forces produced, the resulting flow was laminar and the data of Kline and Shapiro (44), and Langhaar (21) (represented by equations 7.1 and 7.7 respectively) have been used to cover the range of entrance Reynolds numbers, ($10^{-6} \leq (L/D)/Re_D < 5 \times 10^{-1}$), for which the flow is non-isothermal developing and laminar. For entrance Reynolds numbers greater than 5×10^{-1}, the frictional loss associated with Poiseuille-type flow and calculated from equation 7.9 is assumed. Attempts at including the data of Al-Nasri and Unny (49) represented by equation 7.8 resulted in a lack of continuity as the range of entrance Reynolds numbers progressed from that associated with Poiseuille-type flow to that of developing flow represented by Langhaar's data. The data of Al-Nasri and Unny being empirically determined may be more reliable, but unlike that of Langhaar, does not provide the necessary link between Poiseuille-type flow and developing flow at the lower range of entrance Reynolds number over which the correlation of Kline and Shapiro is valid. "Minor" frictional loss coefficients for laminar, isothermal flow in curved sections of the insulated connecting pipes, are taken from the Beck (55) and Kittredge (56) data represented by equations 7.16 to 7.18. Correlations, namely equations 7.20 and 7.21,

FIGURE 7.5

Schematic diagram of flows through the solar water heater under conditions of buoyancy-induced flow

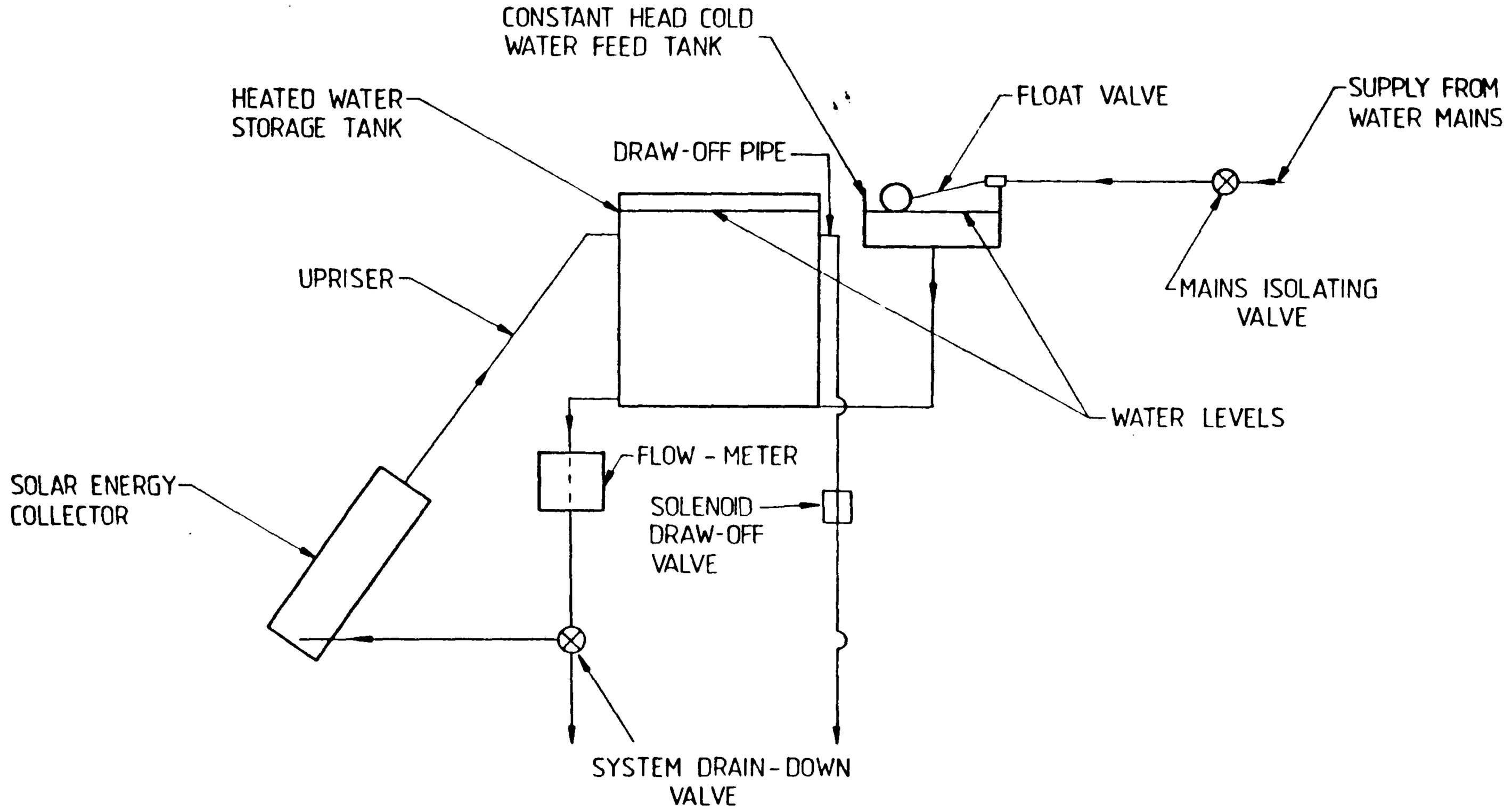
CONSTANT HEAD COLD
WATER FEED TANK
HEATED WATER
STORAGE TANK
DRAW-OFF PIPE
FLOAT VALVE
SUPPLY FROM
WATER MAINS
UPRISER
MAINS ISOLATING
VALVE
WATER LEVELS
FLOW - METER
SOLAR ENERGY
COLLECTOR
SOLENOID
DRAW-OFF
VALVE
SYSTEM DRAIN-DOWN
VALVE

presented in the Engineering and Science Data Units (58,59) are used to calculate frictional losses within tee sections.

The use of friction factor correlations for isothermal developing flow (21,44) in estimating frictional losses in the collector risers resulted in a predicted mass flow rate which was 20% higher than the measured value. The use of the Bishop et al (53) correlation for frictional losses under non-isothermal developing flow conditions given by equation 7.14 reduced the discrepancy between the predicted and measured mass flow rates to 12%. The correlation derived by Addlesee (52) (represented by equation 7.11) for friction factors as a function of Reynolds number alone for thermally destabilised flow was found to predict a loss coefficient for the risers which gave overall predicted flow rates agreeing with the experimental values to within 2% (see figure 7.6). The Addlesee correlation (52) was therefore retained in the computer simulation to calculate frictional losses in the riser pipes. Figure 7.7 shows a plot of the variations in the relative magnitudes of the mean calculated friction factors for the riser pipe over the period of the test based on identical experimental values of flow and temperature for the three sets of correlations, notably

i) developing isothermal flow (21,44),

ii) Bishops correlation for developing nonisothermal flow (53) and

iii) Addlesees equation for nonisothermal flow (52).

A step function of 600 Wm^{-2} was initially used in the test. However this was found to produce oscillations in the experimentally measured flow rate. These oscillations were caused by the low initial water flow-rate through the collector at the onset of the power step function. The low flow-rates cause high mean collector and upriser temperatures resulting in a corresponding high buoyancy induced pressure differential and the flow rate rapidly increases. As the flow rate increases, the mean collector and therefore the mean upriser temperature drop thereby reducing the buoyancy pressure differential. Consequently the flow-rate drops rapidly. This process is repeated until a combination of flow-induced frictional damping and reduced

FIGURE 7.6

Experimental and predicted buoyancy-induced mass flow rate in response to a thermal step input

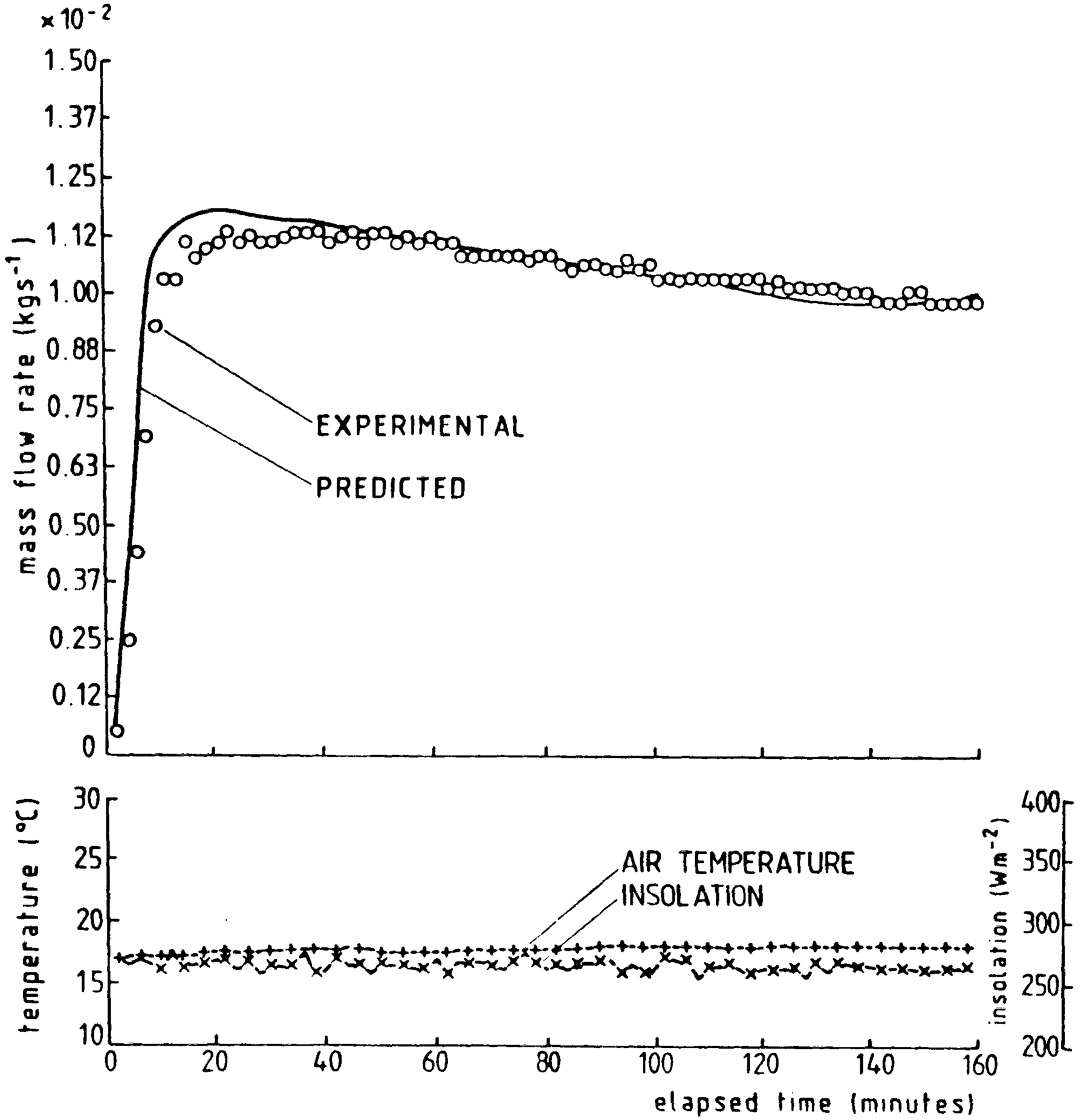
x 10⁻²
1.50
1.37
1.25
1.12
1.00
0.88
0.75
0.63
0.50
0.37
0.25
0.12
0
mass flow rate (kgs⁻¹)
EXPERIMENTAL
PREDICTED
30
25
20
15
10
temperature (°C)
AIR TEMPERATURE
INSOLATION
400
350
300
250
200
insolation (Wm⁻²)
0
20
40
60
80
100
120
140
160
elapsed time (minutes)

FIGURE 7.7

A comparison of calculated friction factors based on the measured mass flow rate in the period prior to steady state flow conditions.

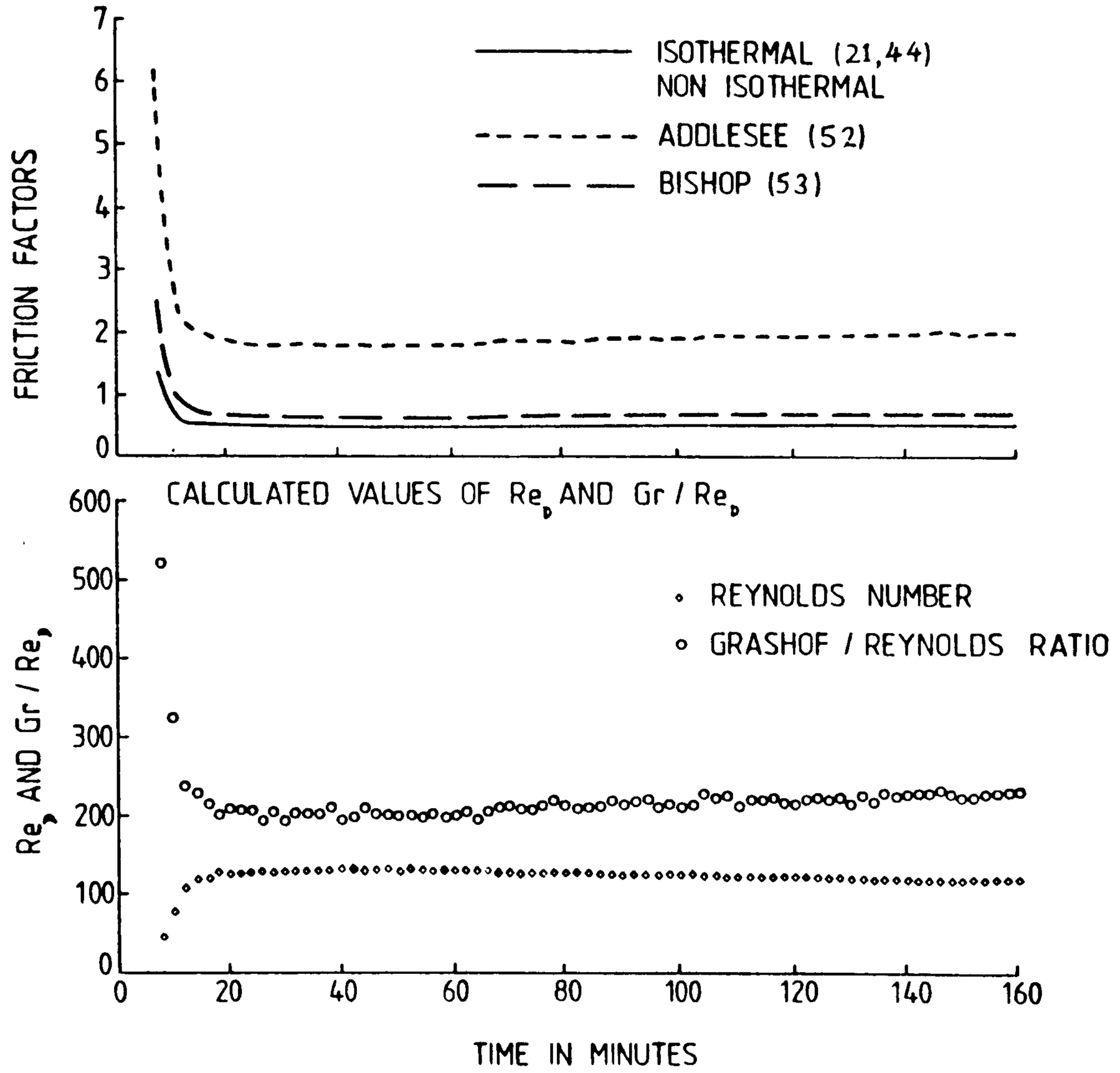
ISOTHERMAL (21,44)
NON ISOTHERMAL
ADDLESEE (52)
BISHOP (53)
FRICTION FACTORS
CALCULATED VALUES OF Re_D AND Gr / Re_D
REYNOLDS NUMBER
GRASHOF / REYNOLDS RATIO
Re, AND Gr / Re,
TIME IN MINUTES

buoyancy pressures due to the presence of warm water in the storage tank causes the oscillations to cease. A lower simulated insolation level of 300 Wm^{-2} was therefore used in the test. This had the effect of reducing the Reynolds numbers of the flows in the system thereby increasing the corresponding mean friction factors for each component. The increased damping meant that after rapidly reaching a maximum value (see figure 7.6), the flow rate gradually decreased as the cool water in the store was displaced by warmer water from the collector and the buoyancy forces integrated around the thermosyphon circuit decreased. Small oscillations were still discernable at this reduced step in the insolation level in both the experimental and predicted flow rates.

7.3 A Comparison of Measured and Predicted Results Using "Real" Insolation and Draw-Off Data.

Measured values of global insolation and water draw-off patterns were obtained from one of three occupied dwellings currently being monitored and which have been retro-fitted with thermosyphon solar-energy water-heaters (28). The measured insolation was simulated experimentally by regulating, via the microcomputer, the electrical power supply to the solar-collector heaters. Similarly, the thermal load on the system was experimentally reproduced by the controlled opening and closing of the solenoid valves giving a draw-off pattern equivalent to that produced by the occupants of the house. Identical operating conditions were used in the computer simulation and the variation of the predicted temperatures and flow rates over a 24 hour period were compared with the corresponding experimental values.

The measured global insolation values were recorded using a Kipp and Zonen type CM 5/6 solarimeter (Kipp and Zonen, Delft, Holland) mounted on, and in the plane of, the SSE-facing roof of one of the three houses being monitored. The recorded values are therefore those due to radiation incident on a plane at an angle (40°) to the horizontal. From the available data, a relatively clear day in early January was chosen. The total recorded incident solar radiation over this day was 11.111280 MJm^{-2}.

Water from the solar hot water store was drawn off by the occupants using a "third tap" system. This meant that in addition to the conventional hot and cold water tap in the house, a third tap was installed which allowed water to be tapped off directly from the solar store. The total mass of water drawn off by the occupants from this third tap on the day chosen, was 49 kg.

The thermosyphon solar energy water heater shown schematicly in figure 7.5 was used to simulate the chosen insolation and draw-off conditions. The test was run in "real time" so that an insolation value recorded at a particular time of day was simulated experimentally at the corresponding time. This ensured a more realistic variation in the ambient temperature (of the laboratory) which varied sinusoidally over the day. The experiment was started-up at approximately mid-day and allowed to run until 24-00 hours of the same day before the monitoring commenced. The performance was then monitored and the results recorded over a 24 hour period.

Figure 7.8 shows the variation of the experimental and predicted mean store temperatures over the day when the values of the imposed insolation and draw-off patterns and the measured ambient and mains temperature are used as input data to the computer simulation. The predicted mean store temperatures agree to within a mean deviation of 0.4^{o}C of the corresponding measured values over the period being simulated. The highest deviation from this mean error value is at 7-30 hours, just before the onset of the insolation period when the predicted store temperature drops to 0.8^{o}C below the corresponding measured value. During the period between 0-00 and 7-30 hours, reverse circulation occurs and the mean predicted Reynold number of the flow is approximately 10 - a value well below the stated minimum in the range for which the friction factor correlations are valid. This has evidently resulted in an under-estimate of the frictional losses at such low Reynolds numbers and consequently the reverse flow rate is higher than the actual value giving higher predicted over-night thermal losses.

Good agreement is shown between the measured and predicted solar collector inlet and outlet temperatures over the duration of the

FIGURE 7.8

Experimental and predicted diurnal variations within a thermosyphon solar energy water heater under "real" operating conditions, of

(a) mass flow rate

(b) mean store temperature, and

(c) collector inlet and outlet temperatures

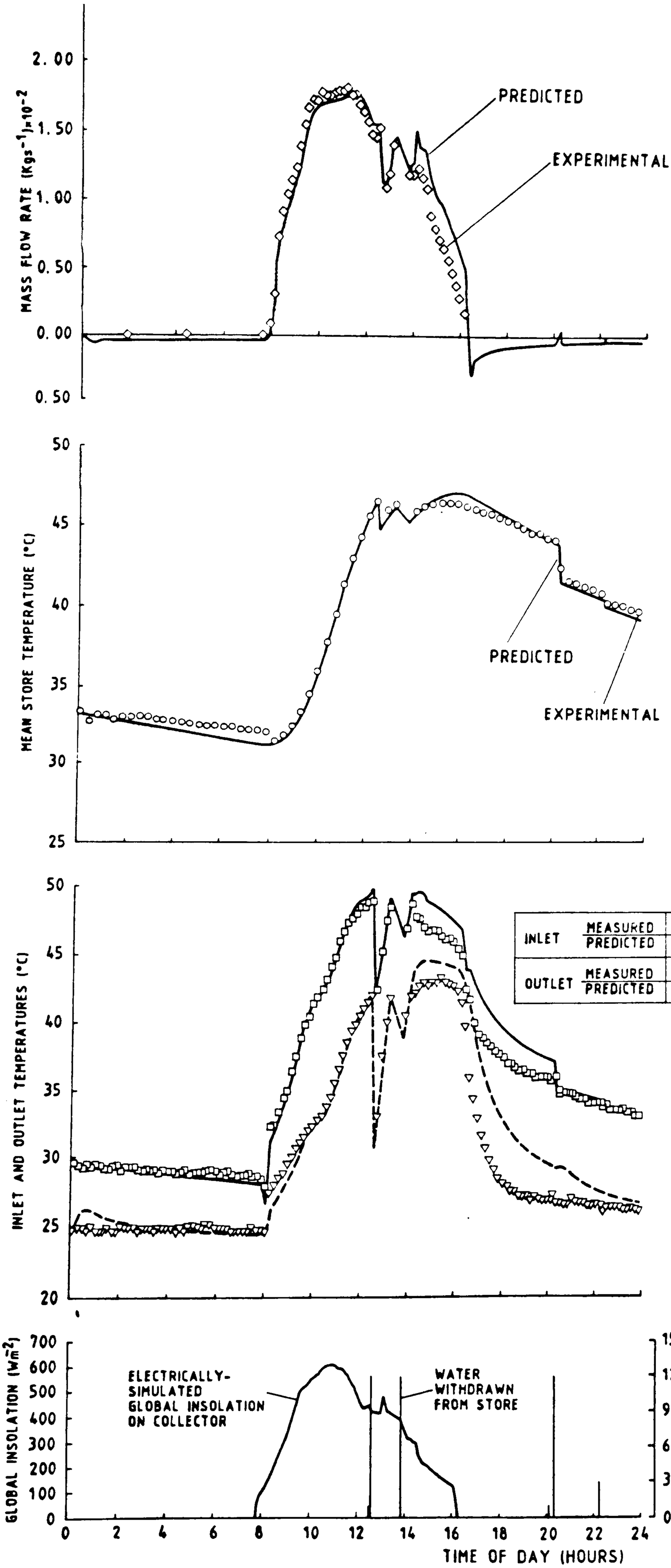
MASS FLOW RATE (Kgs⁻¹)x10⁻²
2.00
1.50
1.00
0.50
0.00
0.50
PREDICTED
EXPERIMENTAL
MEAN STORE TEMPERATURE (°C)
50
45
40
35
30
25
PREDICTED
EXPERIMENTAL
INLET AND OUTLET TEMPERATURES (°C)
50
45
40
35
30
25
20
INLET
MEASURED
PREDICTED
OUTLET
MEASURED
PREDICTED
GLOBAL INSOLATION (Wm⁻²)
700
600
500
400
300
200
100
0
ELECTRICALLY-SIMULATED GLOBAL INSOLATION ON COLLECTOR
WATER WITHDRAWN FROM STORE
MASS OF WATER DRAWN-OFF (kg)
15
12
9
6
3
0
0
2
4
6
8
10
12
14
16
18
20
22
24
TIME OF DAY (HOURS)

insolation period (see figure 7.8). After the termination of the insolation period, the predicted differences between collector inlet and outlet temperatures ($T_{c,o} - T_{c,in}$) are significantly lower than the experimental values. This was consistant with the previously indicated higher predicted reverse flow rates. However, to put these temperature discrepancies into perspective, although the predicted value of $T_{c,o}-T_{c,i}$ in the hour immediately after sun set was $5^{o}C$ compared with a measured value of $7.5^{o}C$, because the (predicted) reverse flow rate at this time is 0.0008 kgs^{-1} the resulting difference between the measured and predicted rate of heat loss from the store is approximately only 8.36 W.

The predicted flow rates shown in figure 7.4 correspond to within a mean deviation of 7% of the measured values over the insolation period. Values of measured flow rate were not recorded during periods of reverse circulation as "signal cut-off" by the inductive flowmeter occurs below a minimum value corresponding to a positive flow rate of 10^{-4} kgs^{-1}.

The large fall-off and subsequent recovery in the measured flow rate immediately after water had been drawn off from the store was correctly predicted by the analysis. This reduced flow rate occurs as the water drawn off is replenished by cooler water at the mains supply temperature being introduced at the base of the store. This cooler fluid enters the collector and the resulting increase in fluid density in the risers and upriser pipes reduces the pressure differential between the fluid in these components and that of the store. A subsequent fall in the flow rate ensues. The reduced flow rate causes fluid temperatures in the collector to increase; the fluid density falls and a higher flow rate is rapidly restored. Similarly, a decrease in the predicted reverse flow rate occurs when water is drawn off and may briefly induce forward circulation as was observed in both the predicted and measured flow rates immediately following the 12 kg draw-off made at approximately 20-20 hours.

The thermal output of a solar water heater as water is withdrawn from the store is calculated from

$$Q_{sol} = M_L C_w (\bar{T}_{s,L} - T_m)$$

equation 7.22

where $\bar{T}_{s,L}$ is the mean temperature of the draw-off water. The total measured thermal output due to the seven draw-offs made over the day was measured as 4.27 ($\pm$0.06) x 10^6J. The corresponding predicted value was 4.39 x 10^6J. The predicted output although not within the uncertainty ($\pm$1.4%) associated with determining the corresponding measured value was nevertheless in good agreement, the discrepancy between the two values being 2.8%.

CHAPTER EIGHT

THE INITIAL DEVELOPMENT AND PRACTICAL TESTING OF A TECHNIQUE FOR CORRELATING THE DAILY PERFORMANCES OF THERMOSYPHON SOLAR ENERGY WATER HEATERS

8.1 Previous Methods Used in Correlating the Performances of Thermosyphon Solar-Energy Water-Heaters

The identification of basic grouped parameters from which the thermal characteristics of different systems can be determined using the minimum amount of data (experimentally-measured or generated from high level numerical simulations) provides a practical means of determining long-term system performance.

Such an approach for forced circulation solar water heaters, namely the "f-chart" method, upon which some subsequent correlations for thermosyphon systems have been based, was pioneered by Klein et al (61). This analysis was derived from a basic heat balance on an entire solar water heating system represented schematically by the Sankey diagram given in figure 8.1.

The net change of internal energy (predominantly of the store) was assumed to be negligible, an assumption which becomes more valid as the period of integration increases. The solar fraction for a forced circulation system was found to be related to two main parameters X' and Y' defined by

$$X' = A_c F_R U_L (T_{ref} - T_a)\Delta t / Q_{tot} \quad \text{and}$$

equation 8.1

$$Y' = A_c F_R (\tau\alpha)_e H^{tm} / Q_{tot}$$

equation 8.2

where Q_{tot} was the total monthly hot water energy consumption and T_{ref} (= 100°C) an arbitrary reference temperature.

Similar parameters were derived by Liu and Hill (62) but with the mean monthly water supply temperature as the reference temperature.

The f-chart analysis is not directly applicable to thermosyphon systems as the circulating fluid flow rate and therefore the heat removal factor F_R is not constant. A modification of the f-chart method to acount for the variation of F_R with system configuration and operating

FIGURE 8.1

Sankey diagram of the heat flows into and out of a solar energy water heater

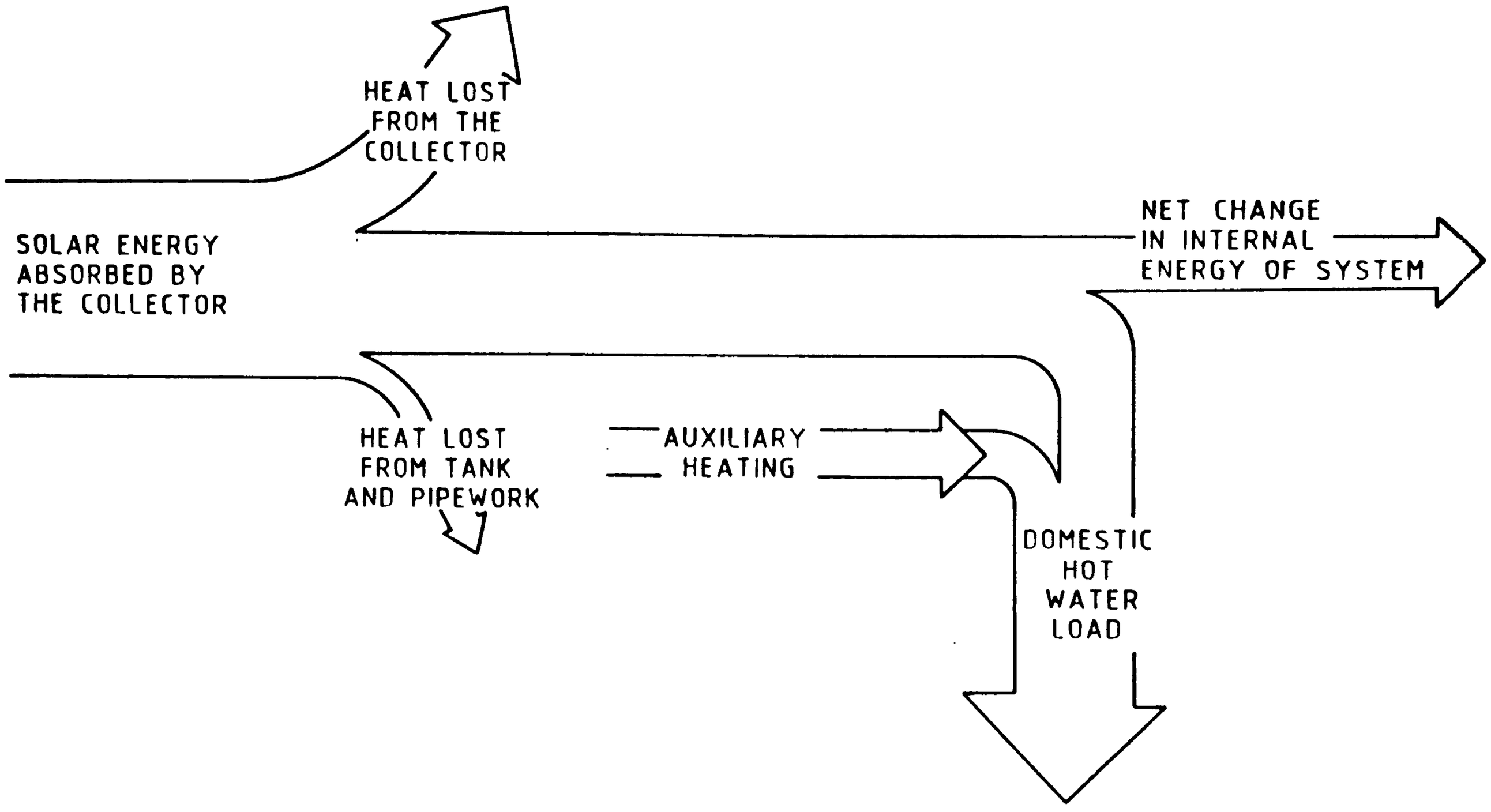
HEAT LOST
FROM THE
COLLECTOR
SOLAR ENERGY
ABSORBED BY
THE COLLECTOR
NET CHANGE
IN INTERNAL
ENERGY OF SYSTEM
HEAT LOST
FROM TANK
AND PIPEWORK
AUXILIARY
HEATING
DOMESTIC
HOT
WATER
LOAD

conditions encountered in thermosyphon solar water heaters has been proposed by Malkin et al (6). The following iterative algorithm is employed;

i) A mean monthly flow rate is assumed from which F_R is calculated and an estimate of the solar fraction obtained using the conventional f-chart method.

ii) From a correlation of mean store temperature against solar fraction (developed using the simulation program, TRNSYS (63)) a mean monthly mean store temperature is then determined.

iii) The degree of stratification based on an analysis by Phillips and Dave (64) enables a mean monthly collector inlet temperature to be calculated from the mean store temperature.

iv) The mean monthly collector outlet temperature can then be determined thereby giving a complete estimate of the temperature variation around the system.

v) Using these temperatures the net buoyancy pressure can be found and by equating this with the fluid frictional losses, a new estimate of the mean monthly flow rate is calculated.

vi) The process is then repeated using the most recent flow rate until the solar fraction calculated in step (i) converges to a constant value.

A comparison between the annual solar fraction predicted using TRNSYS (in thermosyphonic mode) and the value calculated from the modified f-chart indicated agreement to within an RMS error of 2.6%.

Morrison and Sapsford (4) correlated the experimental results obtained from a number of representative thermosyphon solar-energy water-heaters using the non-linear relationship,

$$f' = a(H/Q_{tot}) + b(H/Q_{tot})^2 + c(T_L - T_a)/Q_{tot}$$

equation 8.3

where T_L is the required delivery temperature of the hot water.

The coefficients a, b and c were determined by a least squares correlation of the monthly average data for each system. In order to reduce scatter of the data due to residual energy in the store, mean values of H and Q_{tot} evaluated over a minimum period of integration of ten days was required. At least three months of these averaged values were required to produce a characteristic curve. This characteristic curve was found to be valid only within a narrow band corresponding to the values measured during the test procedure. The curve produced by equation 8.3 is only representative of the performance of the system under test and the results cannot be extrapolated to predict the performance of other systems. As with the f-chart correlations, implicit in this analysis is the assumption that any water consumed is heated in part by the solar hot water system. This is not always the case as systems are sometimes employed (28) whereby in addition to the conventional hot and cold taps, a "third tap" is installed with which water can be drawn directly from the solar store.

More recently, the so-called "Input/Output" method has been gaining popularity in Europe and Australia as a standard test method for determining the performances of individual systems (both forced and buoyancy-driven) based on a relatively small number of short-term tests. The technique involves identifying the climatic parameters which affect system performance and carrying out a series of tests in which the thermal performances (the outputs) are measured when only one of these parameters (the inputs) are varied. Morrison and Tran (65) used H/Q and $(T_L - T_m)/Q_{tot}$ as the primary climatic parameters and investigated the functional relationship between these parameters using the TRNSYS (63) simulation model. By maintaining $(T_L - T_a)/Q_{tot}$ at constant values, a linear relationship was observed between the measured solar fraction, f' and H/Q_{tot}. A series of linear curves were produced for different values of $(T_L - T_m)/Q_{tot}$. Both the gradients and ordinate intercepts of these curves were themselves a linear function of $(T_L - T_m)/Q_{tot}$. So for the purposes of determining the long term performance of a system, the solar fraction of the particular system can be expressed in the form

$$f' = a + [b(T_L - T_m)/Q_{tot}]H/Q_{tot} + c(T_L - T_m)/Q_{tot}$$

equation 8.4

As with previous techniques, the results have to be averaged over a period of days (between 5 and 15) in order that the difference in the internal energy of the store between the beginning and end of the test period is small compared with the total heat delivered by the system. An advantage of this as an individual test technique, but a disadvantage as an approach to producing correlation charts with a more universal application, is that all exogenous system parameters are implicit in the constants a, b and c. This test method is currently in the process of being adopted by the Standards Association of Australia (66).

Two further refinements in the use of Input/Output test data in determining long term system performance have been proposed by Collares-Pereira (67). Energy "carry-over" due to unused hot water in the store at the end of the period for which the thermal performance is to be determined is approximated by a store temperature based on prevalent insolation levels and ambient temperatures. Also, more representative performance data is predicted from the experimentally determined Input/Output characteristics by modifying the thermal output calculated from mean measured meteorological data. This is acheived using a function which describes the probability of obtaining solar radiation values between zero and the maximum possible for that location and time of year. This probability function has been shown to correlate strongly with the local clearness index, K_s when averaged over one month or longer.

A method of determining the performance of thermosyphon solar water heaters based on predicted or measured daily rather than monthly data has been proposed by Song and Zhang (3). This has the advantage that the amount of data required to characterise the thermal performance of the system is greatly reduced. The system is characterised by the theoretical diurnal variation of the steady-state mean store temperature that would exist if the thermal capacitance of the water store was negligible and a sinusoidal insolation pattern is assumed.

The actual mean store temperature only corresponds to the steady-state value when the minimum or maximum diurnal temperatures occur towards (ideally) the onset and end respectively of the insolation period. The mean store temperature variation is then approximated by fitting a simple sinusoidal function such that the characteristic steady-state curve is intercepted at the time of day at which the minimum and maximum temperatures occur. The time of day at which minima and maxima occur are also expressed in a graphical form as functions of basic system parameters. The analysis used to produce these correlation charts for thermosyphon systems was similar to that used by Close (7) and therefore suffers from the same limitations - primarily that accurate mean store temperature prediction depends on the assumption of identical mean store and collector temperatures. In estimating the amount of heat capable of being delivered by the system, the draw-off of solar water from the store is assumed to take place at the end of the insolation period.

The above literature review on correlation techniques suggested further developments in the following areas.

i) A method of correlating performance data had to be developed in which the amount of required data would be considerably reduced. This would make feasable the use of the numerical model in determining long term thermal performance.

ii) The identification of grouped system parameters which are specific to thermosyphon solar water heaters would provide a step towards a more universal set of correlations for these systems and a move away from the current practice (6) of employing a cumbersome and over simplified iterative method in determining the buoyancy driven flow rate for use in a modified f-chart design procedure.

iii) The development of an analysis in which the thermal output depends on the amount of water withdrawn from the store rather than simply the amount of energy incident on the collector. This would result in a design technique in which the applicability can be widened to include third tap as well as preheat methods of hot water delivery.

8.2 The Derivation of an Initial Analysis.

To identify daily system thermal performance parameters for thermosyphon solar energy water heaters which could be correlated, a simplified analysis representative of the primary heat transfer processes within a generic system was undertaken. It was envisaged that such an analysis would

(i) be amenable to an algebraic solution, and

(ii) be of sufficient sophistication for a reasonable approximation of the thermal performance of the system to be gained from the resulting solution to the governing equations.

It was intended that the solar fraction, G, calculated using this simplified analysis would be correlated with the true solar fraction, f', to produce in effect a correction factor for the approximate analysis. A transient heat balance was carried out on a generic solar energy water heater system (see figure 8.2).. By making some basic simplifying assumptions relevant to natural-circulation systems, a first-order differential equation was obtained from which an explicit algebraic solution could be found. A simpler analysis than the following and containing some of the assumptions outlined below was carried out by Place et al (68), but used for predicting, directly, diurnal system performance rather than to establish correction factors. The following assumptions have been made.

i) The collector and storage tank both have the same mean temperature. This assumption is based on experimental observations made originally by Close (7) on multiple pass thermosyphon solar hot water systems.

ii) Upriser and downcomer pipe heat losses are negligible.

iii) Ambient and mains water temperatures are assumed to remain invariant at their respective mean measured values.

iv) The initial store temperature at the onset of the insolation period

FIGURE 8.2

Holistic heat transfer mechanisms for a generic thermosyphon solar-energy water heater

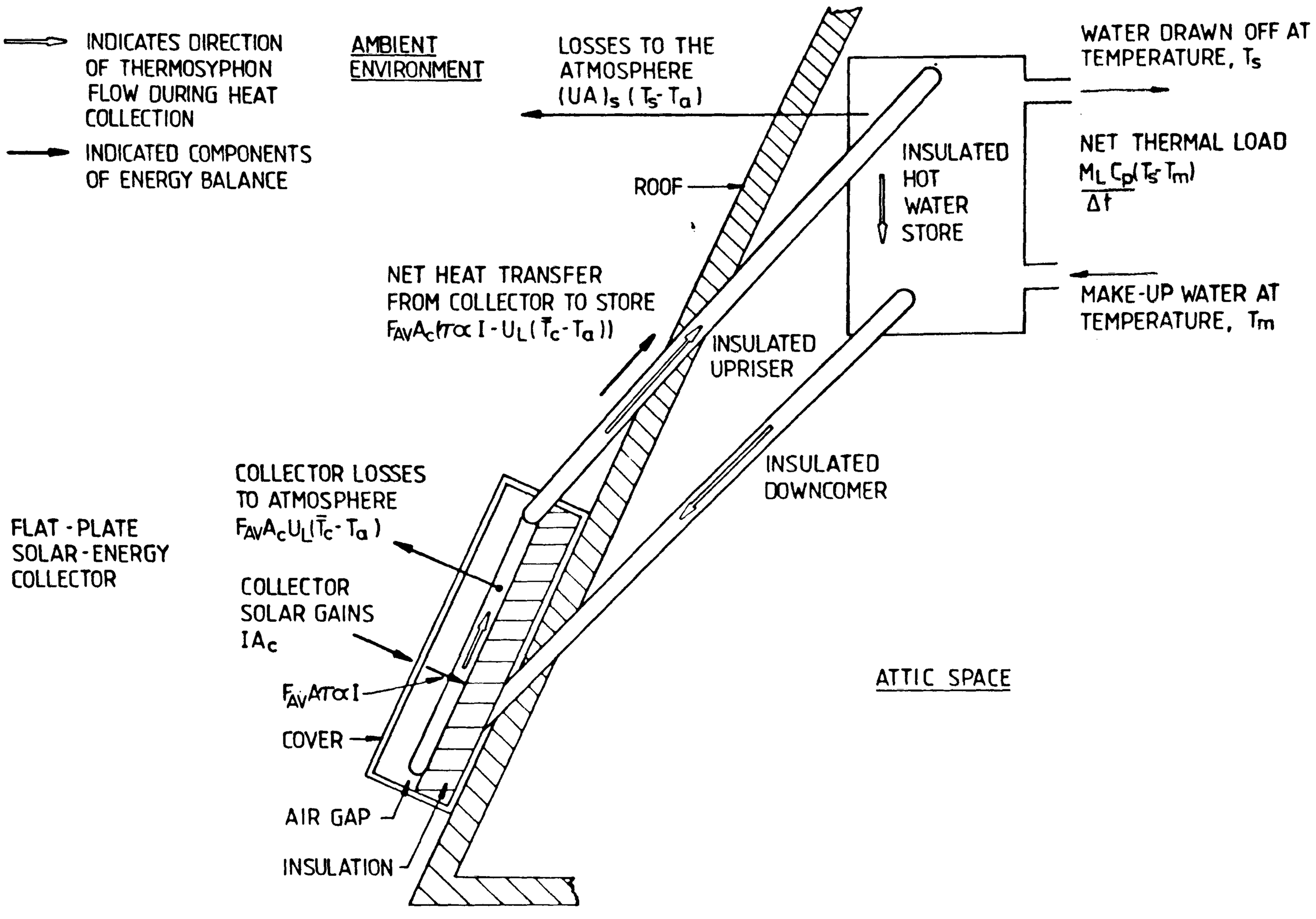
INDICATES DIRECTION OF THERMOSYPHON FLOW DURING HEAT COLLECTION
INDICATED COMPONENTS OF ENERGY BALANCE
AMBIENT ENVIRONMENT
LOSSES TO THE ATMOSPHERE
$(UA)_s (T_s - T_a)$
WATER DRAWN OFF AT TEMPERATURE, T_s
NET THERMAL LOAD
$\frac{M_L C_p (T_s - T_m)}{\Delta t}$
ROOF
INSULATED HOT WATER STORE
NET HEAT TRANSFER FROM COLLECTOR TO STORE
$F_{AV} A_c (\tau\alpha I - U_L (\bar{T}_c - T_a))$
INSULATED UPRISER
MAKE-UP WATER AT TEMPERATURE, T_m
INSULATED DOWNCOMER
COLLECTOR LOSSES TO ATMOSPHERE
$F_{AV} A_c U_L (\bar{T}_c - T_a)$
FLAT-PLATE SOLAR-ENERGY COLLECTOR
COLLECTOR SOLAR GAINS
IA_c
$F_{AV} A \tau\alpha I$
COVER
AIR GAP
INSULATION
ATTIC SPACE

is equal to the mean mains water supply temperature.

v) Water is drawn-off at the mean storage tank temperature.

vi) The total draw-off is assumed to take place at a constant rate over the period of insolation. By introducing the mass of water drawn off as an independent parameter, the analysis is as applicable to 'third tap' as to preheat systems.

vii) The solar radiation intensity, I, is assumed to vary sinusoidally over the duration of the insolation period.

viii) Heat losses due to reverse circulation during the night are negligible.

A heat balance on the system gives

$$M_s C_w \frac{d\bar{T}_s}{dt} = F_{AV}[(\tau\alpha)_e I - U_L(\bar{T}_c - T_a)] - (UA)_s(\bar{T}_s - T_a) - \dot{q}_L$$

equation 8.5

but using assumption (i),

$$\bar{T}_c = \bar{T}_s$$

equation 8.6

The sinusoidal function of assumption (vii) relates total daily radiation incident on the collector by

$$I = (H^{td}/\Delta t)(\pi/2)\sin(\pi t/\Delta t)$$

equation 8.7

Also from (iii),

$$T_a = \bar{T}_a$$

equation 8.8

Using (v) and (vi), the instantaneous load is given by

$$\dot{q}_L = \frac{M_L C_w}{\Delta t} (\bar{T}_s - T_m)$$

equation 8.9

Substituting equations 8.6 to 8.9 into equation 8.5 gives

$$M_s C_w \frac{d\bar{T}_s}{dt} = \frac{F_{AV} A_c (\tau\alpha)_e H^{td} \sin(\pi t/\Delta t)}{2\Delta t} - [F_{AV} A_c U_L + (UA)_s](\bar{T}_s - \bar{T}_a) - \frac{M_L C_w}{\Delta t}(\bar{T}_s - T_m)$$

equation 8. 10

Equation 8.10 can be made dimensionless by defining dimensionless time and temperature as

$$t' = \pi t/\Delta t$$

equation 8.11

and

$$T' = (\bar{T}_s - \bar{T}_a)/(\bar{T}_a - T_m)$$

equation 8.12

so equation 8.10 becomes

$$\frac{dT'}{dt'} + \frac{[F_{AV} A_c U_L + (UA)_s]\Delta t}{M_s C_w} + \frac{M_L}{M_s} T' = \frac{F_{AV} A_c (\tau\alpha)_e H^{td} \sin t'}{2 M_s C_w (T_a - T_m)} - \frac{M_L}{M_s}$$

equation 8. 13

Three dimensional groups therefore emerge at this stage, these being

$$W = \frac{M_L}{M_s} = \frac{\text{MASS OF WATER WITHDRAWN FROM STORE}}{\text{TOTAL MASS OF WATER IN STORE}}$$

equation 8.14

$$Y = \frac{F_{AV} A_c H^{td}}{M_s C_w (T_a - T_m)} = \frac{\text{TOTAL DAILY INSOLATION ABSORBED BY PLATE}}{\text{CHANGE IN INTERNAL ENERGY OF STORE WHEN RAISED FROM MAINS TO AMBIENT TEMPERATURE}}$$

equation 8.15

$$Z = \frac{[F_{AV}A_cU_L+(UA)_s]\Delta t}{(M_LC_w)} = \frac{\text{TOTAL DAILY COLLECTOR AND STORE HEAT LOSS}}{\text{THERMAL CAPACITANCE OF WATER IN STORE}}$$

equation 8.16

Substituting the dimensionless groups W, Y and Z into equation 8.11 gives the dimensionless first order differential equation

$$\frac{dT'}{dt'} + [(V+W)/\pi]T' = (Y/2)\sin t' - W/\pi$$

equation 8.17

Solving equation 8.17 for the dimensionless store temperature T' at any instant t' and applying the boundary condition given by assumption (iv) gives

$$T' = \left[T^i + \frac{(Y/2)\pi^2}{\pi^2 + (V+W)^2} + \frac{W}{(V+W)}\right]\exp[-(V+W)t'] + \frac{(R/2)\pi^2}{\pi^2 + (V+W)^2}\left[\frac{(V+W)}{\pi}\sin(t') - \cos(t')\right] - \frac{W}{(V+W)}$$

equation 8.18

The useful heat delivered by the solar hot water system is

$$Q_{sol} = \frac{M_LC_w}{\Delta t}\int_{t=0}^{\Delta t}(T_s - T_m)dt$$

equation 8.19

If a dimensionless total load factor, Q_{tot}' is defined as

$$Q_{tot}' = \frac{Q_{tot}}{M_sC_w(\bar{T}_a - T_m)}$$

equation 8.20

then the solar fraction, G as predicted by this model will be

$$G = \frac{W}{\pi Q_{tot}'}\int_{t'=0}^{\pi}(T' + 1)dt'$$

equation 8.21

This integral was then evaluated by substituting for T' from equation 8.18 to give

$$G = \frac{W}{Q_{tot}'}\left[\frac{[1 - e^{-(Z + W)}]}{(Z + W)}\left(\frac{(Y/2)\pi^2}{\pi^2 + (Z + W)^2} + \frac{W}{(Z + W)} - 1\right) + \frac{Y(Z + W)}{\pi^2 + (Z + W)^2} - \frac{W}{(Z + W)} + 1\right]$$

equation 8.22

8.3 Using Experimentally-Measured Data to Test the Correlation Technique

As a precursory step, the correlation of the dimensionless parameters W, Y and Z by the function expressed in equation 8.22 was tested using data measured experimentally from the monitoring of a thermosyphon solar energy water heater under conditions of normal domestic usage and the range of climatic conditions associated with an annual seasonal cycle of weather in the U.K. By using this large bank of readily-available data, the viability of correlating performance data on a daily basis using equation 8.22 was established before embarking on a large number of costly and time consuming computer runs using the detailed numerical simulation. Further, this initial study provided pointers leading to modifications. The implementation of the latter provided the basis of an improved and extended analysis.

The data was collected from the monitoring of three basically-identical thermosyphon solar-energy water-heaters retro-fitted to three adjacent occupied houses in Wharley End, Bedfordshire (28). The systems employed both differing frost-protection and heat-delivery strategies. Because of the availability of data due primarily to the reliability of the system, the results of the indirectly-heated solar water heater have been used to investigate the veracity of the analysis presented in the previous section. In this system, an aqueous solution with 35% by volume propylene-glycol flowed through a closed circuit comprising the collector, a single-wall heat exchanger in the hot water store, and the connecting pipes. The collectors consisted of two single-glazed selectively-coated flat-plate absorbers each of two square meters

aperture area, and manufactured from light gauge copper. The collector units were mounted on the roof tiles with fixing bolts through the rafters. An external view of of the installation is shown in figure 8.3. The collectors were linked by 25 mm internal-diameter flow and return pipes to a two hundred litre unpressurised hot-water store located in the apex of the loft space, together with a twelve litre cold water header tank. A second header tank connected to the primary circuit of the heat exchanger acted as the glycol make-up tank. A supply pipe provided solar-heated water to additional "third taps" located above the kitchen sink, the bathroom wash basin and the bath.

The temperatures of the following were measured at regular intervals;-

(i) the outside ambient environment,

(ii) the solar heated water at five equidistant locations along the vertical axis of the store,

(iii) the collectors inlet and outlet, and

(iv) the cold water mains.

All the temperatures were measured using copper/constantan thermojunctions. The global insolation incident on the plane of the collectors is measured with a Moll-Gorzynski pyranometer inclined appropriately. In addition, when hot water was used, the temperatures and volumes of water withdrawn from the solar-energy water-heater, the conventional water heating system and the cold water supply were measured using thermojunctions and turbine flowmeters.

The data logging was accomplished by a modular system in which a BBC Model B microcomputer was used in conjunction with a multi-application peripheral system (MAPS) manufactured by Harlyn Automation. Both the computer and this peripheral were equipped with the IEEE-488 instrument interface. The data acquisition software was developed to collect sensor readings at regular intervals (eg. half hourly) and at the beginning and end of any hot water draw-off, with the data then being stored on a floppy disk.

FIGURE 8.3

External view of installed thermosyphon solar-energy water heaters

The values of the mean ambient and mains water supply temperature and the total insolation and mass of solar water drawn off from the store were calculated from the available data in order to determine the daily values of the dimensionless groups W, Y and Z defined by equations 8.14, 8.15 and 8.16 respectively. The daily solar fraction, $(f')^{td}$, was determined from

$$(f')^{td} = \sum \frac{M_L C_w (\bar{T}_{S,L} - T_m)}{Q_{tot}}$$

equation 8.23

where $\bar{T}_{S,L}$ is the mean temperature of all the axially-placed thermocouples in the store contained within a distance from the top of the store corresponding to the volume of the water withdrawn. The duration of the insolation period t was calculated using the method outlined by Duffie and Beckman (23).

Using the experimental data collected, calculated values of the solar fraction function, G, using equation 8.22 when plotted against the measured solar fraction, $(f')^{td}$ as defined in equation 8.23 gave a good correlation over the period for which the data was available at the time (18th June 1985 to 30th December 1985). The correlation (shown in figure 8.4) has a correlation coefficient of 0.97. From the best fit straight line a correction coefficient could be determined that relates the actual solar fraction to be delivered by the system to that predicted by the above analysis, such that

$$(f')^{td} = 0.836G$$

Despite these encouraging results, this approach was found to have limitations when applied to other systems. The particular indirect thermosyphon solar-energy water-heater investigated was a multiple-pass system in which the assumption of equal mean store temperatures of the store and collector would be valid. Limited data available from the other two direct systems indicated excessive flow restrictions whithin the thermosyphoning loop resulting in predominantly non-linear temperature profiles within the stores. The measured solar fractions

FIGURE 8.4

Initial correlation of measured daily solar fraction $(f')^{td}$ with predicted value G for an indirect solar energy water heater over a period from 18th June to the 30th December

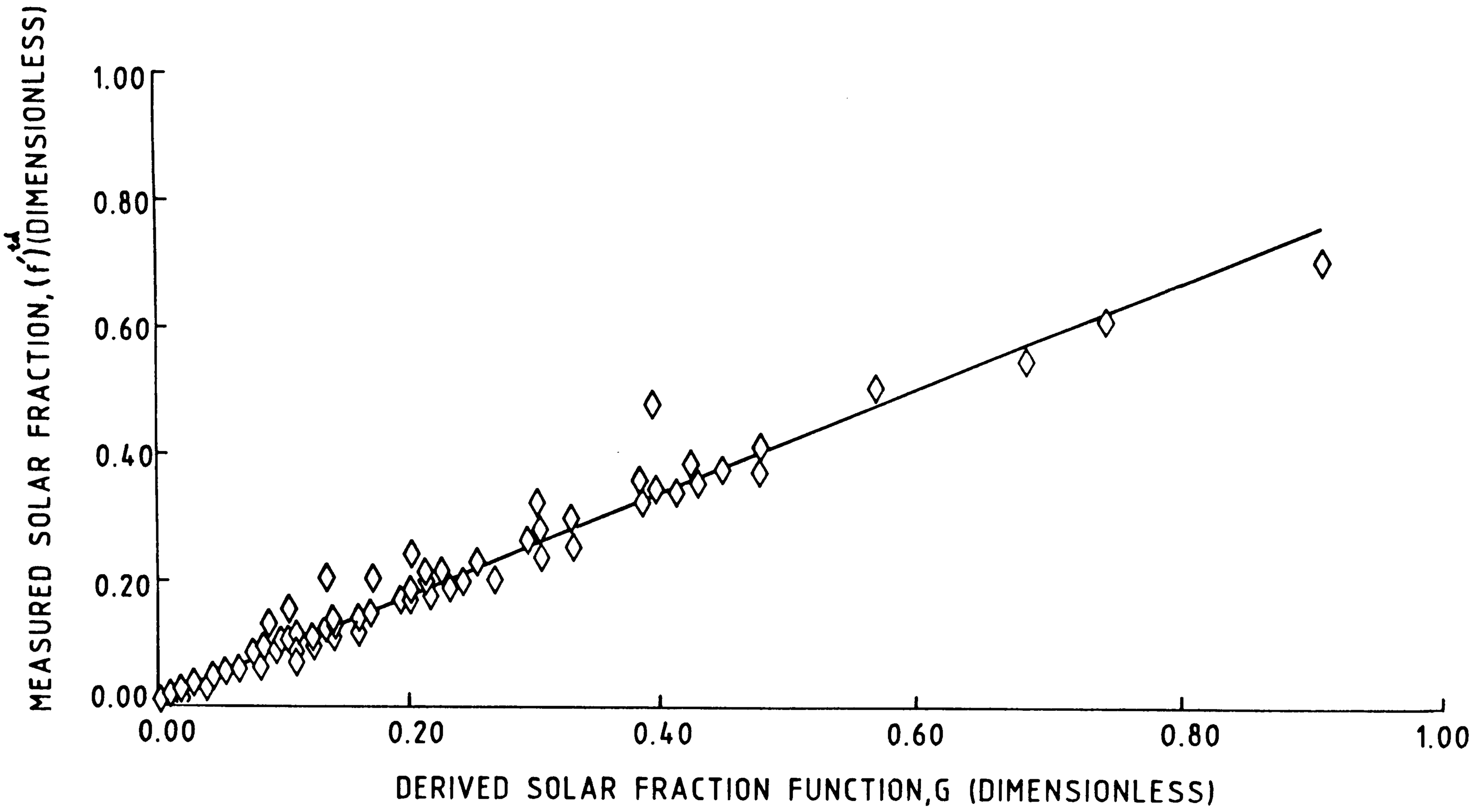
MEASURED SOLAR FRACTION, (f')^{cd} (DIMENSIONLESS)
1.00
0.80
0.60
0.40
0.20
0.00
0.00
0.20
0.40
0.60
0.80
1.00
DERIVED SOLAR FRACTION FUNCTION, G (DIMENSIONLESS)

for these systems therefore correlated relatively poorly with the predicted solar fraction defined in equation 8.16 giving typically, correlation coefficients of 0.89 and 0.91.

8.4 A Simplified Analysis

The main shortcomming of the above approach was the element of rigidity inherent in the interdependence of the dimensionless variables W, Y and Z which is necessarily introduced by the use of a complex function (equation 8.22) in determining values of G. A greatly simplified approach was therefore adopted in which, instead of using a single explicit function representative of an approximate solar fraction, a series of simple ratios of dimensionless variables was derived implicit in which was the solar fraction.

The simplifications in the analysis took the form of changes to assumptions (vi) and (vii) given on page 118. These now became:

vi) The total draw-off of water from the solar store was assumed to take place as a single event at the end of the insolation period.

vii) The solar radiation intensity remains invariant over the day at the mean measured value.

In this analysis, the differential equation is solved in its original dimensional form although the emergent grouped parameters are dimensionless. An instantaneous heat balance on the system gives with assumption (i)

$$M_s C_w \frac{d\bar{T}_s}{dt} = F_{AV}A_c(\tau\alpha)_e H^{td}/\Delta t - [F_{AV}A_c U_L + (UA)_s](\bar{T}_s - T_a)$$

equation 8.24

Using assumptions (ii) and (vii), equation 8.24 becomes, after making the substitution $\psi = T_s - T_a$ and rearranging,

$$\frac{d\psi}{dt} + \frac{[F_{AV}A_c U_L + (UA)_s]\psi}{M_s C_w} = \frac{F_{AV}A_c(\tau\alpha)_e H^{td}}{M_s C_w \Delta t}$$

equation 8.25

The solution to equation 8.25 using assumption (iv) as a boundary condition gives

$$\psi = \frac{[F_{AV}A_c(\tau\alpha)_e H^{td} - [F_{AV}A_c U_L + (UA)_s]\Delta t(T_m - T_a)]}{F_{AV}A_c U_L \Delta t} \times [1 - \exp[-(F_{AV}A_c U_L + (UA)_s)\Delta t/(M_s C_w)]]$$

equation 8.26

The difference in the mean store temperature between the beginning and the end of the insolation period is therefore

$$\psi^e - \psi^i = [F_{AV}A_c(\tau\alpha)_e H^{td} - [F_{AV}A_c U_L + (UA)_s]\Delta t(T_m - T_a)] \times [1 - \exp[-(F_{AV}A_c U_L + (UA)_s)\Delta t/(M_s C_w)]]$$

equation 8.27

From assumptions (v) and (vi), the solar fraction can be expressed as

$$(f')^{td} = \frac{M_L C_w(\psi^e - \psi^i)}{Q_{tot}}$$

equation 8.28

Substituting equation 8.27 into equation 8.28 and rearranging gives

$$\frac{(f')^{td}Q_{tot}}{M_L C_w(T_m - T_a)[1-\exp[-(F_{AV}A_c U_L + (UA)_s)\Delta t/(M_s C_w)]]}$$

$$= \frac{F_{AV}A_c(\tau\alpha)_e H^{td}}{[F_{AV}A_c U_L + (UA)_s]\Delta t(T_m - T_a)} - 1$$

equation 8.29

Equation 8.29 can then be expressed in terms of the previously defined dimensionless variables Y and Z given by equations 8.15 and 8.16 respectively and a further dimensionless variable X where,

$$X = \frac{(f')^{td}Q_{tot}}{M_L C_w(T_a - T_m)} = \frac{\text{TOTAL HEAT DELIVERED BY SYSTEM}}{\text{CHANGE IN INTERNAL ENERGY OF WATER DRAW OFF WHEN RAISED FROM MAINS TO AMBIENT TEMPERATURE}}$$

equation 8.30

In terms of these dimensionless variables, equation 8.30 becomes

$$\frac{X}{1 - e^{(-Z)}} = \frac{Y}{Z} + 1$$

equation 8.31

Equation 8.31 therefore indicates a linear relationship between $X/[1-e^{(-Z)}]$ and Y/Z.

Using experimental data collected from the indirectly heated system, a plot of $X/[1-e^{(-Z)}]$ against Y/Z for the 250 days monitored, is shown in figure 8.5. A strongly linear relationship is observed with a correlation coefficient of 0.96. The apparent scatter of the data points about the origin in figure 8.5 is due to slight seasonal variations in the functional relationship between the dimensionless parameters. This is illustrated by figure 8.6 for data monitored over the month of September where the scatter is minimal about the origin. The correlation coefficient for this month is 0.99 and is typical of the values obtained for the individual months.

A table of the equations representing the best straight lines through the daily data split up into months is given in table 8.1. There is evidence of gradual seasonal variations in the gradients of these lines.

Inspection of the dimensionless groups X, Y and Z indicate that the linear relationship (shown graphically in figure 8.5) between the grouped parameters obtained using data measured from the particular thermosyphon solar-energy water heater described is applicable to other systems. However, in addition to the parameters in the dimensionless groups namely $F_{AV}(\tau\alpha)_e$, $F_{AV}U_L$, $(UA)_s$, A_c and M_s which define the system configuration and thermal characteristics, the performances of buoyancy-driven systems also depend on other factors such as

(i) the position of the store relative to the collector,

(ii) the pipework arrangement,

FIGURE 8.5

$X/[1 - e^{(-Z)}]$ and Y/Z correlated over a period of 250 days using measured data from an indirectly heated thermosyphon solar-energy water-heater.

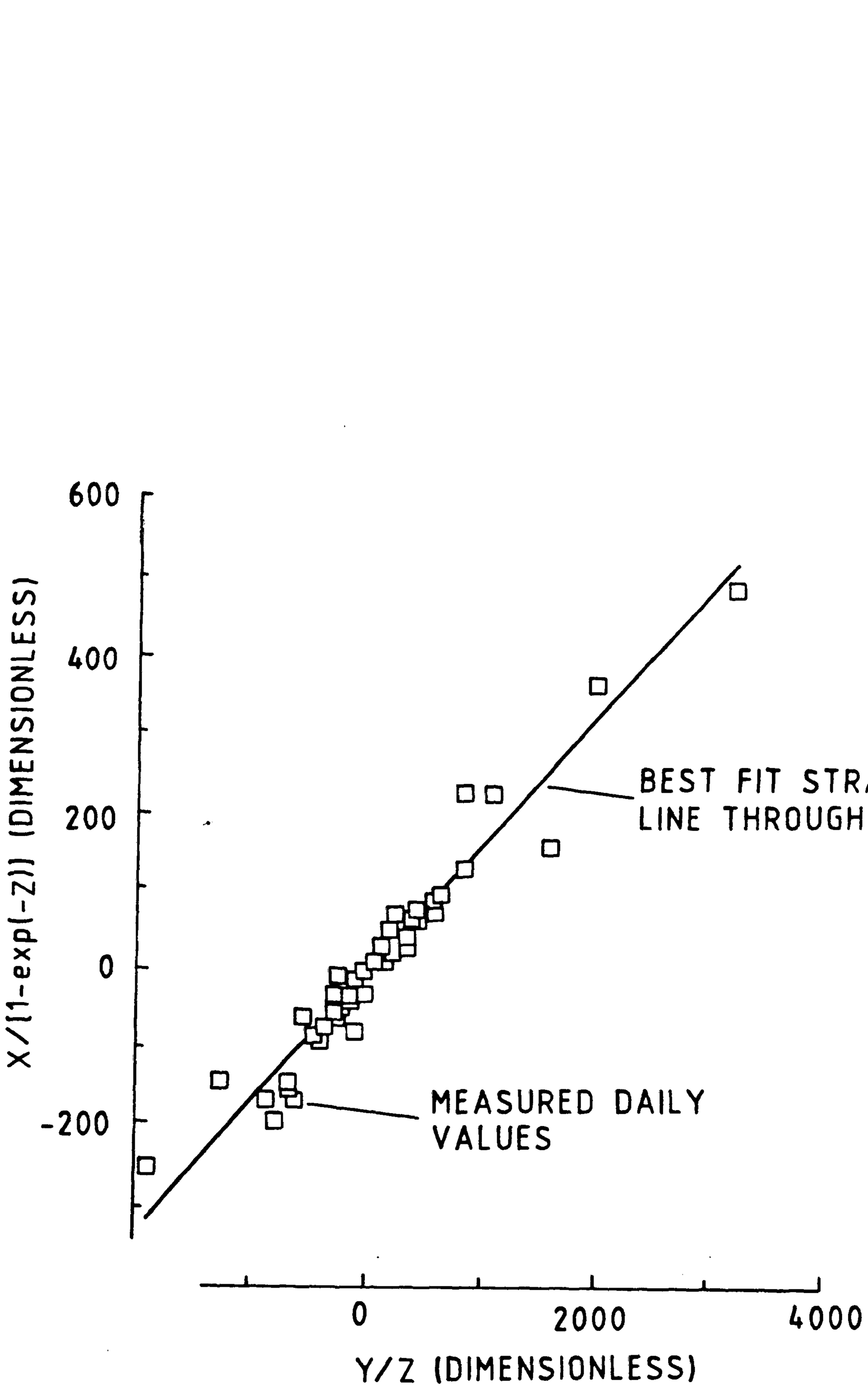
600
400
200
0
-200
X/(1-exp(-Z)) (DIMENSIONLESS)
BEST FIT STRAIGHT LINE THROUGH DATA
MEASURED DAILY VALUES
0
2000
4000
Y/Z (DIMENSIONLESS)

FIGURE 8.6

$X/[1 - e^{(-Z)}]$ and Y/Z correlated over the month of September using measured data from an indirectly heated thermosyphon solar-energy water-heater.

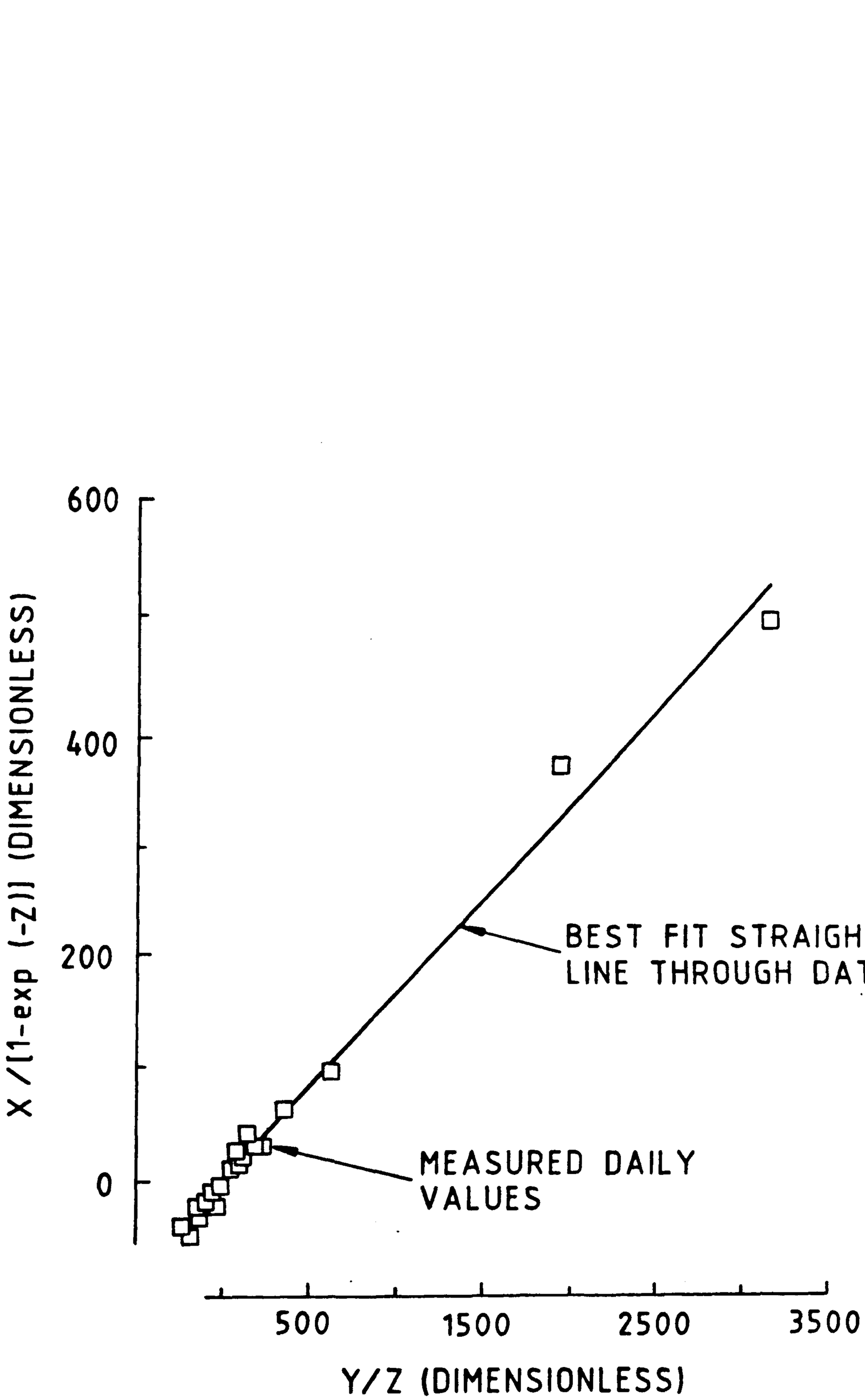
600
400
200
0
X /(1-exp (-Z)) (DIMENSIONLESS)
BEST FIT STRAIGHT
LINE THROUGH DATA
MEASURED DAILY
VALUES
500
1500
2500
3500
Y/Z (DIMENSIONLESS)

Table 8.1 Gradients of characteristic curves from the monitoring of an indirectly-heated thermosyphon solar-energy water-heater

month	year	gradient
October	1985	0.21
November	1985	0.25
December	1985	0.40
January	1986	0.22
February	1986	0.22
March	1986	0.20
April	1986	0.16
May	1986	0.12
June	1986	0.12
July	1986	0.13
August	1986	0.20
September	1986	0.17

(iii) prevalent flow regimes and

(iv) frictional fluid flow losses.

A possible measure of the influence of these other factors might be the relationship between the store and collector temperatures. An initial investigation using monitored data from the installed unit in use, indicated a constant temperature difference between the daily mean collector ($\bar{T}_c$) and store ($\bar{T}_s$) temperature over the insolation period. Figure 8.7 shows a plot of the daily $\bar{T}_c$ against $\bar{T}_s$ for the month of August indicating a linear relationship. The best straight line through the data gave

$$\bar{T}_c = 1.00\bar{T}_s - 1.41$$

equation 8.32

with a correlation coefficient of 0.97. Rearranging equation 8.32 gives

$$\bar{T}_s - \bar{T}_c = 1.41$$
$$= \beta$$

equation 8.33

In effect, this difference, β, between daily values of the mean store and collector temperatures is an indication of thermal stratification effects within the store and the degree to which the system behaviour deviates from the implied assumptions made by Close(7). This can be illustrated by considering the temperature-height diagram for a solar water heater shown schematically in figure 8.8. If heat losses from the upriser and downcomer pipes are considered small, then the isotherms a-d and b-c will be parallel. From the geometry of the resulting parallelogram a-b-c-d, the mean store and mean collector temperatures must be equal. The only way in which the mean of the store temperature profile c-d can deviate from the mean of the linear collector profile b-a (and therefore deviate from a Close(7) type model), is for the profile c-d to be non-linear. Therefore as the value of β increases, the characteristic store profile becomes more highly non-linear.

FIGURE 8.7

Correlation of the mean collector and hot water store temperatures each averaged over single periods of insolation using measured data from an indirectly heated thermosyphon solar-energy water-heater.

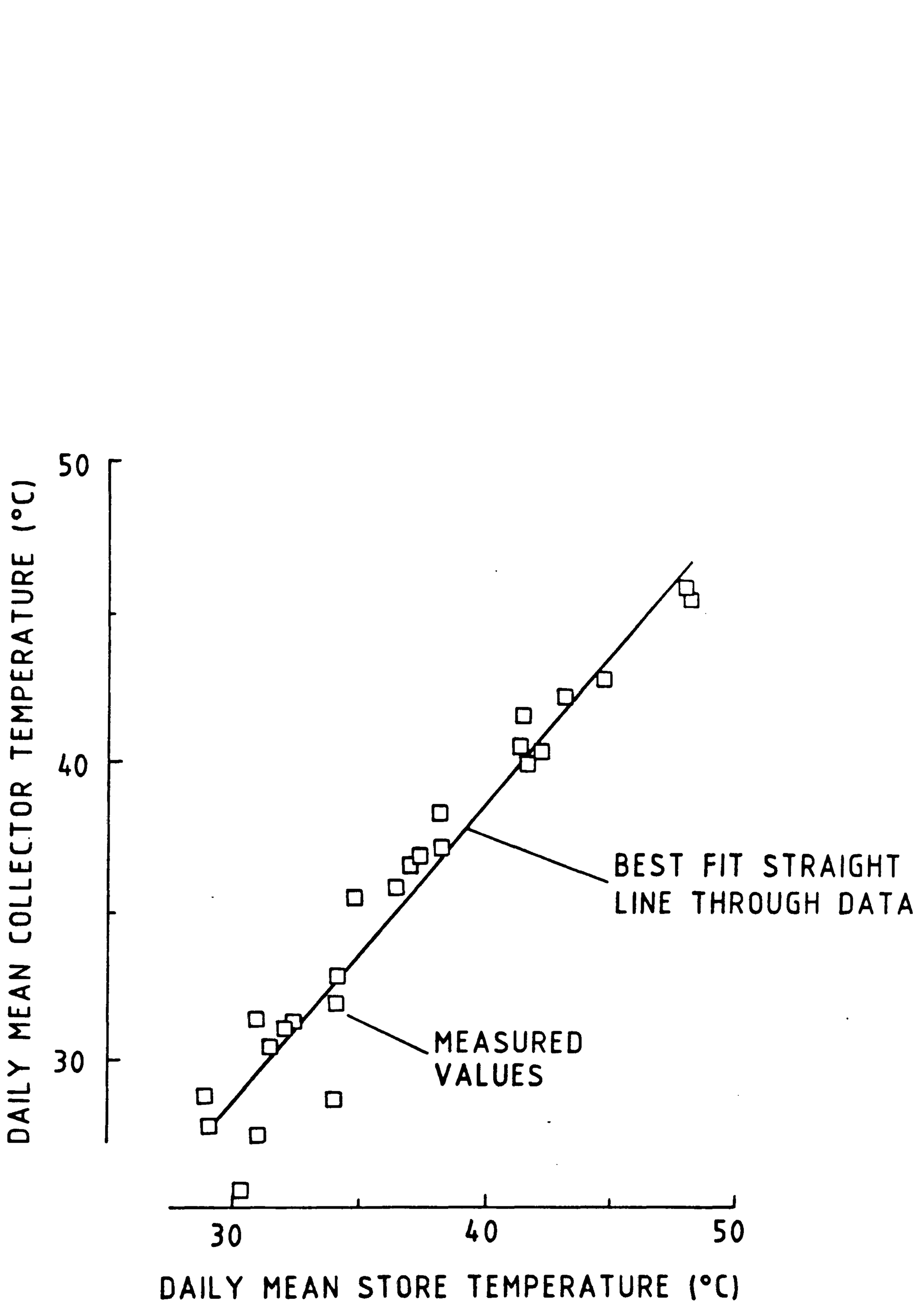
DAILY MEAN COLLECTOR TEMPERATURE (°C)
50
40
30
BEST FIT STRAIGHT
LINE THROUGH DATA
MEASURED
VALUES
30
40
50
DAILY MEAN STORE TEMPERATURE (°C)

FIGURE 8.8

Schematic representation of a solar-energy water-heater and the effect of different values on an associated temperature-height diagram.

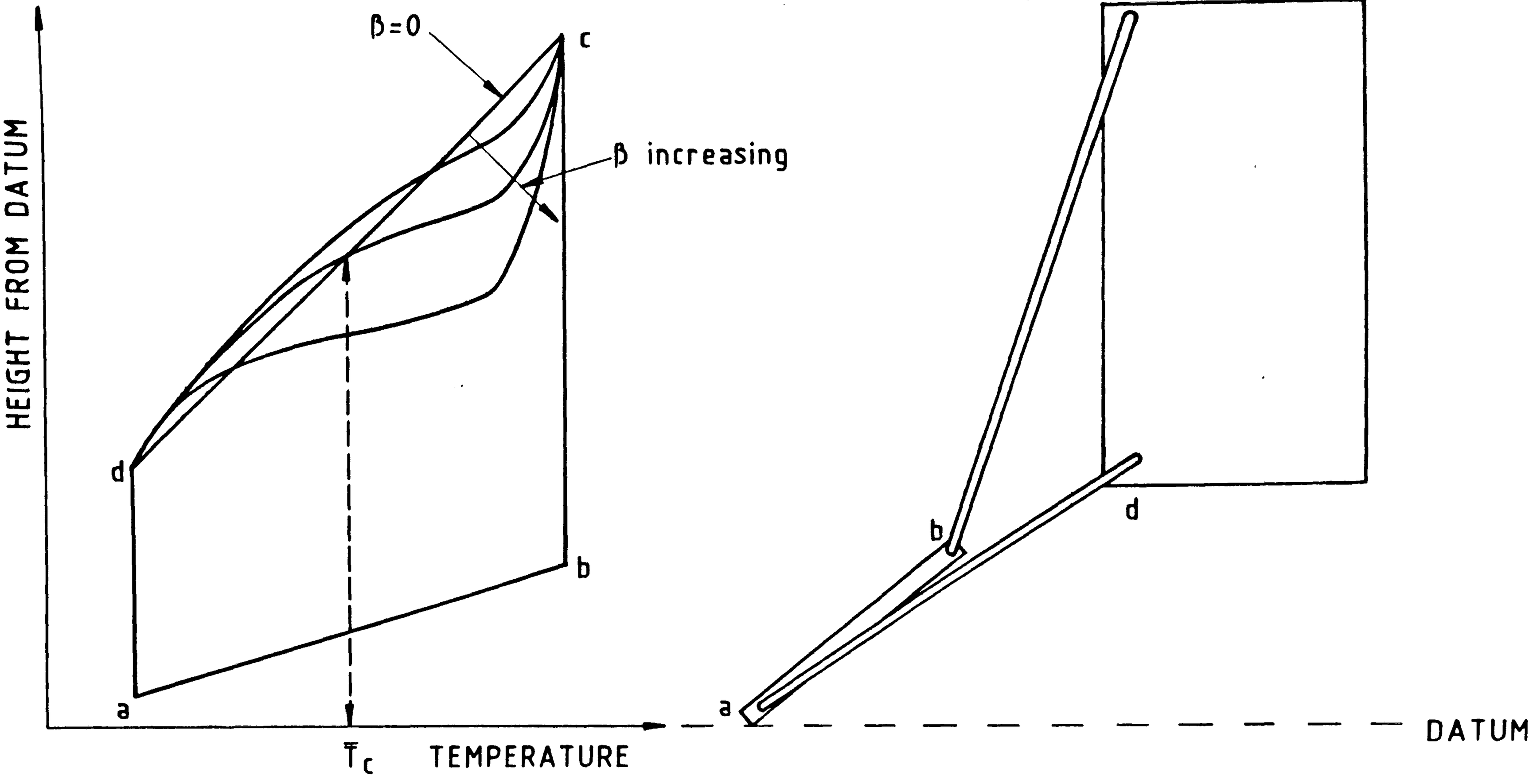
HEIGHT FROM DATUM
β=0
β increasing
c
d
b
a
T_c
TEMPERATURE
c
b
d
a
DATUM

Introducing into the analysis a constant temperature difference β, between the store and collector results in the dimensionless group Y being redefined as,

$$Y = \frac{F_{AV}A_c[(\tau\alpha)_e H^{td} + U_L\beta\Delta t]}{M_s C_w(T_a - T_m)}$$

equation 8.34

If successful, the use of this modified value of Y, would result in a correlation with a potentially more universal application. The characteristic thermal performance of any system could then be determined by establishing the relationship between the value of β and exogenous system parameters.

The practicability of these initial ideas were tested more rigorously using the validated high level simulation model. Based on the subsequent findings reported in the following sections, the correlating techniques were refined and extended.

CHAPTER NINE

THE CHOICE OF APPROPRIATE INPUT DATA FOR THE SIMULATION MODEL SUITABLE FOR CORRELATING SYSTEM PERFORMANCE UNDER U.K. WEATHER CONDITIONS

9.1 Weather Data

The method of correlating the thermal performances of thermosyphon solar water heaters was to be established for the climatic conditions and domestic hot water consumption patterns prevalent in the U.K.

Although the relationship between the correlating parameters derived in section 8 are not explicitly location dependent, the possible effects on parameters such as the transmittance of the collector cover and heat transfer rates in the system necessitated the use of meteorological data specific to the U.K.. The applicability of derived characteristic curves representing the thermal performances of systems to less temperate climates is in itself an area for future study.

Recommendations from the technical department of The Chartered Institution of Building Services Engineers (C.I.B.S.E.) (69) indicated the use of the C.I.B.S.E. Example Weather Year as the most appropriate source of data to use as inputs to the simulation model. The C.I.B.S.E. Example Weather year established (for the south of England) as running from the 1st. of October 1964 to the 30th of September 1965 is an example or reference year recommended by a task group of the C.I.B.S.E. and was originally set up "for the purpose of facilitating comparative predictions of energy consumption in buildings" (70). The weather station at which the data for the Example Weather Year was measured is situated at Kew - latitude 51^{o} 28'N, longitude 0^{o} 19'W and at a height of 5m above sea level. At the request of the Building Research Establishment, computer tapes of combined solar radiation and meteorological data for the 10 year period 1959 to 1968 using data recorded at the Kew Observatory have been prepared by the Meteorological Office. Access to this data was gained via the Meteorological Data Base System which was developed on the Science and Engineering Research Council's Central Computing Facility, a large IBM computer complex at the Rutherford Appleton Laboratory. The weather data has been recorded on an hourly basis. Table 9.1 is an extract from a typical weather data file, indicating the nature and accuracy of the available data. A hard copy of the C.I.B.S.E. Example Weather Year data for Kew is also available in a much condensed form (70).

Table 9.1 Sample listing from a Kew weather data file for June 1st 1965

Key to abreviated file headings:

GSR	Total global solar radiation	(Wm^{-2})
DSR	Diffuse solar radiation	(Wm^{-2})
SS	Sunshine duration	(hrs x 10^{-1})
DBT	Dry bulb temperature	(^{o}C x 10^{-1})
WBT	Wet bulb temperature	(^{o}C x 10^{-1})
ATPR	Atmospheric pressure	(Nm^{-2})
WS	Wind speed	(ms^{-1} x 10^{-1})
WD	Wind direction	(degrees)
RA	Rainfall amount	(m x 10^{-4})
RD	Rainfall duration	(minutes)
WCLD	Weather code (see handbook (78))	

Where a reading has not been recorded, the number -32768 is substituted.

GSR	DSR	SS	DBT	WBT	ATPR	WS	WD	RA	RD	WCLD	
0	0	0	87	77	10120	28	335	0	0-32768		01066
0	0	0	88	77	10119	33	345	0	0-32768		
0	0	0	88	75	10120	39	350	0	0-32768		
0	0	0	86	75	10120	41	355	0	0-32768		
6	6	0	87	75	10122	39	5	0	0-32768		
31	31	0	88	77	10128	36	10	0	0-32768		
83	73	0	89	77	10131	41	10	0	0	2188	
161	139	0	97	81	10138	49	20	0	0-32768		
261	209	1	108	89	10143	54	30	0	0-32768		
306	244	2	106	94	10146	46	30	1	6	8188	
254	224	0	116	99	10148	39	35	5	12-32768		
175	153	0	124	99	10149	39	105	0	0-32768		
179	164	0	109	102	10157	31	115	7	24	8188	
194	182	0	121	107	10160	28	45	18	30-32768		
133	127	0	126	109	10161	23	45	1	12-32768		
107	102	0	127	114	10164	10	70	1	6	8088	
98	93	0	130	111	10165	15	55	0	0-32768		
102	97	1	133	109	10166	26	25	0	0-32768		
97	90	0	140	115	10166	28	15	0	0	2577	
46	45	0	138	112	10171	33	5	0	0-32768		
10	10	0	132	109	10174	39	0	0	0-32768		
0	0	0	119	102	10181	39	5	0	0	266	
0	0	0	108	95	10186	39	10	0	0-32768		
0	0	0	96	86	10191	44	15	0	0-32768		

9.2 Water Supply Temperature

The thermal performances of all solar water heaters are strongly dependent on the mains (ie. cold) water supply temperature. However, available data is scant and of dubious relevance. Ground water temperature measurements made in the London area (71) indicated a wide range of location-dependent values. Further, it has been suggested (71) that the water supplied to domestic appliances is approximately equal to the roof-space rather than ground-water temperatures. The best data available on the temperature of the water supplied as make-up water to solar water heater systems is that obtained from the Wharley End houses described in the previous section. If it is assumed that the water supply temperature is related to that of the roof space, which in turn will be a function of the prevalent weather conditions, then the variation over the year of the supply temperature as measured at Wharley End cannot be used directly in simulating the cold water supply temperature associated with the Example Weather Year. A correlation was therefore sought which would relate the water supply temperatures monitored at the Wharley End houses to the prevalent insolations and ambient temperatures. This correlation was then used to predict the water supply temperature associated with the weather conditions measured at the Kew Observatory in 1964-5. This was accomplished by considering a simple thermally steady-state energy balance on the roof space of the house containing the water supply tank which is in turn in thermal equilibrium with the surrounding loft space. If the water supplied from the cold store is equal to the roof space temperature, then there is the implicit assumption that the rate of heat transfer due to cold water entering the store from outside the building at the ground temperature and leaving at the roof-space temperature is small compared with the heat transfer between the bulk of the water and the surrounding roof space. The energy balance over a period of time Δt then becomes,

$$[(A\alpha)_R I + A_R U_{l,R}(T_a - T_m) + A_C U_{l,C}(T_{ref} - T_m) + \frac{NrV_R(\rho C)_a(T_a - T_m)}{3600}]\Delta t = 0$$

(i) (ii) (iii) (iv)

equation 9.1

where the terms of equation 9.1 represent,

i) Energy gains due to solar radiation incident on the roof surface,

ii) heat transfer to the ambient via conduction and ventilation through the fabric of the roof,

iii) heat transfer through the ceiling with the remainder of the house which is assumed to be maintained at a temperature of T_{ref}

iv) heat transfer with the ambient due to air infiltration

Equation 9.1 simplifies to

$$\frac{[A(T_a - T_m) + B(T_{ref} - T_a)]\Delta t}{H} + 1 = 0$$

equation 9.2

where

$$A = \frac{A_C U_{1,C} + A_R U_{1,R} + N r V_R (\rho C)_a / 3600}{(A\alpha)_R}$$

and

$$B = \frac{A_C U_{1,C}}{(A\alpha)_R}$$

So, from equation 9.2,

$$\frac{A(T_a - T_m)\Delta t}{H} \quad \& \quad \frac{B(T_a - T_{ref})\Delta t}{H}$$

The period, Δt (in seconds) over which the insolation levels and the ambient and mains temperatures were integrated was taken as being a month. This was because the water supply temperature was not expected

to follow the relatively large daily fluctuations experienced by the insolation and ambient temperatures. By implication, the water supply temperature was therefore assumed to remain invariant over each month.

No attempt was made to give the resulting correlation any degree of universality by evaluating the constants A and B, as the uncertainty involved in estimating the component parameters of A and B would have been too great. Instead, $(T_a-T_m)\Delta t/H$ was plotted directly against $(T_a-T_{ref})\Delta t/H$ as shown in figure 9.1 to give a correlation relating the mains water supply temperature (assumed equivalent to the roof space temperature) and prevalent weather conditions, for the roof construction existing on the Wharley End houses. However, since the roofs on the Wharley End houses were of a type common to a large proportion of the U.K. housing stock, the results of the correlation were taken as being representative of a typical terraced building. The temperature T_{ref} at which the houses were assumed to be maintained by the occupants was not known and was determined by trial and error as the value for which the best correlation was obtained. By this means a value for T_{ref} of $18^{o}C$ was established. The best straight line through this data gives the relationship

$$\frac{(T_a - T_{ref})\Delta t}{H^{tm}} = \frac{1.9603(T_a - T_m)\Delta t}{H^{tm}} + 0.0082$$

equation 9.3

The correlation coefficient for the data points was 0.98.

Applying equation 9.3 to the Kew data, values for the monthly variation in the water supply temperature were obtained (see figure 9.2) corresponding to the Example Weather Year of 1964-5.

9.3 Hot Water Consumption Patterns

Previous studies have indicated that the diurnal pattern of hot water withdrawal has a significant effect on system behaviour (62-75). The correlating technique developed in section 8 when tested using the experimentally measured data demonstrated a marked insensitivity to the wide variety of diurnal draw-off patterns imposed on the system by the

FIGURE 9.1

Correlating $t\ (T_a - T_m)/H^{tm}$ with $t\ (T_a - T_m)/H^{tm}$ using mean monthly daily data from the monitoring of the Wharley End houses

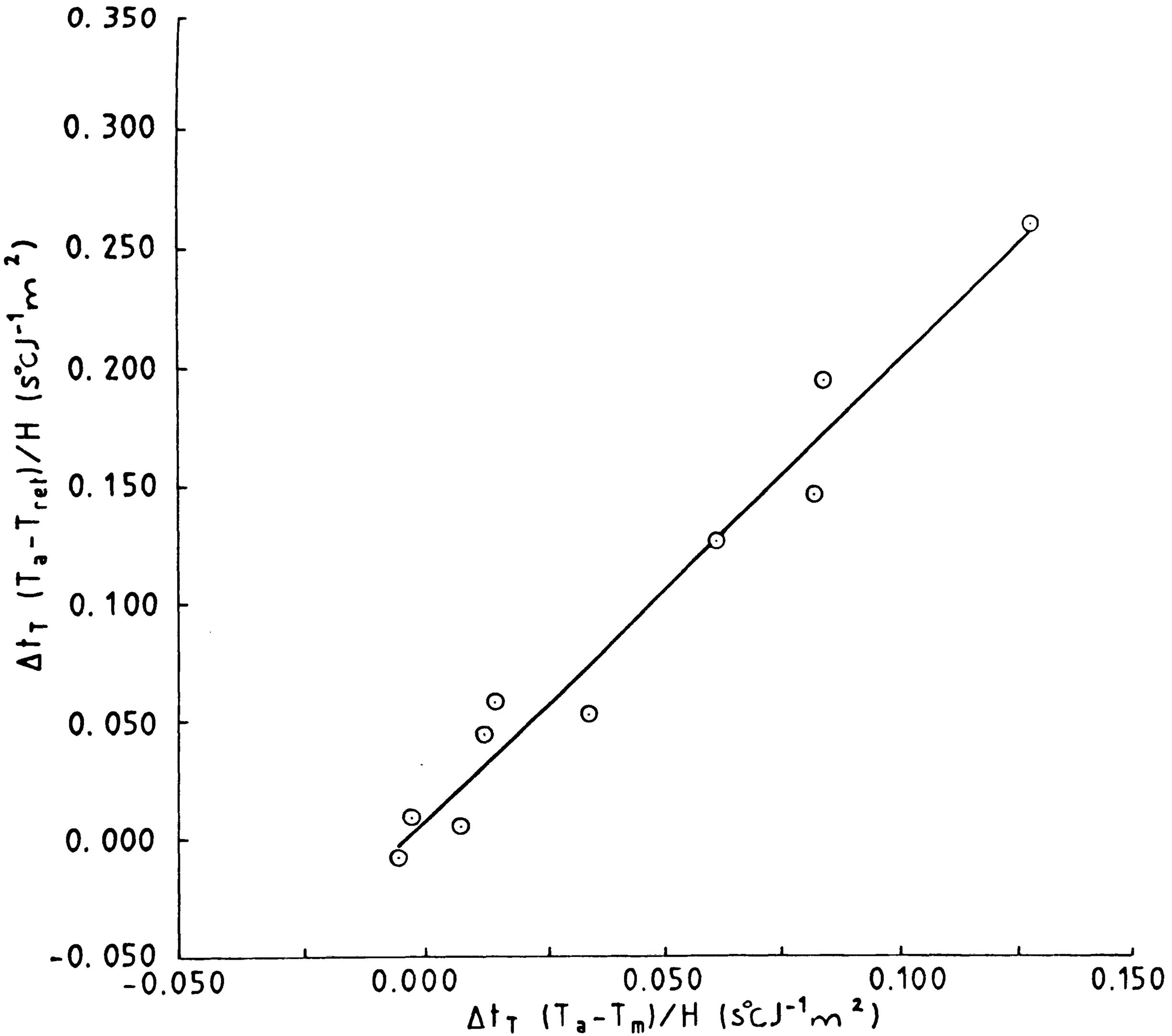
0. 350
0. 300
0. 250
0. 200
0. 150
0. 100
0. 050
0. 000
-0. 050
Δt_T $(T_a-T_{ref})/H$ $(s°CJ^{-1}m^2)$
-0.050
0.000
0.050
0.100
0.150
Δt_T $(T_a-T_m)/H$ $(s°CJ^{-1}m^2)$

FIGURE 9.2

Total global radiation, mean monthly ambient and the predicted mean monthly mains cold water supply temperature

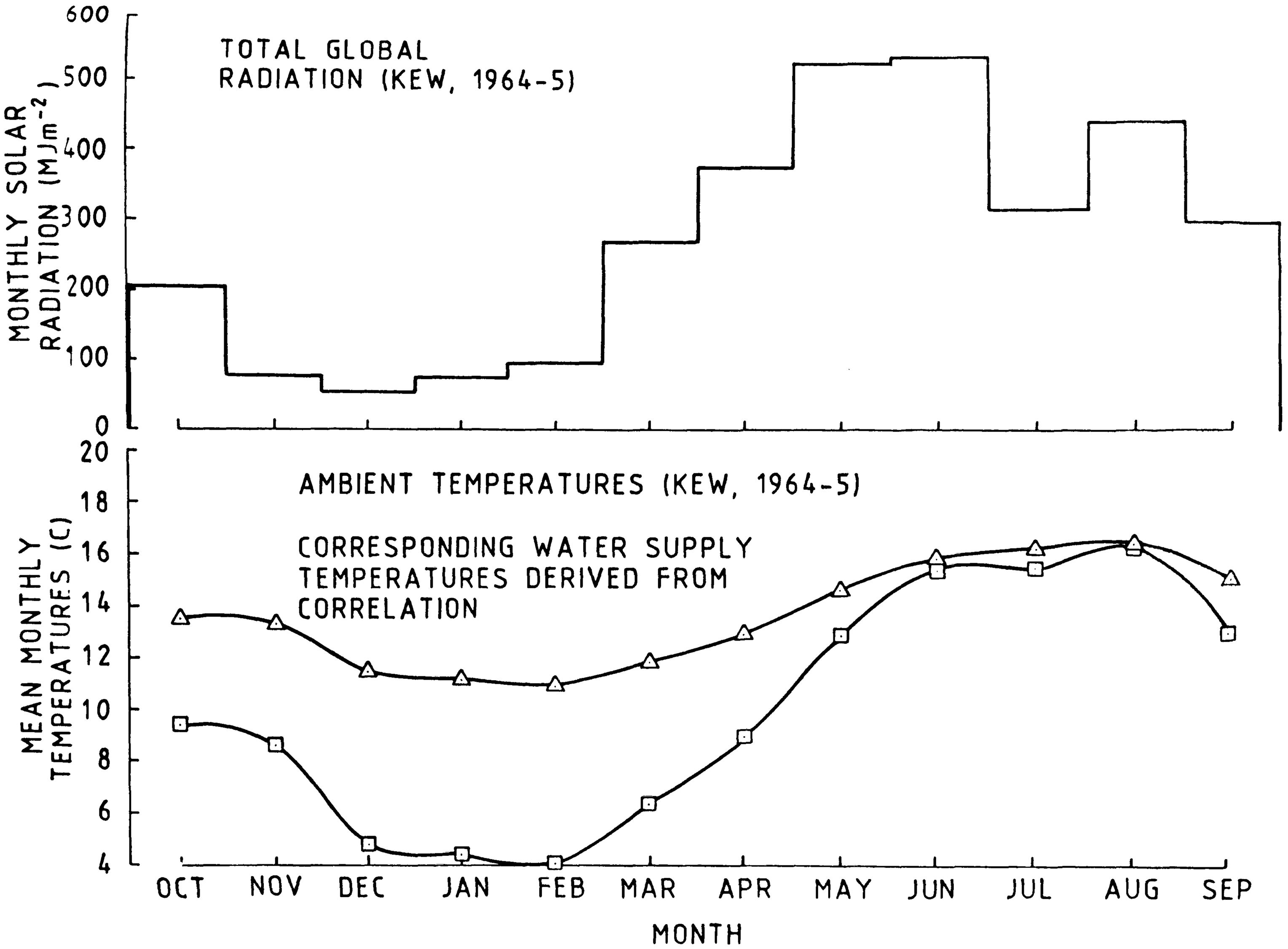
TOTAL GLOBAL
RADIATION (KEW, 1964-5)
MONTHLY SOLAR RADIATION (MJm⁻²)
600
500
400
300
200
100
0
AMBIENT TEMPERATURES (KEW, 1964-5)
CORRESPONDING WATER SUPPLY
TEMPERATURES DERIVED FROM
CORRELATION
MEAN MONTHLY TEMPERATURES (C)
20
18
16
14
12
10
8
6
4
OCT
NOV
DEC
JAN
FEB
MAR
APR
MAY
JUN
JUL
AUG
SEP
MONTH

occupants. However because of the possible effects on performance of underlying monthly or seasonal trends, it was considered prudent to choose an example of hourly draw-off profiles monitored in the U.K. Again, the most comprehensive and readily available source of data was that collected during the monitoring of the Wharley End houses (28). Draw-off patterns for the mass of conventionally heated water consumed were averaged to give a characteristic hourly diurnal draw-off profile for each month. These are shown on a seasonal basis in figures 9.3 (a)-(d). When applying these draw-off profiles to the simulation model, the total hourly draw-off was assumed to take place uniformly over the course of that particular hour, rather than as a single instantaneous event on the hour. The thermosyphon solar-energy water-heater being simulated employs a preheat, rather than a "third tap", method of heat delivery. The mass of solar heated water drawn off from the store is thus identical to that consumed via the "conventionally"- heated water system.

The measured temperature of the water heated conventionally was found to be constant (due to the fixed setting of the thermostat for the immersion heater.) at 46^{o}C with a standard deviation over the year of only 3^{o}C. In calculating the daily energy requirement for water heating purposes, the required delivery temperature was assumed constant at 46^{o}C. The resulting daily energy consumption on water heating for each month was therefore calculated from

$$Q_{tot} = M_L C_w (46 - T_m)$$

equation 9.4

9.4 Applying the Data to the Numerical Simulation

Hourly values of insolation, ambient temperatures, windspeeds (effecting heat losses by forced convection from the glass collector cover), relative humidity and atmospheric pressures (used in the calculation of effective sky temperatures) for the C.I.B.S.E. Example Weather Year (Kew), taken from the data base described in the previous sections, were used as inputs to the model. Intermediate values were calculated by a process of linear interpolation between the hourly values. The mains water supply temperatures were calculated on a

FIGURE 9.3

Mean monthly diurnal water draw-off profiles (from the Wharly End houses) for

(a) Autumn (September - November)

(b) Winter (December - February)

(c) Spring (March - May)

(d) Summer (June - August)

a) AUTUMN

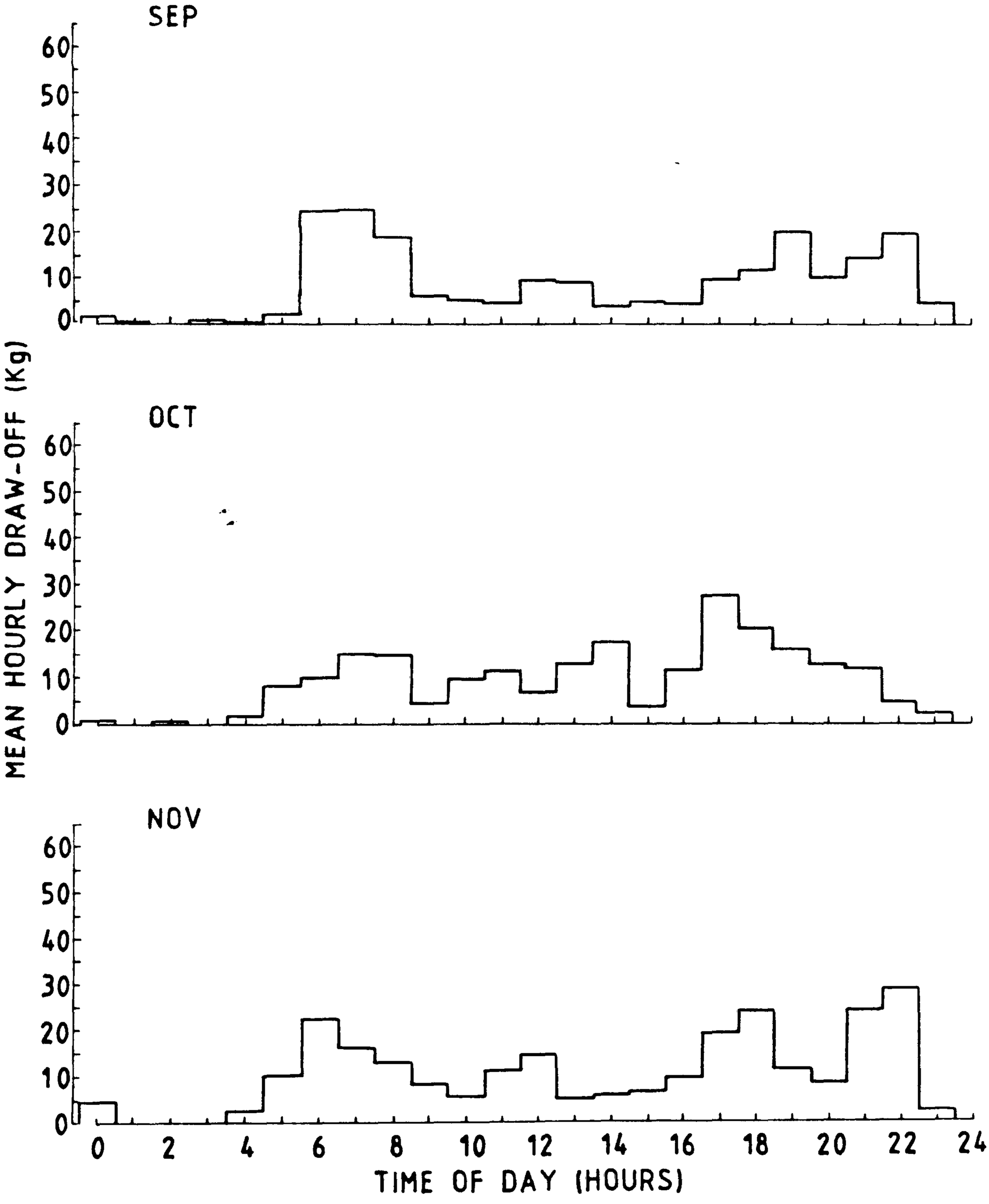
SEP
OCT
NOV
MEAN HOURLY DRAW-OFF (Kg)
0
10
20
30
40
50
60
0
2
4
6
8
10
12
14
16
18
20
22
24
TIME OF DAY (HOURS)

b) WINTER

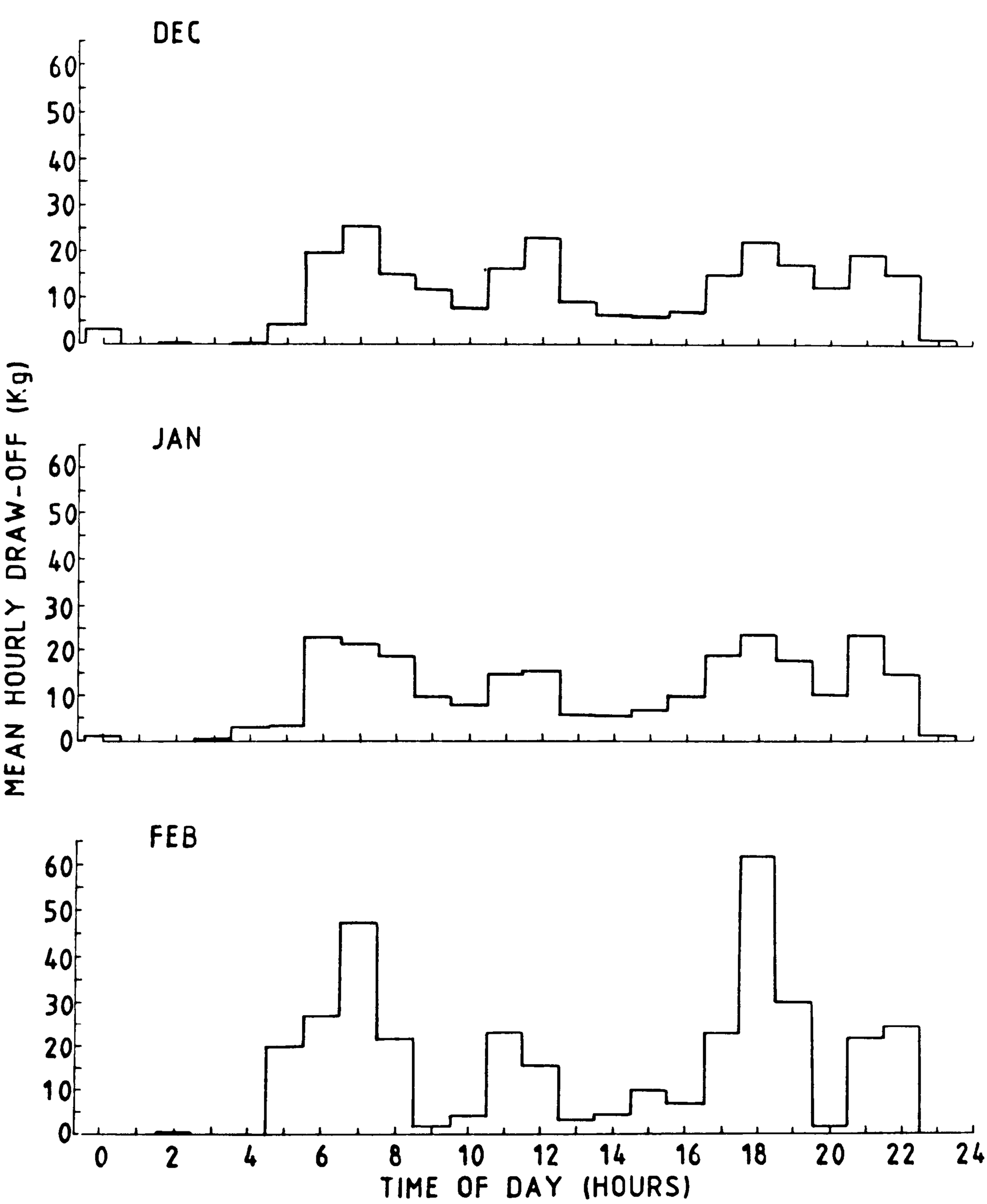
DEC
JAN
FEB
MEAN HOURLY DRAW-OFF (Kg)
0
10
20
30
40
50
60
0
2
4
6
8
10
12
14
16
18
20
22
24
TIME OF DAY (HOURS)

c) SPRING

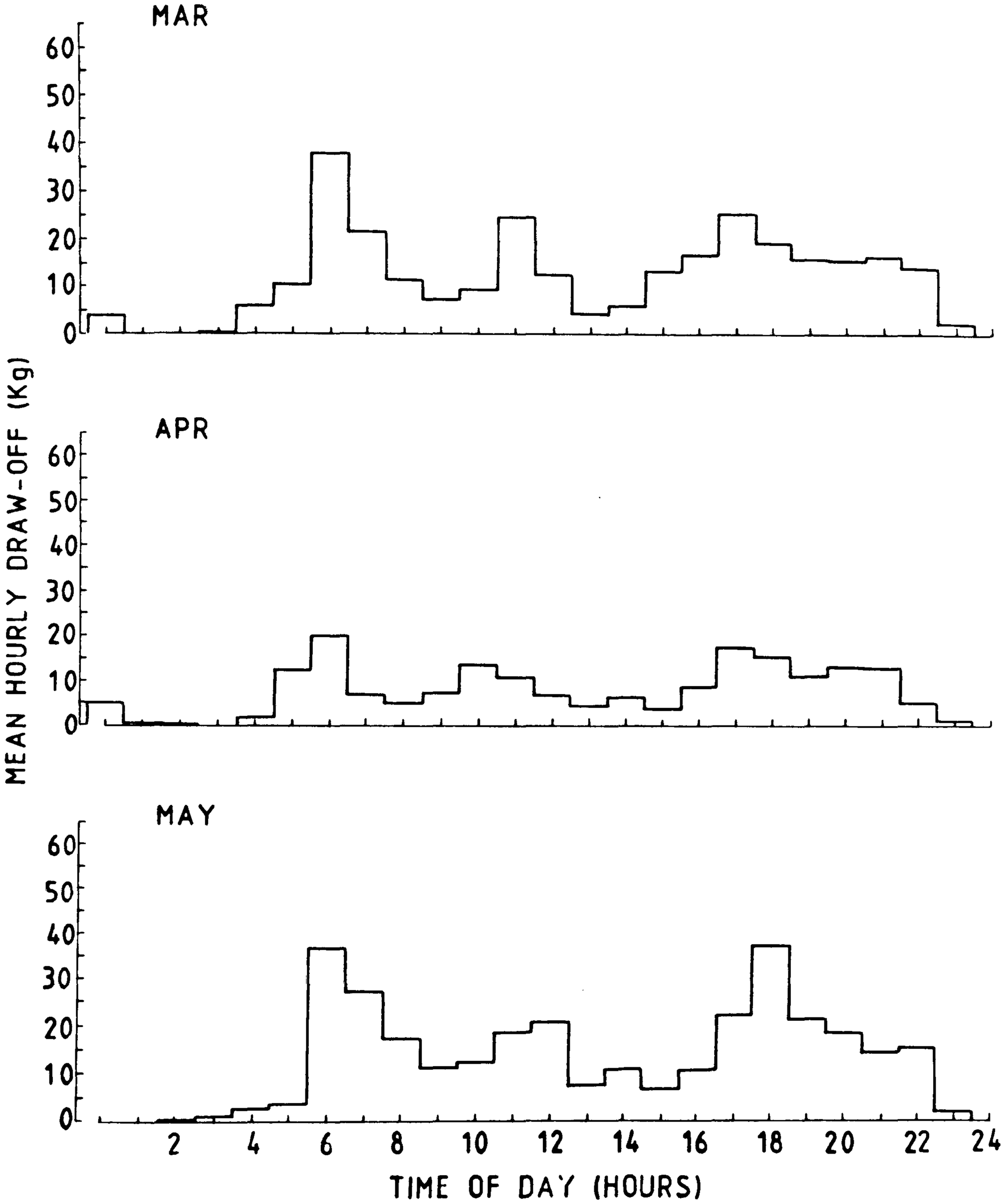
MAR
APR
MAY
MEAN HOURLY DRAW-OFF (Kg)
0
10
20
30
40
50
60
2
4
6
8
10
12
14
16
18
20
22
24
TIME OF DAY (HOURS)

d) SUMMER

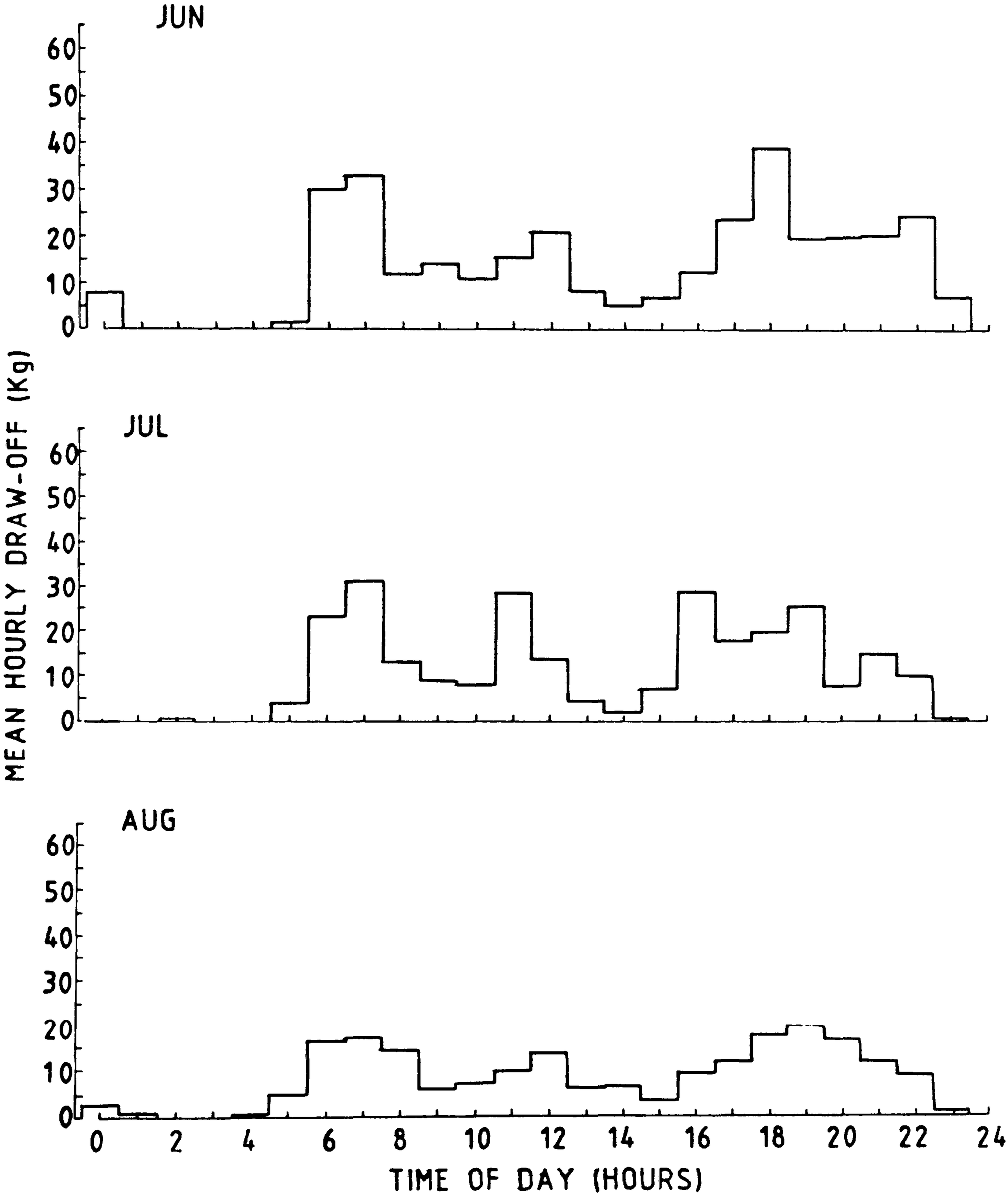
JUN
JUL
AUG
MEAN HOURLY DRAW-OFF (Kg)
0
10
20
30
40
50
60
0
2
4
6
8
10
12
14
16
18
20
22
24
TIME OF DAY (HOURS)

monthly basis using the correlation developed in section 9.2. Where as the collector and storage tank under laboratory test conditions were both exposed to the same ambient temperatures, most conventional domestic solar energy water heaters installed in the U.K. are of the distributed type with the storage tank mounted within the roof space. Based on the premiss (71) of equivalent roof-space and mains water supply temperatures, the heat losses through the insulated store walls were therefore assumed to take place between the fluid in the store and a heat sink at the mains water supply temperature rather than the outside ambient temperature. This involved the substitution of T_m for T_a in the energy equations and associated boundary conditions for a section of fluid within the store given by 3.10, 3.11 and 3.12. The monthly-averaged hourly diurnal solar-water draw-off profiles obtained from the monitoring of the Wharley End houses were implemented in the simulation model by assuming the draw-off to be made at a constant rate over each corresponding hour rather than as an instantaneous hourly event. This enabled a finite draw-off rate (a parameter in the storage tank energy equations) to be established.

CHAPTER TEN

ESTABLISHING THE ACCURACY OF THE CORRELATION TECHNIQUE IN DETERMINING LONG TERM SYSTEM PERFORMANCE

The correlation technique derived in section 8 was applied to thermal performance data generated by the validated high level numerical simulation.

The two collectors simulated were identical in size and construction to the Gull-Air model described in appendix B giving a total collector area of 4 m^2. A 780 kg capacity, 0.48 m diameter, copper-walled store was assumed in the simulation. This was mounted such that the downcomer pipe entered the tank at a height of 2 m above the collector inlet and the upriser pipe was connected at a height of 3 m above the same datum. A more detailed description of this system simulated in the program "YEARUN" is given in appendix L.

The high level simulation model was run for a total of 8 months from March to October. As the predicted buoyancy-driven flow rates decreased over the months in which lower insolation levels predominated, correspondingly smaller time steps were necessary in the simulation in order to obtain a solution for the momentum and energy equations. For the majority of the days during the months of November to February, despite the use of very small time steps (down to 0.1 seconds) the Gauss-Seidel technique used in the numerical solution of the J simultaneous equations for the J nodal temperatures, failed to produce a solution. Stable but relatively large amplitude oscillations in temperature and flow rate values during the iterative procedure, ensued. This may have been due in part to the approximating polynomials used in determining the physical properties of the circulating water. As the fluid temperature approaches freezing point, the accuracies of the polynomials decreases at the extremes of range for which these correlations are valid.

From the scant predicted thermal performance data obtained during these winter months, the collector fluid temperatures consistently dropped below the freezing point for water. This occurred not only over the night when radiative energy losses to the sky were high, but also for upto 2 hours at either end of the insolation period. In practice, an automatically-activated solenoid valve, as part of the frost protection system on such directly heated systems, causes the collector to be

drained down at 2 ($\pm$ 2)^{o}C (76). The system, which, during these periods of low insolation will not be contributing greatly to the annual solar fraction, will supply still less of the available solar radiation as heat, as it will have been drained down for a significant part of what is, at that time of year, a relatively short insolation period. Inspection of the predicted flow rates and mean collector fluid temperatures for the winter months confirms that reverse circulation occurs even during the insolation periods, causing a decrease in the enthalpy of the store . This will further reduce the daily solar contribution on such days. Reverse circulation will continue to occur unless the level of insolation is high enough to raise the collector fluid temperature above that of the mean store temperature. Other factors such as snow and ice on the collector cover obscuring the absorber plate, would also further decrease the expected contributions to the annual solar fraction during winter, when for the 4 months from November to February, only 9% of the total annual global radiation occurs.

In summary, it was considered that an annual solar fraction based on the eight months predicted thermal performance data constituted a realistic active operation period for a directly heated system.

A plot of daily values of X/[1-exp(-Z)] against Y/Z is shown in figure 10.1 for the simulated period of operation from March to October. The correlation coefficient for these values over the 245 days was 0.97. As with the correlations obtained using data from the Wharley End houses (see table 8.1), seasonal variations in the gradients (listed in table 10.1) of the best straight lines are observed, with the gradient at a minimum in June and increasing symmetrically in the months on either side of the summer solstice.

All 8 of the characteristic curves given in table 10.1 were used to predict the solar contribution during the days included within each of the appropriate months, from which an annual solar fraction was calculated. The same meteorological data base as was used in the high level simulation model was employed, but using mean daily rather than hourly values. The daily solar fraction was calculated from

FIGURE 10.1

Correlation of X/[1 - exp(-Z)] against Y/Z using simulated thermal performance data

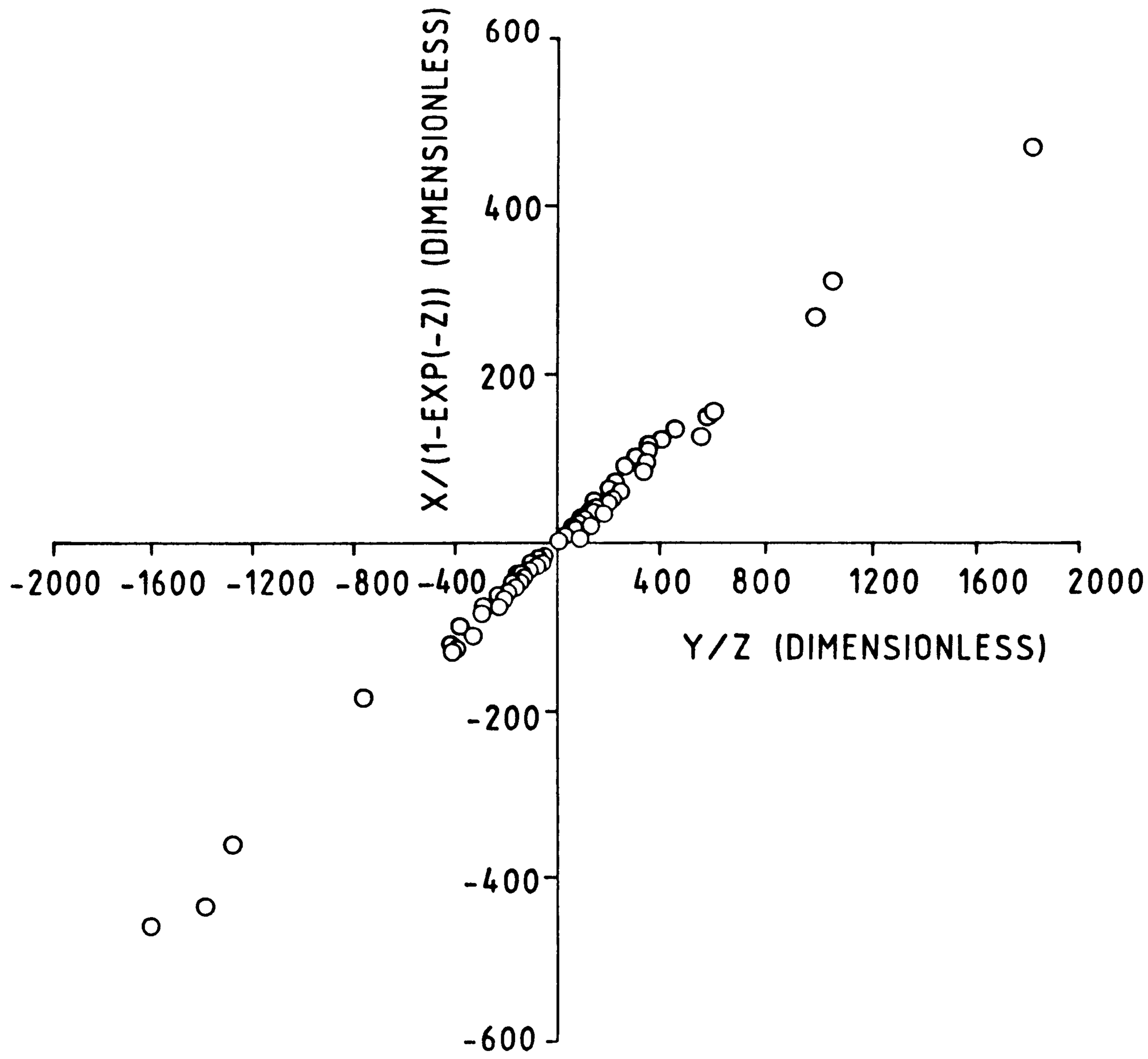
X/(1-EXP(-Z)) (DIMENSIONLESS)
600
400
200
-200
-400
-600
-2000
-1600
-1200
-800
-400
400
800
1200
1600
2000
Y/Z (DIMENSIONLESS)

Table 10.1 Gradients of characteristic curves for the months of March to October from the simulation "YEARUN".

month	gradient
March	0.3654
April	0.2876
May	0.2828
June	0.2629
July	0.2487
August	0.3497
September	0.3417
October	0.3608

$$X/[1-\exp(-Z)] = m(Y/Z)$$

equation 10.1

where m represents the appropriate gradients of the characteristic curves (given in table 10.1). At this stage, the constant representing a value for the ordinate intercept when X/[1-exp(-Z)] was plotted against Y/Z, was discarded as the value of this constant was small compared with values of Y/Z. Characteristic curves therefore only differed due to variations in the value of the gradient, m. Substituting into equation 10.1 for X (as defined in equation 8.30) and rearranging gives, for the diurnal solar thermal contribution during day id of month im,

$$(Q_{sol})^{id,im} = (M_L C_w)^{im}[(T_a)^{id,im} - (T_m)^{im}][m^{im}(Y/Z)^{im,id}(1-\exp(-z))^{im,id}]$$

equation 10.2

The annual solar fraction was then calculated from,

$$(f'_{cor})^{iy} = \frac{\sum_{im=1}^{8} \sum_{id=1}^{(Nd)^{im}} (Q_{sol})^{id,im}}{\sum_{im=1}^{12} (Nd)^{im}(Q_{tot})^{im}}$$

equation 10.3

where $(Nd)^{im}$ was the total number of days in month im. The predicted annual solar fraction using this method was 0.329 compared with 0.336 for the corresponding value calculated using the high level simulation model. This represents a discrepancy of 2.1%.

In view of the observed seasonal variations in the characteristic curves, if the correlation technique is to succeed as a tool for reducing to a minimum the amount of either simulated or experimentally-obtained thermal performance data required in order to make long term performance predictions, then data collected over a relatively short period should be made at a suitably representative

time of the year. The equations of the best straight lines through the 8 individual monthly sets of data were therefore used in turn to predict the annual solar fraction. The method of calculation of the annual solar fraction (during which a positive solar contribution was made for a total of 245 days), was redefined using the gradient of the characteristic curve for month im as,

$$(f'_{cor})^{iy} = \frac{\sum_{id=1}^{245} (Q_{sol})^{id,im}}{\sum_{im=1}^{12} (Nd)^{im}(Q_{tot})^{im}}$$

equation 10.4

The subsequent errors, (in the predicted anual solar fraction) incurred when using the characteristic curves for the months of March to October are shown in figure 10.2 where the error, $(e_{cor})^{iy}$, is given by,

$$(e_{cor})^{iy} = 100(f'_{sim} - f'_{cor})^{iy}/(f'_{sim})^{iy}$$

equation 10.5

Distinct minima of -3.0% and +3.0% were observed to occur in the months of May and June respectively. Values increased symmetrically on either side of these months to produce, respectively, errors of -34.0% and -32.0% for the months of March and October corresponding to the onset and end of the active period of this particular directly heated system.

Without embarking on a more exhaustive series of simulations in which the annual performances of a large number of different systems are investigated using the high level simulation model, it cannot be stated categorically that the characteristic curve obtained for the single month of June will always produce predicted annual performances, to within an accuracy of 3%. However, general observations on the seasonal availabilty of solar radiation energy in the U.K. sugests that the selection of simulated thermal performance data for June in order to produce a characteristic curve which gives the most accurate prediction of the annual solar fraction, can be used as a general result

FIGURE 10.2

Error incurred in predicting the annual solar fraction using the characteristic curves for the months of March to October

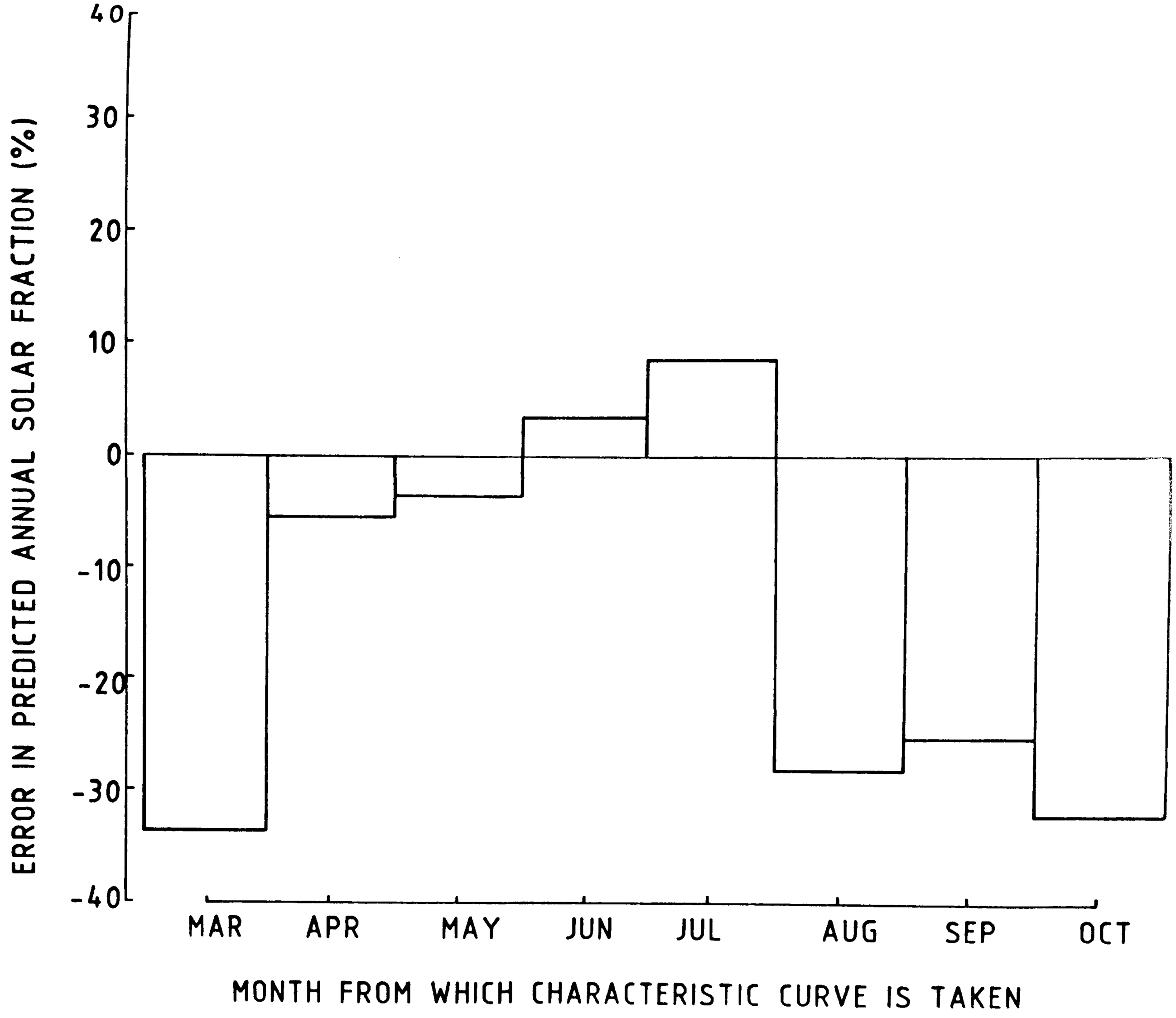
40
30
20
10
0
-10
-20
-30
-40
ERROR IN PREDICTED ANNUAL SOLAR FRACTION (%)
MAR
APR
MAY
JUN
JUL
AUG
SEP
OCT
MONTH FROM WHICH CHARACTERISTIC CURVE IS TAKEN

applicable, with a comparable degree of confidence, to other systems. Most of the total global radiation available annually in the U.K. occurs in a very limited number of months. Figure 9.2 for the Example Weather Year indicates that approximately 33% of the annual global radiation, or 36% of the radiation available during the active period of the thermosyphon system being investigated, occurs in the months of May and June. This would imply that the largest monthly solar contributions of any system to the total annual hot water requirements would also occur at this time. The least error in the prediction of the annual solar fraction would therefore be expected (and is indeed observed in figure 10.2, for the system investigated) with the use of thermal performance data collected during these two months. June was therefore selected, for the purposes of investigating other systems as producing a characteristic curve from which the most accurate prediction of the annual solar fraction could be made. Equation 10.1 was therefore modified and the basic equation upon which all future performance predictions were made using this correlation technique was given by

$$X/[1-\exp(-Z)] = m_J(Y/Z)$$

equation 10.6

where m_J was the gradient of the characteristic curve obtained from thermal performance data pertinent to the month of June.

For the purposes of calculating the maximum power output required of an auxiliary heater to work in conjunction with a solar energy water heater, it is of some considerable importance that not only is the annual solar fraction accurately predicted but so also are the individual daily or monthly values. The cumulative solar fraction and associated error over the year calculated by using equation 10.6, is shown in figure 10.3. Apart from an initial discrepancy of approximately -20%, during the month of March, there is generally good agreement between the correlation technique and high level model over the year.

A method of further reducing the number of calculations required in determining an annual solar fraction was investigated. Using daily

FIGURE 10.3

Comparison of cumulative solar fraction calculated from the numerical simulation model with corresponding values determined from:

1) the correlation technique based on daily data and

2) the correlation technique based on daily mean monthly data

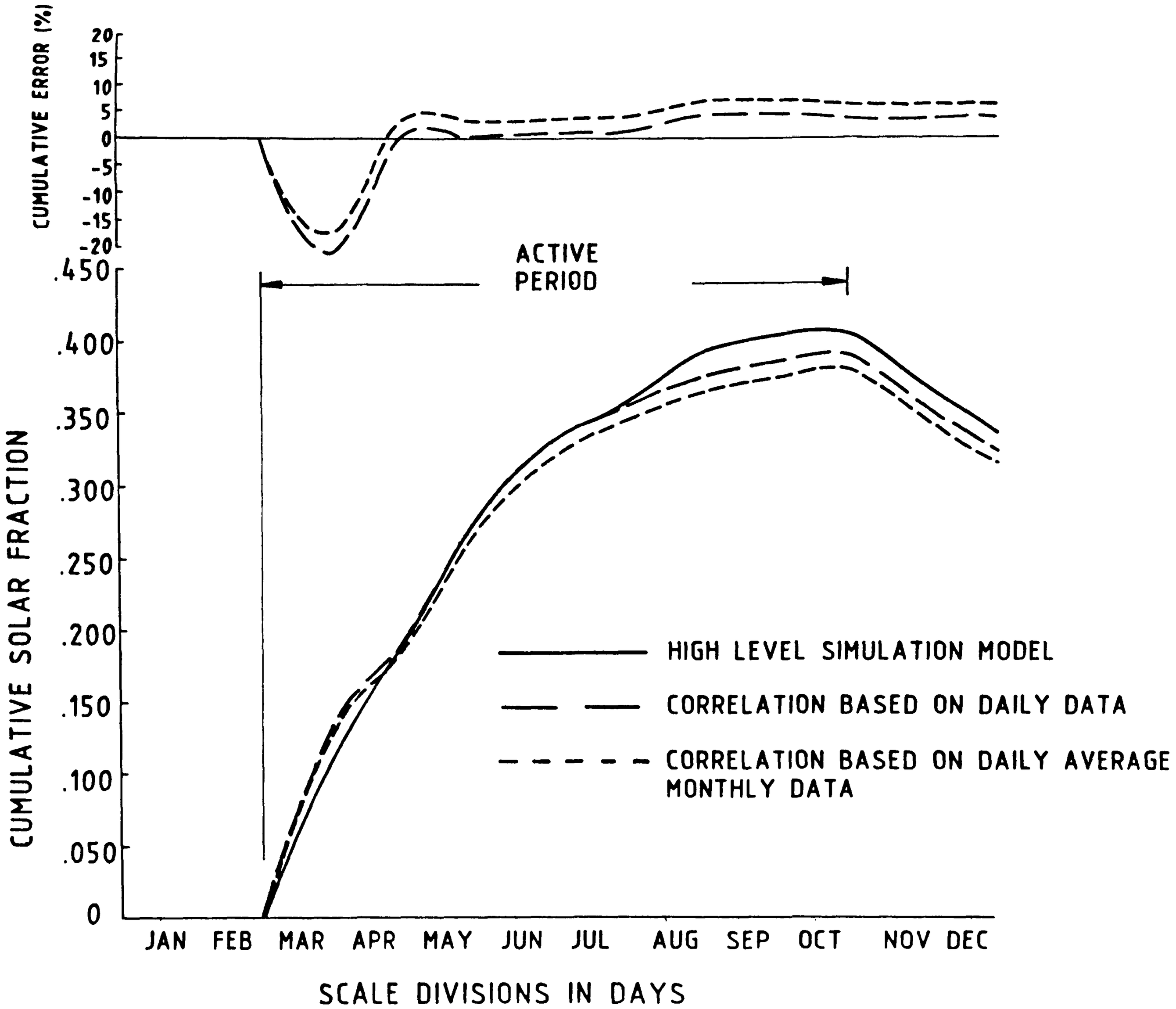
CUMULATIVE ERROR (%)
20
15
10
5
0
-5
-10
-15
-20
ACTIVE PERIOD
CUMULATIVE SOLAR FRACTION
.450
.400
.350
.300
.250
.200
.150
.100
.050
0
JAN FEB MAR APR MAY JUN JUL AUG SEP OCT NOV DEC
SCALE DIVISIONS IN DAYS
HIGH LEVEL SIMULATION MODEL
CORRELATION BASED ON DAILY DATA
CORRELATION BASED ON DAILY AVERAGE MONTHLY DATA

average monthly data, a single calculation giving a representative predicted daily solar contribution for that particular month was determined using, as before, the single characteristic gradient for June. To determine the total monthly solar contribution this daily value was assumed to remain invariant over the month and was therefore simply multiplied by the number of days in the month so that the annual solar fraction became

$$(f'_{cor})^{iy} = \frac{\sum_{im=1}^{8} (Nd)^{im}(\bar{Q}_{sol})^{im}}{\sum_{im=1}^{12} (Nd)^{im}(Q_{tot})^{im}}$$

equation 10.7

where $(\bar{Q}_{sol})^{im}$ was the daily solar contribution calculated using mean daily values of T_a, T_m and H^{td} averaged over month im. Using this method, the predicted annual solar fraction was within +6.3% of that calculated using the high level simulation model. The variation in cumulative solar fraction over the year (shown in figure 10.3) deviates little from that based on daily rather than monthly-average daily weather data. Using this approach, the number of basic calculations have therefore been reduced from 245 to 8 with a relatively small decrease in accuracy. This brings the above method of calculating an annual solar fraction from a limited amount of data, within the realms of the "hand calculation" with an acceptable degree of accuracy.

In summary, the analysis developed in chapter 8 was shown to provide an accurate method of characterising the performance of an individual system. A good estimate of the annual heat delivery of a system could be calculated using only 30 days simulated thermal performance data, so long as this data was obtained for the month of the year for which the highest total global radiation occurs. This was taken as the month of June for the UK. By taking mean monthly diurnal values of T_a, T_m and H^{td}, the heat delivery using the correlation technique can be determined using only eight representative diurnal calculations with a relatively small decrease in the accuracy of the prediction.

The relationship between individual characteristic curves for a range of different systems is investigated in the following section.

CHAPTER ELEVEN

TOWARDS A MORE UNIVERSAL CORRELATION

11.1 The Need for and Choice of, a Method of Comparison for System Behaviour Type.

The correlation technique was shown in chapter 10 to be a suitable method, given a limited amount of thermal performance data, of characterising the performance of a specific thermosyphon solar-energy water heater over the wide range of climatic conditions expected during seasonal weather variations in the U.K.. The presence of basic parameters which describe both the configurations and thermal performances of system components (such as A_c, M_s, M_L, F_{AV}, $(\tau\alpha)_e$, U_L, $(UA)_s$) in the correlating dimensionless parameters X, Y and Z, rather than those pertinent simply to applied weather conditions (for example $\bar{T}_a$, T_m, H^{td}, and Δt), infer a degree of universal application of the results given in section 10, to systems with other configurations. This would indeed be valid if by varying any of the dimensionless parameters, the degree to which the system exhibited multiple-pass behaviour remained invariant. Because the relationship beteen relative magnitudes of X, Y and Z and the degree of multiple-pass behaviour (and therefore the degree to which the system conforms to the Close(7) assumption of equal mean store and collector temperatures), is unknown, this in effect limits the characteristic curve obtained for any simulation, to being representative only of that particular system. For example, if a system with a larger collector area than that used in section 10 is simulated (in effect an increase in the value of Z), the change in the relative temperatures of the collector and store would result in higher flow rates under the same operating conditions. The mean daily circulation number, Np (that is, the mean daily number of times the water within the store has been replaced by the circulating fluid) will have increased and the thermal characteristics will therefore have undergone an unquantifiable change.

In section 8, a strongly linear relationship between the mean daily store and collector temperatures during the insolation period indicated a possible means of characterising the degree of stratification within the store (and therefore the degree of multiple pass behaviour) of an indirectly heated solar energy water heater. A

similar linear relationship was observed for the data obtained from the directly heated system simulated using "YEARUN". A linear regression algorithm carried out on mean daily values of the simulated collector and store temperatures for the month of June, gave a value of β (as defined in equation 8.33) of 2.10°C. When values of Y modified acording to the definition given in equation 8.34 were implemented using this value of β, the degree of scatter in the correlation given by equation 8.24 was increased considerably from that observed when values of Y as defined originally in equation 8.15 were used. The correlation coefficient for June was reduced from 0.99 to 0.92. More significantly, the slope of the correlating curve using a finite value of β in the definition of Y given by equation 8.34 as opposed to that of 0°C implicit in that derived in the original analysis where Y is defined by equation 8.15, remained invariant at 0.263. Had the "empirically" determined constant difference, β, between the mean store and collector temperatures been a true measure of the degree of stratification, the introduction into the definition of Y of this value should transform this, as with all other characterstic curves for which an appropriate value of β has been determined, onto a single universal curve the slope of which would be unity. A possible reason for the failure of the constant-β approach may be that although a constant temperature difference was observed between the collector and store on a mean daily basis, this same value was not representative of a suitable effective instantaneous temperature difference when integrated over the insolation period.

The value of β as an effective method of relating the thermal performances of all thermosyphon solar-energy water-heaters to a universal correlation was therefore abandoned. An alternative approach was adopted in which the dimensionless gradients of the characteristic curves for June as defined by equation 10.6, were used directly as a comparative method of investigating system performances.

11.2 The Effects of Collector Area and Store Size on the Gradient of the Characteristic Curve

A reference thermosyphon solar-energy water heater was defined and effects of changes on the characteristic curve determined using weather data for the month of June. The basic configuration of the reference system was chosen (arbitrarily) as comprising a single, 2 m^2 area (Gull-Air type) collector coupled via the minimum amount of well-insulated, 0.025 m diameter copper pipe to a 0.5 m diameter, copper-walled, 195 kg store insulated with 0.07 m of glass fibre. The store was positioned such that the upriser pipe entered the top of the store at a vertical height of 1.5 m relative to a datum line corresponding to the vertical position of the collector inlet pipe. Further details of the reference and other systems used in the initial parametric study simulated by the basic program "PARASIM" are given in appendix L.

An investigation was undertaken into the effects on the gradients, m_J, of changes in the primary dimensionless system parameter, Z evaluated, for reference purposes, for the month of June (Z_J). This was carried out initially by varying the collector area of the reference system from 0.5 m^2 to 5 m^2 , giving a corresponding range of values of Z_J from 0.19 to 0.72 for a total of 6 systems (designated in appendix L by the programs PARASIM 0-5). The rate of change of the resulting characteristic gradients, with corresponding changes in Z_J, were observed from figure 11.1, to be high at low values of Z_J and to decrease as the magnitude of Z_J increased. A maximum, constant gradient of approximately 0.3 occurred for values of Z_J greater than 0.54. When the collector area increases relative to the store capacity, the system temperatures are such that the buoyancy-driven flow-rates around the system increase. With this progressive increase, the conditions are therefore approached in which the assumption (pertinent to multiple-pass systems) made in the initial analysis, of equivalent mean store and collector temperatures, becomes valid. For the relative position of the collector and store, used in the reference system, the degree of multiple-pass behaviour is sufficient for the above assumption to be valid at and above values of Z_J greater than 0.54 and

FIGURE 11.1

Variation of m_J with Z_J due to changes in collector area alone

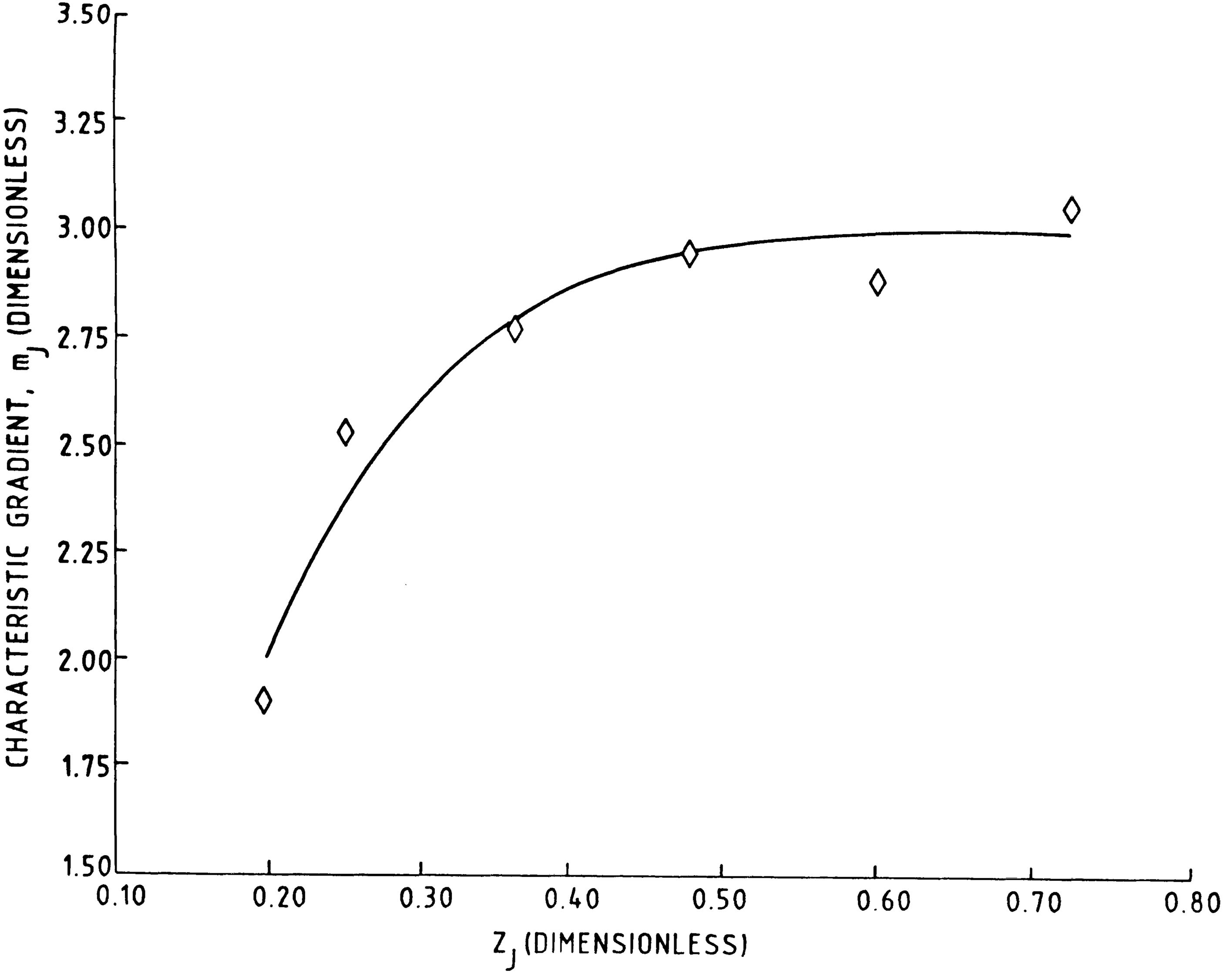
CHARACTERISTIC GRADIENT, m_J (DIMENSIONLESS)
3.50
3.25
3.00
2.75
2.50
2.25
2.00
1.75
1.50
0.10
0.20
0.30
0.40
0.50
0.60
0.70
0.80
Z_J (DIMENSIONLESS)

the thermal performances of systems with values of Z_J greater than 0.54 could therefore be represented by a single characteristic curve.

A further series of nine simulations were run using the programs PARASIM 6-14 in which the dimensionless group Z_J was varied by changing the thermal mass of the store in addition to the collector area. A total of 6 different store capacities ranging from 107 kg to 1107 kg, were investigated. Figure 11.2 shows a plot of the resulting gradients against corresponding mean monthly values of the parameter Z_J using data from these simulation runs. For comparison purposes, figure 11.2 also includes values from PARASIM 0-5 in which changes in Z_J were achieved by varying the area alone, the mass of the store remaining constant at the reference value of 195 kg. Figure 11.2 indicates both a higher degree of scatter and an underlying apparent change in the relationship between m_J and Z_J when compared with figure 11.1 in which a relatively orderly variation of m_J with Z_J due to area changes alone, is exhibited. At first sight this would throw doubt on the credibility of Z_J as a dimensionless ratio fundamental to the performance of thermosyphon solar energy water heaters. However, when Z_J is plotted against corresponding values of the mean daily circulation number (Np) made by the circulating water as shown in figure 11.3 for all the systems investigated (PARASIM 0-14), a basicaly linear relationship emerges, regardless of whether Z_J is varied due to changes in the store size or collector area. Because the linear relationship observed in figure 11.3 also contains data from the 6 simulations PARASIM 0-5 in which a positive functional dependence is observed between m_J and Z_J (due to the effects of Z_J on Np), then changes in the gradient, m_J which conform to the same relationship as that shown in figure 11.1 must also be occurring for the simulations PARASIM 6-14. The fact that these orderly changes are not apparant in figure 11.2 must mean that the resulting changes in the gradients are "swamped" by additional changes in m_J due to another factor which although dependent on the mass of the store is independent of the circulation number. It also follows that because the effect of Z_J on system performance is essentially dependent on the corresponding circulation number, it is independent of this additional store-capacity-dependent factor.

By changing the mass of the store alone in the reference system, not

FIGURE 11.2

Variation of m_J with Z_J due to changes in collector area and store capacity

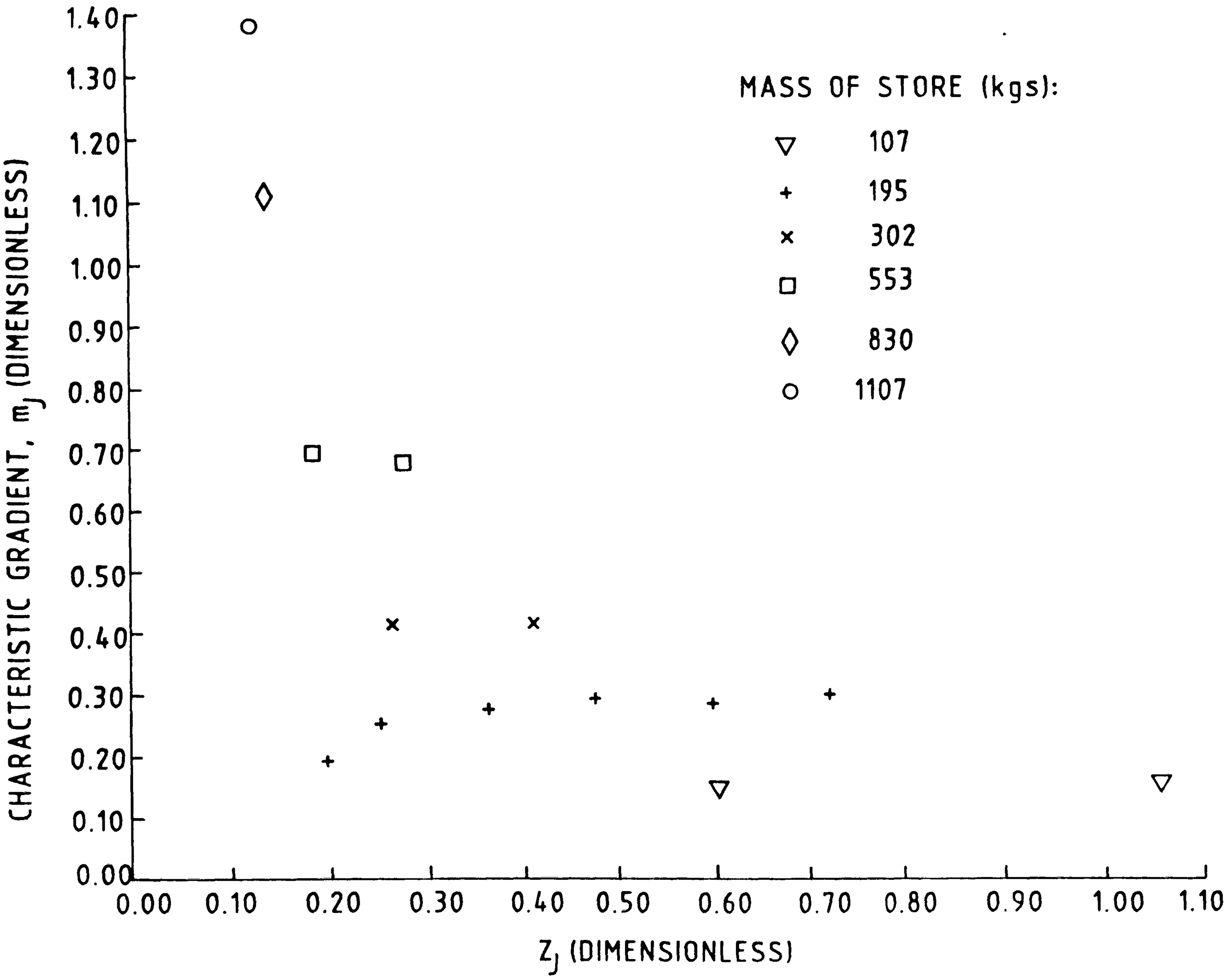
MASS OF STORE (kgs):
107
195
302
553
830
1107
CHARACTERISTIC GRADIENT, m_j (DIMENSIONLESS)
1.40
1.30
1.20
1.10
1.00
0.90
0.80
0.70
0.60
0.50
0.40
0.30
0.20
0.10
0.00
0.00 0.10 0.20 0.30 0.40 0.50 0.60 0.70 0.80 0.90 1.00 1.10
Z_j (DIMENSIONLESS)

FIGURE 11.3

Variation of circulation number, Np with Z_J due to changes in collector area and store capacity

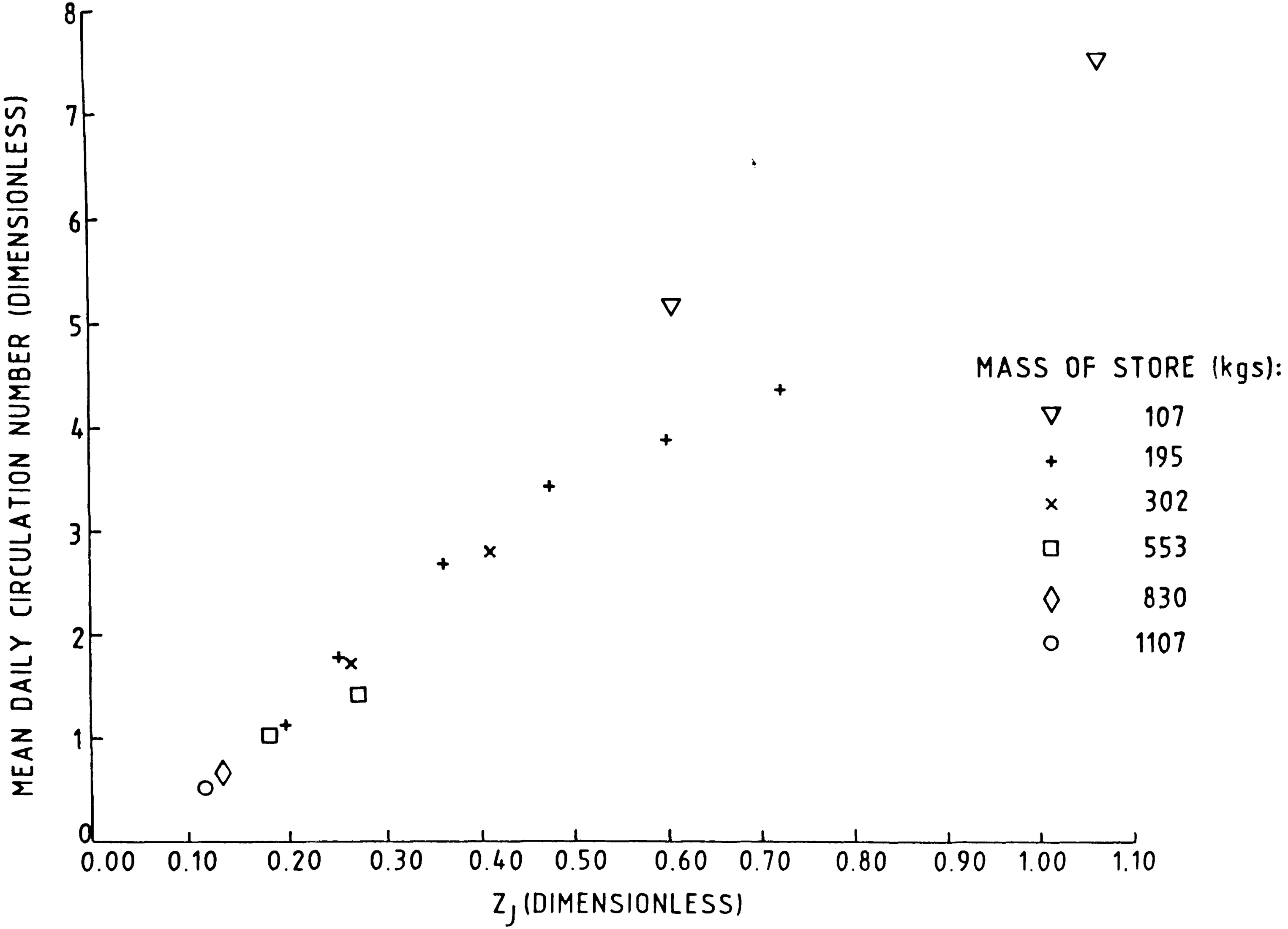
MEAN DAILY CIRCULATION NUMBER (DIMENSIONLESS)
0
1
2
3
4
5
6
7
8
0.00
0.10
0.20
0.30
0.40
0.50
0.60
0.70
0.80
0.90
1.00
1.10
Z_J (DIMENSIONLESS)
MASS OF STORE (kgs):
107
195
302
553
830
1107

only does this change the value of Z_J, but also, since the total daily draw-off remains constant, affects the relative magnitudes of the total daily draw-off and the mass of the store. The ratio of the total daily mass of water drawn off, to the mass of water in the store, although not explicitly apparent as an independent variable in the correlating function given by equation 8.31 had emerged previously as the dimensionless variable W defined, during the derivation of the more sophisticated analysis, in equation 8.14. The gradients of the characteristic curves obtained from the simulations PARASIM 0-14 are shown plotted against W in figure 11.4. The variations in the gradients due to W are seen to be large relative to those changes in which W remains constant whilst Z_J (and therefore the mean daily circulation number) alone, are varied.

One of the reasons for this variation of gradient with W, which is primarily independent of the circulation number, is due to the assumption made in section 8.3 that the draw-off of water takes the form of a single event at the end of the insolation period. The reasoning behind this assumption was that the value of the final store temperature predicted by the simple analysis, no-matter how high, would be some function of the total amount of heat collected by a particular system. The fact that equation 8.31 gives a strong linear correlation for an individual month is in itself a verification of the veracity of this assumption when W remains invariant. In reality, the amount of water withdrawn from the store during the insolation period affects the mean store temperature. This in turn affects both the temperature of the draw-off water and the heat loss from the collector and so, ultimately, the relationship between X, Y and Z. The variation of the gradients of the characteristic curves with W is therefore a reflection of the difference between the actual performance and that predicted by the load-independent analysis on which equation 8.31 is based.

Accounting for changes in the gradient, m_J, with W also allows for a thermodynamic anomaly introduced into the simplified analysis, by the use of the above assumption. This is: if water is assumed to be drawn off at the end of the insolation period and at the temperature of the store, then when the mass of water withdrawn is greater than that within the store itself, (ie. $W > 1$) then the amount of energy

FIGURE 11.4

Variation of m_J with W, due to changes in collector area and store capacity

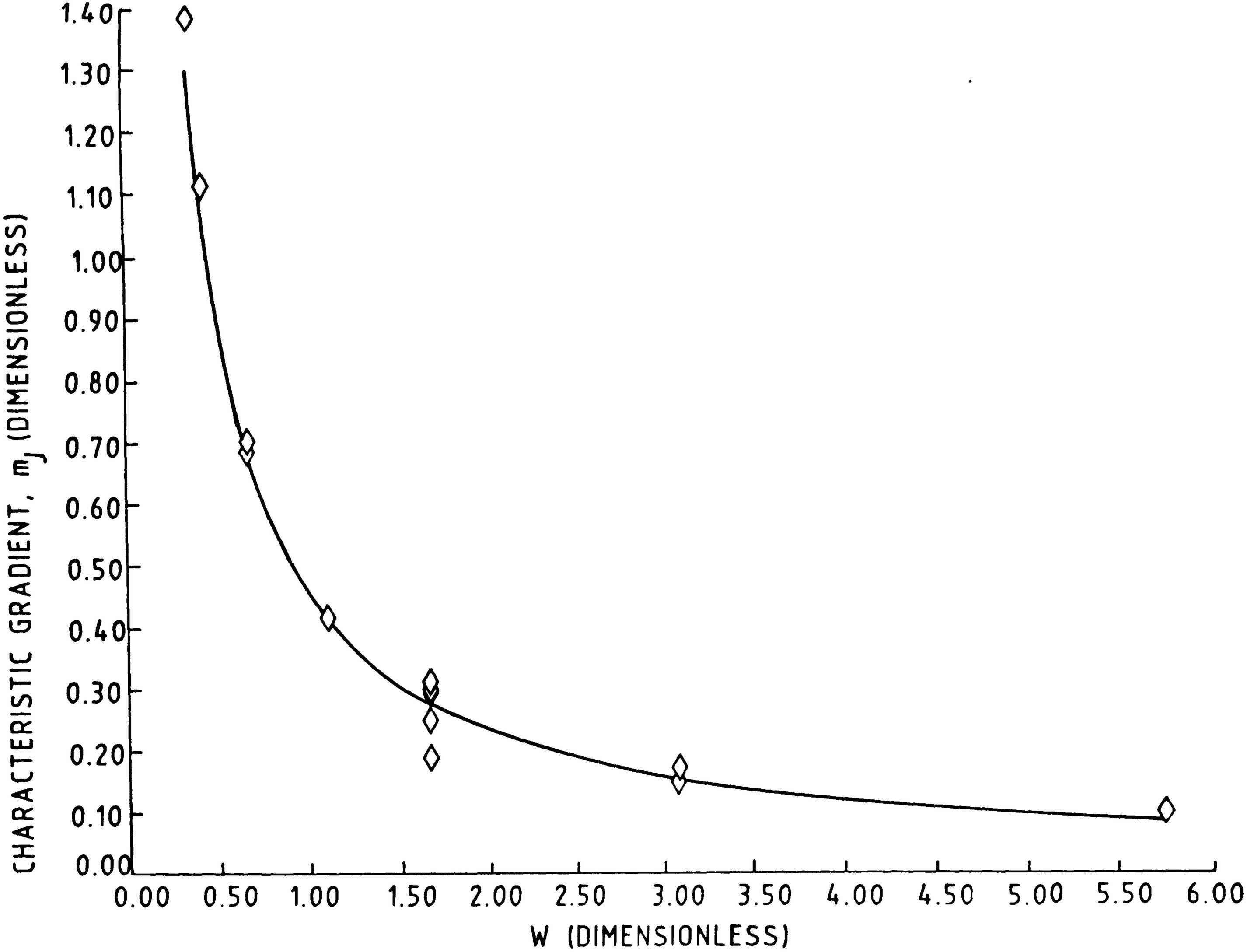
CHARACTERISTIC GRADIENT, m_J (DIMENSIONLESS)
1.40
1.30
1.20
1.10
1.00
0.90
0.80
0.70
0.60
0.50
0.40
0.30
0.20
0.10
0.00
0.00 0.50 1.00 1.50 2.00 2.50 3.00 3.50 4.00 4.50 5.00 5.50 6.00
W (DIMENSIONLESS)

extracted will be greater than that contained within the store. This would contradict the conservation of energy.

The variation of m_J with W has implications for the use of this correlation technique as a test method for individual systems. In chapter 10, it was suggested that the thermal performance of a system could be characterised using data from a single month of operation. It is evident that this is a realistic proposal only if, during the tests, the mean mass of water withdrawn from the system (ie. the value of W) is representative of the normal expected daily water consumption. Further tests on the individual system in which W is varied by using different daily loads could form the basis of a means of extrapolation by which the results could be made applicable to a range of values of W likely to be encountered by the system under test.

11.3 Development of a Universal Correlation

Three primary observations made in section 11.2, suggest a method of characterising all thermosyphon solar-energy water heaters. In summary, these are:

i) Any change in the gradient (from that of a reference system) of the characteristic curve has a component which is a function of the circulation number.The circulation number is a function of Z_J.

ii) The remaining component of any changes in the gradient are due to the effects of water draw-off on system performance, is largely independent of the circulation number and is a function of W.

iii) For a fixed value of W, the gradient of a characteristic curve is essentially constant after a certain maximum value of Z_J (and hence circulation number) has been exceeded. Because from i), Np is independent of W, this maximum value of Np will apply to all values of W.

The effect of changing the relative vertical orientation of the store and collector, from that of a reference system, will be to change the flow rate and therefore the mean daily circulation number of the

system. As with changes in Z_J, this will have the effect of altering the gradient of a reference characteristic curve. If the height of the store is increased relative to the collector, the circulation number will increase and the maximum gradient above which all systems can be characterised will be acheived at a lower value of Z_J than will occur in the reference system. Conversely, a reduction in the relative heights of the collector and store to a value less than that of the reference system, will result in a decrease in the circulation number and the maximum gradient will occur at a higher value of Z_J. A family of curves is therefore required using a fixed arbitrary value of W, each of which relate the gradient to the dimensionless parameter, Z_J for different relative collector/store heights. All the curves will converge to the same maximum gradient, this value being dependent on the magnitude of W chosen. The relationship between the displacement of the gradient from the maximum value represented by these family of curves, because the circulation number is independent of W, will be valid for all values of W. From these family of curves, a system can then be chosen for which the gradient of the characteristic curve is a maximum. Using this system, a plot similar to that in figure 11.4 of $m_{J,max}$ against W, can be determined and which will then be representative of the performance of all systems in which the maximum circulation number (beyond which no further change in the gradient occurs), has been exceeded.

A simple two-stage algorithm can now be used to determine the gradient of the characteristic curve for any system.

1) Using the required daily value of W for the system under consideration, the gradient (of a system in which the maximum circulation number has been exceeded) can be determined from the plot of $m_{J,max}$ against W.

2) For the value of Z_J and the relative collector/store orientation of the system being considered, using the family of curves described above, the required displacement (which is due to circulation number effects and is independent of W) to transform the maximum gradient onto that of the actual gradient is determined.

The assumption of equivalent mean store and collector temperatures made in determining equation 8.31 is an implicit statement of the relationship between component temperatures and the flow rates in a thermosyphon solar energy water heater. The problem therefore arrises in the choice of a suitably representative group of system parameters (including such parameters as the relative vertical orientation of the store and collector) which become applicable when correlating the performances of systems in which the above assumption of equivalent mean store and collector temperatures, does not apply. An analysis similar to the simplified approach presented in section 8.3 was therefore developed in which a fully mixed store was assumed, thereby requiring an explicit knowledge of the interaction between

(i) the relative configurations of components,

(ii) the component temperatures and

(iii) buoyancy-driven flow-rates.

The solution of the resulting differential equations was an instantaneous time dependent store temperature given by,

$$\frac{(\tau\alpha)_e I - U_L \gamma^e}{(\tau\alpha)_e I - U_L \gamma_m} = \exp[F_{AV} A_c U_L \Delta t/(M_s C_w)]$$

$$\text{x} \exp\left[\underbrace{\frac{U_L [F_{AV} A_c U_L \Delta t/(4K^* C_w)]^{0.5}}{[(\tau\alpha)_e I - U_L \gamma_m]^{0.5}}}_{\text{(i)}} \underbrace{\left(\frac{[(\tau\alpha)_e I - U_L \gamma_m]^{0.5}}{[(\tau\alpha)_e I - U_L \gamma^e]^{0.5}} - 1 \right)}_{\text{(ii)}} \right]$$

equation 11.1

where K^* is a system constant given by

$$K^* = \frac{\pi \rho \gamma g (h_3 - h_2/2)}{128 \left[L_r/(N D_r^4) + L_p/D_p^4 \right]}$$

equation 11.2

Term (i) in equation 11.1 is the solution to equation 8.25 for a system in which equivalent mean store and collector temperatures are assumed.

The actual thermal performances of most systems are intermediate between that predicted by a fully stratified and that of a fully mixed store. Term (ii) could therefore be interpreted as being representative of the temperature difference β (defined by equation 8.33) between the mean store and collector temperatures. As was suggested in section 11.1, β as represented by term (ii) in equation 11.1, is not a constant over the day. An explicit expression for the instantaneous store temperature was not obtained and the integration over the insolation period could therefore not be determined. However, the constant K^* was retained as a variable representative of the effects on β and therefore on thermal performance, of system-related parameters. More specifically, K^* as defined by equation 11.2 is the linear coefficient representing the change in flow rate per unit change in temperature between the mean store and collector temperatures (ie. per unit change in an instantaneous value of β). K^* therefore has units of $kgs^{-1}{}^{o}C^{-1}$. A dimensionless form of K* was defined as,

$$K = \frac{\rho \gamma g \Delta T_{ref}[h_3 - h_2/2]}{\nu \dot{m}_{ref}[L_r/(ND_r^4 + L_p/D_p^4)]}$$

equation 11.3

The reference temperature difference ΔT_{ref}, and mass flow rate, m_{ref}, otherwise arbitrarily chosen, were such that values of K were of a convenient order of magnitude. The values chosen were,

$\Delta T_{ref} = 10^{o}C$ and,

$\dot{m}_{ref} = 10^{-1}\ kgs^{-1}$

The thermal performance of a direct thermosyphon solar-energy water-heater was therefore shown to be dependent upon five primary dimensionless groups, namely, K, W, X, Y and Z. It was anticipated that these dimensionless groups would not undergo any further changes in their respective definitions and it was decided at this stage to allocate these terms an appropriate form of appellation. With the exception of the dimensionless group, W, technical terms which described concisely, the physical significance of the dimensionless

groups, could not be determined. In such cases these dimensionless groups were named after early pioneers in the field of thermosyphon solar-energy water-heaters. The designated terms were:

K (equation 11.3) Bailey (78) Number

W (equation 8.14) Specific Load Ratio

X (equation 8.30) Brooks (79) Number

Y (equation 8.15) Heywood (80) Number

Z (equation 8.16) Yellot (81) Number

Values of Z determined for the month of June (namely Z_J) were referred to as reference Yellot numbers.

A reference system was now defined as having a collector area of $2m^2$, and a store mass of 280 kg, the upriser entering the store at a vertical distance of 1.788m above the collector inlet. These gave values for the Bailey, K, specific load, W, and reference Yellot numbers, Z_J of 15.16, 1.169 and 0.271 respectively. For a fixed value of the relative vertical positioning of both the store and collector and the mass of the store, the area of the collector was varied from $1m^2$ to $11m^2$ giving values of Z_J which change correspondingly over the range 0.195 to 1.074.

As the size of the collector varied, so too did the minimum length of pipe work (calculated in the subroutines PRNODE and PDNODE given in appendix I), required to connect the collector to the store. Inspection of equation 11.3 reveals that such changes in the values of L_p will result in the value of K varying over a series of simulations in which the relative vertical positioning of the store and collector was invariant. The variation in Bailey number, K, over such a series of simulations due to changes in L_p was however found to be small when compared with changes due to varying $(h_3 - h_2/2)$. A mean value of Bailey number was therefore taken as being suitably representative of each of these groups of simulation runs.

The simulated relative vertical positioning of the store and collector was varied from that of the reference system to give five mean values of Bailey number, K ranging from 4.3 to 30.5. At Bailey numbers greater than 16, the characteristic gradient had converged to a constant value at values of Z_J less than 1.074. The further simulation of systems up to this maximum chosen value of Z_J were, for these cases deemed unnecessary. Also, at these higher values of Z_J and K, the flow rates were high and a small time step was required in the numerical solution (down to 5s), leading to the excessive use of computer time. Further details of the systems simulated to produce this family of curves is given in appendix L.

The gradients of the characteristic curves were found to converge to a maximum value of 0.429. Since the maximum gradient was a - then unknown - function of the arbitrarily chosen value of the specific load, W, only the displacement Δm_J of the gradient from a maximum value, rather than the absolute value of the gradient was of relevance. Values of Δm_J over the stated range of Z_J for different values of the Bailey number,K, are shown in figure 11.5. A correlating function relating the displacements of the characteristic gradients of this set of simulated sytems (PARASIM 15-41) to their respective system parameters, is given by,

$$\Delta m_J = 2.541 \times 10^{-3} + 0.780(m^*) + 1.967(m^*)^2$$

equation 11.4

over the range

$$0 < m^* \leq 0.15$$

where,

$$m^* = 0.195 \exp[(0.402 - 0.387K)Z_J]$$

Data gained from the systems simulated in PARASIM 15-41 are shown plotted as a function of m^* in figure 11.6. Equation 11.4 has an associated correlation coefficient of 0.94.

FIGURE 11.5

Displacement Δm_J of the gradients of the characteristic curves due to variations in the reference Yellot number ,Z_J for different Bailey numbers,K.

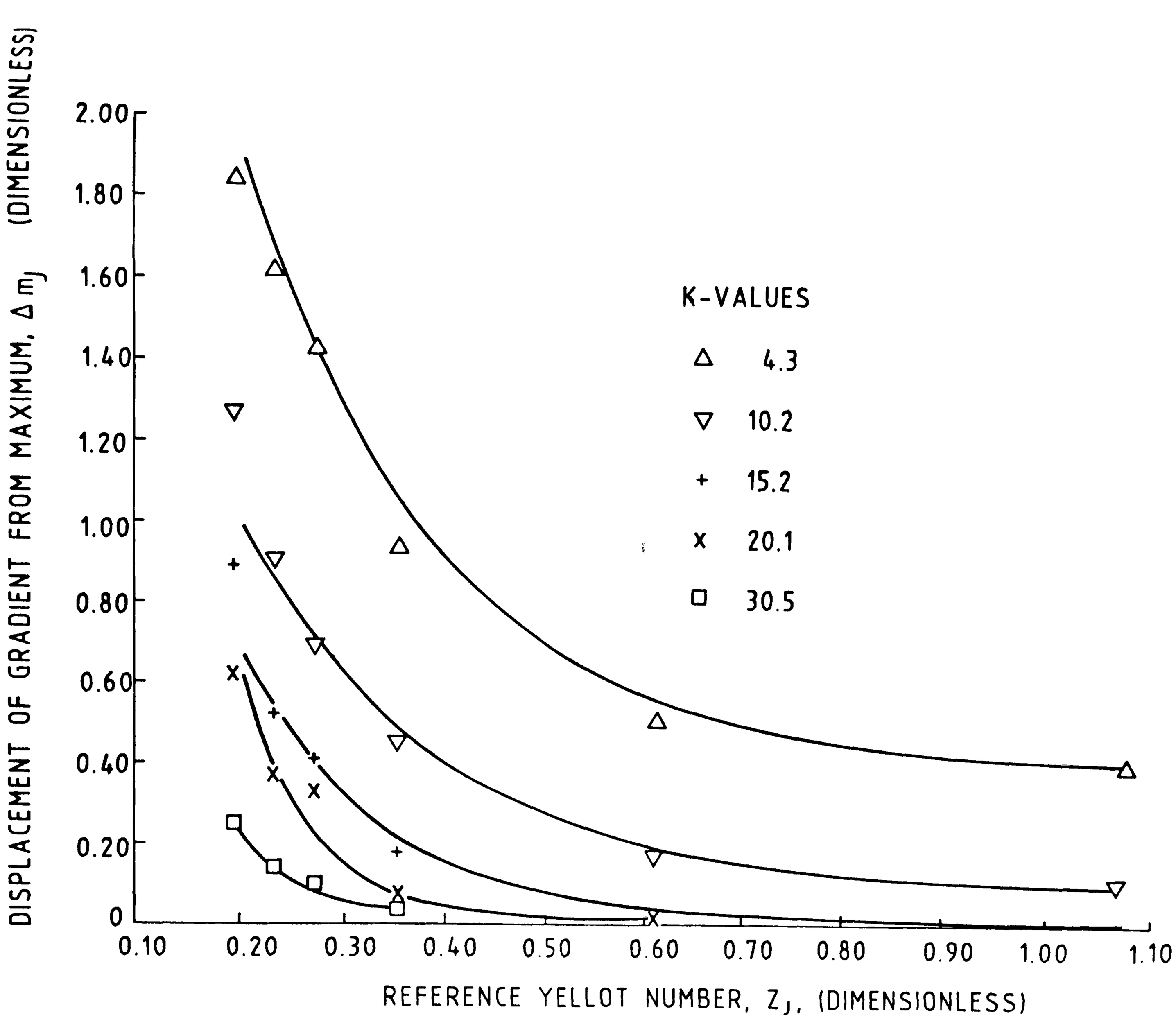
DISPLACEMENT OF GRADIENT FROM MAXIMUM, Δ mJ (DIMENSIONLESS)
2.00
1.80
1.60
1.40
1.20
1.00
0.80
0.60
0.40
0.20
0
0.10
0.20
0.30
0.40
0.50
0.60
0.70
0.80
0.90
1.00
1.10
REFERENCE YELLOT NUMBER, ZJ, (DIMENSIONLESS)
K-VALUES
Δ 4.3
▽ 10.2
+ 15.2
x 20.1
□ 30.5

FIGURE 11.6

Displacement Δm_j of the gradients of the characteristic curves due to variations in the correlating function m^*

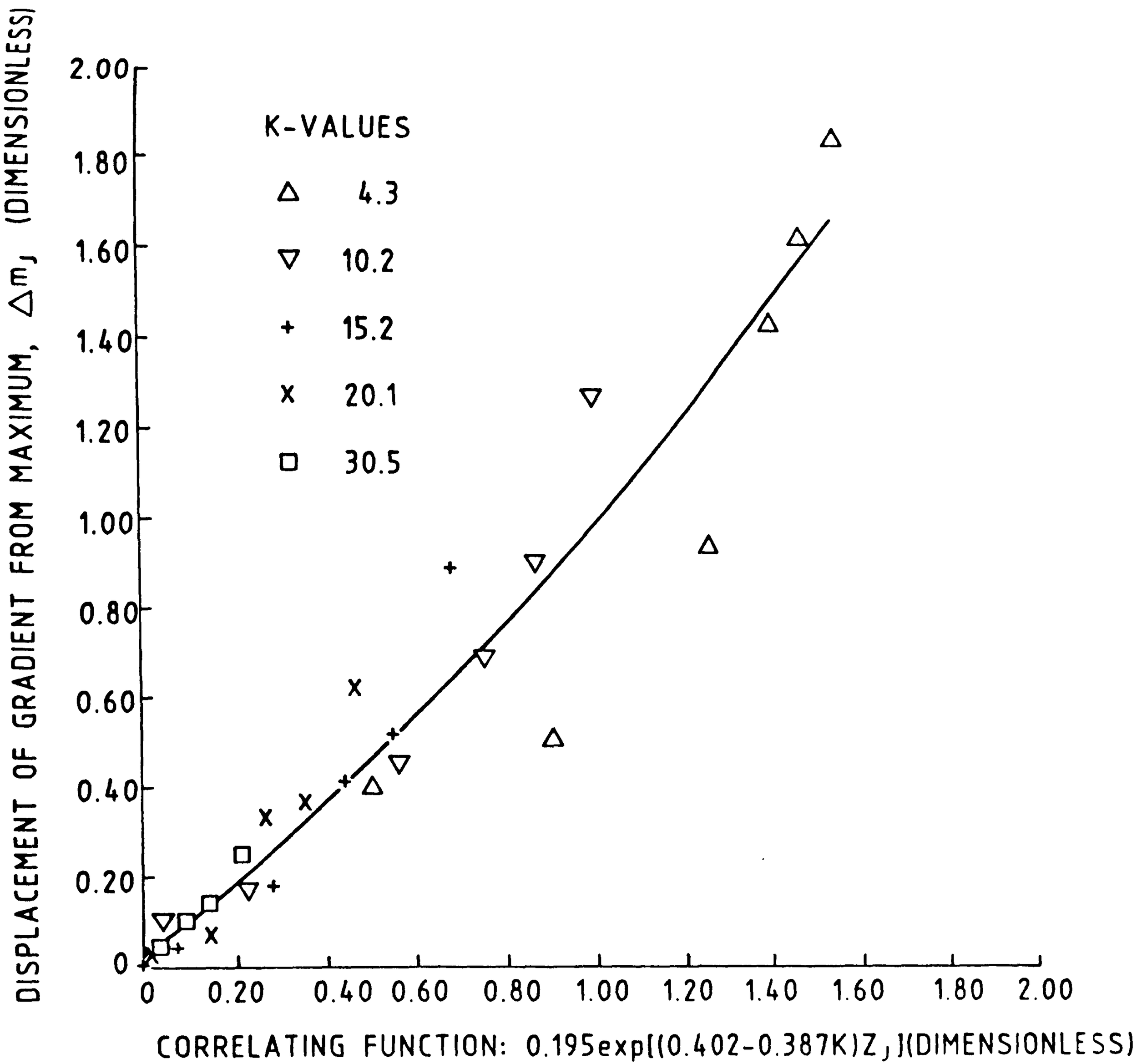
K-VALUES
4.3
10.2
15.2
20.1
30.5
DISPLACEMENT OF GRADIENT FROM MAXIMUM, Δm_J (DIMENSIONLESS)
CORRELATING FUNCTION: $0.195\exp[(0.402-0.387K)Z_J]$(DIMENSIONLESS)
0
0.20
0.40
0.60
0.80
1.00
1.20
1.40
1.60
1.80
2.00

Equation 11.4 is universally applicable to all systems within the stated range and was shown in section 11.2 to be largely independent of the specific load, W.

The relationship between the absolute value of the maximum gradient $m_{J,max}$ and the specific load, W, was investigated by varying the value of the mass of water in the store in the six simulations PARASIM 40 and 42-46. The chosen reference system was taken as PARASIM 40 with K, W and Z_J values of 31.2, 1.169 and 0.272 respectively. With the high K value, this ensured that the gradient deviated by a negligible amount from the maximum value of 0.429 (due to changes in Z_J) as the mass of the store varied. The mass of the store was varied over the range 47kg to 560kg with a corresponding variation in W from 6.8 to 0.6. A logarithmic plot of the maximum gradients, $m_{J,max}$ as a function of the load ratio, W, is shown in figure 11.7. The best fit line through this data is given by,

$$m_{J,max} = 0.4817(W)^{-0.937}$$

equation 11.5

for $0.5 \leq W \leq 6.8$

The associated correlation coefficient of equation 11.5 is 0.999.

Within the stated range, equation 11.5 represents the second of two universal curves and is predominantly independent of values of Z_J and K.

FIGURE 11.7

Variation of values of $m_{J,max}$ as a function of the specific load, W

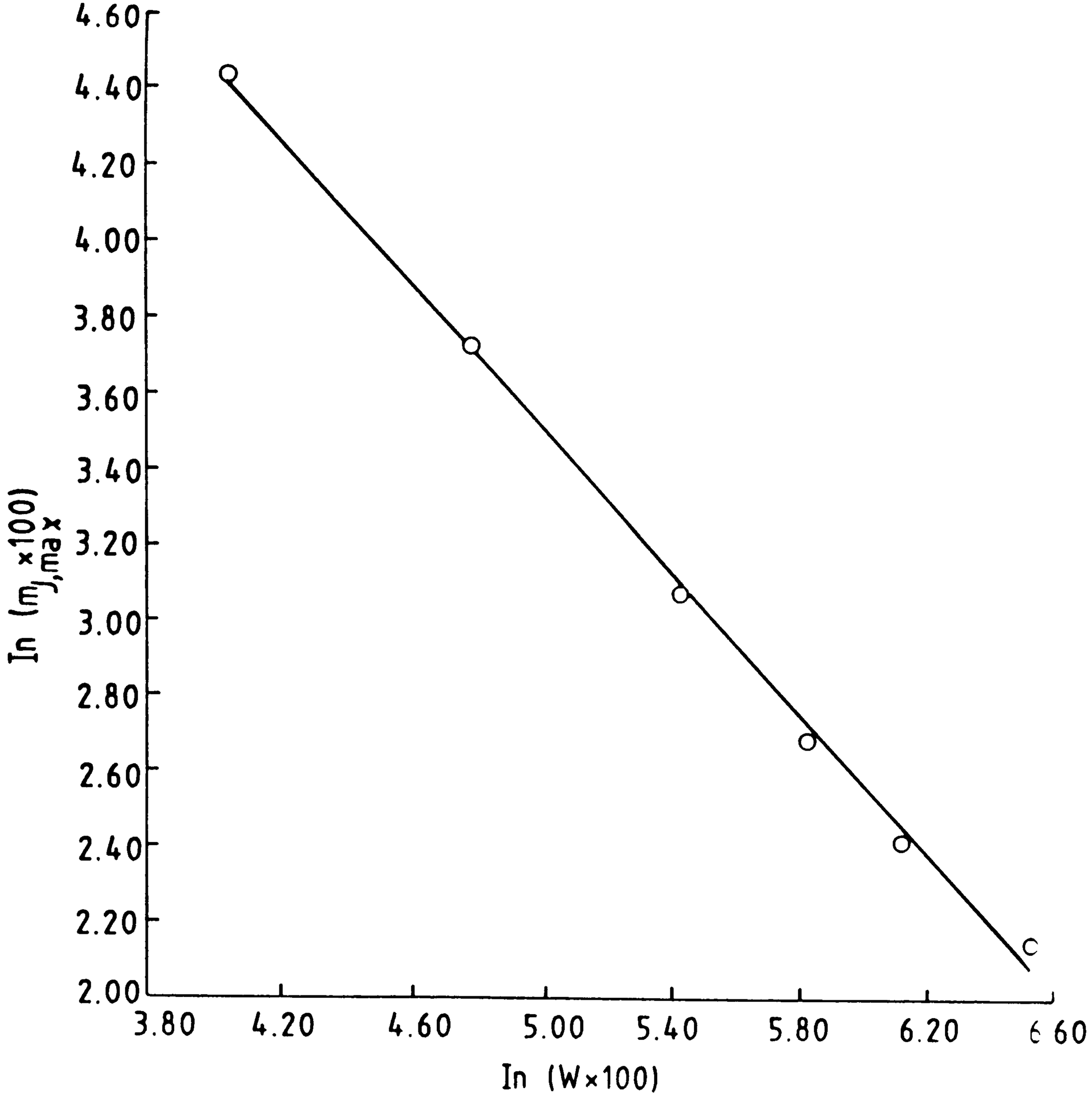
4.60
4.40
4.20
4.00
3.80
3.60
3.40
3.20
3.00
2.80
2.60
2.40
2.20
2.00
In ($\eta_{J,max}$ ×100)
3.80
4.20
4.60
5.00
5.40
5.80
6.20
6.60
In (W×100)

11.4 Accuracy of Prediction of the Universal Correlations

From equation 10.6, the performance of any direct thermosyphon solar-energy water heater can be represented by a characteristic curve of the form,

$$X = m_J(Y/Z)[1-\exp(-Z)]$$

equation 11.6

For small changes in X due to errors in estimating m_J

$$\Delta X = (Y/Z)[1-\exp(-Z)]\,\Delta m_J$$

equation 11.7

$$\text{So, } \frac{\Delta X}{X} = \frac{\Delta f'_{cor}}{f'_{cor}} = \frac{\Delta m_J}{m_J}$$

equation 11.8

where X, f'_{cor} and m_J are the differences in the respective values between those calculated using the universal correlations and those obtained using performance data obtained for a specific system (as was reported in section 10). The values of X, f'_{cor} and $m_{J,max}$ are those obtained from performance data for a specific system. Because of the high correlation coefficient (0.999) associated with the relationship between the maximum gradient, $m_{J,max}$ and the specific load, W, errors in determining the gradient of the characteristic curve were assumed to be dominated by errors in calculating the gradient displacement Δm_J. The errors were therefore analysed in terms of factors affecting Δm_J, namely the Bailey and Yellot numbers, K and Z. Using equations 11.4 and 11.5 for the universal correlations, values of $\Delta m_J/m_J$ and therefore $\Delta f'_{cor}/f'_{cor}$ were calculated for all twenty seven of the systems used in determining equation 11.4 (designated by PARASIM 15-41).

A weak relationship was observed, for constant values of K, between the parameter Z_J and the errors incurred (due to the use of the universal correlations), in determining the solar fraction. Typical correlation coefficients beteen $\Delta f'_{cor}/f'_{cor}$ and Z_J were of the order

of 0.7. As a qualitative observation, the majority of the exceptionally high errors occurred at low values of Z_J.

By determining the mean magnitude of the error for each of the five sets of tests (PARASIM 15-20,21-26,27-32,33-37 and 38-41) representing the simulations in which five different K values were investigated, a distinct decrease in the associated error was observed for increasing values of K. These mean values of $\Delta f'_{cor}/f'_{cor}$ are shown plotted in figure 11.8 as a function of K. An error function representing the best curve through these points is

$$e = 14.52(K)^{-0.52}$$

equation 11.9

where e is expressed as a percentage. The correlation coefficient is 0.904.

The fact that these errors represented values averaged over a range of systems in which Z_J varies between 0.195 and 1.074, required that the uncertainty in stating an error value be qualified by an associated expected deviation of the error from the mean. The standard deviation of the errors from their means are therefore also given in figure 11.8. This data can be represented, with a correlation coefficient of 0.899, by the function,

$$\sigma' = 19.54(K)^{-1.067}$$

equation 11.10

The value of σ' is a percentage. Inspection of figure 11.8 indicates that at low values of K, corresponding to low circulation numbers, the uncertainty in predicting the performance of a system is high. This association of low circulation number with high uncertainty of prediction is corroborated by the observation made earlier in this section that low values of Z_J produced higher errors.

The use of equation 11.9 indicates expected mean errors which vary from 7.1% for a K value of 4 (typical of a same-level, single pass system) to 2.5% for a K value of 30 (a distributed, multiple-pass system). As

FIGURE 11.8

Results of the error analysis as a function of the Bailey number, K;

a) mean error e as a function of K, incurred using the universal correlations to determine the gradient of a characteristic curve when compared with the corresponding value obtained form daily thermal performance data for an individual system

b) corresponding deviation of errors from the mean value

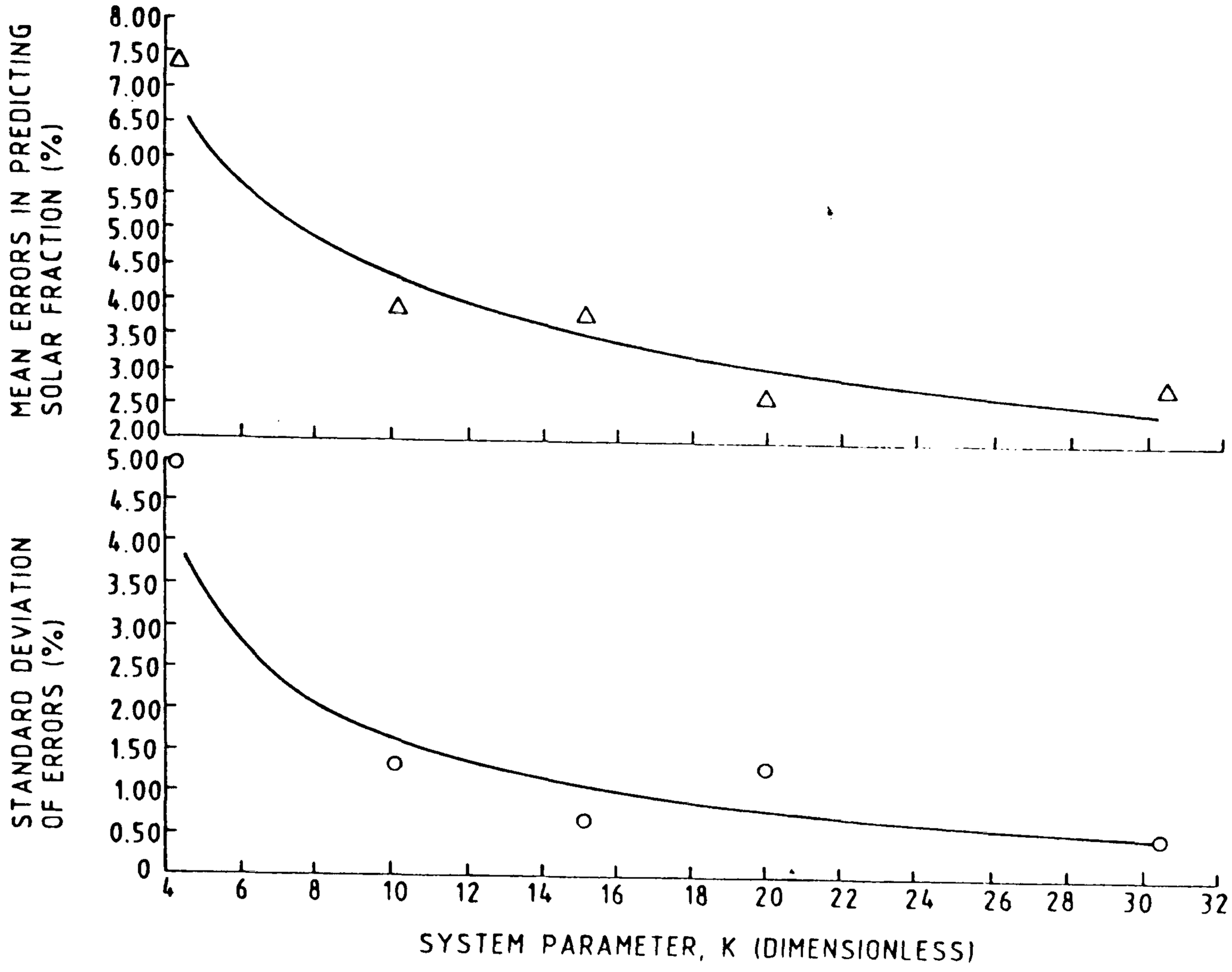
MEAN ERRORS IN PREDICTING SOLAR FRACTION (%)
8.00
7.50
7.00
6.50
6.00
5.50
5.00
4.50
4.00
3.50
3.00
2.50
2.00
STANDARD DEVIATION OF ERRORS (%)
5.00
4.50
4.00
3.50
3.00
2.50
2.00
1.50
1.00
0.50
0
4
6
8
10
12
14
16
18
20
22
24
26
28
30
32
SYSTEM PARAMETER, K (DIMENSIONLESS)

previously stated, these errors represent a deviation of the performance of a system as a result of using equations 11.4 and 11.5 to predict the characteristic gradient as compared with the predicted performance when a characteristic curve is obtained from thermal performance data for an individual system. The accuracy reported in section 10 in predicting the annual solar fraction from a characteristic curve was given as $\pm$3% when compared with the high level simulation model. Also, the error associated with the heat delivery as predicted by the numerical simulation model was, when compared in section 7.3 with experimental data, a further $\pm$2.8%. A modification to equation 11.9 to give a more realistic estimate of the total error associated with the use of the universal correlations represented by equations 11.4 and 11.5 would therefore be,

$$e = \pm[5.8 + 14.52(K)^{-0.52}]$$

equation 11.11

Equation 11.11 indicates mean total errors of between $\pm$12.9% and $\pm$8.3% over the range of K values between 3 and 30 respectively.

11.5 A Worked Example in Using the Corelations to Predict the Daily Solar Fraction

The components of a thermosyphon solar-energy water heater have the specifications listed in table 11.1. The operating conditions (for a typical day in June) are given in table 11.2.

Evaluating the parameters K, W, Y and Z from equations 11.3, 8.14, 8.15 and 8.16 respectively,

$$K = \frac{\rho_w \gamma_w g \Delta T_{ref}(h_3 - h_2/2)}{\gamma_w \dot{m}_{ref}[L_r/(ND_r^4) + L_p/D_p^4]} = \frac{998 \times 2.1\times10^{-4} \times 9.81 \times 10 \times (1.8-0.7/2)}{1.002\times10^{-6}\times10^{-1}[1/(8\times0.015^4)+8.72/0.025^4]}$$

$$= 12$$

$$W = \frac{M_L}{M_S} = \frac{208}{297}$$

$$= 0.7$$

$$Y = \frac{F_{AV}A_c(\tau\alpha)_e H^{td}}{M_s C_w(\bar{T}_a - T_m)} = \frac{0.9x2x0.72x19.2x10^6}{297x4190x(16 - 15)}$$

$$= 20$$

$$Z = \frac{F_{AV}A_c U_L \Delta t}{M_s C_w} = \frac{0.9x2x3.5x59220}{297x4190}$$

$$= 0.3$$

Also, since the thermal performance is being determined for the reference month of June,

$$Z_J = Z$$

$$= 0.3$$

A three stage algorithm is used to determine the dimensionless parameter, X from which the solar fraction can be calculated. A nomogram, shown in figure 11.9, has been devised to provide a graphical means of determining the solar fraction.

1. DETERMINE THE DEVIATION, Δm_J (DUE TO CIRCULATION NUMBER EFFECTS) OF THE CHARACTERISTIC GRADIENT FORM THE MAXIMUM VALUE, $m_{J,max}$

From equation 11.4,

$$\Delta m_J = 2.541x10^{-3} + 0.78(m^*) + 1.967(m^*)^2$$

where

$$m^* = 0.195\exp[(0.402-0.387K)Z_J] = 0.195\exp[(0.402-0.387x12)x0.3]$$

$$= 0.055$$

and so,

$$\Delta m_J = 2.541x10^{-3} + 0.78x0.055 + 1.967x0.055^2$$

$$= 0.051$$

This stage corresponds to the first quadrant of the nomogram

Table 11.1 Details of the configuration and thermal data for the thermosyphon solar-energy water-heater used in a sample calculation

Collector area, (A_c)	= 2	m^2
Average collector fin efficiency factor, (F_{AV})	= 0.9	
Effective transmittance -absorptance product, for collector absorber plate and cover, ($\tau\alpha$)$_e$	= 0.72	
Overall steady-state heat-loss coefficient for the collector, (U_L)	= 3.5	$Wm^{-2}{}^oC^{-1}$
Storage tank heat loss coefficient, (UA)$_s$	= 3	W^oC^{-1}
Number of risers in collector(N)	= 8	
Mass of water in the store, (M_s)	= 297	kg
Vertical height from collector inlet to inlet at top of store, (h_3)	= 1.8	m
Vertical height between collector inlet and outlet, (h_2)	= 0.7	m
Length of riser pipe, (L_r)	= 1	m
Internal diameter of riser pipe, (D_r)	= 0.015	m
Total length of connecting pipework (L_p)	= 8.72	m
Internal diameter of connecting pipework, (D_p)	= 0.025	m

Table 11.2 Operating conditions, thermal load and fluid properties used the sample calculation

Total daily global solar radiation,$(H)^{td}$	= 19.2	MJm^{-2}
Mean daily ambient temperature,$(\bar{T}_a)$	= 16	^oC
Cold water mains supply temperature,(T_m)	= 15	^oC
Day length,(Δt)	= 59220s	
Total daily mass of water removed from store,(M_L)	= 208	kg
Required hot water supply temperature,(T_L)	= 46	^oC

All physical properties of water are evaluated at the mains cold water supply temperature. The values used are,

Density,(ρ_w)	= 998	kgm^{-3}
Dynamic viscosity,(μ_w)	= 10^{-3}	Nsm^{-2}
Kinematic viscosity,(ν_w)	= $1.002x10^{-6}$	m^2s^{-1}
Specific heat capacity,(C_w)	= 4190	$Jkg^{-1}{}^oC^{-1}$
Cubic expansivity,(γ_w)	= $2.1x10^{-4}$	$^oC^{-1}$

FIGURE 11.9

Nomogram representing the design formulae given by equations 11.4, 11.5 and 10.6

W: specific load

W=2.0 W=1.5 W=1.2 W=1.0 W=0.8 W=0.7 W=0.6

W=3.0

W=5.0

0.00 0.10 0.20 0.30 0.40 0.50 0.60 0.70 0.80 0.90

characteristic gradient

X10⁻¹

2.00 1.80 1.60 1.40 1.20 1.00 0.80 0.60 0.40 0.20 0.00

displacement of gradient from max value

K: Bailey number

K= 4

K= 5

K= 7

K= 9

K=12

K=16

K=21

K=27

0.00 0.10 0.20 0.30 0.40 0.50 0.60 0.70 0.80 0.90 1.00 1.10 1.20

Z : reference Yellot number

Z: Yellot number

Z=0.2

Z=0.3

Z=0.4

Z=0.5

Z=0.6

Z=0.7

Z=0.8

Z=0.9

Z=1.0

Z=1.1

Y= -80 Y= -60 Y= -40 Y= -30 Y= -20 Y= -10 Y= -5 Y= 5 Y= 10 Y= 20 Y= 30 Y= 40 Y= 60 Y= 80

Y: Heywood number

-60 -50 -40 -30 -20 -10 0 10 20 30 40 50 60

X: Brooks number

2. DETERMINE THE MAXIMUM GRADIENT FOR THE SYSTEM AND SUBTRACT THE GRADIENT DISPLACEMENT, Δm_J, TO GIVE THE ACTUAL GRADIENT, m_J, OF THE CHARACTERISTIC CURVE.

Using equation 11.5,

$$m_{J,max} = 0.4817(W)^{-0.937} = 0.4817(0.7)^{-0.937}$$
$$= 0.673$$

The actual gradient, m_J is then given by,

$$m_J = m_{J,max} - \Delta m_J = 0.673 - 0.051$$
$$= 0.622$$

Using the nomogram, the value of m_J can be read off from the second quadrant (moving anticlockwise).

3. USING THE CHARACTERISTIC CURVE, CALCULATE X FROM WHICH THE SOLAR FRACTION CAN BE DETERMINED.

Rearranging the appropriate characteristic curve as defined by equation 10.6,

$$X = \frac{m_J(1 - e^{-Z})Y}{Z} = \frac{0.622x(1 - e^{-0.3})x20}{0.3}$$
$$= 10.71$$

This calculation corresponds to the third and fourth quadrants of the nomogram.

From the definition of X given in equation 8.30, the daily solar fraction can be determined from,

$$(f'_{cor})^{td} = \frac{XM_L C_w(T_a - T_m)}{Q_{tot}}$$

The total thermal load, Q_{tot} when M_L kg of water are heated from the

mains cold water supply temperature, T_m to the required temperature of T_L ^oC is,

$$Q_{tot} = M_L C_w (T_L - T_m) = 208x4190x(46 - 15)$$
$$= 27.02x10^6 J$$

So the daily solar fraction is,

$$(f'_{cor})^{td} = \frac{10.7x208x4190x(16-15)}{27.02x10^6}$$
$$= 0.345$$

The estimated mean error band, e associated with this value for the daily solar fraction is, from equation 11.11,

$$e = \pm [5.8 + 14.52(K)^{-0.52}] = \pm [5.8 + 14.52x12^{-0.52}]$$
$$= \pm 6.8\%$$

Strictly speaking, equation 11.11 refers to errors incurred in predicting annual solar fractions. The cumulative error over a year occurs predominantly as a result of using the characteristic curve for June in order to predict the performance over the entire year. Since in this example, the characteristic curve for June has been used to predict the performance of a system in that same month, the error will be less than the value calculated above.

CHAPTER TWELVE

CONCLUSIONS AND FUTURE RESEARCH

12.1 Conclusions

The development of a high level numerical model has been shown, by comparison with experimental data, to be a successful method of simulating the performances of thermosyphon solar-energy water-heaters. By the testing of each component of the water heater, the veracity of the analyses developed for the individual components has been determined. With the exception of the collector absorber plate for which a two dimensional analysis was adopted, a one dimensional approach (in the direction of the bulk fluid flow within each component) was found to give predicted temperature profiles which were well within the error bands associated with the corresponding measured values.

An indoor test facility has been developed which enabled a variety of radiation and water draw-off patterns to be simulated; both step inputs and "real" insolation patterns were shown to be feasable in terms of the microcomputer-based control and monitoring techniques employed. This facility was thus both more comprehensive and flexible than previous indoor solar water heating system simulators that have adopted a similar approach (82,83,84). The flexibility afforded by this software-based facility, made practical the overall validation approach of individual component testing. The main limitations of such a system were found to be the dual requirements of the electrical heater mats of:

(i) high power density (and therefore high heater temperatures), and

(ii) a flexible electrically-insulating covering layer with good thermal contact with the collector absorber plate.

The resulting compromise of electrical heater mats with a power density of approximately 600 Wm^{-2} was only a limitation when simulating "real" conditions. Both the transient and steady-state performances of components over a wide range of thermal conditions were not subject to such limitations as other performance parameters such as flow rate and component inlet temperatures could be varied to extend the range of conditions against which the numerical model could be validated.

The use of a non-invasive electromagnetic inductive flow meter was shown to be successful in measuring thermosyphonic flow rates under normal conditions of forward circulation. The particular instrument employed was not suitable for measuring reverse flows. However, experiences with this instrument at low forward-circulating mass flow-rates indicated that, had it been capable of measuring reverse circulation, the zero-offset errors caused by the deposition on the electrodes of small impurities from the circulating fluid, would be of a greater order of magnitude than normal reverse circulation flows.

The predicted performance of the collector under steady-state conditions agreeed closely with experimental values. The predicted effects of conduction within the collector absorber plate in a direction parallel to and opposite in direction to the flow of water in indicated a highly non-linear temperature profile along the length of the absorber plate at low flow rates. When the performance was simulated for the case of one dimensional conduction (between the collector fin base and tip) under identical conditions, the corresponding temperature profile was observed to be linear. The simulated mean absorber plate temperatures and therefore the predicted efficiencies for the two cases considered were, for all practical purposes, identical. For the purposes of steady-state prediction, a Hottel-Whillier-Bliss-type analysis was therefore deemed adequate for the modelling of collector performance. The main advantages of a two dimensional absorber plate analysis was demonstrated by the good agreement between the predicted and measured response time without recourse to an effective heat capacitance for the absorber plate in which there is a non-uniform temperature distribution.

A simple five-node finite difference mesh was found to give excellent agreement between the predicted and measured transient and steady state thermal responses of the connecting (upriser and downcomer) pipe work.

Experimental measurements of the penetration depths at the inlet to a high aspect ratio (diameter/height), vertical store at low Reynolds number, laminar flow indicated negligible local mixing in this area over a range of Richardson number flows. An equalisation test carried

out under *no*-flow conditions identified conduction in the copper walls of the storage tank as being the predominant cause of thermocline relaxation effects.

Correlating functions used in the prediction of frictional fluid losses in pipes under conditions of isothermal and non-isothermal flow, were collated. Where possible, using existing data, new correlating functions have been derived either as an attempt to improve on existing functions or where, previously, such functions had not been developed. These functions were used in the numerical simulation and the resulting predicted flow rates were compared with corresponding measured values. The use of a non-isothermal correlation in determining the friction factors within the collector riser pipes were found to give predicted flow rates which were significantly more accurate than those obtained with the previously-used isothermal, developing-flow correlations.

Good agreement was shown to exist between the measured and predicted heat output of a thermosyphon solar-energy water-heater when operating under "real" conditions of insolation and water draw-off.

An analysis was developed from which five dimensionless groups consisting of parameters pertaining to the dimensions and thermal characteristics of individual components of a thermosyphon solar-energy water-heater and the prevalent operating conditions, were identified. The functional relationship between these dimensionless groups and diurnal system performance (using the validated numerical simulation) has been derived. Using the correlation technique developed and by the choice of appropriate test conditions, a characteristic thermal performance curve could be determined. Thirty days was shown to be a sufficient test period from which a performance curve could be determined. Using such a curve, the calculated annual solar fraction was in good agreement with the corresponding value computed from the numerical simulation. As a test method for individual systems, this technique, because it was based on a transient analysis, represented a considerable saving in the duration of the required test period when compared with previous methods in which monthly rather than diurnal test periods are necessary.

Using the numerical simulation model, values representing the characteristic gradients of a wide range of systems operating under the same conditions of hot water water draw-off were shown to be a function of the corresponding mean diurnal circulation numbers. The gradient of the characteristic curve was shown also to be a function of the specific load (the ratio of the diurnal water draw-off to the mass of the store). Two universal curves were therefore developed in which the characteristic curves were correlated against,

1) the dimensionless groups containing system-related parameters which affect the mean diurnal circulation number, and

2) the specific load ratio.

These two curves formed the basis of a technique by which the thermal performance of any directly-heated thermosyphon solar-energy water-heater (within a stated range) could be predicted, based on detailed system-related and water draw-off data.

12.2 Future Areas of Research

The following is a summary of possible areas for further investigation based on, and beyond the scope of, this present study.

1) The relationship between jets of fluid entering a stratified store, the store size and relaxation of the thermocline are well documented for turbulent flow. The same is not the case for laminar jets. Although negligible mixing was observed over the range of conditions investigated in this study, a larger range of store types need to be investigated using either a three dimensional store analysis or an empirical approach to determine the penetration depth of a laminar jet into a stratified store as a function of the state and flow rate of the fluid and the dimensions of the storage tank and inlet pipe. Such a correlation would then permit the extension of the one dimensional storage tank analysis to more complex storage tank configurations (eg. horizontal, cylindrical stores) with a greater degree of confidence.

2) Using the currently available flow loss relationships, predicted

flow rates during periods of reverse circulation are too high, thereby over estimating the store losses during the night. At these low Reynolds number flows, fully developed and, since there is no longer solar radiation incident on the absorber plate, isothermal (Poiseuille-type) flow would be expected in the riser pipes. However, even by retaining the non-isothermal friction factor correlation in the calculation of frictional losses during these periods, the under estimate of the flow losses persists. It is evident that at these low Reynolds numbers, there is sufficient heat loss from the collector to cause a high degree of thermal destabilisation and a relationship from which appropriate friction factors can be determined during reverse circulation, needs to be developed.

3) A system employing a direct method of heat delivery to the storage tank was investigated as an initial step towards the investigation of more complex systems. Many thermosyphon solar-energy water-heaters employ indirect methods of heat delivery. The inclusion in the storage tank simulation of a heat exchanger would therefore be a logical step. A term in the analysis, similar to that developed by Webster et al (22), to account for the thermal penalties incurred by the introduction of a heat exchanger and the correlation method for performance prediction, could be determined resulting in a modification of the dimensionless parameters used in correlating system performance.

4) The presence of fluid properties within the Bailey number suggests an investigation into the possible application of the system performance correlations presented in this study to thermosyphon air heaters. The mass of the store would have to be replaced by an effective thermal capacitance for the load (ie. the fabric of a room or building). The frictional losses at the collector inlet and outlet vents could be represented by an equivalent pipe length in the Bailey number.

5) The universal correlations developed in this study were generated using the numerical model to simulate the thermal performances of thermosyphon solar-energy water heaters under U.K. weather conditions. Although none of the dimensionless correlating parameters are explicitly location-dependent, the veracity of the universal

correlations when applied to climates other than that experienced in the U.K. needs to be established using alternative meteorological data bases as inputs to the numerical simulation.

REFERENCES

1. G L Morrison and H N Tran, "Simulation of the
Long Term Performance of Thermosyphon Solar
Water Heaters", Solar Energy, 33, 515-526, 1984.

2. B J Huang and C T Hsieh,"A Simulation
Method for Solar Thermosyphon Collector",
Solar Energy, 35, 31-43, 1985.

3. Z P Song and H J Zhang, "Prediction
of System Performance
of Solar Water Heaters for a Specified Locality",
Solar Energy, 28, 433-441, 1982.

4. G L Morrison and C M Sapsford, "Long Term Performance of
Thermosyphon Solar Water Heaters",
Solar Energy, 30, 341-350, 1983.

5. P A Hobson, B Norton and S N G Lo, "Demonstration of
Thermosyphon Solar-Energy Water Heating in
a Group of Three Dwellings", EEC Technical Report No.4,
Project Number SE 034/83, April, 1986.

6. M P Malkin, S A Kline and J A Duffie, "A Design
Method for Thermosyphon Solar Domestic Hot Water Systems",
Solar Engineering-1986, Proc. of the ASME Solar Energy
Conf., Aneheim, California, April, 1986.

7. D J Close, "The Performance of Solar Water Heaters
with Natural Circulation",
Solar Energy, 6, 33-40, 1962.

8. C L Gupta and H P Garg, "System Design
in Solar Water Heaters with Natural Circulation",
Solar Energy, 12, 163-182, 1968.

9. K S Ong,"A Finite Difference Method to Evaluate the
Performance of a Solar Energy Water Heater",
Solar Energy, 16, 131-147, 1974.

10. K S Ong,"An Improved Computer Program for
the Thermal Performance of a Solar Water Heater",
Solar Energy, 18, 183-191, 1976.

11. J W Baughn and D A Dougherty, "Experimental Investigation
and Computer Modeling of a Solar Natural Circulation System",
Proc. 1977 Annual Meeting of the Am. Sec. of
ISES, 1, 4.25-4.29, 1977.

12. G L Morrison and D B J Ranatunga,"Transient
Response of a Thermosyphon Solar Collector",
Solar Energy, 26, 55-61, 1980.

13. B J Huang,"Similarity Theory of a Solar Water Heater with
Natural Circulation", Solar Energy, 25, 191-198, 1980.

14. M Vaxman and M Sokolov, "Effects of Connecting Pipes in
in Thermosyphonic Solar Systems", Solar Energy, 37,
323-330, 1986.

15. M F Young,"Solar Domestic Hot Water Systems:
A Comparative Study and Storage Tank Investigation",
Ph.D Thesis, University of California, Davis USA, 1980.

16. A Mertol, W Place, T Webster and R Greif, "Detailed Loop Model
Davis Analysis of Liquid Thermosypons with Heat Exchangers",
Solar Energy, 27, 367-386, 1981.

17. D E Riddle,"Modelling the Transient Performance of
Natural Circulation Solar Hot Water Systems",
Numerical Methods in Thermal Problems, 4, 1029-1039, 1985.

18. P Pierson and R. Javelas, "Etude Theoretique et Experimentale d'un Chauffe-Eau Solaire avec Echangeur et Fonctionaumont Naturelle" (in French), Revue Generale de Thermique, 22, 467-482, 1983.

19. B Norton and S D Probert, "Thermosyphon Solar Energy Water Heaters", Advances in Solar Energy, 3, 125-170, 1986.

20. B Norton and S D Probert, "Achieving Thermal Rectification in Natural Circulation Solar Energy Water Heaters", Applied Energy, 14, 211-225, 1983.

21. H L Langhaar, "Steady Flow in the Transitional Length of a Straight Tube", ASME Jour. App. Mech., 9, 55-58, 1942.

22. T L Webster, J P Coutier, J W Place and M Tavana, "Experimental Evaluation of Solar Thermosyphons with Heat Exchangers", Solar Energy, 38, 219-231, 1987.

23. J A Duffie and W Beckman,"Solar Engineering of Thermal Processes",John Wiley, NY,USA,1980.

24. A Shitzer, D Kalmanoviz, Y Zvirin and G Grossman, "Experiments With a Flat Plate Solar Water Heating System in Thermosyphonic Flow", Solar Energy, 22, 27-35, 1978.

25. R H Kirchhoff and M Billups,"A Two Dimensional Heat Transfer Model of a Flat Plate Collector", ASME Conference Paper Number 76-WA/Sol-2, ASME New York, USA, December, 1976.

26. P P Rao, J E Francis and T J Love (Jnr.), "Two Dimensional Analysis of a Flat Plate Solar Collector", Journal of Energy, 1, 5-12, September-October, 1977.

27. D E Prapas, B Norton, E Milonidis and S D Probert,"Response Function for Solar-Energy Collectors", Solar Energy, 40, 549-562, 1988.

28. B Norton, P.D. Fleming, S.N.G. Lo and S.D. Probert, "Data Acquisition from Thermosyphon Solar-Energy Water Heaters for a Terrace of Three Dwellings", Proc. of UK-ISES Workshop on Solar Energy and Building Design, Birmingham, UK, April, 1985.

29. J G Hare, "Specification of Flat Plate Solar Collector" Gull Air Ltd, Fort Fareham,Hampshire,UK, 1984.

30. B M Cross, "Thermal Performance Test of a Flat Plate Solar Collector Submitted for Test by Gull Air Ltd.", Rep. No. 1162, SEU No. 486.Energy Equipment Testing Service, University College Cardiff, Cardiff, Wales.

31. Anon, "International Thermocouple Reference Tables for Copper/Constantan", TC Limited, Uxbridge, UK.

32. Anon, "Mounting and Operating Instructions - Magnetic Inductive Flow Meter with Line Frequent Field", Eckart, Stuttgart, W-Germany.

33. C Sherman, D Byard, J Mason, "Effect of Vertical Wall Conductance on Temperature Relaxation in Thermally Stratified Liquid Thermal Storage Tanks", Procs. of ISES conf., Atlanta, Georgia, May, 1979.

34. J S Turner, "Jets and Plumes with Negative or Reversing Buoyancy", J. Fluid Mechanics, 26, 4, 779-792, 1966.

35. Z Lavan and J Thompson, "Experimental Study of Thermally Stratified Hot Water Storage Tanks", Solar Energy, 19, 519-524, 1977.

36. B J Sliwinsky, A R Mech, T S Shih,
"Stratification in Thermal Storage During Charging",
Procs. of International Heat Transfer Conf.,
EU-6.149, Toronto, Canada, 1978.

37. R Cohen, "Commissioning and Experimental Work on a
Thermal Energy Storage Test Facility, PhD Thesis,
Cranfield Institute of Technology, Bedford, UK, 1986.

38. Anon, "Methods of Test for the Thermal Performance
of Solar Collectors", British Standards
Institution, DD77, 1982.

39. K G T Hollands, T E Unny, G D Raithby and L Konicek,
"Free Convection Heat Transfer Across Inclined Air Layers",
Trans. of ASME, Jour. of Heat Transfer, 98, 189-193, 1976.

40. E M Sparrow, J W Ramsey and E A Mass,
"Effect of Finite Width on Heat Transfer and
Fluid Flow About an Inclined Rectangular Plate",
Trans. of ASME, Jour. of Heat Transfer, 101, 2, 1979.

41. C P Kothandaraman and S Subramanyan,"Heat and
Mass Transfer Data Book", 3rd Ed, Wiley Eastern, New Delhi, 1977.

42. Anon, "Methods of Testing to Determine the Thermal
Performances of Solar Collectors", ASHRAE Standard 93-77,
ASHRAE, New York, USA, 1977

43. S Goldstein, "Modern Developments in Fluid Dynamics",
Oxford University Press, Oxford, UK, 1938.

44. S J Kline and A H Shapiro, "Experimental
Investigation of the Effects of Cooling
on Friction and on Boundary-Layer Transition for
Low Speed Gas Flow at the Entry of a Tube",
NACA Report, Technical Note 3048, 1953.

45. T Tatsumi,"Stability of the Laminar Inlet-Flow Prior
to the Formation of the Poiseuille Regime,
Jour. of the Physical Soc. of Japan, 7, 489-495, 1952.

46. W D Campbell and J C Slattery,"Flow in the Entrance
of a Tube",ASME Jour. of Basic Engineering, 85, 41-45, 1963.

47. E M Sparrow and S H Lin, "Flow Development
in the Hydrodynamic Regions of Tubes and Ducts",
Pysics of Fluids, 7, 338-347, 1964.

48. F Kreith and R Einstadt, "Pressure Drop and Flow Characteristics
of Short Capiliary Tubes at Low Reynolds Numbers",
Trans. ASME, 79, 1070-1078, 1957.

49. S A Al-Nasri and T Unny, "Developing Laminar
Flow in the Inlet Length of a Smooth Pipe",
Applied Scientific Reasearch, 36, 313-332, 1980.

50. G A Kemeny and E V Somers, "Combined Free and Forced-Convective
Flow in Vertical Circular Tubes: Experiments with
Water and Oil", ASME Jour. of Heat Transfer, 84, 339-346, 1962.

51. H F Crevling, J F De Paz, J Y Baladi and R J Schoenhals,
"Stability Characteristics of a Singlephase Free
Convective Loop", Jour. of Fluid Mechanics, 67, 65-84, 1975.

52. A J Addlesee, "Frictional Resistance of Low Reynolds
Number Flows Destabilised by Heat Transfer",
Letters in Heat and Mass Transfer, 7, 249-255, 1980.

53. A A Bishop, J M Willis and R A Markley, "Effects of
Buoyancy on Laminar Upward Flow Friction Factors
in Cylindrical Tubes", Nuclear Engineering
and Design, 62, 365-369, 1980.

54. Anon,"Pressure Losses in Curved Ducts:Single Bends", Engineering Science Data Units (ESDU), Item Number 83037, Technical Editing and Reproductions Ltd., London, 1983.

55. C Beck, "Laminar Flow Friction Losses in 90 Constant Circular Cross-Section Bends", Jour. of the American Society of Naval Engineers, 56, 366-388, 1944.

56. C P Kittredge and D S Rowley, "Resistance Coefficients for Laminar and Turbulent Flows Through One-Half Inch Valves and Fittings, ASME, 78, 1759-1766, 1959.

57. D A Crow and R Wharton, "A Review of Literature on the Division and Combination of Flow in Closed Conduits", British Hydromechanics Research Assosiation, Report TN937, Cranfield, UK, 1968.

58. Anon, "Pressure Losses in Three-Leg Pipe Junctions: Combining Flow", ESDU, Item Number 73023, Technical Editing and Reproductions Ltd., London, 1973.

59. Anon, "Pressure Losses in Three-Leg Pipe Junctions: Dividing Flow", ESDU, Item Number 73022, Technical Editing and Reproductions Ltd., London, 1973.

60. F Kreith, "Principles of Heat Transfer", Third Edition, Intex Press, New York, 1973.

61. S A Klein, W A Beckman and J A Duffie, "A Design Procedure for Solar Heating Systems", Solar Energy, Vol.18, 113-127, 1976.

62. S T Liu and J E Hill, "A Proposed Technique for Correlating the Performance of Solar Domestic Water Heating Systems", ASHRAE Transactions, 85, part (i), 96-109.

63. S A Klein and contributers, "TRNSYS, a Transient System Simulation Programme. Report 38-11". Solar Energy Laboratory, University of Wisconsin, USA, April, 1981.

64. W F Phillips and R N Dave, "Effects of Stratification on the Performance of Liquid-Based Solar Heating Systems", Solar Energy, 29, 111-120, 1982.

65. G L Morrison, N H Tran, "Correlation of Solar Water Heater Test Data", Solar Energy, 39, 135-142, 1987.

66. Anon, "Solar Water Heating Systems; Progress Towards the Development of Performance Test Methods", Non Nuclear Eñergies, BSI Private Circulation, Doc. No. 87/70509, Octtober 1986.

67. M Collares Pereira, "Solar Systems Long Term Performance Prediction Based on I-O Test Results", Procs. of the CEC Collector and System Testing Group Meeting, 205-211, Seville, December, 1986.

68. W Place, M Daneshyar, R Kammerud, "Mean Monthly Performance of Passive Solar Water Heaters", Procs. of the 4th National Passive Solar Conference, Kansas City, Missouri, October 3rd-5th, 1979.

69. D Rowe (CIBSE Technical Officer), Private Comunication re: CIBSE Example Weather Years, Delta House, London, September, 1987.

70. K M Letherman, F M Wai, "Condensed Statistics on the CIBSE Example Weather Year-Kew", Technical Note, Building Services Engineering Research and Technology, 1, 3, 157-159, 1980.

71. E A R Hithchin (British Gas), Private Comunications, August 1987.

72. J E Braun and A H Fanney, "Design and Evaluation of Thermosyphon Solar Water-Heating Systems", Procs. of the Annual Conference of the American Solar Energy Society, Minneapolis, Minnesota, USA, 283-288, June, 1983.

73. B Norton and S D Probert, "Characteristics of Thermosyphonic Solar-Energy Water-Heaters", Procs. of the Fourth International Conference on Energy Options-The Role of Alternatives in The World Energy Scene, Institution of Electrical Engineers, London, England, 39-42, April, 1983.

74. G L Morison, C M Sapsford, "Performance of Domestic Solar Water Heaters", Procs. of the Conference of the Australian-New Zealand Section of the International Solar Energy Society, Sydney, Australia, November, 1981.

75. M F Young and J B Bergquam, "The Performance of a Thermosyphon Solar Domestic Water System with Hot-Water Withdrawl", Solar Energy, 3, 655-658, 1984.

76. S N G Lo, B Norton, P A Hobson, "Demonstration of Thermosyphon Solar-Energy Water Heating in a group of Three Dwellings", Final Report to the Commision of the European Communities, Project No. SE 03483, December, 1987.

77. W A Smith, J K Page and J L Thomson, "A Metiorological Data Base System for Architectural and Building Engineering Designers", S.E.R.C. Handbook, 1, 2nd edition, September 1983.

78. W J Bailey, "Solar Heaters", U.S. Patent No. 966, 070, 1910.

79. F A Brooks, "Solar Energy and its Use for Heating Water in California", Agricultural Experimental Station Bulletin, 602, University of California, Berkeley, California, 1936.

80. H Heywood, "Solar Energy for Water-and-Space Heating", Journal of Institute of Fuel, 27, 334-352, 1954.

81. J I Yellot and R Sobotka, "An Investigation of Solar Water Heater Performance", ASHRAE Transactions, 7, 425-453, 1964.

82. A H Fanney, "Analytical and Experimental Analysis of Procedures for Testing Solar Domestic Hot Water Systems", PhD Thesis, Virginia Polytechnic Institute and State University, Blacksburg, Virginia, USA, 1981.

83. J Pascal Coutier, "Laminar Convection with Buoyancy in Tube Flows with a Surrounding Liquid Medium", PhD Thesis, University of California, Berkeley, USA, 1983.

84. J T Gidney, "The Development of a Design Procedure for Thermosyphon Solar Water Heaters", MSc. Thesis, Cranfield Institute of Technology, Bedford, UK, 1985.

85. R P Benedict, "Fundamentals of Pipe Flow", John Wiley and sons, USA, 1977.

APPENDICES

APPENDIX A:

STABILITY CRITERIA FOR THE FINITE-DIFFERENCE APPROXIMATION TO A GENERAL HEAT-TRANSFER EQUATION

An equation equivalent to those derived in chapter 2 in which conductive, and convective heat transfer processes are represented, will be of the general form,

$$\frac{\partial T}{\partial t} + A\frac{\partial T}{\partial x} = B\frac{\partial^2 T}{\partial x^2} + C(T_a - T)$$

equation A.1

where A, B and C are positive constants. A finite difference approximation for equation A.1 may be determined such that the future temperature of a particular node $(T_k)^{t+1}$ in terms of both the current node temperature $(T_k)^t$, and the temperature of adjacent nodes may be expressed either explicitly or implicitly. In its explicit form, equation A.1 becomes

$$\frac{(T_k)^{t+1}-(T_k)^t}{\Delta t} + A\frac{(T_k-T_{k-1})^t}{\Delta x} = B\frac{(T_{k+1}-2T_k+T_{k-1})^t}{\Delta x^2} + C[T_a-(T_k)^t]$$

equation A.2

Rearranging equation A.2 gives

$$(T_k)^{t+1} = (T_k)^t[1-(A/\Delta x+2B/\Delta x^2+C)\Delta t]+[(A/\Delta x+B/\Delta x^2)\Delta t](T_{k-1})^{t+1} + (B\Delta t/\Delta x^2)(T_{k+1})^t + C\Delta t T_a$$

equation A.3

Inspection of equation A.3 indicates that in order that thermodynamic laws are obeyed, the coefficients of the temperature terms must take on positive values. This may be illustrated by assuming $(T_{k-1})^t$ and $(T_{k+1})^t$ have values which are equal to, but lower than, the current temperature $(T_k)^t$ of the node in question. If then, the coefficient of $(T_k)^t$ in equation A.3 is negative, this would result in the predicted future temperature $(T_k)^{t+1}$ taking on a value which is lower than the

surrounding nodes, $(T_{k-1})^t$ and $(T_{k+1})^t$ and the ambient temperature T_a. This would imply, in direct contradiction to the second law of thermodynamics as stated by Clausius, that heat has been transferred from a lower to a higher temperature without any external application of work. The criteria for stability in equation A.3 (from the coefficient of $(T_k)^t$) is therefore

$$(A/\Delta x + 2B/\Delta x^2 + C)\Delta t \prec 1$$

or, in terms of the limits imposed on the time step Δt,

$$\Delta t \prec (A/x + 2B/x^2 + C)^{-1}$$

If the finite difference form of equation A.1 is expressed such that $(T_k)^{t+1}$ is implicit in the approximation as has been done for equations 3.1 to 3.15, then this would give

$$\frac{(T_k)^{t+1}-(T_k)^t}{\Delta t}+\frac{A(T_k-T_{k-1})^{t+1}}{\Delta x}=\frac{B(T_{k+1}-2T_k+T_{k-1})^{t+1}}{\Delta x^2}+C[T_a-(T_k)^{t+1}]$$

equation A.4

and rearranging equation A.4 to give $(T_k)^{t+1}$ as the subject,

$$(T_k)^{t+1}=[(T_k)^t+(A\Delta t/\Delta x+B\ t/\Delta x^2)(T_{k-1})^{t-1}+(B\Delta t/\Delta x^2)(T^{k+1})^{t+1}+C\Delta tT_a]/[1+A\Delta t/\Delta x+2B\Delta t/\Delta x^2+C\Delta t]$$

equation A.5

Since A, B and C, as previously stated, have positive values, then all the node and ambient temperature coefficients will also be positive for all values of Δx and Δt. Solving for a temperature field using equations of the implicit form represented by A.5, will therefore result in a numerical procedure which is unconditionally stable. The only bounds limiting the chosen time and space steps, is the desired accuracy of the solution.

APPENDIX B:

DESCRIPTION OF SOLAR COLLECTOR

Name of manufacturer: Gull Air Ltd.

Name of collector: Maxsun

Transparent covers:

  number: 1

  thickness: 0.005 m

  effective aperture dimensions: 1.975 m x 0.98 m

Absorber plate:

  material: copper

  thickness: 0.0007m

  surface treatment: Maxorb selective foil

  surface absorptivity: 0.97

  surface emissivity: 0.11

  manufacturing process: fins mechanically bonded to 0.015 m diameter copper tubes

Thermal insulation:

  thickness: 0.100 m

  material: glass fibre

Casing material: GRP

Total mass of collector with water: 63 kg

Gross dimensions of collector: 2.015 m x 1.015 m x 0.11 m.

Maximum operating temperature: 100 ^{o}C.

Acceptable heat transfer fluids: water, water/antifreeze.

APPENDIX C:

STORAGE TANK CONFIGURATION AND THE POSITIONING OF THERMOCOUPLES

The store was constructed from a commercially available cylindrical tank with 0.0007 m thick copper walls. The base of the tank was internally-domed and the top was uncovered. The maximum store capacity was 0.1159 m^3 and the water level within the tank was adjusted using the adjacent constant head tank to give an actual volume of 0.111 m^3 of water. Upriser, downcomer, draw-off and the constant head tank inlet ports were brazed directly onto the store wall. The points of entry of the upriser and downcomer pipes were belled to reduce flow resistance. Thermocouples were mounted axially in the store on a 0.01 m diameter glass fibre rod. The low thermal conductivity of this material minimised the possibility of axial heat transfer down the rod. The dimensions of the store, positioning of the ports and placement of the thermocouples are given in figure C.1.

The effective volume of the section of the store below the downcomer port was calculated by assuming that the dome forms a segment of a sphere of radius, r, shown in figure C.1. The segment protrudes into the store a distance of 0.082 m and the radius of the segment in the plane of the store base was taken as being equivalent to that of the store (0.245 m). By the ratio of intercepting perpendicular chords for a circle, the radius of the sphere segment will be given by

$$0.082(2r - 0.082) = (0.245)^2$$

from which $r = 0.4070$ m

The volume of the sphere segment can be calculated from the integral

$$V = \pi \int_{(0.407-0.082)}^{0.407} (r^2 - y^2)dy$$

FIGURE C.1

The dimensions and positioning of thermocouples within the storage tank

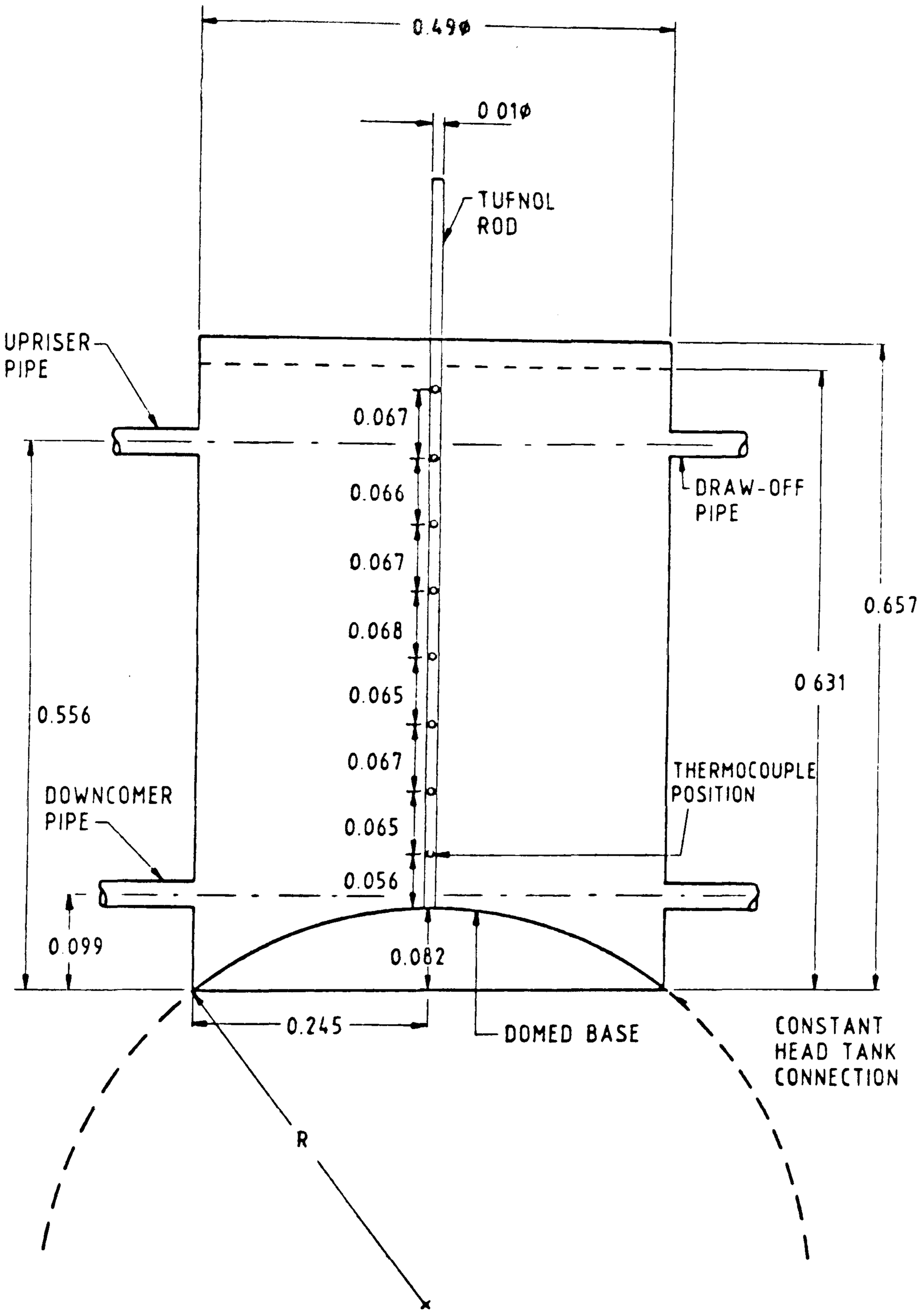
0.490
0 010
TUFNOL
ROD
UPRISER
PIPE
0.067
0.066
0.067
0.068
0.065
0.067
0.065
0.056
DRAW-OFF
PIPE
0.657
0 631
0.556
THERMOCOUPLE
POSITION
DOWNCOMER
PIPE
0.099
0.082
0.245
DOMED BASE
CONSTANT
HEAD TANK
CONNECTION
R

which gives

$$V = r^2 y - \frac{y^3}{3}\Bigg|_{0.325}^{0.407}$$

and so $V = 0.008020\ m^3$

The volume of the store below the centre line of the downcomer port in the absence of the spherical segment is $0.018669\ m^3$. The actual volume of the store section below the downcomer port is therefore given by,

$0.018669 - 0.008020 = 0.010649\ m^3$.

The estimated uncertainties in store measurements were $\pm$ 0.001 m for the store heights and, because of the degree of flexibility of the copper tank walls, $\pm$ 0.002 m for the store radius. This gave an error band of $\pm$ $0.0021\ m^3$ or approximately $\pm$ 2% for the overall volume of water contained in the tank.

APPENDIX D:

MONITORING AND CONTROL DIAGRAM

A flow diagram of the monitoring and control software is shown in figure D.1. The complete program in listing D.1 written in BBC basic follows. The program is designed to read meteorological data (previously measured at an alternative location) and the corresponding draw-off pattern from an occupied dwelling, and simulate these operating conditions whilst simultaneously monitoring the experimental response of a thermosyphon solar water heater. The procedures and functions used in other programs (such as those in which a thermal step function was imposed on the system via the power supplied to the collector heater mats), represented a subset of those given in the following listing.

FIGURE D.1

Flow diagram of monitoring and control program

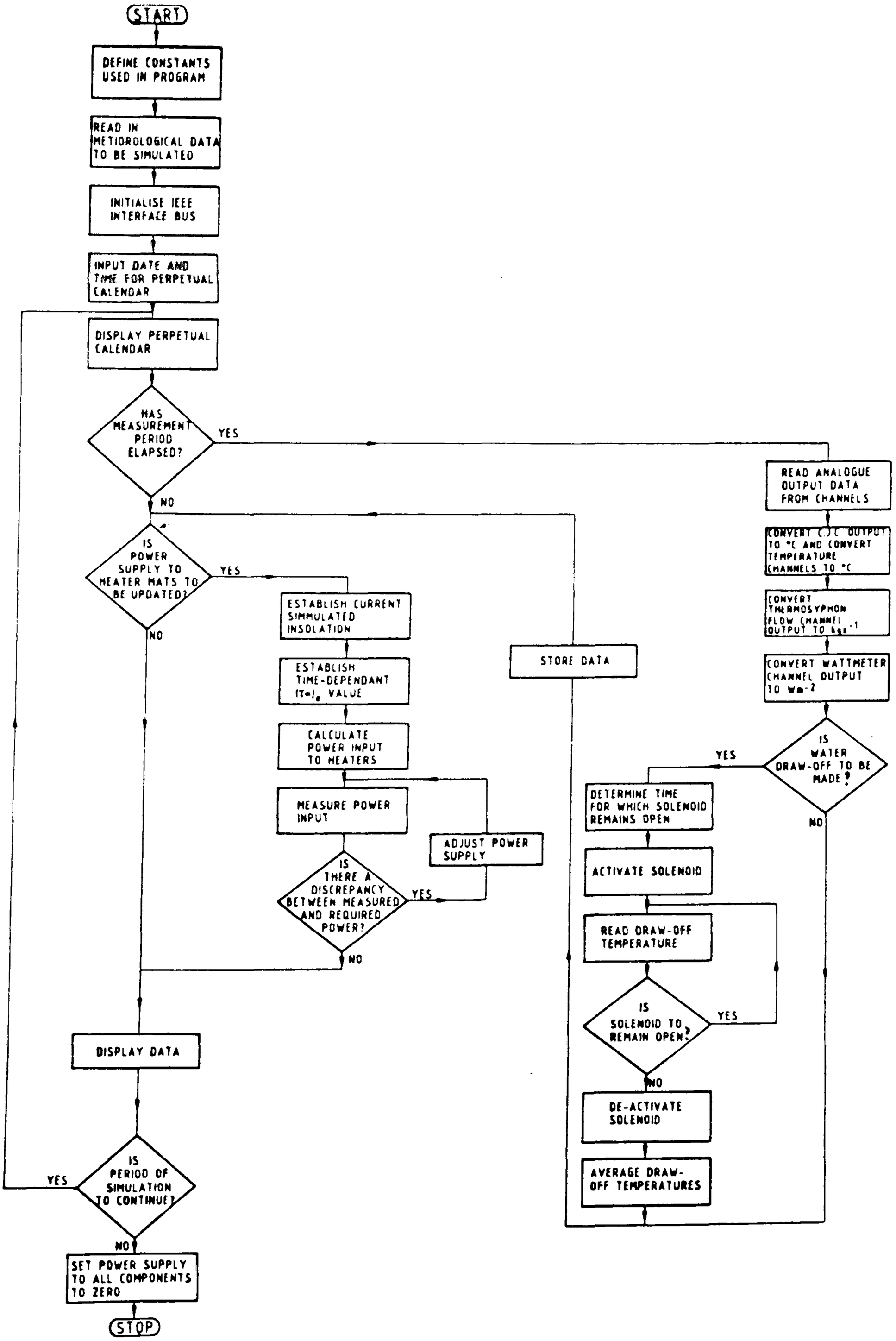
START
DEFINE CONSTANTS USED IN PROGRAM
READ IN METIOROLOGICAL DATA TO BE SIMULATED
INITIALISE IEEE INTERFACE BUS
INPUT DATE AND TIME FOR PERPETUAL CALENDAR
DISPLAY PERPETUAL CALENDAR
HAS MEASUREMENT PERIOD ELAPSED?
YES
NO
READ ANALOGUE OUTPUT DATA FROM CHANNELS
CONVERT C.J.C. OUTPUT TO °C AND CONVERT TEMPERATURE CHANNELS TO °C
CONVERT THERMOSYPHON FLOW CHANNEL OUTPUT TO kgs-1
CONVERT WATTMETER CHANNEL OUTPUT TO Wm-2
IS WATER DRAW-OFF TO BE MADE?
YES
NO
DETERMINE TIME FOR WHICH SOLENOID REMAINS OPEN
ACTIVATE SOLENOID
READ DRAW-OFF TEMPERATURE
IS SOLENOID TO REMAIN OPEN?
YES
NO
DE-ACTIVATE SOLENOID
AVERAGE DRAW-OFF TEMPERATURES
STORE DATA
IS POWER SUPPLY TO HEATER MATS TO BE UPDATED?
YES
NO
ESTABLISH CURRENT SIMMULATED INSOLATION
ESTABLISH TIME-DEPENDANT $(T\alpha)_e$ VALUE
CALCULATE POWER INPUT TO HEATERS
MEASURE POWER INPUT
IS THERE A DISCREPANCY BETWEEN MEASURED AND REQUIRED POWER?
YES
NO
ADJUST POWER SUPPLY
DISPLAY DATA
IS PERIOD OF SIMULATION TO CONTINUE?
YES
NO
SET POWER SUPPLY TO ALL COMPONENTS TO ZERO
STOP

LISTING D.1

The monitoring and control program

```
   10 ONERRORGOTO350
   20 MODE7
   30 REM DIMENSION ARRAYS
   40 DIMv$(3,9),v(3,9),T(3,9),R%(1,5),F%(1,5),B(12),hur(200),mnt(200)
,slr(200),lde(200),PT(3)
   50 REM DEFINE CONSTANTS
   60 REM USED IN PROGRAM
   70 PROCconstants
   80 REM INPUT DIURNAL METEOROLOGICAL
   90 REM DATA FOR SIMMULATION
  100 PROCreadin
  110 REM INITIALISE IEEE DEVICE
  120 PROCinitialise
  130 REM ESTABLISH DATE AND TIME
  140 REM FOR WHICH SIMMULTION
  150 REM WILL BE RUN.SET CLOCK.
  160 PROCgetdatetime
  170 REM START MONITORING AND
  180 REM CONTROL SEQUENCE
  190 REPEAT
  200   REM ESTABLISH CURRENT TIME,
  210   REM SCAN SENSORS AND ACTIVATE
  220   REM CONTROL DEVICES AT APPROPRIATE
  230   REM INTERVALS
  240   PROCshowtime
  250 UNTILday = dayend
  260 REM END MONITORING SEQUENCE
  270 REM
  280 REM ERROR HANDLING ROUTINE
  290 REM SHUTS DOWN POWER SUPPLY TO
  300 REM ALL CONTROLLED DEVICES
  310 REM EITHER AT END OF SIMMULATION
  320 REM PERIOD OR ALL ERRORS OTHER
  330 REM THAN PURPOSELY GENERATED
  340 REM FILE HANDLING ERRORS
  350 IFERR=223THENCLOSE#Y:GOTO120
  360 *IEEE
  370 volt=0:FORdac%=1TO3:PROCset(volt,dac%):NEXT
  380 *D.
  390 *DR.0
  400 PRINTTAB(0,22);ERL:REPORT
  410 END
  420 REM END OF PROGRAM
  430 REM ------------------------
  440 DEFPROCinitialise
  450 REM INITIALISE IEEE INTERFACE
  460 CLOSE#0
  470 *IEEE
  480 cmd%=OPENIN("COMMAND")
  490 data%=OPENIN("DATA")
  500 PRINT#cmd%,"BBC DEVICE NO",0
  510 PRINT#cmd%,"CLEAR"
  520 REM CONVERT VALUE OF volt IN
  530 PRINT#cmd%,"REMOTE ENABLE"
  540 PRINT#cmd%,"UNTALK"
  550 PRINT#cmd%,"UNLISTEN"
  560 ENDPROC
```

```
570 REM ------------------------
580 DEFPROCgetdatetime
590 REM SET THE INTERNAL CLOCK AT
600 REM THE CURRENT "REAL" TIME.
610 REM DATE SET AT DAY CORRESPONDING
620 REM TO DATE AT WHICH METIOROLOGICAL
630 REM DATA RECORDED.
640 IFyear%<99THENyear%=year%+1900
650 PRINTTAB(0,0)"time at which simulation starts"
660 REPEAT
670   PRINTTAB(5,10);"Hours ";
680   INPUThour
690 UNTILhour>1ANDhour<24
700 REPEAT
710   PRINTTAB(5,12);"Minutes ";
720   INPUTminute
730 UNTILminute>1ANDminute<60
740 CLS
750 TIME=100*60*(minute+60*hour)
760 PRINTTAB(0,10);CHR$(141);"     NOW INSERT DATA DISC":PRINTTAB(0,
11);CHR$(141);"    NOW INSERT DATA DISC"
770 PRINTTAB(0,13);CHR$(141);"       AND PRESS RETURN":PRINTTAB(0,14
);CHR$(141);"       AND PRESS RETURN"
780 INPUT""cont$:IFcont$<>""GOTO800
790 CLS
800 ENDPROC
810 REM ------------------------
820 DEFPROCshowtime
830 REM DETERMINE CURRENT TIME.
840 REM SCAN SENSORS, UPDATE
850 REM POWER SUPPLY TO HEATERS
860 REM AND MAKE WATER DRAW_OFF
870 REM AT APPROPRIATE TIME.
880 REM DISPLAY PERPETUAL CALENDAR
890 IFTIME>8640000THENTIME=TIME-8640000
900 hour=TIMEDIV360000MOD24
910 minute=TIMEDIV(100*60)MOD60
920 second=TIMEDIV100MOD60
930 IF(hour=0ANDminute=0ANDlastminute=59)THENPROCincdate:REM See 115
0
940 lastminute=minute
950 PRINTTAB(0,0);"Date= "day;" ";
960 RESTORE970
970 DATA Jan,Feb,Mar,Apr,May,June,July,Aug,Sept,Oct,Nov,Dec
980 FORX=1TOmonth
990   READmonth$
1000 NEXTX
1010 PRINTmonth$;" ";year%;" ";
1020 PRINT"GMT= ";
1030 IFhour<10THENPRINT" ";
1040 PRINT;hour;" : ";
1050 IFminute<10THENPRINT" ";
1060 PRINT;minute;" : ";
1070 IFsecond<10THENPRINT" ";
1080 PRINT;second;" ";
1090 IF oldday<>day THENPROCduration(day,month)
1100 IFsecond=0THENPROCkaytime:PROCrec
1110 IFsecond=0ANDminute MOD5=0THENPROCsolar(KJ%,extrap)
1120 ENDPROC
```

```
1130 REM ------------------------
1140 DEFPROCincdate
1150 REM INCREMENT DAY,MONTH OR YEAR
1160 day=day+1
1170 IF(month=2)AND(day>29)THENday=1:month=3
1180 IF(month=2)AND(day=29)THENIFNOTFNLEAP(year%)THENday=1:month=3
1190 IFday>31THENday=1:year%=year%+1
1200 IFmonth>12THENmonth=1:year%=year%+1
1210 ENDPROC
1220 REM ------------------------
1230 DEFFNLEAP(Y)
1240 REM DETERMINE LEAP YEAR
1250 IFYMOD4=0AND(YMOD100<> 0ORYMOD400=0)THEN=TRUEELSE=FALSE
 1260 REM-----------------------------
 1270 DEFPROCrec
 1280 REM INITIALLY CLOSE ALL CHANNELS.
 1290 REM SCAN TEN CHANNELS INDIVIDUALLY
 1300 REM IN EACH OF THE TWO MODULES.
 1310 REM APPLY CONVERSION FACTORS,
 1320 REM RECORD DATA THEN DISPLAY
 1330 REM ALL CURRENT READINGS
 1340 REM ON THE SCREEN.
 1350 LD%=0:TEM=0:CNT%=0:REP%=0
 1360 FORM%=67TO68
 1370 FORSCANadd%=65TO69:SCANadd$=CHR$(SCANadd%):PROCopenscan("7",SCAN
add$):NEXT
 1380 FORSCANadd%=65TO69:SCANadd$=CHR$(SCANadd%):PROCopenscan("6",SCAN
add$):NEXT
 1390    FORN%=0TO9
 1400      IFM%=68ANDN%=7THEN1540
 1410      m$=CHR$(M%)
 1420      n$=STR$(N%)
 1430       PROCscan("7",m$,n$,200)
 1440      IF(M%=67ANDN%=0)OR(M%=68ANDN%=8)THENADCrange$="0"ELSEADCrang
e$="3"
 1450      IFM%=67ANDN%=1THENPROCcold:GOTO1540
 1460      IFM%=68ANDN%=9ANDlde(KJ%)     0ANDKJ%     KOLD%THENPROCload(KJ
%)
 1470      v(M%-67,N%)=FNadc("6","F",ADCrange$,2000)
 1480      IFM%=67ANDN%=0THENGOTO1540
 1490      v(M%-67,N%)=v(M%-67,N%)-ZERO
 1500      IFM%=68ANDN%=8THENPROCflow(v(1,8),T(1,0)):GOTO1540
 1510      VT=v(M%-67,N%)+CJV
 1520      T(M%-67,N%)=INT(0.5+10*(-0.104797+VT*(25.9454E3+VT*(-6.895E5
+VT*2.3512E7))))/10
 1530      IFLD%=1THENCNT%=CNT%+1:TEM=TEM+T(M%-67,N%):GOTO1460
 1540   NEXTN%
 1550 NEXTM%
 1560 IFCNT%<>0THENT(1,9)=INT(0.5+10*(TEM/CNT%))/10:DRW=T(1,9):KOLD%=K
J%ELSET(1,9)=0
 1570 PROCdisc
 1580 PROCdisplay
 1590 ENDPROC
```

```
1600 REM ------------------------
1610 DEFPROCdisc
1620 REM RECORD DATA AND CORRESPONDING
1630 REM TIME OF MEASUREMENT ON DISK
1640 REM IN FILE " .RD". IF FILE
1650 REM DOES NOT ALREADY EXIST,THEN
1660 REM ERROR GENERATED AND FILE
1670 REM CREATED IN ERROR
1680 REM HANDLING ROUTINE.
1690 *D.
1700 *DR.2
1710 IFREC%=0THENREC%=1:X=OPENOUT("£.RD")ELSEX=OPENUP("£.RD"):PTR#X=E
XT#X
1720 BPUT#X,day
1730 BPUT#X,month
1740 BPUT#X,year%-1900
1750 BPUT#X,hour
1760 BPUT#X,minute
1770 insol1=INT(insol/(2*100)):insol2=INT(insol/2-100*insol1)
1780 BPUT X,insol1:BPUT X,insol2
1790 IFCNT%<>0THENBPUT#X,MASS ELSEBPUT#X,0
1800 FORM%=67TO68:FORN%=0TO9
1810     CHAN=10*T(M%-67,N%)
1820     CHAN1=INT(CHAN/100):CHAN2=INT(CHAN-100*CHAN1)
1830     BPUT#X,CHAN1:BPUT#X,CHAN2
1840 NEXTN%:NEXTM%
1850 CLOSE#X
1860 *IEEE
1870 ENDPROC
1880 REM ------------------------
1890 DEFPROCdisplay
1900 REM DATA DISPLAYED ON SCREEN
1910 CLS
1920 PRINTTAB(0,2)
1930 FORN%=0TO9:PRINTT(0,N%),T(1,N%):NEXTN%
1940 PRINTTAB(0,20);"VALVE CLOSED"
1950 PRINTTAB(0,21);"LAST DRAW-OFF = ";MASS;" kg     "
1960 PRINTTAB(0,22);"MEAN TEMP. OF DRAW-OFF WATER = ";DRW;" C   "
1970 PRINTTAB(0,23);"INSOLATION = ";INT(insol);" Wm-2 "
1980 PRINTTAB(0,24);"ACTUAL POWER = ";INT(watts/2);" Wm-2 "
1990 ENDPROC
2000 REM ------------------------
2010 DEFPROCduration(day,month)
2020 REM CALCULATE SUNRISE AND
2030 REM SUNSET HOURS
2040 RESTORE2050
2050 DATA0,31,59,90,120,151,181,212,243,273,304,334
2060 FORN=1TOmonth:READnday:NEXTN:nday=nday+day
2070 dec=23.45*(PI/180)*SIN((PI/180)*360*(284+nday)/365)
2080 solang=ABS(ACS(-TAN(dec)*TAN(lat)))
2090 solang=43200-INT(solang*3600/(PI/12))
2100 hstart=solang DIV 3600:mstart=(solang MOD 3600) DIV 60
2110 solang=86400-solang
2120 hend=solang DIV 3600:mend=(solang MOD 3600) DIV 60
2130 period=(hend-hstart)*3600+(mend-mstart)*60
2140 oldday=day
2150 ENDPROC
```

```
2160 REM ------------------------------
2170 DEFPROCsolar(KJ%,extrap)
2180 REM CALCULATE INSTANTANIOUS
2190 REM SIMULATED ANGLE-DEPENDANT
2200 REM TRANSMITTANCE_ABSORPTANCE
2210 REM PRODUCT AND THEREFORE
2220 REM POWER INPUT TO HEATERS
 2230 instant=hour*3600+minute*60
 2240 port=(hour-hstart)*3600+(minute-mstart)*60
 2250 IF instant>(hstart*3600+mstart*60) AND instant<(hend*3600+mend*6
0) THEN insol=slr(KJ%)+extrap*(slr(KJ%+1)-slr(KJ%)) ELSE insol=0
 2260 omega=PI*(instant-43200)/43200
 2270 a1=SIN(dec)*SIN(lat)*COS(beta)
 2280 a2=-SIN(dec)*COS(lat)*SIN(beta)*COS(gama)
 2290 a3=COS(dec)*COS(lat)*COS(beta)*COS(omega)
 2300 a4=COS(dec)*SIN(lat)*SIN(beta)*COS(gama)*COS(omega)
 2310 a5=COS(dec)*SIN(beta)*SIN(gama)*SIN(omega)
 2320 theta=ACS(a1+a2+a3+a4+a5)
 2330 talfa=0.88*(1-0.05*(1/COS(theta)-1)-0.03*(1/COS(theta)-1)ç2)
 2340 IFtalfa<0THENtalfa=0
 2350 IF(talfa*insol) > 550THENinsol=550/talfa
 2360 watts=2*talfá*insol
 2370 PROCpower(watts)
 2380 ENDPROC
 2390 REM ------------------------------
 2400 DEFPROCconstants
 2410 REM CONSTANTS RELEVANT TO
 2420 REM SIMULATED GEOGRAPHICAL
 2430 REM LOCATION AND ATTITUDE
 2440 REM OF COLLECTOR
 2450 lat=52*PI/180:REM Latitude
 2460 beta=52*PI/180:REM Collector angle
 2470 gama=0:REM Azimuth angle
 2480 solmax=400:REM Max. Insolation
 2490 G%=10:REM ensures relays are closed prior to reading next module
 2500 K%=0:REM K% used as marker for PROCdisc if there has been previo
us error message
 2510 lastminute=0
 2520 oldday=0
 2530 KOLD%=0
 2540 MASS=0
 2550 DRW=0
 2560 REC%=0
 2570 spower%=0
 2580 watts=0
 2590 insol=0
 2600 ENDPROC
```

```
 2610 REM ----------------------------
 2620 DEFPROCpower(watts)
 2630 REM SUPPLY POWER VIA D.A.C.
 2640 REM TO HEATER MATTS. CHECK
 2650 REM POWER SUPPLIED USING FEED
 2660 REM -BACK SYSTEM.
 2670 FORSCANadd%=65TO69:SCANadd$=CHR$(SCANadd%):PROCopenscan("7",SCAN
add$):NEXT
 2680 FORSCANadd%=65TO69:SCANadd$=CHR$(SCANadd%):PROCopenscan("6",SCAN
add$):NEXT
 2690 LOCALm,c,i%
 2700 IFwatts < 20THENPROCset(0,1):T(1,7)=0:GOTO3020
 2710 IFspower%=1THENGOTO2810
 2720 RESTORE2730
 2730 DATA0,0,4,0.3,8,0.4,13,0.5,21,0.6,33,0.7,50,0.8,67,0.9,93,1,150,
1.2,185,1.3,220,1.4,270,1.5,317,1.6,367,1.7,422,1.8,475,1.9,530,2,583,
2.1,640,2.2,692,2.3,753,2.4,813,2.5
 2740 DATA870,2.6,925,2.7,977,2.8,1029,2.9,1072,3,1118,3.1,1165,3.2,12
08,3.3,1247,3.4,1282,3.5,1316,3.6,1333,3.7,1372,3.9,1393,4.1,1412,4.5,
1415,5
 2750 READP1,V1
 2760 READP2,V2
 2770 IF(watts>=P1)AND(watts<=P2)THENGOTO2800
 2780 P1=P2:V1=V2
 2790 GOTO2760
 2800 volt=((V2-V1)/(P2-P1))*(watts-P1)+V1:spower%=1
 2810 vt=volt
 2820 FORIP%=1TO3
 2830   IF vt < 0.4THEN vt=0.4 ELSEIF vt > 5 THEN vt=5
 2840   PROCset(vt,1)
 2850   FORIRP%=1TO4
 2860     PROCscan("7","D","7",200)
 2870     PT(IP%)=FNadc("6","F","1",2000)
 2880   NEXTIRP%
 2890   PT(IP%)=(PT(IP%)-ZERO)*1272.26034+5.574365
 2900   PRINTTAB(0,IP%+13)PT(IP%);"   ";watts
 2910   IFIP% > 1THENGOTO2940
 2920   IF PT(IP%) > watts THEN vt=volt-0.1
 2930   IF PT(IP%) < watts THEN vt=volt+0.1
 2940   IFIP% <> 2THENGOTO2980
 2950   IF PT(2)<> PT(1) THEN m=(vt-volt)/(PT(2)-PT(1)) ELSE m=0
 2960   c=volt-m*PT(1)
 2970   vt=m*watts+c
 2980 NEXTIP%
 2990 volt=vt
 3000 IFABS(PT(3)-watts)/watts > 0.05THENGOTO2810
 3010 T(1,7)=INT(PT(3)/2)
 3020 ENDPROC
```

```
 3030 REM ------------------------
 3040 DEFPROCset(volt,dac%)
 3050 REM SET VOLTAGE OUTPUT FROM
 3060 REM D.A.C. TO volt ON
 3070 REM CHANNEL dac%
 3080 PROCbinary(volt)
 3090 REM Set up comand string
 3100 dac$=CHR$(dac%+48)
 3110 com$="F"+dac$+"X0Y"+LSN$+"Z"+"F"+dac$+"X1Y"+MN$+"Z"+"F"+dac$+"X2
Y"+MSN$+"Z"
 3120 REM Set up output setting string
 3130 out$="F"+dac$+"X3Z"
 3140 W%=OPENIN("7")
 3150 PRINT#cmd%,"LISTEN",W%,"EXECUTE"
 3160 FORX=0TO200:NEXTX
 3170 PRINT#data%,com$
 3180 FORX=0TO200:NEXTX
 3190 PRINT#data%,out$
 3200 FORX=0TO200:NEXTX
 3210 PRINT#cmd%,"UNLISTEN"
 3220 CLOSE#W%
 3230 ENDPROC
 3240 REM ------------------------
 3250 DEFPROCbinary(volt)
 3260 REM CONVERT VALUE OF volt IN
 3270 REM BASE 10 INTO BINARY
 3280 REM EQUIVALENT
 3290 FORN=1TO12:B(N)=0:NEXTN
 3300 CT%=INT(0.5+volt*409.5)
 3310 N=0
 3320 N=N+1
 3330 B(N)=CT%MOD2
 3340 CT%=CT%DIV2
 3350 IFCT%=0THENGOTO3360ELSEGOTO3320
 3360 FORI=1TO12 STEP 4
 3370   BASE10=0
 3380   N=0
 3390   FORJ=I TO (I+3)
 3400     BASE10=BASE10+B(J)*(2çN)
 3410     N=N+1
 3420   NEXTJ
 3430   B(I)=BASE10
 3440 NEXTI
 3450 LSN%=B(1)
 3460 MN%=B(5)
 3470 MSN%=B(9)
 3480 LSN$=CHR$(LSN%+48)
 3490 MN$=CHR$(MN%+48)
 3500 MSN$=CHR$(MSN%+48)
 3510 ENDPROC
```

```
3520 REM----------------------------
3530 DEFFNadc(IEEEadd$,ADCadd$,ADCrange$,ADCdel%)
3540 REM ANALOGUE INPUT PAIR IS
3550 REM SWITCHED ONTO A.D.C. FOR
3560 REM MEASUREMENT. CORRECT RANGE
3570 REM IS SELECTED FOR INPUT SIGNAL
3580 ADC%=OPENIN(IEEEadd$)
3590 PRINT#cmd%,"LISTEN",ADC%,"EXECUTE"
3600 PRINT#data%,ADCadd$+ADCrange$
3610 FORI%=0TOADCdel%:NEXT
3620 PRINT#cmd%,"UNLISTEN"
3630 PRINT#cmd%,"TALK",ADC%
3640 INPUT#data%,RESULT$
3650 PRINT#cmd%,"UNTALK"
3660 PRINT#cmd%,"UNLISTEN"
3670 CLOSE#ADC%
3680 l$=LEFT$(RESULT$,1)
3690 m$=MID$(RESULT$,2,1)
3700 r$=RIGHT$(RESULT$,1)
3710 A=ASCl$-64
3720 B=ASCm$-64
3730 C=ASCr$-64
3740 N=256*C+16*B+A
3750 IFADCrange$="0"factor=1
3760 IFADCrange$="1"factor=0.1
3770 IFADCrange$="2"factor=0.01
3780 IFADCrange$="3"factor=0.001
3790 =factor*(N-2048)/204.8
3800 REM----------------------------
3810  DEFPROCopenscan(IEEEadd$,SCANadd$)
3820 REM ENSURE ALL CHANNELS OPEN
3830 REM PRIOR TO SCANNING
3840 REM OF SUBSEQUENT MODULE
3850 SCAN%=OPENIN(IEEEadd$)
3860 PRINT#cmd%,"LISTEN",SCAN%,"EXECUTE"
3870 PRINT#data%,SCANadd$+"JT"
3880 PRINT#cmd%,"UNLISTEN"
3890 CLOSE#SCAN%
3900 ENDPROC
3910 REM-------------------------------
3920 DEFPROCcold
3930 REM READ REFFERENCE TEMPERATURE
3940 REM ON COLD JUNCTION CARD.
3950 ZERO=0:FORNZ%=1TO5:ZERO=ZERO+FNadc("6","F",ADCrange$,2000):NEXTN
Z%:ZERO=ZERO/5
 3960 v(0,0)=v(0,0)-ZERO
 3970 CJT=10*v(0,0)
 3980 T(0,0)=INT(0.5+10*CJT)/10
 3990 CJV=-2.308E-6+CJT*(3.8616E-5+CJT*(4.4503E-8-CJT*2.6741E-11))
 4000 ENDPROC
```

```
4010 REM----------------------------
4020 DEFPROCload(KJ%)
4030 REM OPEN SOLENOID VIA
4040 REM D.A.C. TO SIMULATE
4050 REM REQUIRED WATER DRAW-OFF
4060 LD%=1
4070 IFREP%=1THEN4140
4080 MASS=1de(KJ%)
4090 DELTA=-0.618623+4.898028*MASS
4100 SWH=TIME/100+DELTA
4110 volt=3:dac%=2:PROCset(volt,dac%)
4120 PRINTTAB(0,20);"VALVE OPEN:DRAW-OFF = ";MASS;" kg "
4130 REMOpen solenoid valve
4140 IF((TIME/100)"=SWH)THEN4150ELSE4170
4150 volt=0:dac%=2:PROCset(volt,dac%):LD%=0
4160 PRINTTAB(0,20);"VALVE CLOSED                    "
4170 REP%=1
4180 ENDPROC
4190 REM----------------------------
4200 DEF PROCreadin
4210 REM INPUT METEOROLOGICAL DATA
4220 REM FROM FILE "].IN".
4230 *D.
4240 *DR.2
4250 Y=OPENIN" .IN"
4260 INPUT Y,day,month,year%,house
4270 dayend=day+2
4280 KT%=0
4290 REPEAT
4300   KT%=KT%+1
4310   INPUT#Y,hur(KT%),mnt(KT%),slr(KT%),1de(KT%)
4320   PRINThur(KT%),mnt(KT%),slr(KT%),1de(KT%)
4330 UNTILEOF#Y
4340 CLOSE£Y
4350 ENDPROC
4360 REM----------------------------
4370 DEFPROCkaytime
4380 REM EXTRAPOLATE BETWEEN BLOCKS
4390 REM OF METEOROLOGICAL DATA
4400 REM TO GIVE INSTANTANIOUS
4410 REM SIMULATED OPERATING
4420 REM CONDITIONS
4430 tme=hour*3600+minute*60
4440 KJ%=0
4450 KJ%=KJ%+1
4460 tm1=hur(KJ%)*3600+mnt(KJ%)*60
4470 IFKJ%=KT%THENtm2=86400ELSEtm2=hur(KJ%+1)*3600+mnt(KJ%+1)*60
4480 IFtme > tm1 OR tme>= tm2 THENGOTO4450
4490 extrap=(tme-tm1)/(tm2-tm1)
4500 ENDPROC
4510 REM----------------------------
4520 DEFPROCflow(vf,tf)
4530 REM CONVERT ANALOGUE SIGNAL FROM
4540 REM FLOW-METER INTO VELOCITY.
4550 REM VELOCITY CONVERTED TO MASS
4560 REM FLOW-RATE USING LOCAL WATER
4570 REM TEMPERATURE READING.
4580 fset=1:frange=0.25:farea=PI*(0.025ç2)/4:CALIB=1.045
4590 ro=751.76968+1.89344*(tf+273)-(3.59707E-3)*(tf+273)ç2
4600 T(1,8)=CALIB*1000*((vf-2.05)*fset*frange*farea*ro/8.2)
4610 T(1,8)=INT(0.5+10*T(1,8))/10
4620 ENDPROC
```

APPENDIX E:

FLOW METER CALIBRATION

A constant mass flow rate of water through the vertically mounted inductive flow meter was maintained using the configuration described in section 5.1. A series of consecutive readings were taken for a constant mass flow-rate through the flow meter and the maximum deviation from the mean of all the flow readings was established. This process was repeated for constant flow rates of 0.005, 0.010 and 0.020 kgs^{-1}. The maximum deviation was found to be a constant 0.0002 kgs^{-1} and this value was taken to be the uncertainty associated with this particular flow meter.

The flow rate, $\dot{m}$ as indicated by the inductive flow meter was calibrated against a method in which a mass of water, M, passing through the meter was collected over a measured time period, t. The collected water was decantered into a measuring cylinder and the measured volume converted into a mass reading using the density of the collected water at the measured temperature. In order that uncertainties associated with the collection method of flow rate measurements are of a lower order than those of the inductive flow meter, a minimum collection time had to be established. For small perturbations,

$$\Delta\dot{m} = \frac{\partial \dot{m}}{\partial t}\Delta t + \frac{\partial \dot{m}}{\partial M}\Delta M$$

equation E.1

and since $\dot{m} = M/t$, equation E.1 can also be expressed as

$$\Delta\dot{m} = \frac{\Delta M - \dot{m}\Delta t}{\Delta t}$$

equation E.2

Rearranging equation E.2, the minimum collection time, t required to give a flow reading of approximately $\dot{m}$, accurate to $\pm\ \Delta m$ is

$$t = \frac{\Delta M - \dot{m}\Delta t}{\Delta \dot{m}}$$

equation E.3

With associated uncertainties of 0.005 kg and 0.5 s for ΔM and Δt respectively, the collection time used in the calibration of the flow meter was calculated from

$$t = \frac{0.005 - 0.5\dot{m}}{0.0002}$$

equation E.4

The linear calibration curve is shown in figure E.1. The best straight line through the data which also passes through the origin was found to be

$$\dot{m}_1 = 1.04\dot{m}_2$$

equation E.5

where $\dot{m}_1$ and $\dot{m}_2$ represent the direct and flow meter measurements respectively.

FIGURE E.1

Flow meter calibration curve

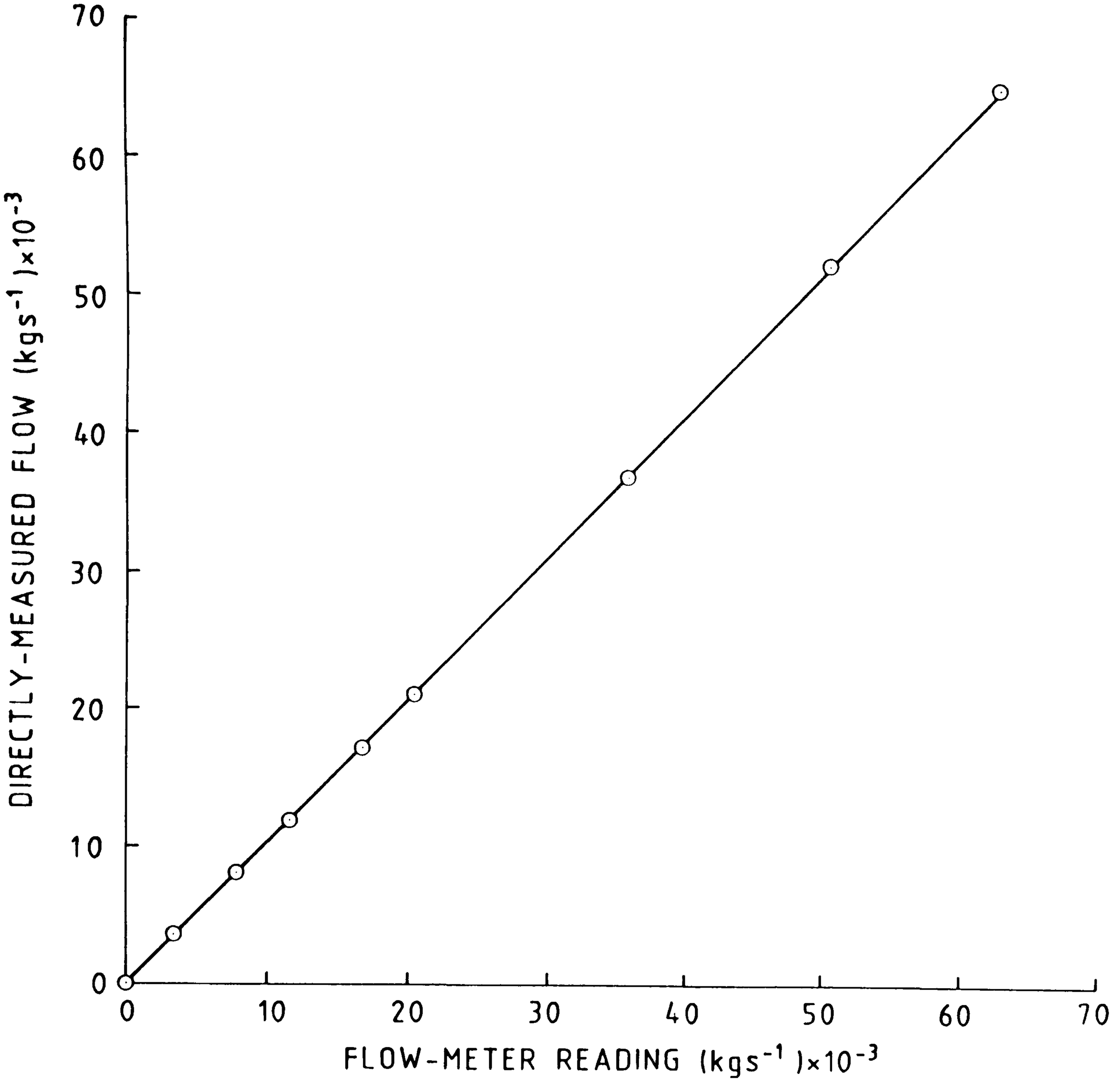
DIRECTLY-MEASURED FLOW (kgs^{-1})×10^{-3}
FLOW-METER READING (kgs^{-1})×10^{-3}
0
10
20
30
40
50
60
70

APPENDIX F:

WATTMETER CALIBRATION

The power supply to the collector heater mats was varied (via signals supplied by the D.A.C. to the phase angle trigger module) between 0 and 1200 W in steps of between 100 and 200 W. The corresponding analogue output from the wattmeter being calibrated was adjusted to vary over the range 0 to 1 volt. This analogue output was calibrated against the measured power input to the heaters using a Feedback EW604 electronic wattmeter connected in series. The estimated uncertainty in measurements taken using the Feedback wattmeter was $\pm$1%. At each power step, the power supplied to the heaters was left to settle to a constant value as the heater mats reached a steady-state temperature. This minimised any errors due to the time lag introduced between reading the Feedback wattmeter and taking the corresponding analogue reading of the meter being calibrated. The best straight line through the calibration data shown in figure F.1 was found to be,

$$w = 5.6+1272.3v \ (W)$$

equation F.1

FIGURE F.1

Calibration curve for the analogue-output wattmeter

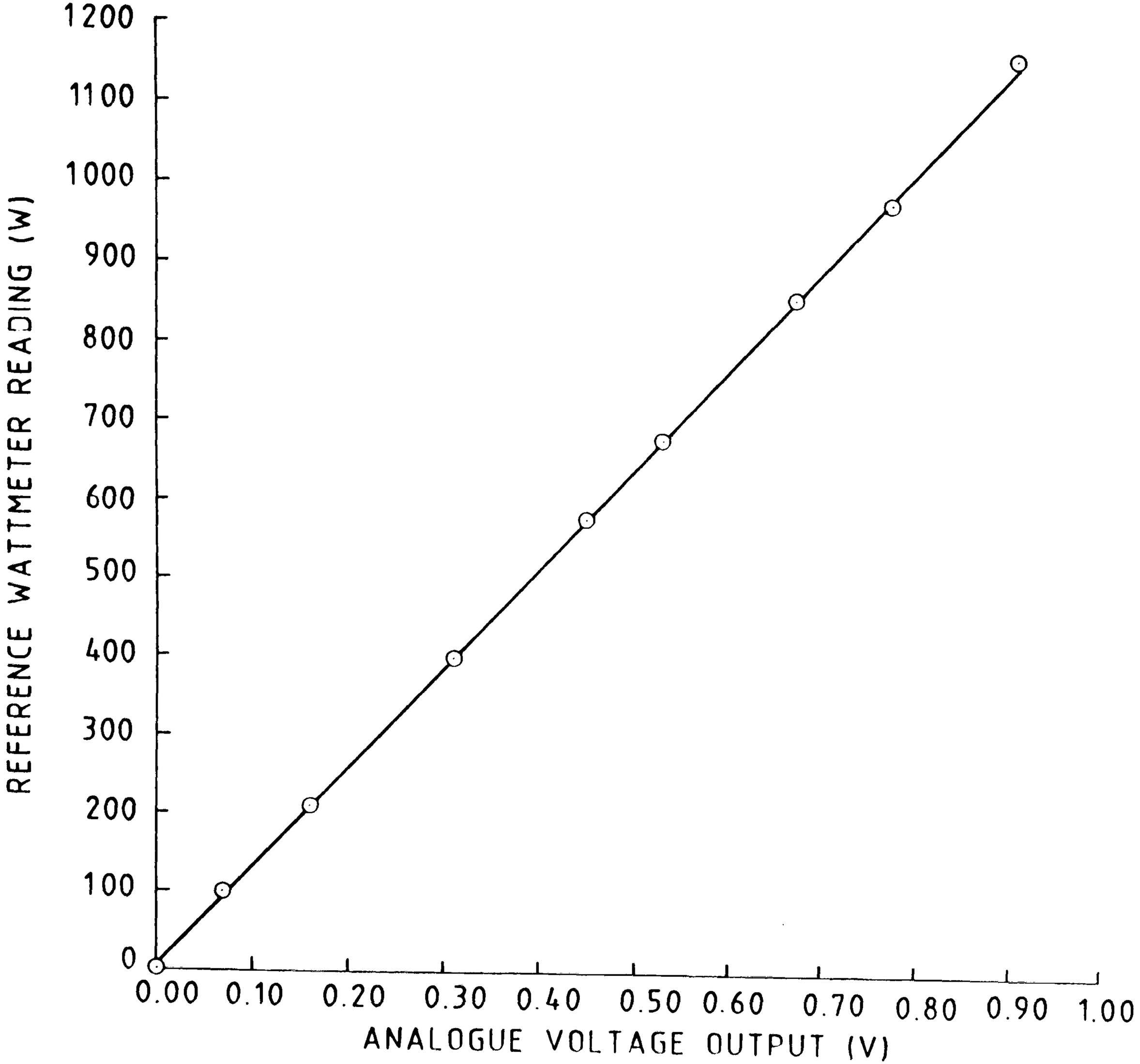
REFERENCE WATTMETER READING (W)
1200
1100
1000
900
800
700
600
500
400
300
200
100
0
0.00
0.10
0.20
0.30
0.40
0.50
0.60
0.70
0.80
0.90
1.00
ANALOGUE VOLTAGE OUTPUT (V)

APPENDIX G:

WATER DRAW-OFF CALIBRATION

A timed signal supplied by the D.A.C. to the relay opened the solenoid valve for a fixed period of time. The water drained off from the store during this period was collected and measured by decanting into a measuring cylinder. This was repeated for various time steps giving water draw-offs of between 0 and 15 kg. The relationship between the time interval and mass of water drained off was found to be linear over the range of the calibration. The best fit straight line to the data was

$$t = -0.62 + 4.898M \text{ (s)}$$

equation G.1

Since the time interval set by the microcomputer can be determined to the nearest 0.01 of a second the errors associated with making a controlled draw-off using the calibration curve, will be dominated by the accuracy with which the mass of the water was determined (this being $\pm$ 0.05 kg).

FIGURE G.1

Water draw-off calibration curve

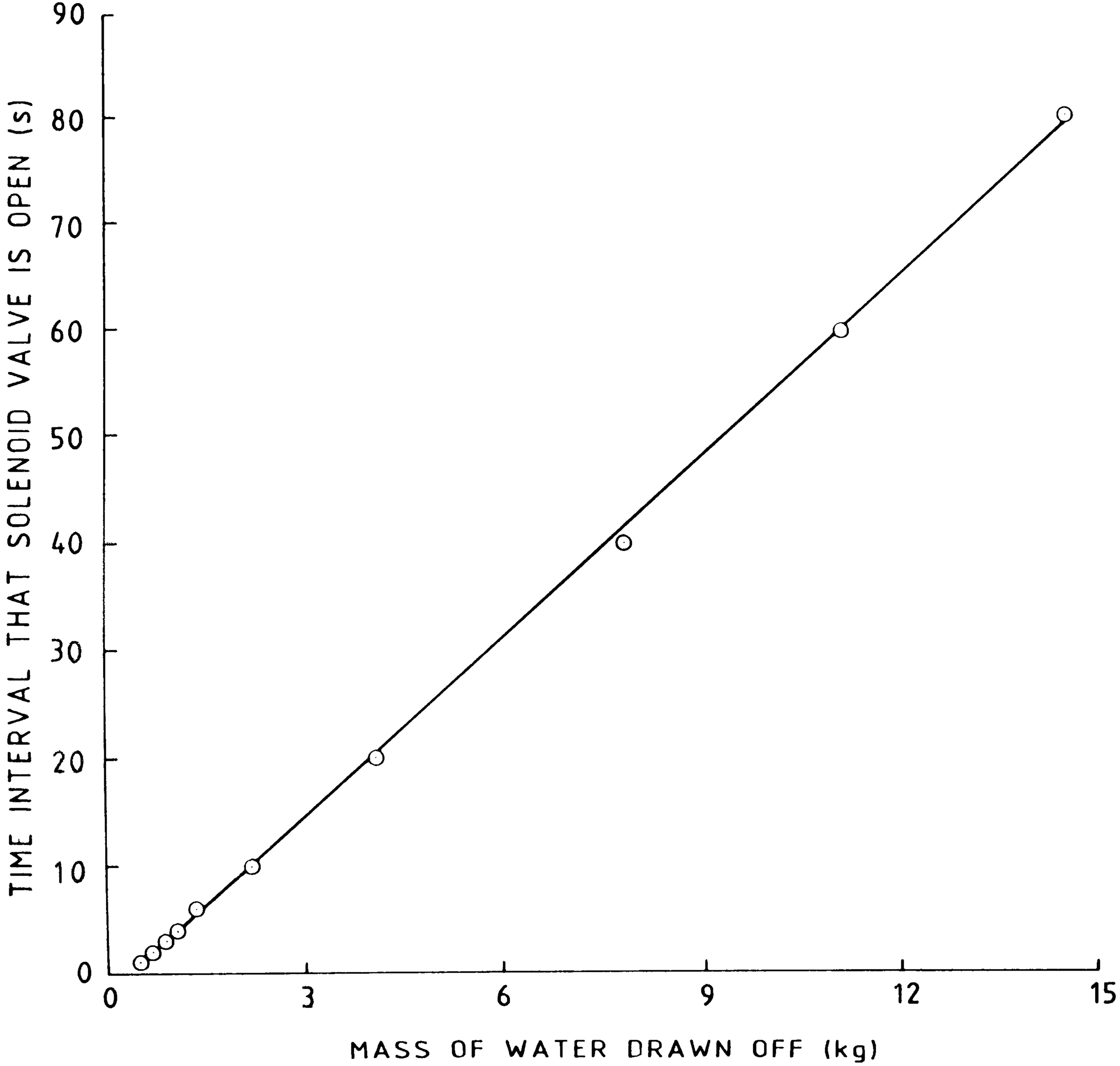
TIME INTERVAL THAT SOLENOID VALVE IS OPEN (s)
90
80
70
60
50
40
30
20
10
0
0
3
6
9
12
15
MASS OF WATER DRAWN OFF (kg)

APPENDIX H:

HEAT TRANSFER CORRELATIONS USED IN THE SIMULATION MODEL

In determining the heat loss by buoyancy driven convection between the collector plate and the glass cover, when mounted at an angle, Θ , between 0 and 75 from the horizontal, the correlation given by equation H.1 and derived by Hollands et al (39) is suggested (23)

$$Nu=1.44\left[1-\frac{1708}{GrPr\cos(\Theta)}\right]^{+}\left[1-\frac{1708[\sin(1.8\Theta)]^{1.6}}{GrPr\cos(\Theta)}\right]+[(GrPr\cos(\Theta)/5830)^{0.33}-1]^{+}$$

equation H.1

The superscripts $(\ )^{+}$ denotes a positive value for the quantity in brackets if this quantity is greater than zero and a value of zero otherwise. The characteristic length in determining Gr is taken as the thickness of the air cavity.

Equation H.2 is used in determining the predominantly forced convective heat loss due to wind across the top of the collector (40).

$$Nu = 0.86Re^{0.5}Pr^{0.33}$$

equation H.2

for $2 \times 10^4 \leq Re \leq 9 \times 10^4$ Equation H.2 will also give acceptable values of Nu for laminar air flows ie. $Re \leq 2 \times 10^4$

Other more "standard" engineering correlations taken from (41) are:

For forced convection due to fluid flow in a circular duct (the convective heat transfer between collector fluid and tubes)

$$Nu = 3.66 + \frac{0.00668(D/L)RePr}{1 + 0.04[(D/L)RePr]^{0.67}}$$

equation H.3

for Re $\lesssim$ 2000

For buoyancy driven convection from the lower surface of an inclined plane (collector back losses)

$$Nu = 0.27[Gr\cos(\Theta)Pr]^{0.25}$$

equation H.4

for $3x10^5 \lesssim GrPr \lesssim 3x10^{10}$

The characteristic length is taken as the longest edge of the collector.

The rate of heat transfer by radial conduction between the inner and outer surfaces of a cylinder of length, L, with respective surface temperatures of T_1 and T_2 is given (60) as

$$q = \frac{-2\pi kL(T_2 - T_1)}{In(D_2/D_1)}$$

equation H.5

where D_1 and D_2 are the internal and external cylinder diameters respectively. From the definition of the "U-value" as the heat loss per unit area per unit degree temperature differential, equation H.5 becomes

$$U = \frac{2k}{D_1 In(D_2/D_1)}$$

equation H.6

In establishing the conductive heat transfer coefficients for the top, base and walls of the store, the insulant surrounding the cylindrical store was sectioned off into two conical "plugs" and a tapered cylinder as shown in figure H.1. A steady state energy balance due to heat transfer by conduction through these sections was derived and the resulting equations solved to determine firstly the heat overall heat transfer rate and then the effective heat transfer coefficient.

FIGURE H.1

Schematic diagram of insulant around the storage tank

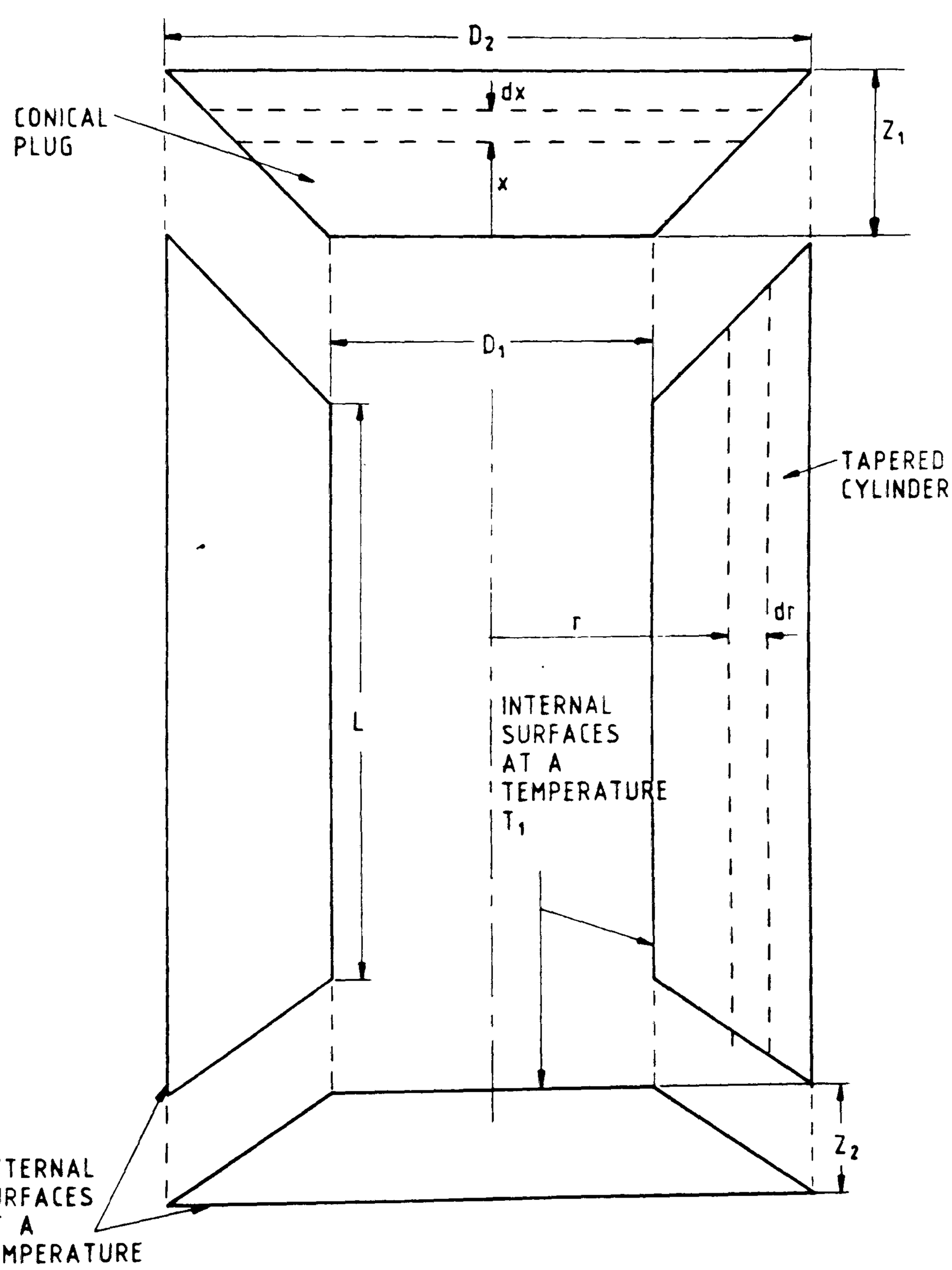
D2
dx
CONICAL
PLUG
Z1
x
D1
TAPERED
CYLINDER
dr
r
L
INTERNAL
SURFACES
AT A
TEMPERATURE
T1
Z2
EXTERNAL
SURFACES
AT A
TEMPERATURE
OF T2

For the plug sections representing the insulant on the top and base of the store, a heat balance gives

$$\frac{d}{dx}[(ZD_1 + (D_2 - D_1)x)^2 \frac{dT}{dx}] = 0$$

equation H.7

Solving equation H.7, gives a temperature profile through the plug of

$$T = T_1 + \frac{(T_2 - T_1)zD_1D_2}{(D_1 - D_2)[zD_1 + (D_2 - D_1)x]} + \frac{(T_1 - T_2)D_2}{D_1 - D_2}$$

equation H.8

By establishing the rate of heat transfer at the inner surface (which is equivalent to the heat transfer rate through any plane through the plug), the effective heat transfer coefficient becomes

$$U = \frac{kD_2}{zD_1}$$

equation H.9

Similarly for the tapered cylinder (shown in figure H.1) formed by the insulant around the walls of the storage tank, a steady state energy balance for the conductive heat transfer through the walls gives

$$\frac{d}{dr}[r(L(D_2 - D_1) + (z_1 + z_2)r) \frac{dT}{dr}] = 0$$

equation H.10

from which, after solving for the radial temperature distribution, the effective heat transfer coefficient was determined as

$$U = \frac{kL(D_2-D_1)}{In\left[\frac{r_2[L(D_2-D_1)+(z_1+z_2)r_1]}{r_1[L(D_2-D_1)+(z_1+z_2)r_2]}\right][L(D_2-D_1)+(z_1+z_2)r_1]r_1}$$

equation H.11

APPENDIX I

THE MAIN SIMULATION PROGRAM

A flow diagram representing the main numerical simulation program is given in figure I.1.

The subroutines within this program (written in FORTRAN 77) and which have been referred to in the main body of the text are given in listing I.1. The remainder of the program containing the solution method has not been included in this listing and is available at the Cranfield Computer Centre.

FIGURE I.1

Flow diagram representing the main numerical simulation program

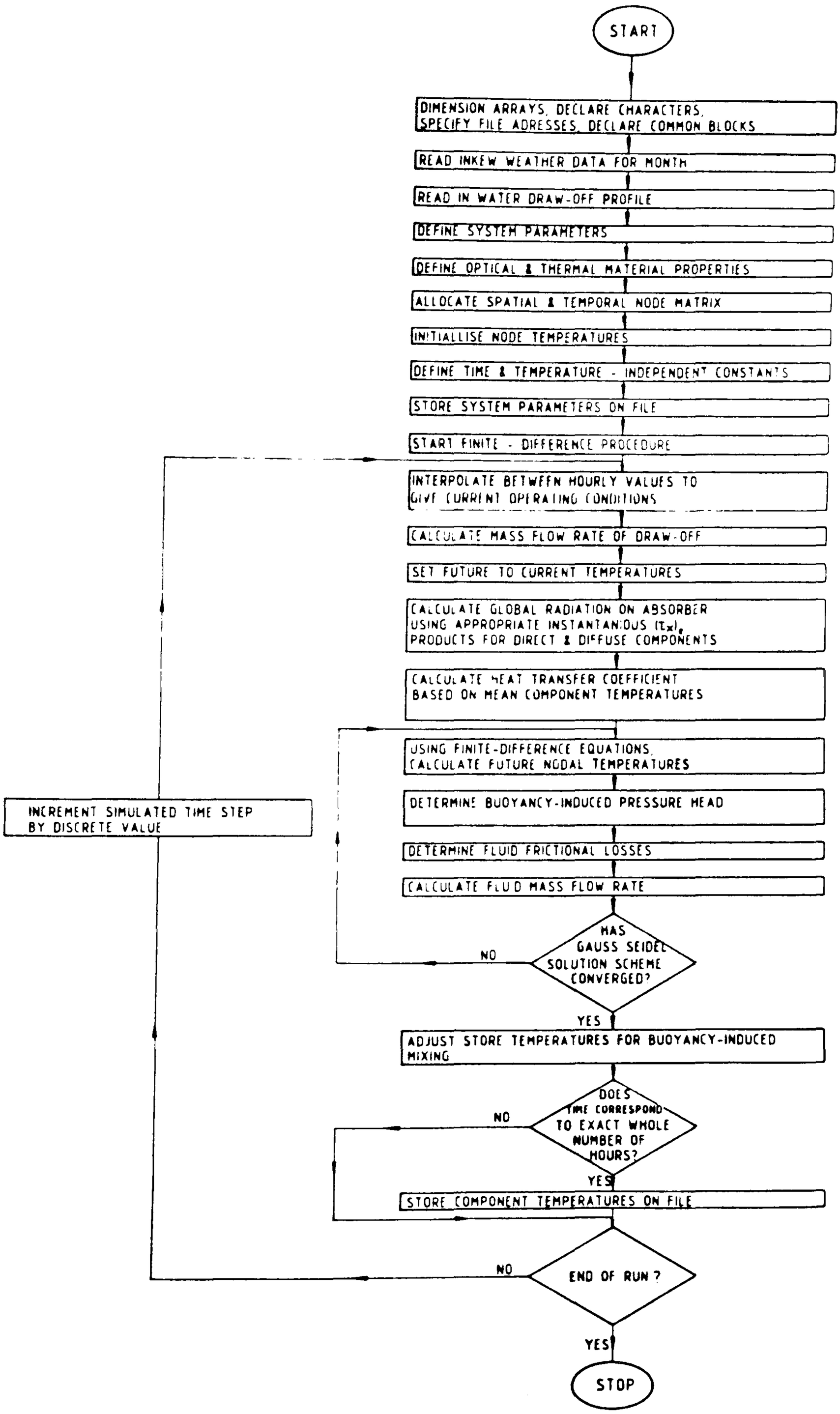
START
DIMENSION ARRAYS, DECLARE CHARACTERS, SPECIFY FILE ADRESSES, DECLARE COMMON BLOCKS
READ INKEW WEATHER DATA FOR MONTH
READ IN WATER DRAW-OFF PROFILE
DEFINE SYSTEM PARAMETERS
DEFINE OPTICAL & THERMAL MATERIAL PROPERTIES
ALLOCATE SPATIAL & TEMPORAL NODE MATRIX
INITIALLISE NODE TEMPERATURES
DEFINE TIME & TEMPERATURE - INDEPENDENT CONSTANTS
STORE SYSTEM PARAMETERS ON FILE
START FINITE - DIFFERENCE PROCEDURE
INTERPOLATE BETWEEN HOURLY VALUES TO GIVE CURRENT OPERATING CONDITIONS
CALCULATE MASS FLOW RATE OF DRAW-OFF
SET FUTURE TO CURRENT TEMPERATURES
CALCULATE GLOBAL RADIATION ON ABSORBER USING APPROPRIATE INSTANTANEOUS (τ_α), PRODUCTS FOR DIRECT & DIFFUSE COMPONENTS
CALCULATE HEAT TRANSFER COEFFICIENT BASED ON MEAN COMPONENT TEMPERATURES
USING FINITE-DIFFERENCE EQUATIONS, CALCULATE FUTURE NODAL TEMPERATURES
DETERMINE BUOYANCY-INDUCED PRESSURE HEAD
DETERMINE FLUID FRICTIONAL LOSSES
CALCULATE FLUID MASS FLOW RATE
HAS GAUSS SEIDEL SOLUTION SCHEME CONVERGED?
NO
YES
ADJUST STORE TEMPERATURES FOR BUOYANCY-INDUCED MIXING
DOES TIME CORRESPOND TO EXACT WHOLE NUMBER OF HOURS?
NO
YES
STORE COMPONENT TEMPERATURES ON FILE
INCREMENT SIMULATED TIME STEP BY DISCRETE VALUE
END OF RUN ?
NO
YES
STOP

LISTING I.1

Annotated listing of subroutines referred to in text

```
C     ********************************************************************
C     ********************************************************************
C     FUNCTIONS AND SUBROUTINES USED IN THE SIMULATION
C     **********  AND REFERED TO IN TEXT  ************************
C     ********************************************************************
C     ********************************************************************
C
      SUBROUTINE PDNODE(IPD,PDSX,PDCX,SDY,SDZ,
     1     PDTL,DPD,IBGD,BGDDZ,IEDD,EDDDZ)
C
C     ALLOCATE NODES AND NODE SPACING TO DOWNCOMER
C
C     IPD-NUMBER OF NODES IN DOWNCOMER
C     PDSX,PDCX-LENGTH OF HORIZONTAL SECTION OF PIPE
C     ASSOCIATED WITH THE STORE AND COLLECTOR RESPECTIVELY
C     SDY,SDZ-VERTICAL AND HORIZONTAL DISTANCE OF STORE
C     OUTLET FROM COLLECTOR INLET.
C     ALL OTHER VALUES CALCULATED WITHIN SUBROUTINE
C
C     SHORTEST LENGTH OF ANGLED PIPE BETWEEN END OF
C     HORIZONTAL SECTIONS.
      D=SQRT(SDZ**2+SDY**2)
C     TOTAL LENGTH OF PIPE
      PDTL=PDSX+D+PDCX
C     NODE SIZE
      DPD=PDTL/IPD
      J=0
10    J=J+1
C     FRACTIONS OF NODES WHICH "OVERLAP" BETWEEN
C     HORIZONTAL AND ANGLED SECTIONS OF DOWNCOMER
C     (USED IN DETERMINING BUOYANCY FORCES)
      IF(J*DPD.LT.PDSX)GOTO 10
      IBGD=J
      BGDDZ=J*DPD-PDSX
      J=0
20    J=J+1
      IF(J*DPD.LT.PDTL-PDCX)GOTO 20
      IEDD=J
      EDDDZ=PDTL-PDCX-(J-1)*DPD
      RETURN
      END
C     ********************************************************************
      SUBROUTINE PRNODE(IPR,PRSX,PRCX,SRY,SRZ,CL,CQ,
     1     PRTL,DPR,IBGR,BGRDZ,IEDR,EDRDZ)
C
C     ALLOCATE NODES AND NODE SPACING TO UPRISER
C
C     IPR-NUMBER OF NODES IN UPRISER
C     PRSX,PRCX-HORIZONTAL LENGTHS ASSOCIATED WITH STORE
C     AND COLLECTOR.
C     SRY,SRZ-VERTICAL AND HORIZONTAL DISTANCES BETWEEN
C     HORIZONTAL SECTIONS OF PIPE
C     CL-COLLECTOR LENGTH
C     CQ-ANGLE OF COLLECTOR FROM HORIZONTAL
      A=SRY-CL*SIN(CQ)
```

```
      B=SRZ-CL*COS(CQ)
C     DETERMINE SHORTEST LENGTH OF ANGLED PIPE
C     BETWEEN HORIZONTAL SECTIONS OF PIPE.
      D=SQRT(A**2+B**2)
      PRTL=PRSX+D+PRCX
C     LENGTH OF UPRISER NODE
      DPR=PRTL/IPR
      J=0
C     DETERMINE "OVERLAP" IN NODES BETWEEN HORIZONTAL
C     AND ANGLED SECTIONS
10    J=J+1
      IF(J*DPR.LT.PRCX)GOTO 10
      IBGR=J
      BGRDZ=J*DPR-PRCX
      J=0
20    J=J+1
      IF(J*DPR.LT.PRTL-PRSX)GOTO 20
      IEDR=J
      EDRDZ=PRTL-PRSX-(J-1)*DPR
      RETURN
      END
C     ************************************************
      SUBROUTINE THMWTR(E,C,V,D,P,CON)
C
C     THERMAL PROPERTIES OF WATER AT LOCAL BULK TEMPERATURE
C
C     E-BULK WATER TEMPERATURE, C-SPECIFIC HEAT CAPACITY,
C     V-VISCOSITY, D-DENSITY, P-PRANDTL NUMBER,
C     CON-THERMAL CONDUCTIVITY.
      C=5514.14753-8.431099*E+0.0133153571*(E**2.)
      V=(23724.55980-131.01922*E+0.18329*(E**2))
     1     *(10.0**-6)
      D=751.76968+1.89344*E-3.59707*(10.0**-3)
     1     *(E**2)
      P=187.91633-1.04839*E+1.47713*(10.0**-3)
     1     *(E**2)
      CON=(-480.45054+5.84468*E-7.32574*(10.0**-3)
     1     *(E**2))*(10.0**-3)
      RETURN
      END
C     ************************************************
      SUBROUTINE THMAIR(E,C,V,D,P,CON)
C
C     THERMAL PROPERTIES OF AIR AT LOCAL BULK TEMPERATURE
C
C     E-BULK AIR TEMPERATURE, C-SPECIFIC HEAT CAPACITY,
C     V-VISCOSITY, D-DENSITY, P-PRANDTL NUMBER,
C     CON-THERMAL CONDUCTIVITY.
      C=(1.01587-1.30868*(10.0**-4)*E+3.14590*(10.0**-7)
     1     *(E**2))*1000
      V=(0.15047+6.47242*(10.0**-3)*E-2.82057*(10.0**-6)
     1     *(E**2))*(10.0**-5)
      D=2.05762-3.4364*(10.0**-3)*E+1.59657*(10.0**-6)
     1     *(E**2)
      P=0.81940-5.1394*(10.0**-4)*E+4.68542*(10.0**-7)
```

```
     1       *(E**2)
        CON=(7.39167*(10.0**-4)+9.6945*(10.0**-3)*E
     1       -3.20764*(10.0**-6)*(E**2))*0.01
        RETURN
        END
C       ************************************************************
        FUNCTION CNAIR1(E1,E2,Y,Q,N)
C
C       HEAT LOSS COEFFICIENT FROM UPPER OR LOWER SURFACE
C       OF INCLINED PLANE DUE TO BUOYANCY-DRIVEN
C       CONVECTION
C
C       E1,E2-PLATE AND AIR TEMPERATURES RESPECTIVELY
C       Y-CHARACTERISTIC LENGTH OF PLATE
C       Q-ANGLE OF PLATE FROM VERTICAL ( > 0 RADS.)
C       N-(=0 FOR LOWER SURFACE,=1 FOR UPPER SURFACE)
        G=9.81
        E=(E1+E2)*0.5
        CALL THMAIR(E,C,V,D,P,CONA)
c       GRASHOF NUMBER FLUID PROPERTIES BASED ON MEAN
C       OF PLATE AND AIR TEMPERATURES.
        GR=G*(1/E)*ABS(E1-E2)*(Y**3)*(D**2)*(COS(Q))
     1       /(V**2)
        RA=GR*P
        CONST=0.54
        EX=0.25
        IF(N.EQ.1.AND.E1.GT.E2.AND.RA.GE.(2*10.0**7))THEN
        CONST=0.14
        EX=0.33
        END IF
        IF(N.EQ.1.AND.E1.LT.E2)THEN
        CONST=0.27
        EX=0.25
        END IF
        IF(N.EQ.0.AND.E1.GT.E2)THEN
        CONST=0.27
        EX=0.25
        END IF
        IF(N.EQ.0.AND.E1.LT.E2.AND.RA.GE.(2*10.0**7))THEN
        CONST=0.14
        EX=0.33
        END IF
        CNAIR1=CONST*(RA**EX)*CONA/Y
        RETURN
        END
C       ************************************************************
        FUNCTION UVAL1(E,EAIR,CON,D,H,Q,N)
C
C       OVERALL U-VALUE FOR HORIZONTAL,INSULATED PLANES
C       WITH BUOYANCY DRIVEN CONVECTION AT EXPOSED SURFACE
C       CORRECTIONS MADE FOR SMALL ANGLES OF INCLINATION
C
C       E,EAIR-INSULATED SURFACE AND AIR TEMPERATURES RESPECTIVE
C       CON,D-CONDUCTIVITY AND THICKNESS OF INSULANT
```

```
C       H-CHARACTERISTIC LENGTH OF EXPOSED SURFACE
C       OF INSULANT
C       Q-ANGLE OF INSULANT SURFACE FROM VERTICAL
C       (PI/2<Q<<0)
C       N(=1 OR 0 FOR UPPER OR LOWER SURFACE OF INSULANT
C       EXPOSED TO AMBIENT)
        E1=(E+EAIR)*0.5
C       HEAT TRANSFER COEFFICIENT FOR CONDUCTION
C       THROUGH INSULANT
        H1=CON/D
C       INITIAL "GUESS" AT EXPOSED INSULANT SURFACE TEMPERATURE
10      H2=CNAIR1(E1,EAIR,H,Q,N)
        IF(H2.GT.0)THEN
C       ESTIMATE OVERALL U-VALUE DUE TO CONDUCTION AND
C       CONVECTION
        HT=1/(1/H1+1/H2)
        ELSE
        HT=H1
        END IF
C       TOTAL HEAT TRANSFER BASED ON LATEST ESTIMATE
C       OF OVERALL U-VALUE
        QT=HT*(E-EAIR)
        OLD=E1
C       CALCULATE NEW VALUE FOR EXPOSED INSULANT SURFACE
        E1=E-QT/H1
C       REPEAT ITERATION IF NECESSARY
        IF(ABS(E1-OLD).GT.0.01)GOTO 10
        UVAL1=HT
        RETURN
        END
C       **********************************************************
        FUNCTION CNAIR2(E1,E2,Y,Q)
C       HEAT TRANSFER COEFFICIENT FOR BUOYANCY-DRIVEN
C       CONVECTION AT A VERTICAL OR NEAR VERTICAL PLANE.
C
C       E1,E2-SURFACE AND AIR TEMPERATURES
C       Y-CHARACTERISTIC LENGTH
C       Q-ANGLE OF PLANE FROM VERTICAL (0<Q<<PI/2)
        G=9.81
        E=(E1+E2)*0.5
        CALL THMAIR(E,C,V,D,P,CON)
C       GRASHOF NUMBER FLUID PROPERTIES BASED ON MEAN
C       PLATE AND AIR TEMPERATURES
        GR=G*(1/E)*ABS(E1-E2)*(Y**3)*(D**2)*(COS(Q))/
     1       (V**2)
        RA=GR*P
        IF(RA.LT.(10.0**9))THEN
        CONST=0.59
        EX=0.25
        ELSE
        CONST=0.13
```

```
      EX=0.33
      END IF
      CNAIR2=CONST*(RA**EX)*CON/Y
      RETURN
      END
C     ***********************************************************
      FUNCTION UVAL2(E,EAIR,CON,D,H,Q)
C
CC    OVERALL U-VALUE FOR VERTICAL INSULATED PLANE
CC    WITH COMPENSATION FOR SMALL DEVIATIONS IN
CC    ANGLE OF PLANE FROM VERTICAL.
CC
C     E,EAIR-INSULATED SURFACE AND AIR TEMPERATURES
C     CON,D-THERMAL CONDUCTIVITY AND THICKNESS OF
C     INSULANT
C     H-CHARACTERISTIC LENGTH OF INSULANT
C     Q-ANGLE OF INCLINATION OF SURVACES FROM VERTICAL
C     (0<Q<<PI/2)
      E1=(E+EAIR)*0.5
      H1=CON/D
C     ITTERATIVE DETERMINATION OF U-VALUE
C     AS FOR CNAIR1
10    H2=CNAIR2(E1,EAIR,H,Q)
      IF(H2.GT.0)THEN
      HT=1/(1/H1+1/H2)
      ELSE
      HT=H1
      END IF
      QT=HT*(E-EAIR)
      OLD=E1
      E1=E-QT/H1
      IF(ABS(E1-OLD).GT.0.0001)GOTO 10
      UVAL2=HT
      RETURN
      END
C     ***********************************************************
      FUNCTION CNAIR3(E1,E2,Y,Q)
C     HEAT TRANSFER COEFFICIENT DUE TO BUOYANCY
C     -DRIVEN CONVECTION AT THE SURFACE OF A
C     HORIZONTAL OR NEAR HORIZONTAL CYLINDER
C
C     E1,E2-TEMPERATURES OF CYLINDER SURFACE AND SURROUNDING
C     AIR, RESPECTIVELY
C     Y-CHARACTERISTIC LENGTH TAKEN AS THE DIAMETER
C     OF THE CYLINDRICAL SURFACE.
C     Q-ANGLE OF INCLINATION OF THE LONGITUDINAL
C     AXIS OF THE CYLINDER (FROM VERTICAL)
      G=9.81
      E=(E1+E2)*0.5
      CALL THMAIR(E,C,V,D,P,CON)
C     GRASHOF NUMBER FLUID PROPERTIES BASED ON MEAN
C     OF THE CYLINDER SURFACE AND AIR TEMPERATURES.
      GR=G*(1/E)*ABS(E1-E2)*(Y**3)*(D**2)*
     1     (COS(Q))/(V**2)
      RA =GR*P
```

```
      IF(RA.LT.(10.0**9))THEN
      CONST=0.53
      EX=0.25
      ELSE
      CONST=0.13
      EX=0.33
      END IF
      CNAIR3=CONST*(RA**EX)*CON/Y
      RETURN
      END
C     ************************************************************
      FUNCTION UVAL3(E,EAIR,CON,D,H,Q)
C
C     OVERALL U-VALUE FOR INSULATED CYLINDERS
C     WITH CENTRELINE HORIZONTAL OR AT SMALL ANGLE FROM HORIZO
C     (HEAT LOSS FROM INSULANT COVERED PIPEWORK)
C
C     E,EAIR-TEMPERATURE OF ENCLOSED SURFACE OF CYLINDER
C     AND SURROUNDING AIR.
C     CON CONDUCTIVITY OF INSULANT
C     D-THICKNESS OF INSULANT
C     H-INSIDE DIAMETER OF INSULATING CYLINDER
C     Q-ANGLE OF INCLINATION OF PIPE LENGTH (FROM VERTICAL)
      PI=3.1415926
      E1=(E+EAIR)*0.5
      H1=2*CON/(H*LOG(1+2*D/H))
      EXT=H+2*D
C     ITTERATIVE METHOD OF DETERMINING U-VALUE
C     SIMILAR TO CNAIR1 AND 2.
10    H2=CNAIR3(E1,EAIR,EXT,Q)
      IF(H2.GT.0)THEN
      HT=1/(1/H1+1/H2)
      ELSE
      HT=H1
      END IF
      QT=HT*(E-EAIR)
      OLD=E1
      E1=E-QT/H1
      IF(ABS(E1-OLD).GT.0.0001)GOTO 10
      UVAL3=HT
      RETURN
      END
C     ************************************************************
      FUNCTION CNAIR4(WIND,EG,EAIR,CL,CW)
C
C     FORCED CONVECTION ON PLANE DUE TO WIND
C
C     WIND-VELOCITY OF WIND
C     EG,EAIR-COOLED SURFACE AND AMBIENT TEMPERATURES
C     CL,CW-LENGTH AND WIDTH OF COOLED SURFACE
      E=ABS(EG+EAIR)*0.5
      CALL THMAIR(E,C,V,D,P,CON)
      Y=4.*(CL*CW)/(2.*(CL+CW))
      RE=D*WIND*Y/V
      UN=0.86*(RE**0.5)*(P**0.3333)
```

```
      CNAIR4=UN*CON/Y
      RETURN
      END
C     ************************************************************
      FUNCTION CNAIR5(E1,E2,Y,Q)
C
CC    HEAT TRANSFER COEFFICIENT DUE TO FREE CONVECTION
CC    ACROSS CAVITY BETWEEN PARALLEL, INCLINED PLANES
CC    (CONVECTIVE HEAT TRANSFER BETWEEN ABBSORBER
CC    PLATE AND COLLECTOR COVER)
C
C     E1,E2-TEMPERATURES OF PARALLEL SURFACES
C     Y-CHARACTERISTIC LENGTH TAKEN AS THE DISTANCE
C     BETWEEN PARALLEL PLANES
C     Q-ANGLE OF PLANES FROM HORIZONTAL.
      IF(ABS(E1-E2).GT.0)THEN
      G=9.81
      E=(E1+E2)*0.5
      CALL THMAIR(E,C,V,D,P,CON)
      RAL=G*(1/E)*ABS(E1-E2)*(Y**3.)*(D**2.)*C/
     1     (V*CON)
      R1=1.44*(1-1708/(RAL*COS(Q)))
      IF(R1.LE.0)THEN
      R1=0.
      END IF
      R2=1-(1708*(SIN(1.8*Q))**1.6)/(RAL*COS(Q))
      R3=-1+(RAL*COS(Q)/5830)**0.333
      IF(R3.LE.0)THEN
      R3=0.
      END IF
      UN=1+R1*R2+R3
      CNAIR5=UN*CON/Y
      ELSE
      CNAIR5=0
      END IF
      RETURN
      END
C     ************************************************************
      FUNCTION CONWTR(EFT,ELT,CTS,CFLOW)
C
CC    CALCULATE FORCED CONVECTION DUE TO LIQUID FLOW
CC    IN DUCT OF CIRCULAR CROSS SECTION
CC
CC    EFT-TEMPERATURE OF DUCT WALL (TAKEN IN
CC    THE RISERS TO BE VALUE AT LONGITUDINAL
C     CENTRELINE OF FIN)
C     ELT-TEMPERATURE OF LIQUID IN DUCT
CC    CTS-CHARACTERISTIC LENGTH TAKEN AS DIAMETER OF DUCT
C     CFLOW-MASS FLOW-RATE OF LIQUID
      PI=3.1415926
      G=9.81
      E=(ELT+EFT)*0.5
      CALL THMWTR(E,C,V,D,P,CON)
C     FLUID PROPERTIES OF REYNOLDS NUMBER BASED ON
C     MEAN OF BULK FLUID AND DUCT WALL TEMPERATURE
```

```
      REY=4*ABS(CFLOW)/(PI*V*CTS)
      IF(REY.GT.6000)THEN
      UN=0.02*(REY**0.8)*(P**0.33)
      ELSE
      UN=4.36
      END IF
      CONWTR=UN*CON/CTS
      RETURN
      END
C     ******************************************************************
      FUNCTION FRICTION(GRASH,REN1,ELOVERD)
C
C     THE MEAN FRICTION FACTOR FOR FLUID FLOW
C     THROUGH A DUCT OF CIRCULAR CROSS-SECTION
C
C     GRASH-DIAMETER GRASHOFF NUMBER; FLUID PROPERTIES
C     BASED ON MEAN TEMPERATURE OF DUCT WALL AND FLUID.
C     REN1-DIAMETER REYNOLDS NUMBER FOR FLOW
C     ELOVERD-LENGTH TO DIAMETER RATIO FOR DUCT
      REN=REN1
      ENTREN=ELOVERD/REN
      IF(GRASH.NE.0.)THEN
C
C     FRICTION FACTORS FOR NON-ISOTHERMAL
C     FULLY DEVELOPED FLOW
C
      FRICTION=600.*(REN**-1.19)
      ELSE
C
C     FRICTION FACTORS FOR ISOTHERMAL, DEVELOPING FLOW
C
      IF(ENTREN.LE.(10.**-3))THEN
      FRICTION=13.74*(ENTREN**0.5)/ELOVERD
      ELSE IF(ENTREN.GT.(10.**-3).AND.ENTREN.LE.10.**-1)THEN
      EN=0.9+0.07*LOG10(ENTREN)
      FRICTION=50.698*(ENTREN**EN)/ELOVERD
      ELSE IF(ENTREN.GT.(1.E-1).AND.ENTREN.LE.0.4)THEN
      EN=1.1+0.11*LOG10(ENTREN)
      FRICTION=64.416*(ENTREN**EN)/ELOVERD
      ELSE IF(ENTREN.GT.0.4)THEN
      FRICTION=64.*ENTREN/ELOVERD
      END IF
      END IF
      RETURN
      END
C     ******************************************************************
      FUNCTION TEE(FL1,FL3,ELT,CTC,NJ)
C
C     FRICTIONAL LOSSES DUE TO FLOW THROUGH A "TEE" SECTION
C
C     FL1-MASS FLOW RATE IN BRANCH
C     FL2-MASS FLOW RATE IN MAIN SECTION APPROACHING BRANCH
C     ELT-LOCAL BULK TEMPERATURE OF FLUID
C     CTC-DIAMETER OF CIRCULAR DUCT
C     NJ(=1 FOR DIVIDING FLOW, =2 FOR JOINING FLOW)
```

```
      PI=3.1415926
      CALL THMWTR(ELT,SPL,VL,ROL,PL,CON)
      IF(NJ.EQ.1)THEN
C
C     SEPARATING FLOW
C
      BRK=0.792-0.304*(FL1/FL3)+0.723*((FL1/FL3)**2)
      END IF
      IF(NJ.EQ.2)THEN
C
C     JOINING FLOW
C
      BRK=0.062+1.207*(FL1/FL3)-0.761*((FL1/FL3)**2)
      END IF
      TEE=BRK/(2.*ROL*(CTC**2.))
      RETURN
      END
C     ************************************************************
      FUNCTION BEND(FLOW,S,ELT,PC)
C
C     FRICTIONAL LOSSES DUE TO LAMINAR FLOW AROUND
C     A 90 DEG. BEND.
C
C     FLOW-MASS FLOW RATE OF FLOW
C     S-DIAMETER OF CIRCULAR DUCT
C     ELT-LOCAL BULK TEMPERATURE OF LIQUID
C     PC-CROSS SECTIONAL AREA OF DUCT
C     ANGLE SUBTENDED BY PIPE SET AT 90 DEG.
      Q=90.
      PI=3.1415926
      CALL THMWTR(ELT,SPL,VL,ROL,PL,CON)
      RE=4*ABS(FLOW)/(PI*VL*S)
C     THE RATIO OF THE RADIUS OF THE BEND TO THE
C     DIAMETER OF THE DUCT IS SET AT 1.5
      RAT=1.5
      DN=RE/((2*RAT)**0.5)
      IF(DN.LE.13.5)THEN
      BRK=1.117*Q*RAT/RE
      ELSE IF(DN.GT.13.5.AND.DN.LE.463.5)THEN
      BRK=0.17*Q*(1+2*RAT)*(RE**-0.72)+(DN-13.5)/450
      ELSE
      BRK=0.17*Q*(1+2*RAT)*(RE**-0.72)+1
      END IF
      BEND=BRK/(2*ROL*(PC**2))
      RETURN
      END
C     ************************************************************
      FUNCTION ENTRANCE(ELT,PC)
C
C     FRICTIONAL LOSSES AS FLUID IS DISCHARGED FROM A DUCT
C     INTO A RESEVOIR OF STILL WATER (IE. FROM THE
C     UPRISER INTO THE STORE)
C
C     ELT-LOCAL BULK TEMPERATURE OF FLUID IN DUCT
C     PC-DIAMETER OF DUCT
```

```
      BRK=1.
      CALL THMWTR(ELT,SPL,VL,ROL,PL,CON)
      ENTRANCE=BRK/(2*ROL*(PC**2.))
      RETURN
      END
C     ***********************************************
      FUNCTION REDUCE(ELT,D1,D2,N)
C
C     FRICTIONAL LOSSES AS FLUID PASSES THROUGH REDUCING
C     OR EXPANDING SECTION
C
C     ELT-BULK FLUID TEMPERATURE
C     D1,D2-INSIDE DIAMETER OF SMALLER AND LARGER
C     PIPE SECTIONS.
C     N(=0 FOR REDUCTION, =1 FOR EXPANSION)
      PI=3.1415926
      CALL THMWTR(ELT,SPL,VL,ROL,PL,CON)
      BRK=(2./3.)*((D1/D2)**4.)-(8./3.)*((D1/D2)**2.)+2.
      IF(N.EQ.0)THEN
      A1=PI*(D1**2.)/4.
      ELSE
      A1=PI*(D2**2.)/4.
      END IF
      REDUCE=BRK/(2.*ROL*(A1**2.))
      RETURN
      END
C     ***********************************************
      FUNCTION DIFFANGLE(CQ)
C
C     EFFECTIVE INCIDENT ANGLE OF ISOTROPIC, DIFFUSE,
C     SKY RADIATION. VALUE IS DEPENDENT ON INCLINATION
C     OF COLLECTOR.
C
C     CQ-ANGLE OF INCLINATION OF COLLECTOR FROM HORIZONTAL
      PI=3.1415926
      CQ1=CQ*180./PI
      DIFFANGLE=PI*(59.68-0.1388*CQ1+0.001497*(CQ1**2.))/180.
      RETURN
      END
C     ***********************************************
      SUBROUTINE SOLANG(KM,KD,TINSTANT,CGAMA,CQ,THI,RDIR)
C
C     ANGLE OF INCIDENCE OF BEAM RADIATION AND RATIO
C     OF OF BEAM RADIATION ON A HORIZONTAL SURFACE TO
C     THAT IN THE PLANE OF THE INCLINED COLLECTOR
C
      DIMENSION KDAY(12)
C     KM,KD,TINSTANT-MONTH,DAY AND TIME OF DAY IN SECONDS
C     CGAMA-SURFACE AZIMUTH ANGLE
C     CQ-ANGLE OF INCLINATION OF THE COLLECTOR
C     QLAT-LATTITUDE
      PI=3.1415926
      QLAT=0.89826
C     DETERMINE DAY OF YEAR
      DATA(KDAY(I),I=1,12)/0,31,59,90,120,151,181,212,243,
```

```
     1       273,304,334/
             KDTOT=KDAY(KM)+KD
C            ANGLE OF DECLINATION
             DEC=23.45*(PI/180.)*SIN((PI/180.)*360.*(284+KDTOT)
     1       /365.)
C            HOUR ANGLE (ASSUMING LONGITUDE OF 0 RADS.)
             OMEGA=PI*(TINSTANT-43200)/43200.
             T1=SIN(DEC)*SIN(QLAT)*COS(CQ)
             T2=-SIN(DEC)*COS(QLAT)*SIN(CQ)*COS(CGAMA)
             T3=COS(DEC)*COS(QLAT)*COS(CQ)*COS(OMEGA)
             T4=COS(DEC)*SIN(QLAT)*SIN(CQ)*COS(CGAMA)*COS(OMEGA)
             T5=COS(DEC)*SIN(CQ)*SIN(CGAMA)*SIN(OMEGA)
C            INCIDENT ANGLE OF BEAM RADIATION
             THI=ACOS(T1+T2+T3+T4+T5)
C            RATIO OF BEAM RADIATION ON AN INCLINED SURFACE
C            TO THAT ON A HORIZONTAL SURFACE ASSUMING THE
C            COLLECTOR LOCATED IN THE NORTHERN HEMISPHERE
C            AND SURFACE AZIMUTH ANGLE OF 0 RADS.
             RDIR=(COS(QLAT-CQ)*COS(DEC)*COS(OMEGA)+SIN(QLAT-CQ)*
     1       SIN(DEC))/(COS(QLAT)*COS(DEC)*COS(OMEGA)+SIN(QLAT)*
     2       SIN(DEC))
             IF(RDIR.LT.0)THEN
             RDIR=0
             END IF
             RETURN
             END
C            ********************************************
             FUNCTION TORALF(THI,CGIND,CGEX,CGD,CFA)
C
C            INSTANTANIOUS TRANSMITTANCE-ABSORPTANCE FACTOR
C
C            THI-ANGLE OF LIGHT INCIDENT ON COLLECTOR COVER
C            CGIND-REFRACIVE INDEX OF COVER
C            CGEX-EXTINCTION COEFFICIENT OF COVER
             PI=3.1415926
             THI=ABS(THI)
             IF(THI.EQ.0)THEN
             THI=0.01
             END IF
             IF(THI.LT.(PI/2))THEN
             THR=ASIN(SIN(THI)/CGIND)
C            PATH LENGTH THROUGH COVER
             PATH=CGD/COS(THR)
C            ABSORPTION LOSSES THROUGH COVER
             TOR1=EXP(-CGEX*PATH)
C            REFLECTANCE AND TRANSMITTANCE OF NORMAL (N)
C            AND PARALLEL (P) COMPONENTS OF INCIDENT LIGHT
             REFN=((SIN(THR-THI))**2)/((SIN(THR+THI))**2)
             REFP=((TAN(THR-THI))**2)/((TAN(THR+THI))**2)
             TORFN=TOR1*((1-REFN)**2)/(1-(REFN*TOR1)**2)
             TORFP=TOR1*((1-REFP)**2)/(1-(REFP*TOR1)**2)
C            MEAN TRANSMITTANCE
             TORM=(TORFN+TORFP)*0.5
C            REFLECTANCE OF DIFFUSE RADIATION (ASSUMED TO
C            HAVE AN EFFECTIVE INCIDENT ANGLE OF PI/3 RADS.)
```

```
      THR6=ASIN(SIN(PI/3)/CGIND)
      REFN6=((SIN(THR6-PI/3))**2)/((SIN(THR6+PI/3))
     1     **2)
      REFP6=((TAN(THR6-PI/3))**2)/((TAN(THR6+PI/3))
     1     **2)
      REFM6=(REFN6+REFP6)*0.5
C     TRANSMITTANCE-ABSORPTANCE PRODUCT AS A
C     RESULT OF SUMMING MULTIPLE REFLECTIONS
C     BETWEEN COVER AND ABSORBER PLATE.
C     RADIATION RE-EMITTED FROM PLATE ASSUMED
C     DIFFUSE (HENSE REFM6)
      TORALF=TORM*CFA/(1-(1-CFA)*REFM6)
      ELSE
      TORALF=0
      END IF
      RETURN
      END
```

APPENDIX J:

ALGEBRAIC SOLUTION TO TIME-DEPENDENT MEAN STORE TEMPERATURES FOR A THERMOSYPHON SOLAR-ENERGY WATER HEATER WITH MIXED STORE CONDITIONS

The actual performance of a thermosyphon solar energy water heater is intermediate between that predicted by analyses using the two extreme assumptions of (i) a linear store profile and (ii) that of fully mixed store conditions. It was therefore anticipated that the results of an analysis in which the latter conditions were assumed, would yield additional parameters of equal relevance to those identified in section 8 where store and collector temperatures were taken as being equivalent. The following assumptions regarding temperature distribution, buoyancy forces and flow losses within the system are made in the mixed store analysis.

i) A fully mixed store.

ii) A linear fluid temperature profile along the length of the collector.

iii) Density is a linear function of temperature.

iv) For the purposes of determining the fluid frictional losses around the thermosyphon loop, fully developed, isothermal, laminar flow exists in all components.

v) Transient terms due to forces arising from unsteady flow, are neglected.

Assumptions regarding solar radiation, water draw-off and heat losses from individual components remain identical to those stated in section 8.3.

Referring to figure J.1, the buoyancy-induced pressure head around the system is given by,

FIGURE. J.1

Schematic illustration of notation used in text

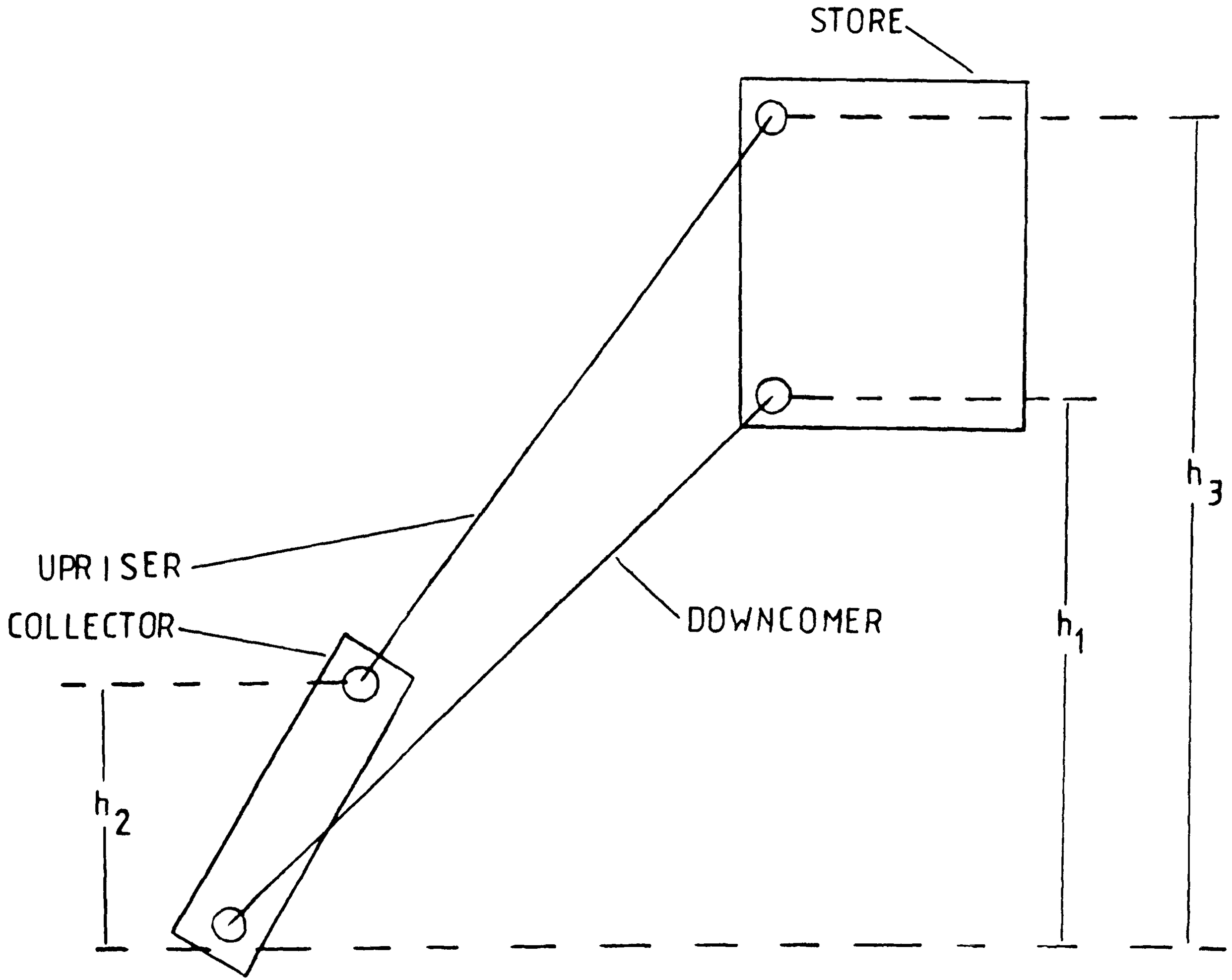
STORE
UPRISER
COLLECTOR
DOWNCOMER
h3
h1
h2

$$\Delta P_{BODY} = (\rho_s g h_3 + \rho_d g h_1) - [\rho_r g h_2 + \rho_u g(h_3 - h_2)]$$

equation J.1

Using assumption (i) for a fully mixed store, $\rho_s = \rho_d$ and so L.1 becomes,

$$\Delta P_{BODY} = \rho_s g h_3 - [\rho_r g h_2 + \rho_u g(h_3 - h_2)]$$

equation J.2

Also, since from assumption (iii) a linear relationship of the form

$$\rho = A + BT$$

equation J.3

exists between fluid temperature and density, then by substituting J.3 into J.2 and rearranging,

$$P_{BODY} = Bg(h_3 - h_2/2)(T_s - T_{c,o})$$

equation J.4

The coefficient, B can be related to the cubic expansivity γ of a liquid by

$$B = -\rho_w \gamma$$

equation J.5

and so equation J.5 for the total buoyancy pressure head becomes,

$$\Delta P_{BODY} = \rho_w \gamma g(h_3 - h_2/2)(T_{c,o} - T_s)$$

equation J.6

Energy losses due to frictional forces within a length of ducting result in a pressure drop across the length of pipe given by,

$$\Delta P_{SURF} = f \frac{L}{D} \frac{\rho v^2}{2}$$

equation J.7

For the laminar flow regime of assumption (iv), the friction factor, f is given by

$$f = 64/Re_D$$

equation J.8

where, in terms of the mass flow rate, the diameter Reynolds number, Re_D is,

$$Re_D = \frac{4\dot{m}}{\pi D \mu_w}$$

equation J.9

Equation J.8 now becomes

$$f = \frac{16\pi D \mu_w}{\dot{m}}$$

equation J.10

Substituting J.10 and mass flow rate for velocity in equation J.7 results, after appropriate manipulation in a general expression for the pressure drop due to frictional forces within a duct:

$$\Delta P_{SURF} = \frac{128 \mu_w L \dot{m}}{\rho_w \pi D^4}$$

equation J.11

But the pressure drop across the riser pipes will be due to a mass flow rate which is a fraction 1/N of the total flow around the thermosyphon loop, so that the total pressure drop from J.11 is,

$$\Delta P_{SURF} = \frac{128 \mu_w}{\pi \rho_w} [L_r/(N D_r^4) + L_p/D_p^4] \dot{m}$$

equation J.12

From assumption (v), frictional and buoyancy pressures are equivalent,

and so by combining J.6 and J.12 and re-arranging, the instantaneous mass flow rate is given by,

$$\dot{m} = \frac{\pi(\rho\gamma)_w g(h_3 - h_2/2)(T_{c,o} - T_s)}{128\nu_w[L_r/(ND_r^4) + L_p/D_p^4]}$$

equation J.13

For the purposes of algebraic expediency the grouped constant, r_1 is defined:

$$r_1 = \frac{\pi(\rho^2\gamma)_w g(h_3 - h_2/2)}{128\mu_w[L_r/(ND_r^4) + L_p/D_p^4]}$$

equation J.14

Also from assumption (ii),

$$T_{c,o} - T_s = 2(\bar{T}_c - T_s)$$

equation J.15

So that J.13 becomes, for the flow around the system,

$$\dot{m} = 2r_1(\bar{T}_c - T_s)$$

equation J.16

A steady-state energy balance on the collector gives (again using assumption (ii)),

$$2\dot{m}C_w(\bar{T}_c - T_s) = F_{AV}A_c[(\tau\alpha)_e I - U_L(\bar{T}_c - T_a)]$$

equation J.17

Substituting J.16 for the flow rate into J.17 gives, after re-arranging,

$$(\bar{T}_c - T_s)^2 + r_3(\bar{T}_c - T_s) + [r_3(T_s - T_a) - r_2] = 0$$

equation J.18

where the lumped parameters r_2 and r_3 are defined respectively as

$$r_2 = \frac{F_{AV}A_c(\tau\alpha)_e I}{4r_1 C_w}$$

equation J.19

$$r_3 = \frac{F_{AV}A_c U_L}{4r_1 C_w}$$

equation J.20

The single root of the quadratic J.18 that would give a positive mass flow rate is given by,

$$\bar{T}_c - T_s = -r_3/2 + [(r_3/2)^2 + r_2 - r_3(T_s - T_a)]^{0.5}$$

equation J.21

A time-dependent energy balance on the store gives, using J.16,

$$M_s C_w \frac{dT_s}{dt} = 4r_1 C_w (\bar{T}_c - T_s)^2$$

equation J.22

The collector temperature can now be eliminated from the energy balance by substituting J.21 into J.22,

$$\frac{dT_s}{dt} = \frac{4r_1}{M_s}\left[\frac{-r_3}{2} + [(r_3/2)^2 + r_2 - r_3(T_s - T_a)]\right]^2$$

equation J.23

The first order differential equation is integrated by successive substitutions, to give, for the temperature of the store at the end of the insolation period,

$$\frac{2}{r_3}\ \mathrm{In}\left[\frac{[(r_3/2)^2-r_3\psi^e+r_2]^{0.5}-r_3/2}{[(r_3/2)^2-r_3\psi^m+r_2]^{0.5}-r_3/2}\right]$$

$$-\ \frac{1}{[(r_3/2)^2-r_3\psi^e+r_2]^{0.5}-r_3/2}\ -\ \frac{1}{[(r_3/2)^2-r_3\psi^m+r_2]^{0.5}-r_3/2}$$

$$=\ \frac{-4r_1\Delta t}{M_s}$$

equation J.24

In practice, the term r_3 is very small when compared with r_1 and r_2, so that J.24 can be approximated to,

$$\frac{r_2-r_3\psi^e}{r_2-r_3\psi_m}\ =\ \exp\left[\frac{-4r_1r_3\Delta t}{M_s}+\ \frac{r_3}{[r_2-r_3\psi_m]^{0.5}}\left(1-\frac{[r_2-r_3\psi^e]^{0.5}}{[r_2-r_3\psi_m]^{0.5}}\right)\right]$$

equation J.25

After substituting for r_1, r_2 and r_3 back into J.25, the store temperature is given by the implicit equation,

$$\frac{F_{AV}A_c[(\tau\alpha)_eI-U_L\psi^e]}{F_{AV}A_c[(\tau\alpha)_eI-U_L\psi_m]}\ =$$

$$\exp\ \frac{-F_{AV}A_cU_L\Delta t}{M_sC_w}\ \exp\left[\frac{U_L[F_{AV}A_c/(4r_1C_w)]^{0.5}}{[(\tau\alpha)_eI-U_L\psi_m]^{0.5}}\left(1-\frac{[(\tau\alpha)_eI-U_L\psi^e]^{0.5}}{[(\tau\alpha)_eI-U_L\psi_m]^{0.5}}\right)\right]$$

equation J.26

APPENDIX K

AN INITIAL COMPARISON OF MEASURED AND PREDICTED PRESSURE DIFFERENTIALS ACROSS A FLAT PLATE SOLAR COLLECTOR WITH FORCED FLOW

K.1 Preliminary Measurements of the Pressure Drop Across a "Gull-Air" Collector

Before completion of the experimental rig described in section 4, a series of measurements of the pressure differentials across the collector were performed. The apparatus used is shown schematically in figure K.1 The purpose of these tests was to ascertain:

i) an order of magnitude for pressure drops across the collector,

ii) the viability of manometer measururements as a method of determining pressure differentials across individual components, and

iii) the veracity of simple flow loss relationships in predicting frictional losses within the collector.

The outlet of the "Gull-Air" collector was connected via a simple isolating gate valve to a constant head tank. The tank was mounted such that the level was at a height of 2.5 m above the inlet to the collector thereby supplying a stable flow of water over a pressure range of 0 Nm^{-2} up to a possible 24500 Nm^{-2} above that of atmospheric. The pressure was measured at two points; short lengths of 0.005 m diameter pipe were brazed onto a section of 0.015 m diameter pipe extending from the collector inlet and outlet. The resulting "tee" was made as close to the collector inlet and outlet as the pipe fittings would permit. Flexible polythene tubing was used to connect the small diameter branch of the "tee" to a pair of glass sight tubes and from the sight tubes onto a T.E.M. manometer. Water flowed from the collector inlet to a drain-away via a flow control valve.

FIGURE K.1

Schematic diagram of apparatus used to measure the pressure differentials across a Gull-Air collector

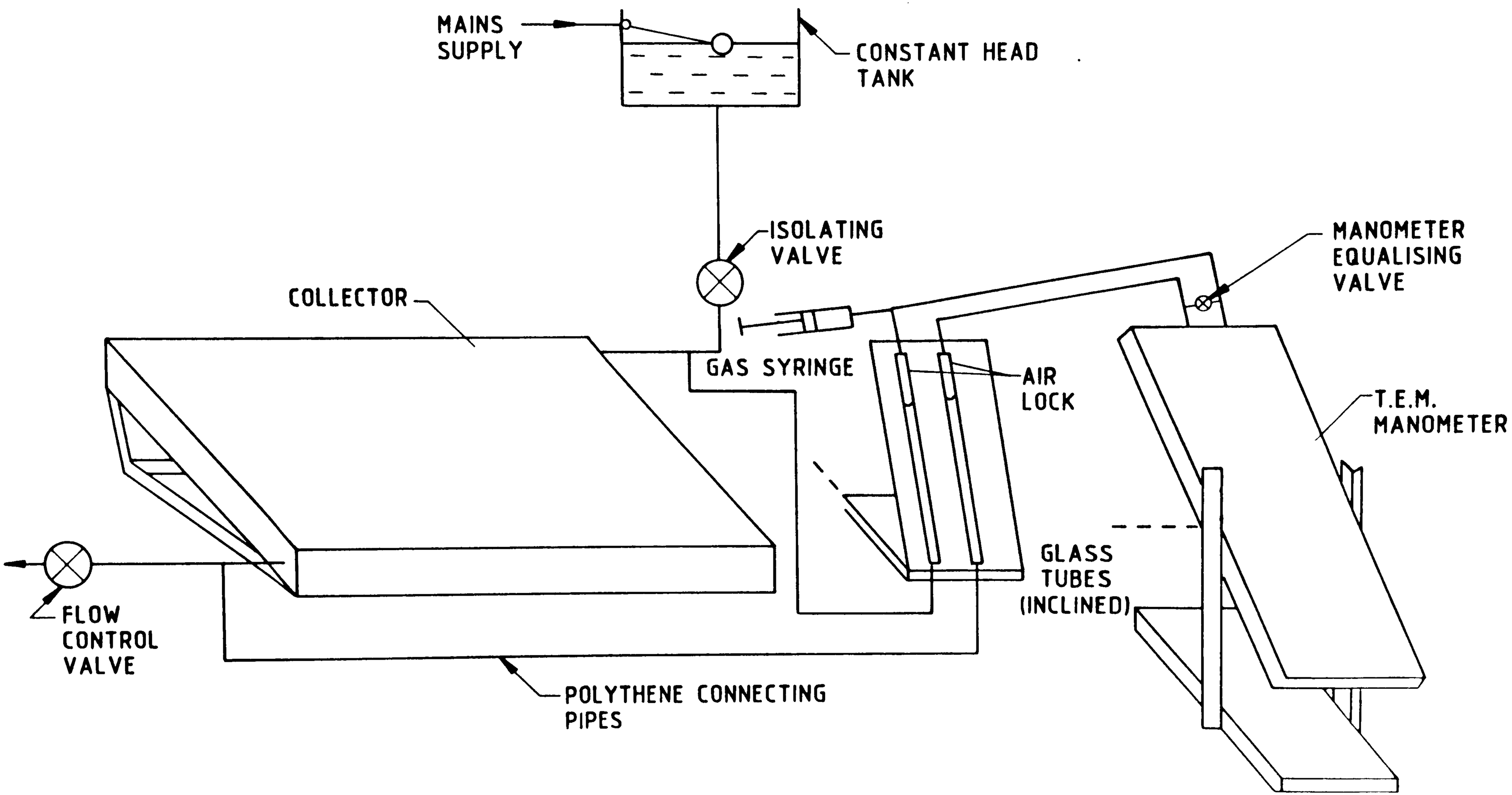
MAINS SUPPLY
CONSTANT HEAD TANK
ISOLATING VALVE
MANOMETER EQUALISING VALVE
COLLECTOR
GAS SYRINGE
AIR LOCK
T.E.M. MANOMETER
GLASS TUBES (INCLINED)
FLOW CONTROL VALVE
POLYTHENE CONNECTING PIPES

Before pressure measurements were taken under flow conditions, the flow control valve was shut and the constant head valve opened. This enabled any air trapped within the collector to escape through the constant head supply line. The manometer equalising valve was then opened and the sight glass was raised until the air lock isolating the manometer from the water within the collector, was visible. This resulted in the respective water levels in both the sight glass and the manometer being equalised to give initial "same level" settings.

The manometer equalising valve was then shut and the flow control valve opened to give the required steady flow rate through the collector. The volume of air within a 250 ml gas syringe in parallel with one of the lines connecting the manometer and sight glass was then adjusted until the water levels within the sight glass were equalised. The reading from the manometer could then be interpreted as representing the pressure drop across the collector alone. The parallel legs of the sight glass were inclined at an angle (from a horizontal datum) considerably less than that of the manometer so that any error in establishing "same level" conditions in this instrument were negligible relative to those incurred in the reading of the manometer. The method of mass flow rate measurement through the collector was similar to that described in appendix E and involved the timed collection of water at the drain-away pipe. The volume measurements made were converted into equivalent mass values using a density based on the measured temperature of the collected water. The pressure drop p, across the collector was then calculated using the relative displacement Δh of the manometer liquid of density ρ_w inclined at an angle θ to the horizontal by

$$\Delta p = \rho_w g \Delta h \sin(\theta)$$

equation K.1

A total of seven flow measurements were taken ranging from 32.5×10^{-3} to 41.7×10^{-3} kgs^{-1}. The experimental results are given in table K.1. During all the pressure measurements, instabilities in the flow caused small oscillations in the liquid within the manometer. Lower values pertinent to typical buoyancy-induced flow rates could not be measured with any degree of confidence as the oscillations within the

Table K.1: Results and associated errors for pressure measurements across a "Gull-Air" collector

Temp.	Pressure			Flow		
T	h		p_r	V	t	m_c
(^oC)	($mx10^{-3}$)	(^{o})	(Nm^{-2})	(m x 10^{-6})	(s) ± 0.2	(kgs^{-1} $x10^{-3}$ ± 0.2
19.0	6.5 ± 0.5	41	42 ± 3	1980	47.3	41.7
19.1	8.5 ± 0.5	30	42 ± 2	1930	46.9	41.0
19.0	7 ± 1	29	36 ± 5	1920	48.9	39.2
18.8	10 ± 1	20	32 ± 3	1940	52.5	36.9
18.8	5 ± 1	20	27 ± 3	1935	54.8	35.2
19.0	6 ± 2	20	21 ± 7	1935	59.2	32.6
19.0	6 ± 2	18	19 ± 6	1925	59.1	32.5

manometer aproached the same order of magnitude as displacements due to the pressure drop across the collector.

K.2 A Comparison of Measured Pressure Drops with those Calculated Using the Measured Flow Rate.

In calculating the pressure drop across the collector, certain simplifying assumptions had to be made, namely:

i) all pipes (ie. the riser and header pipes) in the collector net work are of the same diameter. This is approximately correct in the "Gull-Air" collector.

ii) the individual pressure drop across the first of the eight parallel riser pipes is is equal to the total pressure drop across the collector.

Two flow rates were selected as being within the limited range for which a relatively low degree of uncertainty was associated with the experimental pressure measurements. The flow rates were $41.7 \times 10^{-3} kgs^{-1}$ and $35.2 \times 10^{-3} kgs^{-1}$ respectively giving experimentally measured pressure differentials of 42 Nm^{-2} and 16.6 Nm^{-2}. Using these flow rates, the pressure drop across the riser pipes and "tee" sections were calculated.

1) $\dot{m}_c = 41.7 \times 10^{-3} kgs^{-1}$

The velocity, v within each of the eight risers is given by

$$v = \frac{4\dot{m}_c}{ND_r^2} = \frac{4 \times 0.0417}{8 \times 998.2 \times \times (0.015)^2} = 0.0295$$

The pressure drop due to frictional forces along the riser is given by

$$\Delta p_r = (\rho_w v^2/2)(fL_r/D_r)$$

equation K.2

The Reynolds number of the flow is given by,

$$Re_D = \frac{\rho_w v D_r}{\mu_w} = \frac{998.2 \times 0.0295 \times 0.015}{1002 \times 10} = 441$$

ie. the flow is laminar for which, assuming that the flow is also fully developed and isothermal, the friction factor, f is defined as

$$f = 64/Re_D = 64/441 = 0.145$$

So substituting values into equation K.2, the pressure drop Δp_r is,

$$\Delta p_r = \frac{998.2 \times (0.0295) \times 0.145 \times 1 \times 9.67}{2 \times 0.015} = 4.2$$

"Minor" losses across pipe fittings are characterised by a loss coefficient K_{TEE} such that,

$$\Delta p_{TEE} = K_{TEE} \rho_w v_{TEE}^2 / 2$$

equation K.3

For the "tee" at the riser inlet, using velocity dependent loss coefficient correlation charts (85), in terms of the loss in kinetic energy of the main flow in the lower header pipe approaching the riser,

$$K_{TEE,in} = 0.406$$

so the pressure drop across this section from equation K.3 is,

$$\Delta p_{TEE,in} = \frac{998.2 \times (0.236) \times 0.406}{2} = 11.3$$

Similarly, the loss coefficient for the "tee" section at the top of the riser in terms of the kinetic energy of the flow leaving the riser gives

$$K_{TEE,o} = 0.19, \text{ and } \Delta p_{TEE,o} = 5.28$$

So the total pressure drop across the riser is given by

$$\Delta p_{tot} = \Delta p_{in} + \Delta p_r + \Delta p_o$$

$$= 20.8$$

2) $\dot{m}_c = 35.2 \times 10^{-3}\ kgs^{-1}$

Using a similar method to the above,

$Re_D = 355$
$\Delta p_r = 3.4$
$\Delta p_{TEE,in} = 7.3$
$\Delta p_{TEE,o} = 3.4$
$\Delta p_{tot} = 14.1$

These predicted pressure differentials (Δp), shown plotted in figure K.2 as a function of the flow rate ($\dot{m}_c$)are considerably lower than the corresponding measured values. This may be due to the use of "minor" loss coefficients (85) which have been derived from the correlation of frictional loss under conditions of turbulent fluid flow. A detailed literature survey carried out subsequent to, and partially as a result of, the above series of tests indicated that for entrance Reynolds numbers less than 0.4, developing flow is predominant and the assumption of Poiseuille-type flow results in an underestimate of the pressure losses along a duct. The entrance Reynolds numbers defined in section 7.1.1 as,

$$= (L_r/D_r)/Re_D$$

for the 2 tests considered are,

$$= (1/0.015)/441 = 0.15$$

and

$$= (1/0.015)/355 = 0.19$$

FIGURE K.2

Experimental and predicted pressure differentials plotted against measured mass flow-rate

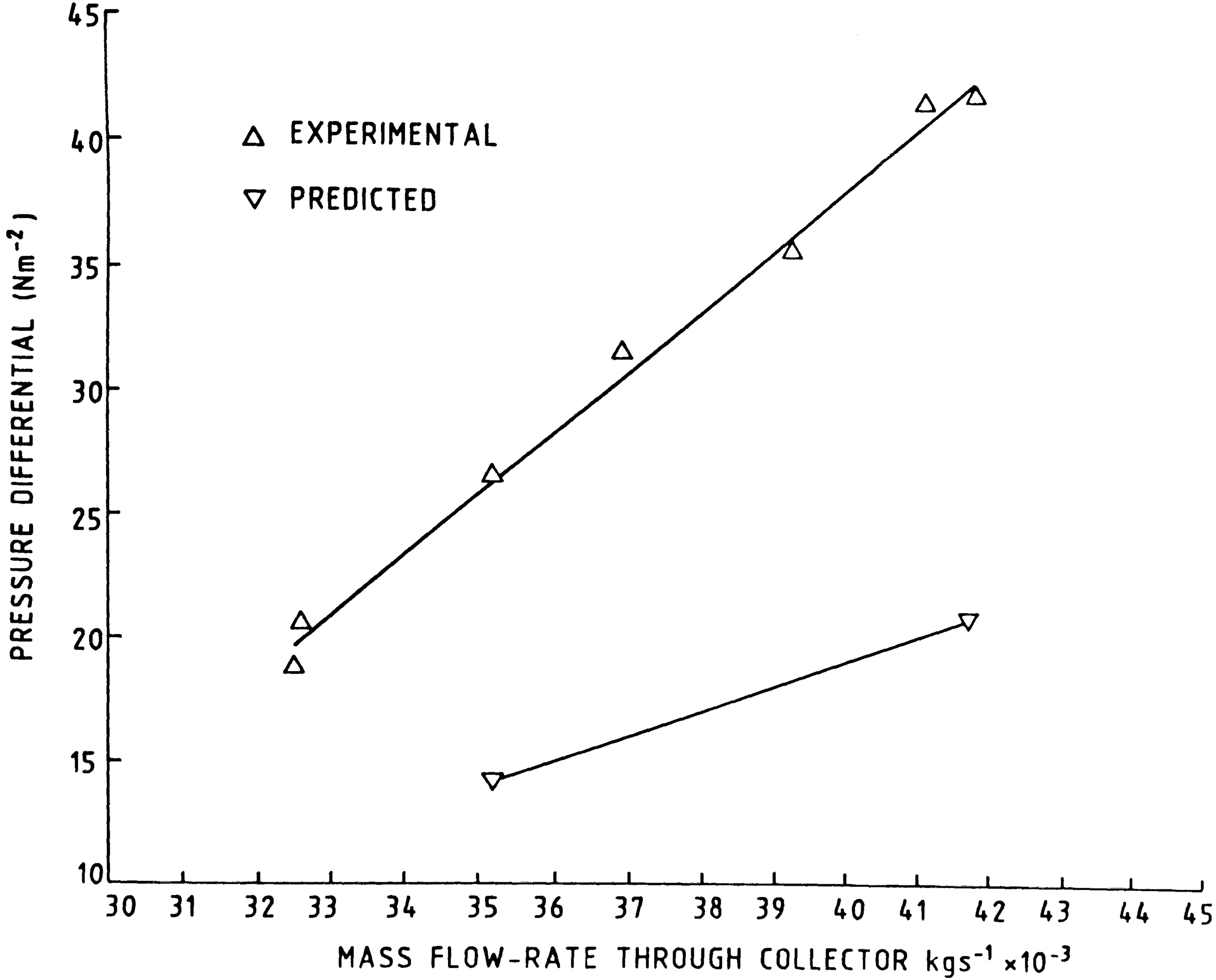
△ EXPERIMENTAL
▽ PREDICTED
PRESSURE DIFFERENTIAL (Nm⁻²)
45
40
35
30
25
20
15
10
30 31 32 33 34 35 36 37 38 39 40 41 42 43 44 45
MASS FLOW-RATE THROUGH COLLECTOR kgs⁻¹ ×10⁻³

both of which would indicate the presence of a developing boundary layer along the riser pipes with the associated increase in the apparent frictional loss coefficient.

APPENDIX L:

DETAILS OF INDIVIDUAL SIMULATION RUNS

All the thermosyphon solar energy water heaters simulated in sections 10 and 11 incorporated a collector model with the basic dimensions and material thermal properties of the "Gull-Air" collector, the specifications of which are given in appendix B. Where the simulated area was greater or less than the 2 m^2 "Gull-Air" collector, the riser length was assumed invariant at 1 m. The area was therefore changed in the simulation runs PARASIM 0-5, 9-11 and 15-41 by varying the width of the collector in effect increasing or decreasing the number of parallel-connected collectors. In order that the fin efficiency factor, F_{AV}, is not changed, the diameter of the riser pipes and the number density of the risers per unit area (or unit of collector width since the length does not vary) remains constant at 4 m^{-2}.

The upriser and downcomer pipes are kept at a constant 0.025 m internal diameter. These pipes were insulated by a 0.025 m annulus of insulant with a conductivity equivalent to that used in the experimental system described in section 4, of 0.04 $Wm^{-1}{}^{o}C^{-1}$. The parameters governing the positioning of the store relative to the collector and which therefore define the pipework geometry are given in figure L.1. The notation used is compatible with that used in the simulation programs. The upriser and downcomer pipe ports enter from opposite sides of the store. The ports in the store were set at equal distances (sdz and srz) of 2 m in the z-direction behind the collector inlet. This value was chosen as being sufficiently large to accommodate all the simulated tank diameters leaving sufficient space for the stores to be housed behind a backwardly-sloping roof. Two horizontal sections of the upriser and downcomer pipework (prcx and pdcx respectively) associated with the collector outlet and inlet were both set at a constant value of 0.2 m. Similar horizontal sections associated with the store (prsx and pdsx) were dependent on the store diameter and collector width. The length of the inclined sections of the upriser and downcomer (d1 and d2) were also calculated based on the shortest distance between the

FIGURE L.1

Schematic diagram of assumed system configuration and the corresponding notation used in the main numerical simulation programs.

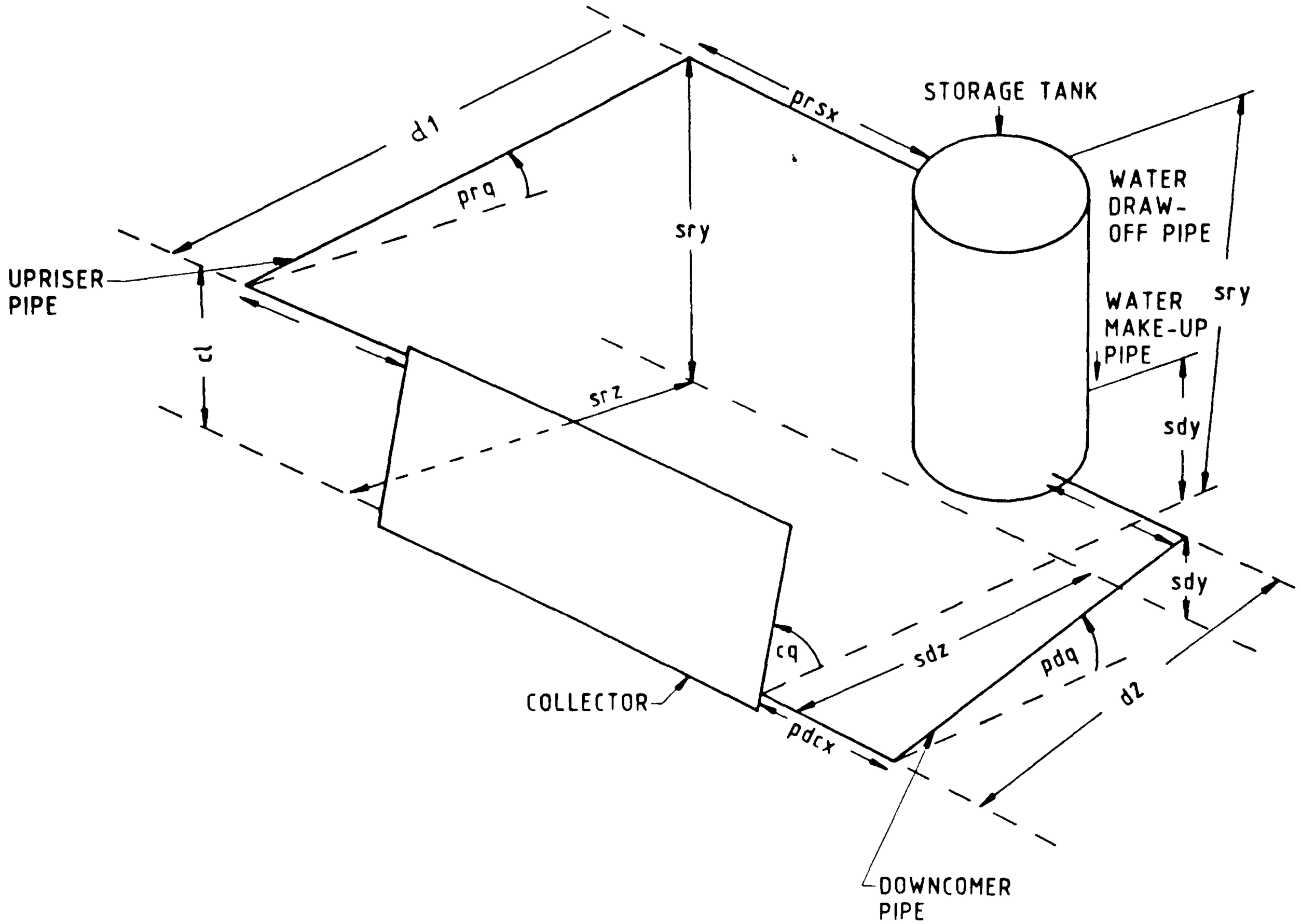
d1
prq
prsx
STORAGE TANK
WATER
DRAW-
OFF PIPE
sry
UPRISER
PIPE
WATER
MAKE-UP
PIPE
sry
srz
d1
sdy
sdy
cq
sdz
pdq
d2
COLLECTOR
pdcx
DOWNCOMER
PIPE

corresponding horizontal sections of the pipework associated with the store and collector. A total of 4 x 90^{o} bends were assumed in all the systems simulated. The simulated storage tanks were assumed to be of circular cross-section. The vertical displacement between the upriser and downcomer entry ports on the store (ie. sry-sdy) were kept at a single value of 0.7 m. The effective mass of the store was changed by varying the tank diameter alone. By this means, the vertical displacement of the upriser and downcomer ports relative to the positioning of the collector remained unaltered at the reference value. The effective thermal capacity of a store can be altered by changing the positioning of the upriser and downcomer entry ports; any water in the store above the upriser inlet will be fully mixed and water below the downcomer port will in effect become a "dead space" from the point of view of thermal storage. In order therefore that the thermal capacitance of these sections of the store remain invariant when the total mass of the store is changed, the positioning of the upriser and downcomer pipes was such that the volume of water (rather than the vertical positioning of the ports) above and below these ports remained fixed at 0.0308 m^3. The parameters varied and corresponding simulation numbers referred to in the main body of the text are given in tables L.1 to L.3.

Table L.1: Data pertinent to system configurations for the simulations YEARUN 1-8

Common data:

Collector area = 4 m^2

Mass of storage tank = 780 kg

Height of upriser port above collector inlet = 3 m

Height of downcomer port above collector inlet = 2 m

month/year	10/64	3/65	4/65	5/65	6/65	7/65	8/65	9/65
designated run number	1	2	3	4	5	6	7	8

Table L.2: Data pertinent to system configurations for the simulations PARASIM 0-14

Common data:

Height of upriser port above collector inlet = 2.48 m

Height of downcomer port above collector inlet = 1.5 m

	mass of store (kg)						
area of collector (m2)		0.5	1	2	3	4	5
	50	-	-	12	-	-	-
	100	-	-	6	-	9	-
	200	0	1	2	3	4	5
	300	-	-	7	-	10	-
	500	-	-	8	-	11	-
	800	-	-	13	-	-	-
	1000	-	-	14	-	-	-

Table L.3: Data pertinent to system configurations for the simulations PARASIM 15-41

Common data:

Mass of storage tank = 280 kg

	h_3 (m)						
area of collector (m^2)		1	1.5	2	3	6	11
	0.788	15	16	17	18	19	20
	1.288	21	22	23	24	25	26
	1.788	27	28	29	30	31	32
	2.288	33	34	35	36	37	-
	4.788	38	39	40	41	-	-